Indian J Chem
SEPTEMBER 1992
CODEN : IJOCAP 31A (9) 645-736 (1992)
ISSN : 0376-4710

INDIAN JOURNAL OF CHEMISTRY

SECTION A

(Inorganic, Bio-inorganic, Physical, Theoretical & Analytical Chemistry)

Published by
PUBLICATIONS & INFORMATION DIRECTORATE, CSIR, NEW DELHI
in association with
THE INDIAN NATIONAL SCIENCE ACADEMY, NEW DELHI

The Treatise on Indian Medicinal Plants

Editors: Asima Chatterjee and Satyesh Chandra Pakrashi

Pages: 172
Price: Rs. 250/-

Ayurveda, the indigenous system of medicine, advocates the application of various Indian herbs in curing many maladies. Several drugs of plant origin are used in Ayurveda.

The Treatise on Indian Medicinal Plants, Vol. I, the first in a series of six volumes, covers 111 plants. The write-up on each plant includes its vernacular name,occurrence and distribution, botanical description, and therapeutic uses along with important chemical constituents of the plant extract. A distinctive feature of the book is inclusion of authentic Sanskrit *slokas*, both in Devnagri and Roman scripts. The *slokas* explain the therapeutic uses of individual plants. A glossary gives the meanings of Sanskrit/Ayurvedic and medical terms. Also, a list of books referred to has been given for ready reference.

The book is profusely illustrated with both coloured and black and white pictures to enable proper identification of plant species.

The editors of the book are eminent scientists in the field. Professor Chatterjee, a Padma Bhushan and a winner of the S.S. Bhatnagar Award, is a chemist of world repute. She is currently the coordinator of the Centre of Advanced Studies on Natural Products, Department of Pure Chemistry, Calcutta University. Dr Pakrashi, the former Director of Indian Institute of Chemical Biology, Calcutta and a Fellow of the Indian National Science Academy is at present a Distinguished CSIR Fellow.

This volume would prove immensely useful to teachers, researchers and specialists in the field of Ayurveda and medicinal plants.

Insight into Scientific Research in Indian Universities & the Institutes of Technology

Rais Ahmed and Madhulika Rakesh

Pages : v + 155
Price : Rs 140/-

The role of scientific research in industry, trade, defence and in the day-to-day life of an individual cannot be over-emphasized. It, therefore, becomes pertinent to take a holistic view not only of the various parameters of research but also to assess its organizational patterns, and human relations, values and attitudes associated with it, which are the main factors responsible for the germination and growth of research *per se*.

Insight into Scientific Research encompasses an exhaustive yet interesting study of the quality, character and efficiency of scientific research in Indian universities and other research institutions.

Several recommendations ranging from adequate financial support, reform of education leading to research, and utilization of research results would enlighten the reader. The book also throws light on what should be the research policy for Indian universities and research institutions.

One of the authors, Professor Ahmed, a Padma Bhushan is a renouned physicist. At present he is Executive Director of the Tertiary Education Commission in Mauritius. The coauthor Ms. Rakesh is an experienced researcher in the field of investigating conditions, process and value systems of scientific research.

Order for the books should be accompanied by M.O./D.D. made payable to **"Publications & Information Directorate"** and sent to:
Sales and Distribution Officer.
PUBLICATIONS & INFORMATION DIRECTORATE
Dr. K.S. Krishnan Marg,
New Delhi-110012.

Well illustrated with graphs and tables, which aid the text, the book should be a valuable possession for all involved in the scientific and technological development of the country.

INDIAN JOURNAL OF CHEMISTRY

Section A: Inorganic, Bio-inorganic, Physical, Theoretical & Analytical Chemistry

Editors: Dr B.C. Sharma, Dr S. Sivakamasundari and Dr S.K. Bhasin
Sr. Scientific Assistant: Geeta Mahadevan

Published by the Publications & Information Directorate (CSIR), Hillside Road, New Delhi 110 012
Director: Dr G P Phondke

The Indian Journal of Chemistry is issued monthly in two sections: A and B. Communications regarding contributions for publication in the journal should be addressed to the Editor, Indian Journal of Chemistry, Publications & Information Directorate, Hillside Road, New Delhi 110 012.

Correspondence regarding subscriptions and advertisements should be addressed to the Sales & Distribution Officer, Publications & Information Directorate, Dr K.S. Krishnan Marg, New Delhi 110 012.
Phone 586301 Gram: PUBLIFORM Telex: 031-77271

The Publications & Information Directorate (CSIR) assumes no responsibility for the statements and opinions advanced by contributors. The Editorial Board in its work of examining papers received for publication is assisted, in an honorary capacity by a large number of distinguished scientists, working in various parts of India.

Annual Subscription: Rs. 400.00 £ 100.00 $ 150.00; 50% discount admissible to research workers and students and 25% discount to non-research individuals on annual subscription.

Single Copy: Rs. 30.00 £ 10.00 $ 15.00

Payments in respect of subscriptions and advertisements may be sent by cheque, bank draft, money order or postal order marked payable to Publications & Information Directorate, Hillside Road, New Delhi 110 012.

Claims for missing numbers of the journal will be allowed only if received within 3 months of the date of issue of the journal plus the time normally required for postal delivery of the journals and the claim.

AUTHOR INDEX

Indian Journal of Chemistry

Sect. A: Inorganic, Bio-inorganic, Physical, Theoretical & Analytical

Vol. 31A NUMBER 9 SEPTEMBER 1992

CONTENTS

(*contd*)

CONTENTS

Authors for correspondence are indicated by (*)

Indian Journal of Chemistry
Vol. 31A, September 1992, pp. 645-646

Communication

Contrasting isomer stabilities of silaboranes and carboranes: $Si_2B_3H_5$ and $C_2B_3H_5$ isomers

Eluvathingal D Jemmis* & G Subramanian
School of Chemistry, University of Hyderabad,
Central Univ. P.O., Hyderabad 500 134

Received 20 April 1992; revised and accepted 3 July 1992

The relative stabilities of the isomers of closo-$Si_2B_3H_5$ have been calculated at the MNDO, HF/6-31G* and MP2/6-31G* levels. Contrary to the results for the corresponding carborane $C_2B_3H_5$ reported earlier, 2,3-$Si_2B_3H_5$ is predicted to be the most stable. The concept of the compatibility of orbitals in overlap is used to rationalize our observation of this reversal of trends in isomer stabilities.

Among the isomers of $C_2B_3H_5$, 1,5-$C_2B_3H_5$ is the most stable[1]. We have developed an explanation based on the compatibility of orbitals in overlap to account for this observation[2]. It occurred to us that the replacement of carbon by silicon could reverse these trends[3]. We now report the relative stabilities of $Si_2B_3H_5$ isomers calculated at the MNDO[4], HF/6-31G*[5] and MP2/6-31G*[6] levels. Contrary to the $C_2B_3H_5$ isomers, 2,3-$Si_2B_3H_5$ is predicted to be the most stable.

The $Si_2B_3H_5$ isomers (**1c, 2c** and **3c**) were first optimized at the MNDO[4] and HF/6-31G*[5] levels. A frequency analysis at the HF/6-31G* level gave one imaginary frequency for **3c**. This was followed to get the lower symmetry structure, **4**. The MNDO relative energies clearly indicated a reversal of the relative energies in comparison to those of the carboranes reported earlier[7]. However, the energies at the HF/6-31G* level of **1c, 2c** and **4** were all comparable. Further optimization at MP2/6-31G* level changed the relative energies such that **4** is lower in energy than **2c** which in turn is lower in energy than **1c** (Table 1).

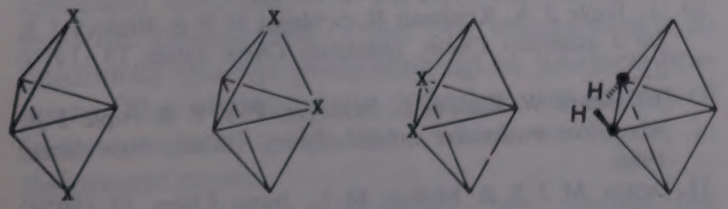

1 (D_{3h}) 2 (C_s) 3 (C_{2v}) 4 (C_s)

(a) X = BH^- (b) X = CH (c) X = SiH ● = Si

Unmarked vertices represent BH

The stability of **1b** compared to **3b** results from the preference of a three-membered borocycle for a capping group with less diffuse orbitals[2]. Hence, carbon is preferred to boron. The same argument would predict that the Si−H with much more diffuse orbitals is an unwelcome cap for the three membered ring. Isomers where the SiH is not a capping group is, therefore, preferred. **4**, where both the capping groups are BH, is more stable. This is not surprising in view of the interatomic distances of the central three-membered ring. For example, the B−B distance is 2.53 Å in **1c** in comparison to the calculated B−B distance of 1.76 Å in H_2B-BH_2 (D_{2h}) (ref. 8). It is possible to represent **1b** and **1c** as classical structures with three sp^2 hybridized borons and two sp^3 hybridized C or Si. The bonding combination of the two Walsh orbitals of the three-membered borocycle with the CH(SiH) orbitals are filled, but at the long B−B distances these MO's contribute mainly towards B−C(Si) binding. In addition, the three π MO's are filled. While there are other factors that also contribute to the relative stabilities of isomers, the concept of compatibility of orbitals in overlap provides an easily arrived at rough guide.

The calculated energies at the HF/6-31G* level for the formal reactions shown below also provide measures of the relative preferences among the C−H and Si−H caps for n-membered borocycles (n = 3-5).

$$1,5\text{-}Si_2B_3H_5 + 1,6\text{-}C_2B_4H_6 \rightarrow 1,5\text{-}C_2B_3H_5 + 1,6\text{-}Si_2B_4H_6$$
$$\Delta E = -30.6 \text{ kcal/mol}$$

$$1,5\text{-}Si_2B_3H_5 + 1,7\text{-}C_2B_5H_7 \rightarrow 1,5\text{-}C_2B_3H_5 + 1,7\text{-}Si_2B_5H_7$$
$$\Delta E = -118.3 \text{ kcal/mol}$$

$$1,5\text{-}Si_2B_3H_5 + B_7H_7^{2-} \rightarrow 1,7\text{-}Si_2B_5H_7 + B_5H_5^{2-}$$
$$\Delta E = -28.4 \text{ kcal/mol}$$

The preference of C−H for smaller ring and Si−H for larger ring is seen from the exothermicities of the above reactions.

We conclude from this study that the relative isomer stabilities are reversed in going from closo carboranes to closo silaboranes. The large diffused nature of the silicon *p*-orbital among other factors

Table 1 – Heats of formation (kcal/mol) at MNDO, total energies (au) at *ab initio* level, relative energies (kcal/mol) and zero-point energies (in kcal/mol) at the HF/6-31G* level for isomers **1a-4** (NIM = number of imaginary frequencies)

Isomer (Symmetry)	MNDO	HF/6-31G* (MP2/6-31G*)[a]	Relative energy			ZPE (NIM)
			MNDO	HF/6-31G*[b]	MP2/6-31G*[b]	
1a (D_{3h})	76.3[c]	−126.05919				
1b (D_{3h})	26.8[d]	−152.68657 (−153.18246)	00.0	0.0	0.0	47.3
2b (C_s)	69.6	−152.61431 (−153.12459)	42.9	45.3	36.3	46.3
3b (C_{2v})	90.2	−152.56581 (−153.08716)	63.5	75.8	59.8	44.3(2)
1c (D_{3h})	112.7	−654.65701 (−655.10897)	35.8	1.5	16.4	35.9
2c (C_s)	99.9	−654.65918 (−655.13087)	23.0	0.5	2.9	36.3
3c (C_{2v})	76.9	−654.65957	00.0	0.3	—	35.9(1)
4 (C_2)		−654.65993 (−655.13555)	—	0.0	0.0	36.3
$Si_2B_4H_6$ (D_{4h})	65.9	−679.96541[e]				
$Si_2B_5H_7$ (D_{5h})	27.3	−705.27537[e]				
$B_7H_7^{2-}$ (D_{5h})	37.3[c]	−176.72273[e]				

[a]Total energies for isomers **1c**, **2c** and **4** optimized at MP2/6-31G* level. Single point MP2/6-31G*/6-31G* for isomers **1b, 2b** and **3b** are taken from ref. 7. Also see ref. 13.

[b]Including ZPE correction after scaling the ZPE by 0.89 (ref. 10).

[c]ref. 11.

[d]ref. 12.

[e]ref. 3.

makes the 1,5-isomer, **1c**, to be less stable compared to **2c** and **4**. In view of the novel 2,3-isomer that is anticipated to be more favourable, attempts at the synthesis of silaboranes based on the trigonal bipyramid should be rewarding[9].

Acknowledgement

The authors thank the Department of Science and Technology, New Delhi, for financial support and Prof. J. Chandrasekhar for suggestions.

References

1 (a) Grimes R N, *Carboranes* (Academic Press, New York), 1970.
(b) Liebman J F, Greenberg A & Williams R E, (Ed.) *Advances in boron and the boranes* (VCH, New York), 1988.
2 Jemmis E D, *J Am chem Soc*, 104 (1982) 7017.
3 Jemmis E D, Subramanian G & Radom L, *J Am chem Soc*, 114 (1992) 1481.
4 Dewar M J S, McKee M L & Rzepa H S, *J Am chem Soc*, 100 (1978) 3607.
5 Hariharan P C & Pople J A, *Theoret chim Acta*, 28 (1971) 213.
6 (a) Moller C & Plesset M S, *Phys Rev*, 46 (1934) 618.
(b) Pople J A, Binkley J S & Seeger R, *Int J quantum Chem Symp*, 10 (1976) 1.
7 McKee M L, *J phys Chem*, 95 (1991) 9273.
8 Whiteside R A, Frisch M J, Binkley J S, DeFrees D J, Schlegel H B, Raghavachari K & Pople J A, *Carnegie-Mellon Quantum Chem Arch*, 2nd Edn. (Carnegie-Mellon, Pittsburg), 1981.
9 Seyferth D, Buchner K, Rees Jr W S & Davis W M, *Angew Chem Int Edn Engl*, 29 (1990) 918.
10 (a) Pople J A, Krishnan R, Schlegel H B & Binkley J S, *Int J quantum Chem, Quantum Chem Symp*, 13 (1979) 225.
(b) Hehre W, Radom L, Schleyer, P V R & Pople J A, *Ab initio molecular orbital theory*, (Wiley, New York) 1986.
11 Dewar M J S & McKee M L, *Inorg Chem*, 17, (1978) 1569.
12 Dewar M J S & McKee M L, *Inorg Chem*, 19, (1980) 2662.
13 Table of cartesian coordinates of isomers **1c-4** can be obtained from the authors.

Indian Journal of Chemistry
Vol. 31A, September 1992, pp. 647-650

Cyclic conjugation in benzo-annelated polyacenes

Ivan Gutman* & Vesna Petrović
Faculty of Science, University of Kragujevac, P.O. Box 60, YU-34000 Kragujevac, Yugoslavia

Received 2 April 1992; accepted 16 June 1992

Conjugation along a particular ring in a polycyclic conjugated molecule can be measured by means of the effect of the ring on total π-electron energy. Using this approach, we have studied cyclic conjugation in mono-, di-, tri- and tetra-benzo polyacenes. The main conclusion of our research is that the Clar aromatic sextet formulas of the benzo-annelated polyacenes provide a reasonable description of their conjugation modes. A few refinements are, however, possible. The extent of cyclic conjugation is found to be minimal in the central region of the polyacene molecule and it monotonically increases towards its two termini. Geminal annelation has an extra increasing effect on cyclic conjugation. Isoarithmic systems are shown to have practically coinciding conjugation modes.

In 1977 S Bosanac and one of the present authors formulated the theoretical basis for the calculation of the effect of an individual ring on the total π-electron energy of a polycyclic conjugated molecule[1,2]. By this a quantitative measure of the thermodynamic effect of cyclic conjugation was obtained which made possible to rationalize the generallized Hückel rule[2,3] as well as a number of other structure-property relations for conjugated π-electron systems[4].

In the early period of the development of this theory the conjugated molecules studied were small and contained only a limited number of cycles. The reason for this is that in order to acquire the numerical value of the energy-effect of an individual cycle it is necessary to perform quite lengthy calculations. For larger polycyclic molecules such calculations cannot be done without the aid of powerful computing machines, which in the seventies were not available to the authors.

Only a few years ago we managed to obtain the first results[5-7] for a few classes of benzenoid hydrocarbons, but even then the studies had to be limited to systems with about ten six-membered rings. By making appropriate improvements in our computer software, now we have been able to extend the examination of the ring energy-effects to benzenoid systems possessing up to fourteen hexagons. This enabled us to complete our studies of benzo-annelated polyacenes which we report in the present paper.

Benzo-annelated polyacenes are among the chemically best studied benzenoid hydrocarbons. Their general structure is depicted in Fig. 1. The hexagon *a* is assumed to be present; the hexagons *b*, *c* and *d* may, but need not be present. Hence, for a given value of n ($n \geq 2$) there are six distinct benzo-annelated polyacenes, possessing either the hexagon *a* or the hexagons *a* & *b* or *a* & *c* or *a* & *d* or *a* & *b* & *c* or *a* & *b* & *c* & *d*.

At least 23 such compounds are known[8,9], in particular all benzo-annelated polyacenes with n = 2, 3 and 4. All these compounds are highly stable aromatic species whose chemical, physical and spectroscopic behaviours are typical of benzenoid hydrocarbons[8,10].

A qualitative insight into the conjugation modes of benzenoid hydrocarbons can be gained by means of the Clar aromatic sextet (CAS) theory[10,11]. In particular, the π-electron structure of the benzo-annelated polyacenes is represented by n-2 or n-3 Clar aromatic sextet formulae. If either the rings *c* or *d* (or both) are present in the molecule, then the number of the respective Clar formulae is n-2. Otherwise a total of n-3 Clar formulae can be drawn. The Clar formulae of benzo-annelated hexacenes (n = 6) are depicted in Fig. 2.

Fig. 2 may serve as an illustration of the following general features of the Clar formulae of benzo-annelated polyacenes:

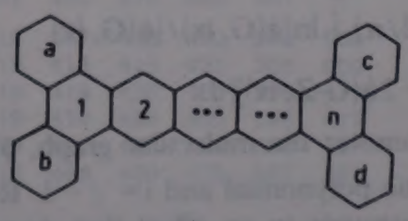

Fig. 1—Benzo-annelated polyacenes and the labelling of their six-membered rings; the ring *b*, *c* and *d* may, but need not be present.

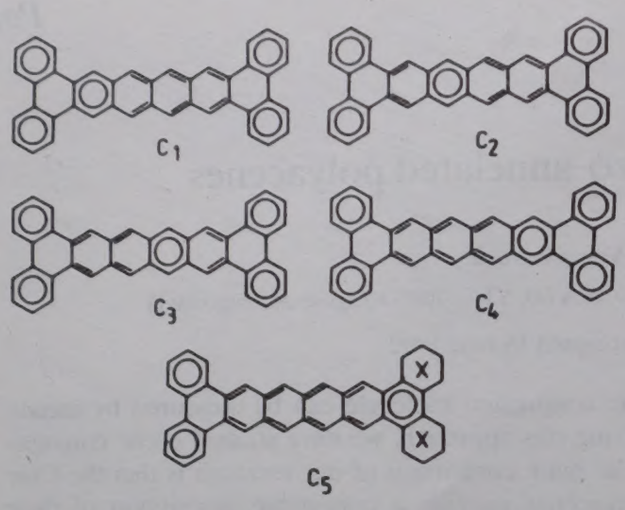

Fig. 2—Clar aromatic sextet formulae of benzo-annelated hexacenes (n=6); the Clar formula C_5 exists only in the case when both the benzene rings *c* and *d* (annelated at the right-hand side of the hexacene fragment) are absent

(a) The rings *a*, *b*, *c* and *d* possess aromatic sextets in all Clar formulae. Consequently, their contribution to the overall cyclic conjugation is expected to be very high.

(b) In all Clar formulae the ring 1 is empty. Consequently, this ring should have only a very small cyclic conjugation effect.

(c) If either the rings *c* or *d* (or both) are present, then in all Clar formulae also the ring n is empty and conclusion (b) applies.

(d) Each Clar formula possesses one additional aromatic sextet that is located in a different hexagon of the linear polyacene fragment. Thus, according to the Clar theory[11] all hexagons of the linear polyacene fragment (except the first and, in certain cases, the last hexagon) should participate with equal intensities in the overall conjugation and their effects should have a medium magnitude.

Method

Details of the theory by means of which we calculate the contribution of an individual cycle in a polycyclic conjugated molecule to the HMO total π-electron energy were outlined elsewhere[1,2]. The effect of the cycle Z (in units of the carbon-carbon resonance integral β) is expressed as,

$$ef(G,Z)=(2/\pi)\int_0^\infty \ln|\phi(G, ix)/[\phi(G, ix) + 2\phi(G\text{-}Z, ix)]|\,dx$$

where G denotes the molecular graph, $\phi(G, x)$ its characteristic polynomial and $i=\sqrt{-1}$. Recall that $ef>0$ corresponds to an effect that decreases the enthalpy, i.e., thermodynamically stabilizes the respective molecule.

Results and Discussion

In Table 1 are collected the ef-values of all six-membered rings of the benzo-annelated polyacenes with $n \leq 10$.

By inspection of the data presented in Table 1, we immediately recognize the following general regularities.

(A) The results of the ef-method essentially agree with the conjugation pattern anticipated by Clar theory: (i) The rings *a*, *b*, *c* and *d* have high ef-values. (ii) The rings adjacent to *a*, *b*, *c* or *d* have very low ef-values. (iii) The rings belonging to the linear polyacene fragment, but not being adjacent to *a*, *b*, *c* or *d* have intermediate ef-values. Because our results are quantitative, we see that the energy-contributions of the full rings (*a*, *b*, *c*, *d*) are 3 to 4 times greater than the "intermediate" energy-contributions of the rings 2, 3, ..., n-1 and are sometimes more than an order of magnitude greater than the effects of the empty rings.

(B) However, the ef-method reveals numerous details in the conjugation pattern which cannot be deduced from Clar-theory-based reasonings. Some of the most significant observations of this kind are listed below under points (C)-(G). According to them, not all Clar formulae are equally plausible; the best are those in which the aromatic sextets are as distant as possible from the centre of the molecule. In other words, in addition to the rings *a*, *b*, *c* and *d*, the aromatic sextets should be preferably located in the rings 2 and n-1 (if *c* and/or *d* are present) or in the rings 2 and n (if neither *c* nor *d* is present).

(C) Two geminally annelated benzene rings increase each other's energy-effects. Hence, where a sole benzene ring contributes by about 0.18 β, two geminal rings contribute each by about 0.20 β. In the same way, an empty ring adjacent to two full rings has a substantially lower energy-effect (about 0.02 β) than an empty ring adjacent to only one full ring (about 0.04 β).

(D) The annelated rings increase the energy-effects also in the non-adjacent rings belonging to the linear polyacence fragment. Their influence, however, attenuates very rapidly. As a consequence, the rings *a* and *b* increase mainly the ef-value of the ring 2 whereas the rings *c* and *d* exhibit an analogous influence on the ring n-1. The ef-values of the rings 2 and n-1 may exceed the ef-values of the other rings in the linear polyacene fragment by a significant amount of 0.01-0.02 β.

(E) If the rings *c* and *d* are absent, then the terminal ring n has an "anomalously" high energy-effect. This result requires that the corresponding

Table 1—Energy-effects of the six-membered rings of the benzo-annelated polyacenes with $n \leq 10$; the ef-values are given in units of $10^{-4}\beta$; the rings are labelled as in Fig. 1

size	annelated benzene rings				six-membered rings of the linear polyacene fragment (1,...,n)									
n	a	b	c	d	1	2	3	4	5	6	7	8	9	10
2	1586	-	-	-	534	1586								
	1910	1910	-	-	242	1910								
	1449	-	1449	-	693	693								
	1465	-	-	1465	689	689								
	1790	1813	1369	-	304	829								
	1725	1725	1725	1725	360	360								
3	1717	-	-	-	431	796	1048							
	2003	2003	-	-	204	908	1116							
	1660	-	1660	-	469	1002	469							
	1665	-	-	1665	469	1001	469							
	1961	1967	1628	-	218	1165	496							
	1939	1939	1939	1939	227	1380	227							
4	1768	-	-	-	413	633	579	926						
	2035	2035	-	-	199	710	609	942						
	1744	-	1744	-	423	695	695	423						
	1745	-	-	1745	423	694	694	423						
	2019	2021	1730	-	202	784	736	428						
	2011	2011	2011	2011	204	835	835	204						
5	1789	-	-	-	412	596	483	521	900					
	2047	2047	-	-	199	666	503	529	903					
	1778	-	1778	-	414	614	519	614	414					
	1779	-	-	1779	414	614	519	614	414					
	2041	2041	1773	-	199	687	543	625	415					
	2037	2037	2037	2037	200	701	570	701	200					
6	1798	-	-	-	414	590	461	443	506	899				
	2052	2052	-	-	200	660	479	449	508	898				
	1793	-	1793	-	414	594	472	472	594	414				
	1793	-	-	1793	414	594	472	472	594	414				
	2049	2050	1791	-	199	664	491	479	597	413				
	2048	2048	2048	2048	199	667	498	498	667	199				
7	1802	-	-	-	415	591	457	427	433	503	902			
	2054	2054	-	-	200	662	474	432	435	503	901			
	1800	-	1800	-	415	592	460	435	460	592	415			
	1800	-	-	1800	415	592	460	435	460	592	415			
	2053	2053	1799	-	200	662	477	440	461	592	415			
	2052	2052	2052	2052	200	662	479	446	479	662	220			
8	1804	-	-	-	417	594	457	425	420	432	504	905		
	2055	2055	-	-	200	664	474	429	421	432	504	905		
	1803	-	1803	-	416	593	457	427	427	457	593	416		
	1803	-	-	1803	416	593	457	427	427	457	593	416		
	2054	2054	1802	-	200	663	475	431	428	458	592	416		
	2054	2054	2054	2054	200	663	475	432	432	475	663	200		
9	1805	-	-	-	417	595	458	425	418	418	432	505	908	
	2055	2055	-	-	201	667	476	429	419	418	432	505	907	
	1804	-	1804	-	417	595	458	425	420	425	458	595	417	
	1804	-	-	1804	417	594	458	425	420	425	458	594	417	
	2055	2055	1804	-	201	666	475	429	420	425	458	594	417	
	2055	2055	2055	2055	201	665	475	430	421	430	475	665	201	
10	1805	-	-	-	418	597	459	426	419	417	419	432	506	909
	2055	2055	-	-	201	668	477	430	419	417	419	432	506	909
	1805	-	1805	-	417	596	459	426	419	419	426	459	596	417
	1805	-	-	1805	417	596	459	426	419	419	426	459	596	417
	2055	2055	1805	-	201	668	476	430	419	419	425	458	596	417
	2055	2055	2055	2055	201	667	476	430	419	419	430	476	667	201

Clar formula (e.g. C_5 is Fig. 2) is given a substantially higher weight than in the ordinary version of the Clar theory[11].

(F) A further peculiar detail seen from Table 1 is the fact that the ef-values monotonically decrease when going from the rings 2 and n-1 towards the centre of the molecule. However, except between the rings 2 & 3 and n-2 & n-1, the respective differences are insignificant. In other words the energy-effects of the rings 3, 4, ..., n-2 are found to be essentially the same (around 0.04 β), a result which is in line with the predictions of the aromatic sextet theory.

(G) As a final remark we call attention to the fact that the dibenzo-polyacenes in which the annelated rings are in position *a* & *c* and *a* & *c'* are classified as isoarithmic[12,13]. Recall that isoarithmic benzenoids have closely similar π-electron properties: coinciding sets of resonance structures and of Clar formulae, identical sextet polynomials etc: In full harmony with this we observe that the energy-contributions of the six-membered rings in the isoarithmic (*a*, *c*)-dibenzo and (*a*,*d*)-dibenzo polyacenes differ insignificantly. For $n \geq 6$ the respective differences are already less than 0.0001 β and, consequently, cannot be seen from Table 1.

References

1 Bosanac S & Gutman I, *Z Naturforsch*, 32a (1977) 10.
2 Gutman I & Bosanac S, *Tetrahedron*, 33 (1977) 1809.
3 Gutman I, *J chem Soc, Faraday Trans*, 2, 75 (1979) 799.
4 Gutman I & Polansky O E, *Theoret chim Acta*, 60 (1981) 203.
5 Gutman I, *Rept mol Theory*, 1 (1990) 115.
6 Gutman I, *Pure appl Chem*, 62 (1990) 429.
7 Gutman I & Agranat I, *Polyc arom Comp*, 2 (1991) 63.
8 Clar E, *Polycyclic hydrocarbons* (Academic Press, London) 1964.
9 Dias J R, *Handbook of polycyclic hydrocarbons, Part A. Benzenoid hydrocarbons* (Elsevier, Amsterdam) 1987.
10 Gutman I & Cyvin S J, *Introduction to the theory of benzenoid hydrocarbons* (Springer-Verlag, Berlin) 1989.
11 Clar E, *The aromatic sextet* (Wiley, London) 1972.
12 Balaban A T & Tomescu I, *Math Chem*, 14 (1983) 155.
13 Balaban A T, *J chem Inf Comput Sci*, 25 (1985) 334.

Indian Journal of Chemistry
Vol. 31A, September 1992, pp. 651-657

Hot atom chemistry in oxyanion targets: Part V†—Pre-activation heat treatment study of recoil ^{56}Mn in permanganates

Shuddhodan P Mishra* & (Miss) Jyoti Singh
Nuclear and Radiation Chemistry Laboratory, Department of Chemistry, Faculty of Science, Banaras Hindu University, Varanasi 221 005 (India)

Received 17 December 1991; revised and accepted 27 February 1992

The effect of pre-heat treatment on the fate of ^{56}Mn recoil atoms originating from (n, γ) reaction in $KMnO_4$, $Ba(MnO_4)_2$ and NH_4MnO_4 targets results in a slight increase in the initial ^{56}Mn retention and decrease in the extent of subsequent thermal annealing. Fletcher-Brown model has been utilized to deduce the kinetic behaviour of the annealing phenomenon which consists of two apparent first order processes for both the pre-heated and untreated permanganates. The implications of the results are explained on the basis of competitive participation of oxidising/reducing inherent crystal defects.

Published literature at our disposal for the processes occurring in radiation damaged solids[1-5] reveals that a precise understanding of the relative importance of the contribution made by pre-activation treatment is still not very clear. The formation of precursors in an irradiated matrix has not yet been established by methods in which the crystals are dissolved for analysis, since on dissolution these species are expected to be changed considerably. However, the nature of these precursors may be investigated by adopting indirect means such as post neutron irradiation heat treatment and pre-irradiation perturbation, e.g., thermal pre-treatment, crushing etc.

The discovery of the effect of the ambient atmosphere on the annealing process supported the redox hypothesis and emphasized involvement of electronic processes[6]. A variety of observations lead to a conclusion that the fate of the fragments generated in the crystalline solids by radiative thermal neutron capture is determined, in part, by the density, and possibly the nature of the defects in the crystals[7]. Theories as to the mechanism of recoil thermal annealing processes, which lead to the once freed recoil species being reincorporated in the chemical form of the parent compound-ion or molecule, invoke the participation of electronic defects in the crystal[8].

Several workers have shown the influence of defects on the initial damage and in the subsequent annealing of radiation damage in lead nitrate[9], potassium bromate[10] and potassium chlorate[9] in some reasonable detail. However, only scanty reports[11-14] have appeared for the pre-activation treatments in permanganates and a convincing scheme for recoil annealing reactions is still lacking. The notion that population of precursors are modified by their transient reactions with inherent crystal defects which influence both initial retention and the extent of annealing motivated us to investigate the effect of pre-irradiation thermal treatment on recoil stabilisation of ^{56}Mn in permanganates ($KMnO_4$, $Ba(MnO_4)_2$ and NH_4MnO_4). These permanganates are of special interest in the present investigation to see the difference between the unusual reduction property of ammonium ion, an alkali metal ion (potassium) as well as an alkaline earth metal ion (barium), i.e. role of counter cations of permanganates during (n, γ) process. The annealing results are fruitfully discussed in the light of kinetic model[15].

Materials and Methods

$Ba(MnO_4)_2$ and NH_4MnO_4 were prepared by the method described in the literature[16,17] and $KMnO_4$ of AR grade was used as received. Targets (300.00 mg) contained in very thin boron-free glass ampoules were irradiated at ambient temperature (303K) for upto 20 hr by paraffin-thermalized neutrons from a 300 mCi Ra-Be neutron source with an integrated neutron flux of 3.2×10^6 n cm^{-2} s^{-1} (11.1 Gbq).

Pre-heat treatments and thermal annealings were accomplished in an electronically controlled oven maintained to within ±0.5°C. Bulk amounts of target materials were pre-heated (heating prior to neutron irradiation), $KMnO_4$ at 423 K, $Ba(MnO_4)_2$ at

†Part IV. S P Mishra & (Miss) Jyoti Singh, *J Radioanal Nucl Chem Lett*, 105 (1986) 363.

403 K and NH_4MnO_4 at 333 K for 2 hr, slowly cooled down to room temperature in a desiccator and are referred to as 'pre-heated samples'. The pre-heat treatment temperatures were chosen well below the decomposition temperatures of the corresponding targets. For post-recoil thermal annealings, the irradiated targets were heated at various desired temperatures for different periods of time before chemical fractionations. The irradiated materials were dissolved in 10.0 ml of doubly distilled water. Chemical analysis of lower valent and parent form was made by the fractional precipitation procedure[18] and the radioactivities of the fractions were counted with the help of an end-window G.M. counter having a constant geometry. The half-life of $^{56}Mn_I$ in the activated permanganate was found to be 154 ± 2 min and no other radioactive species was detected in time-decay analysis and thus the presence of any other isotopic impurity was ruled out. The retention values reported are an average of at least three independent experiments.

The computations of various data were performed using the ICL 1904 computer facility at the B.H.U.

Results and Discussion

The initial retention values for the untreated and pre-heated samples of $KMnO_4$, $Ba(MnO_4)_2$ and NH_4MnO_4 are found to be 12(15), 8(11) and 4(7%) respectively (values in the parentheses are for pre-heated permanganates). It is known that the behaviour of recoil atoms of the same element in a crystal by different nuclear processes is often not exactly the same. Shiokawa and Sasaki[11] explained this difference in alkali metal permanganates due to ^{55}Mn (n, γ) ^{56}Mn and ^{55}Mn $(n, 2n)$ ^{54}Mn reactions. The initial kinetic energy of ^{54}Mn recoils produced by the (n, 2n) reactions is about 1000 times that of ^{56}Mn recoils produced by the (n, γ) reaction., The present data of initial retention shows the trend $KMnO_4 > Ba(MnO_4)_2 > NH_4MnO_4$ for both untreated and pre-heated targets. This is interpreted in terms of the electrostatic character of counter cation. The order of ionisation potential of $Ba > K$ may be responsible for a lower retention value for $Ba(MnO_4)_2$ than $KMnO_4$. Lower affinity of K for electrons results in an increased electron density over the permanganate ion. Consequently, stability of the positively charged metastable species produced by the (n, γ) reactions is facilitated. Due to higher stability, the probability of recombination increases so that higher initial retention is observed in case of potassium permanganate. Few workers[19] explained the increasing behaviour of initial retention in alkali metal permanganates ($LiMnO_4$-$CsMnO_4$) on the basis of ionisation potential of the co-ion and recoil energy. An unusual ammonium ion effect is seen for ammonium permanganate where the initial retention is lower than the values obtained for potassium and barium permanganates. A hot atom reaction in which the recoil fragment strikes and reacts with an ammonium ion is possible, whereby NH_4^+ ions undergo cleavage to produce NH_3 and H^+. NH_3 molecules may get coordinated with recoil species forming a complex and thereby decreasing the possibility of its reformation to acquire the parent form. Harbottle and Sutin[1] explained the lower retention values of ammonium salts than alkali metal salts due to the reduction of recoil fragments by ammonium ion. It is perhaps also explicable by the decomposition of the polyatomic cation followed by diffusion of hydrogen atoms from their original site, so that reformation of the original molecule would then most likely be impossible. Such anomalous retentions have been observed earlier[20] also in case of solid systems of other oxyanions.

A slight increase in initial retention is obtained for pre-heated than untreated permanganates. This trend is also observed for other oxyanions[21,22]. Campbell and Jones[22] reported 20.9% retention after pre-heating $NaBrO_3$ at 245°C for 2 hr as against a value of only 17% for the untreated sample. Some iodates viz., $Cu(IO_3)_2$, $Ca(IO_3)_2$ and I_2O_5 showed a similar trend[23]. Although, the character of defects are not known perfectly, in ionic crystals, electrons and holes are generally considered as inherent defects incorporated into the lattice during crystal preparation. These centres combine or get trapped at defect sites[10] and recoil reaction proceeds through one of the several possible mechanisms, which may involve electronic oxidation or reduction of the recoil fragment, exchange reactions or fragment recombination. By interaction with reducing inherent crystal defects, a small fraction of ^{56}Mn recoils are stabilized in reduced froms in untreated permanganates.

$^{56}Mn^{z+}$	+	e^-	→	$^{56}Mn^{(z-1)+}$
recoil atom		inherent defect		stabilized reduced form

The number of oxidized recoil atoms are increased due to decrease in the concentration of the reducing defects on pre-heating and hence an increase in initial retention is observed in pre-heated targets.

The post-recoil isothermal annealing retentions corresponding to various temperatures and time of annealing for both untreated and pre-heated permanganates are presented in Figs 1-3. It is evident that radiopermanganate fraction increases with the temperature and time of annealing at the cost of lower valent species. Thermal annealing isotherms

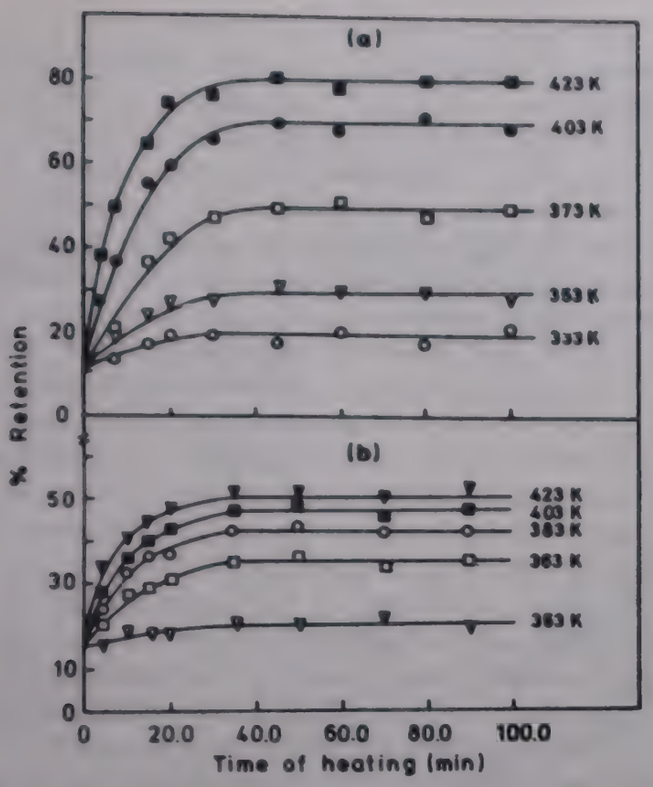

Fig. 1—Isothermal annealing curves for ^{56}Mn recoil in potassium permanganate irradiated by thermal neutrons at room temperature (303 K), (a) untreated (b) pre-heated.

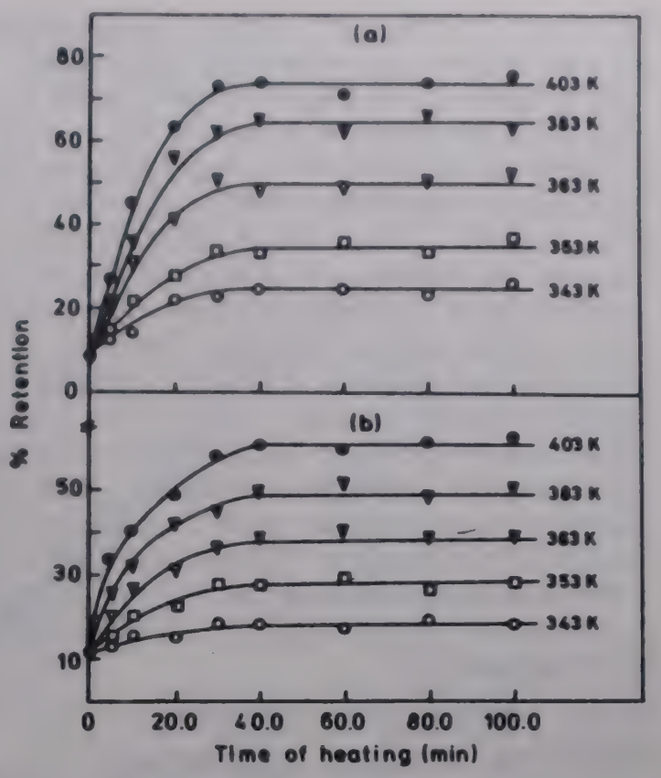

Fig. 2—Isothermal annealing curves for ^{56}Mn recoil in barium permanganate target irradiated by thermal neutrons at room temperature (303 K), (a) untreated (b) pre-heated.

of untreated and pre-heated potassium, barium and ammonium permanganates follow the classical annealing pattern (Figs 1-3); a rather fast rise of retention as a function of heating time and levelling off into temperature-dependent pseudo-plateau. The higher the temperature of anneal, higher is the plateau value. A fairly high retention obtained at higher temperature for both untreated/pre-heated permanganates is accounted by the greater abundance of thermally activated solid state chemical reactions and is supported by earlier works[11,16,24]. A limiting saturation is obtained within ~35 min (80% max.) for $KMnO_4$ and ~40 min (74% max) for $Ba(MnO_4)_2$ (Figs 1 and 2). Shiokawa and Sasaki[11] reported maximum pseudo-plateau of 50% at 180°C for the parent permanganate fragment during thermal annealing of potassium permanganate irradiated by reactor. However, heating of $KMnO_4$ to 180°C increased the retention up to 89% was observed by Teeling *et al.*[14]. As thermal decomposition is triggered by the presence of lattice defects, it is furthermore evident that the recoil site itself will act as a nucleation centre and this may lead to a dramatic change in the fate of the recoil atom itself. In case of NH_4MnO_4, a maximum retention value is observed at 333 and 343 K and saturation is obtained within 20 min (Fig. 3). For this anomaly, the epithermal reduction of recoil fragments through participation of free radicals produced due to radiolytic ef-

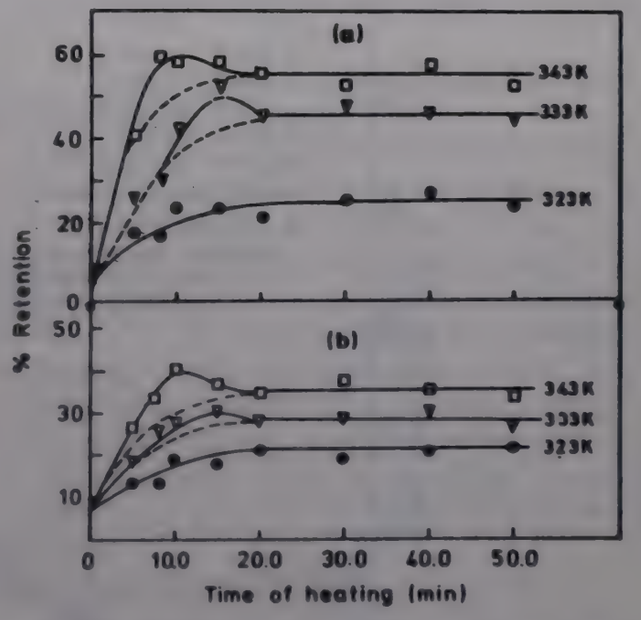

Fig. 3—Isothermal annealing curves for ^{56}Mn recoil in ammonium permanganate irradiated by thermal neutrons at room temperature (303 K), (a) untreated (b) pre-heated.

fects and radiation chemical products of the ammonium group seem to be responsible. Various experimental evidences have been obtained which indicate that the ammonium group in a compound can influence the course of thermal[25] and radiation annealing. In many ammonium salts still more complex isotherms, displaying both maxima and minima in the

retention, are obtained[26] without accompanying gross thermal decomposition of the target material.

Pre-heating of permanganates results in the lowering of the plateau values (Figs 1-3) which is supported by an earlier work[12]. It has been proposed that if sample is heated and cooled again before irradiation, additional lattice defects will be introduced. However, the number will depend on the way by which the target is cooled. An abrupt cooling might result in larger number of defects than when samples are cooled gradually. It is worth recalling that thermal annealing reactions of (n, γ) recoil fragments involve both direct fragment recombination and redox defect controlled processes. In intrinsic annealing of permanganates the recombination proceeds purely by means of thermal activation, while in defect promoted annealing the $^*MnO_2^-$ acts as a recombination centre for electrons and represented by the mechanism:

$$MnO_4^- \rightarrow {}^*MnO_2^- + O_2 \quad \text{recoil step}$$

$$^*MnO_2^- + O_2 \rightarrow {}^*MnO_4^- \quad \text{annealing step}$$

The oxygen remains associated with the particular recoil site[27].

The model of Fletcher and Brown[15] for the recovery of isolated defect pairs has found successful application in the annealing of various systems[1,9,21,23,28]. It is also applied to isothermal annealing (Figs 1-3) of untreated and pre-heated potassium, barium and ammonium permangantes which has been missing in the available literature. The annealing occurs in three stages corresponding to the three different mechanisms of annihilation, viz., close pair, liberation and second order diffusion controlled reactions. Those vacancy interstitial pairs formed with a small separation that the vacancy is still within the strain field of the associated interstitial are supposed to recombine by first order process. For these vacancies a single diffusive movement is most likely to move it closer to the interstitial, where the energy of activation for the next movement will be appreciably lower, so that only the first step is rate controlling. The annealing processes which are governed by a single activation energy in all the three stages can be expressed by the relation $t' = t\nu_0 \exp(-E/kT)$ and the rate law is expressed by, $\phi = f(t/\tau)$, where t is the annealing time, τ is the average jump time of the vacancy in the lat-

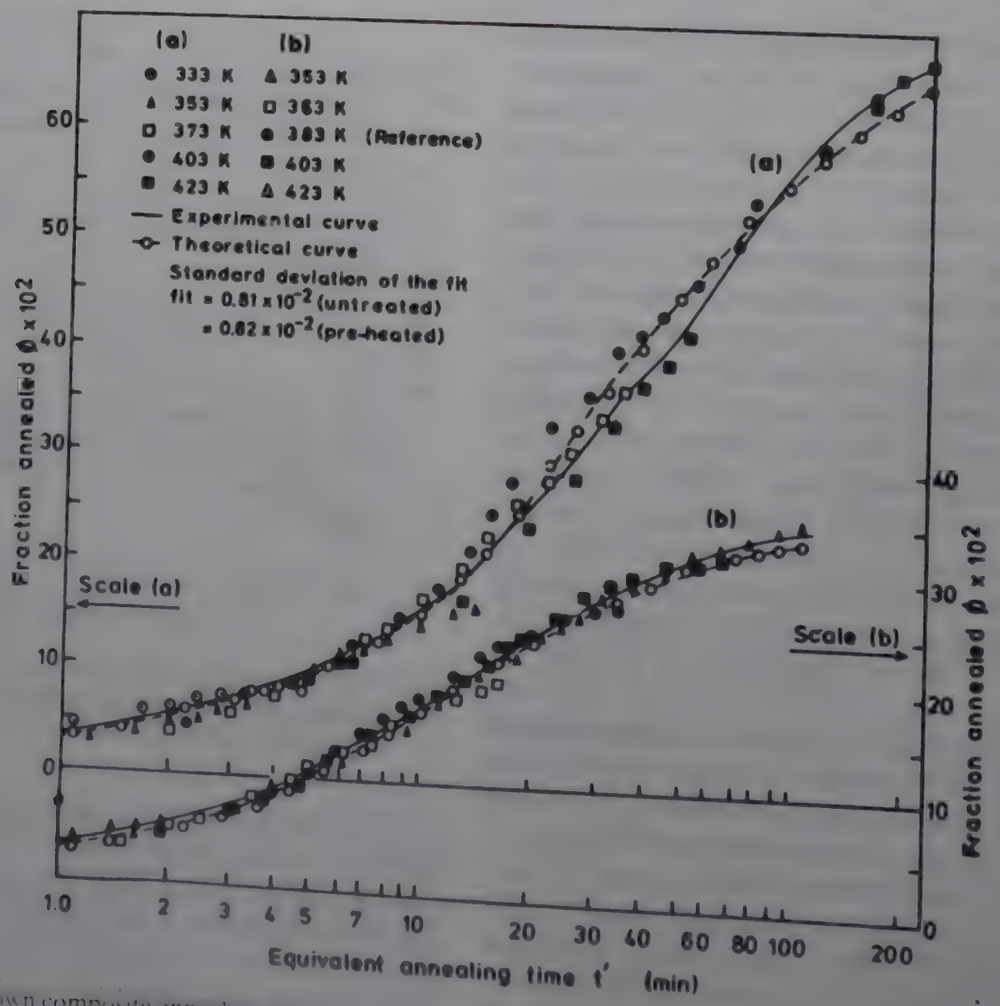

Fig. 4 - Fletcher-Brown composite annealing curve for various recoil fragments in $KMnO_4$ after (n, γ) process. (a) untreated (b) pre-heated.

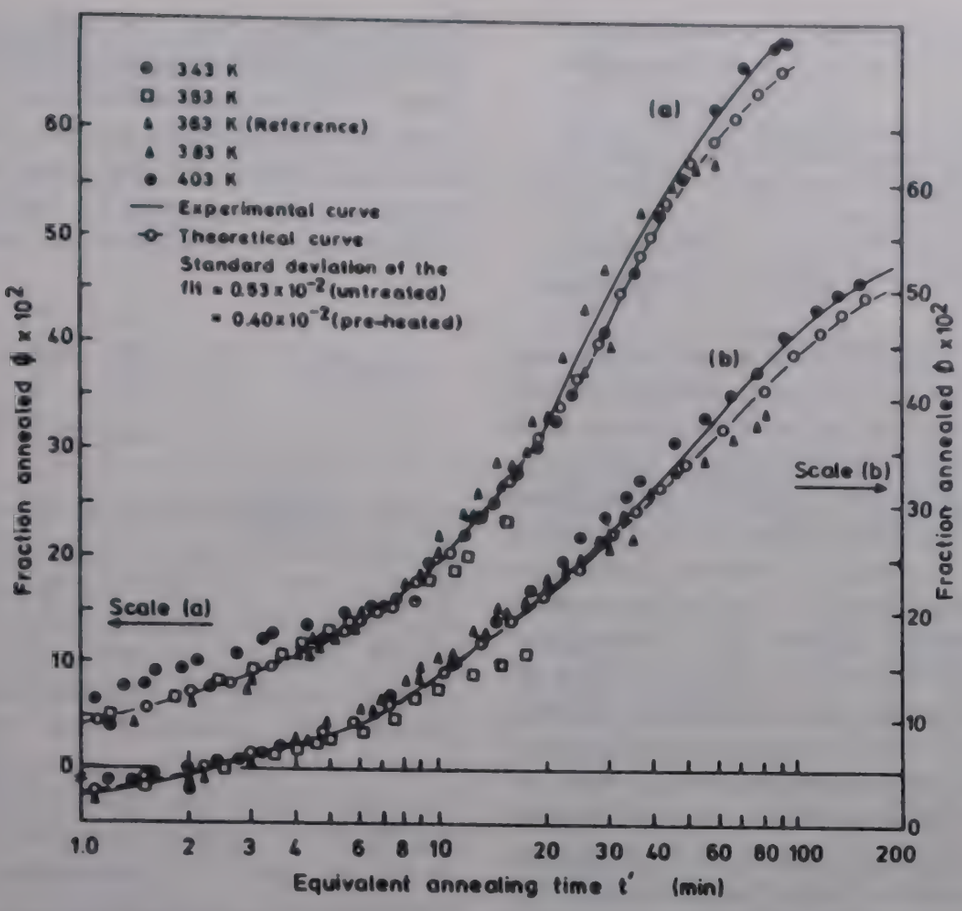

Fig. 5—Fletcher-Brown composite annealing curve for various recoil fragments in $Ba(MnO_4)_2$ after (n, γ) process, (a) untreated (b) pre-heated.

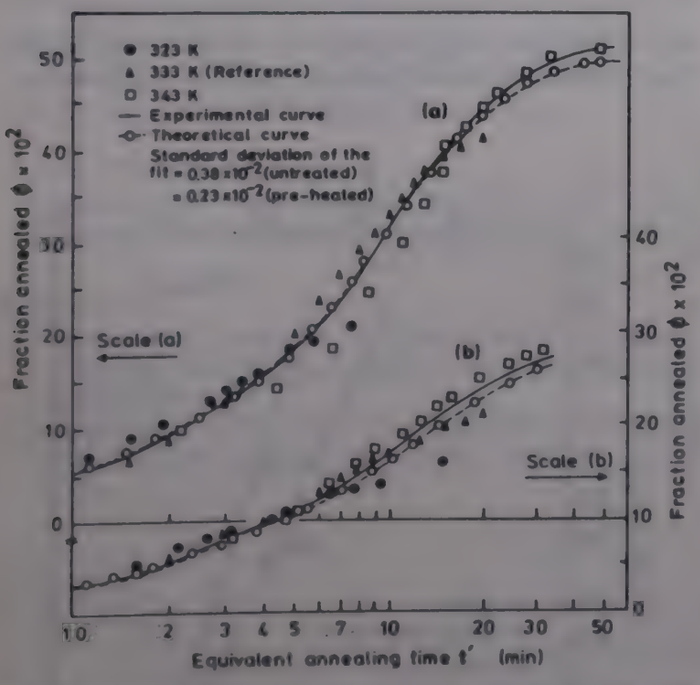

Fig. 6—Fletcher-Brown composite annealing curve for various recoil fragments in NH_4MnO_4 after (n, γ) process, (a) untreated (b) pre-heated.

tice, ν_0 is the frequency factor, E refers to the energy of activation for motion, k is the Boltzmann constant, T is the absolute temperature and $\phi = \frac{(R_t - R_0)}{(R_\infty - R_0)}$ represents fraction annealed at time t. [R_0, R_t and R_∞ are the retention values at time 0, t and saturation respectively.

In the present investigation, the reference temperatures 373K for $KMnO_4$, 363K for $Ba(MnO_4)_2$ and 333 K for NH_4MnO_4 were chosen. The ratio of the time scale of reference temperature to that of any other temperature corresponding to a particular value of ϕ, gave the time adjustment factor for different heating times at that temperature which, in fact, is the necessary condition of this model. It varies for different isotherms of both untreated and pre-heated permanganates. Thus, t', equivalent annealing time for all the points in the isotherm has been calculated as

$$t' = t \cdot \frac{\tau(\text{reference temperature})}{\tau(\text{annealing temperature})}$$

The plot of annealing data ϕ versus the equivalent time (at reference temperature 373 K for $KMnO_4$, 363 K for $Ba(MnO_4)_2$ and 333 K for NH_4MnO_4) are shown in Figs 4-6. It is evident that data are adequately superimposed and fit the equation proposed by the model for permanganates. The annealing isotherms are composed of both fast and slow first order processes[1]. The well fitted continuous curves (Figs 4-6) are represented by following equations for both untreated and pre-heated potassium, barium and ammonium permanganates.

$KMnO_4$ $\phi = 0.81(1-e^{-t/203}) + 0.10(1-e^{-t/10})$] untreated
$= [0.70(1-e^{-t/502}) + 0.21(1-e^{-t/28})]$ pre-heated

$Ba(MnO_4)_2$ $\phi = 0.73(1-e^{-t/506}) + 0.23(1-e^{-t/8})$ untreated
$= [0.61(1-e^{-t/401}) + 0.31(1-e^{-t/19})]$ pre-heated

NH_4MnO_4 $\phi = 0.59(1-e^{-t/203}) + 0.34(1-e^{-t/7})$ untreated
$= [0.49(1-e^{-t/188}) + 0.41(1-e^{-t/10})]$ pre-heated

Thus 81(70), 73(61), 59(49)% of the recoil fragments are annealed by slow first order process and 10(21), 23(31), 34(41) % by fast first order process in untreated and pre-heated $KMnO_4$, $Ba(MnO_4)_2$ and NH_4MnO_4 respectively [values in the parentheses are for pre-heated permanganates]. The slow first order contribution is low in pre-heated permanganates, than untreated samples which also supports the low retention and a lower rate of subsequent thermal annealing in pre-heated samples. First order process reflects that the alteration or removal of the defects may be occurring within single spur of track rather than by interaction between different tracks. A good agreement between the experimental and theoretical curves is seen at lower temperatures with smaller deviations at higher temperatures (Figs 4-6) indicating that at higher temperatures some of the annealing processes are presumably governed by some different (rather additional) mechanisms other than the simple first order recombination.

The logarithm of the relative jump time $(\tau_{(ref)}/\tau_{(T)})$ is found to be linearly dependent on 1/T for all the permanganates (Figs 7-9). The activation energies obtained by least square fit method are presented in Table 1. The same gradation in activation energy is found in both untreated and pre-heated permanganates. It is obvious that the energy of activation for recombination is greater for ammonium permanganate than for potassium or barium permanga-

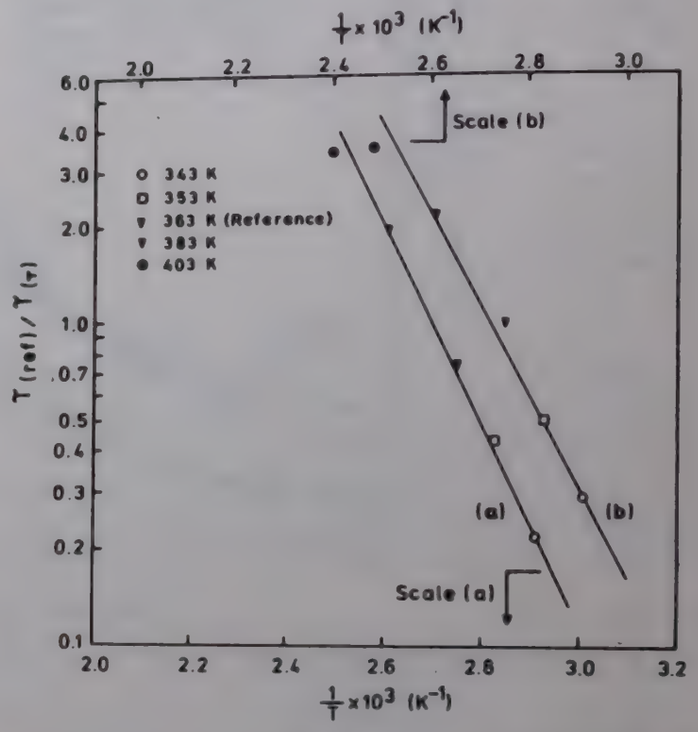

Fig. 8—Variation of relative jump time with the inverse of absolute temperature of thermal annealing in $Ba(MnO_4)_2$, (a) untreated (b) pre-heated.

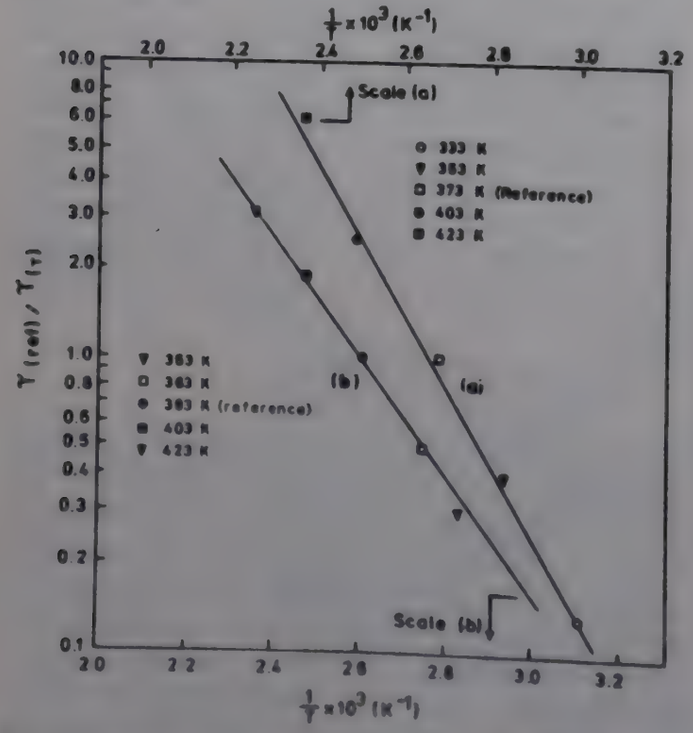

Fig. 7—Variation of relative jump time with the inverse of absolute temperature of thermal annealing in $KMnO_4$, (a) untreated (b) pre-heated.

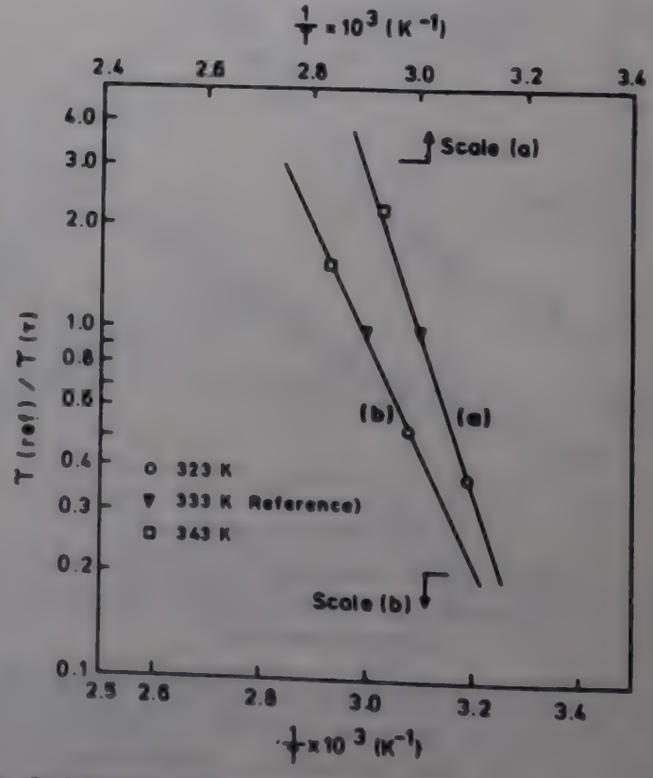

Fig. 9—Variation of relative jump time with the inverse of absolute temperature of thermal annealing in NH_4MnO_4, (a) untreated, (b) pre-heated.

Table 1—Treatment of data on neutron irradiated permanganates† on the basis of Fletcher-Brown model

Compound	Activation Energy	
	kJ mol^{-1}	eV
$KMnO_4$	48 ± 2	0.50 ± 0.03
	(39 ± 6)	(0.41 ± 0.04)
$Ba(MnO_4)_2$	59 ± 3	0.61 ± 0.06
	(54 ± 4)	(0.56 ± 0.03)
NH_4MnO_4	88 ± 5	0.91 ± 0.05
	(63 ± 3)	(0.65 ± 0.02)

†Values for pre-heated permanganates are shown in brackets.

nates. This also supports the low retained fraction in NH_4MnO_4. As annealing proceeds, the concentration of defects is reduced at the same time as the radioactive atoms or fragments recombine, so that the energy of activation rises in untreated sample. However, reintroduction of defects by pre-heating, crushing and irradiating with ionizing radiation will then reduce the energy of activation. The low activation energy suggests that the recoil energy stored in the form of disorder in crystals may be available in overcoming the barrier for recombinations.Same order of magnitude are also reported for other oxyanions[21,23]. It is certain that radiation and thermal annealing processes are defect promoted through electronic and thermal steps and are responsible for the low annealing propensity observed in case of pre-heated permanganates.

Acknowledgement

One of us (JS) is thankful to the CSIR, New Delhi for the award of Research Associateship.

References

1 Harbottle G & Sutin N, *The Szilard-Chalmers reaction in solids. Adv Inorg Chem Radiochem*, (Academic Press, New York) 1 (1959) 267.
2 Maddock A G, *MTP international review of sciences*, Series Two, *Inorganic Chemistry*, (Butterworths, London) 8 (1975) 273.
3 *Chemical effects of nuclear transformations in inorganic systems*, edited by G Harbottle & A G Maddock (North-Holland, Amsterdam) (1979).
4 *Modern hot atom chemistry and its applications*, edited by T Tominaga & E Tachikawa (Springer Verlag, Berlin) (1981).
5 *Hot atom chemistry. Studies in physical and theoretical chemistry*, edited by T Matsuura (Elsevier, Kodansha, Tokyo) 31 (1984).
6 Venkateswarlu K S & Kishore K, *Radiochim Acta*, 15 (1971) 70.
7 Maddock A G & Vargas J I, *Nature*, 184 (1959) 1931.
8 Maddock A G, Treloar F E & Vargas J I, *Trans Faraday Soc*, 59 (1963) 924.
9 Mohanti S R & Pandey V M, *J scient ind Res*, 34 (1975) 196.
10 Andersen T, *Experimental investigation of chemical effects associated with nuclear transformations in some inorganic solids* (University of Aarhus, Denmark) (1968).
11 Shiokawa T & Sasaki T, *Bull chem Soc Japan*, 43 (1970) 801.
12 Van Herk G & Aten A H W *Radiochim Acta*, 17 (1972) 214.
13 Teeling M T A, *Chemical fate of a recoil atom as a function of lattice conditions*, Ph. D. Thesis, Mathematisch Centrum, Amsterdam, (1980).
14 Teeling M T A, Aten A H W & Boersma J, *J inorg nucl Chem*, 42 (1980) 1535.
15 Fletcher R C & Brown W L, *Phys Rev*, 92 (1953) 585.
16 McCallum K J & Maddock A G, *Trans Faraday Soc*, 49 (1953) 1150.
17 Bircumshaw L L & Tayler F M, *J chem Soc Part IV*, (1950) 3674.
18 Mishra S P & Singh J, *J Radioanal Nucl Chem Lett*, 105 (1986) 107.
19 Dedgaonkar V G, Kulkarni S A & Mitra S, *J Radiochem Radioanal Lett*, 51 (1982) 385.
20 Gavrilov V V, Isupov V K & Kirin I S, *Radiokhimiya*, 17 (1975) 130.
21 Mishra S P & Patnaik A, *Int Appl Radiat Isot*, 37 (1986) 955.
22 Campbell I G & Jones G H W, *Radiochim Acta*, 9 (1968) 7; 71.
23 Mishra S P, Patnaik A & Wagley D P, *J chem Soc Faraday Trans.* I, 80 (1984) 47.
24 Apres D J & Harbottle G, *Radiochim Acta*, 1 (1963)188.
25 Getoff N, *Proc Symp Chem Eff Nucl Trans*, Prague, (1964), IAEA, Vienna, II (1965) 279.
26 Getoff N & Nishikawa M, *Nature*, 192 (1961) 61.
27 Harbottle G, *Ann Rev Nucl Sci*, 15 (1965) 89.
28 Brown W L, Fletcher R C & Wright K A, *Phys Rev*, 92 (1953) 591.

Indian Journal of Chemistry
Vol. 31A, September 1992, pp. 658-660

Effect of 3-fluoro-4-cyano substituted benzoates in the formation of induced smectic phases with N-[4-ethoxybenzylidene]-4′-*n*-butylaniline

N K Sharma*, Anila Charak & F Ostereicher†
Liquid Crystal Group, Department of Chemistry, University of Jammu, Jammu 180 004

Received 6 September 1991; accepted 28 February 1992

Diagrams of state of the binary liquid crystalline systems, in which one component is a 4-cyano-3-fluoro substituted benzoates and the other component is N-[4-ethoxybenzylidene]-4′-*n*-butylaniline, have been investigated. The nematic phase shows uninterrupted miscibility in all the binary systems. Induced smectic A phase is observed in all but one diagram of state. The effect of 4-cyano-3-fluoro substitution on induced phases is discussed on the basis of dipole moments.

Isobaric diagrams of state of binary liquid crystalline systems with similar chemical structures of the components constituting the system show, in general, nearly linear phase boundaries. However, binary liquid crystalline systems, in which the components possess different molecular structures, often give unusual diagrams of state. Smectic phases are stabilised in middle concentrations in certain nematogenic mixtures consisting of components with a polar and a non-polar end groups[1]. A model based upon non-polar (N) and polar (P) end groups was provided by Engelen *et al.*[2], in which NP type mixtures were shown to exhibit induced smectic phases, Moreover, mixtures of nematic electron donors and acceptors form induced smectic phases, which exhibit typical charge transfer absorption bands[3]. Furthermore, mixtures consisting of a bilayer (B) and a monolayer (M) liquid crystals also show induced smectic phases[4]. de Jeu *et al.*[5] provided a mathematical explanation for the formation of induced smectic phases.

This paper presents the results of investigations on the mesomorphism in the mixed phases in binary liquid crystalline systems consisting of N-(4-ethoxybenzylidene)-4′-*n*-butylaniline (EBBA) and 3-fluoro-4-cyanobenzoates. The appearance of different modifications and the dependence of transition temperatures on the 3-fluoro-4-cyano end group is discussed.

Materials and Methods

The chemcial names, the structural formulae, the different mesophases and transition temperatures of the liquid crystals used in this paper are as follows:

(a) (4-Cyano-3-fluorophenyl) -4- [4′-*n*-heptyl-cyclohexyl*-benzoate [CFPHCHB]
Cr 84.3 N* 182 Is

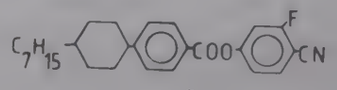

a

(b) (4-Cyano-3-fluorophenyl) - 4 - [4′-(2-methyl-butyl)phenyl]-benzoate [CFPMBPB]
Cr 48 N* 145 Is

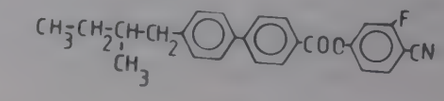

b

(c) (4-Cyano-3-fluorophenyl)-4-[4′-(2-n-pentyl-phenyl]-benzoate [CFPPPB]
Cr 90.5 N* 190 Is

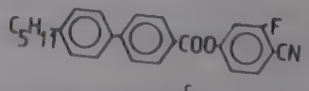

c

(d) (4-Cyano-3-fluorophenyl) -4′-*n*-decylbenzoate [CFPDB]
Cr 55 S_A 57 N* 63 Is

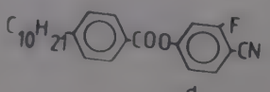

d

(e) (4-Cyano-3-fluorophenyl) - 4 - [4′-(*n*-dodecyloxyphenyl]-benzoate [CFPDOB]
Cr 66.5 (S_A 66) Is

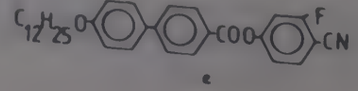

e

† Iwan N. Stranski Institute, Str. des 17. Juni-135, TU Berlin, 1000-Berlin-12, F.R.G.

(f) 4-(4-Cyano-3-fluorophenyl)-phenyl-4-(4'-*n*-heptylphenyl)-benzoate [CFPPHPB]
Cr 85.5 N* 183.5 Is

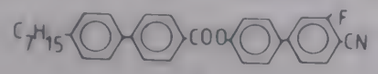

f

(g) N-4-Ethoxybenzylidene-4'-*n*-butylaniline [EBBA]
Cr 35.5 N 80.1 Is

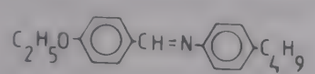

g

The compounds (a)-(f) are benzoates with a 4-cyano-3-fluorophenyl substitution; these were first reported by Kelly and Schad[7]. The synthesis of these compounds for the use of this work was carried out in the laboratories of the Berlin Liquid Crystal Group.

Results and Discussion

All the components used in this study possess nematic or cholesteric phase except CFPDB which possesses additionally smectic A phase and CFPDOB, which shows only monotropic smectic A phase.

The diagrams of state of EBBA, which is a non-polar liquid crystal and a substance with polar 4-cyano-3-fluoro groups attached to the end phenyl ring, were studied. The details of only one representative diagram of state between EBBA and CFPHCHB are given Fig. 1. The nematic* phases of both the liquid crystals were uninterruptedly miscible with each other. The nematic phase also covers the largest area of this system. Neither EBBA nor CFPHCHB possesses smectic A phase, which appears at 64.8°C on the side of EBBA as shown in Fig. 1. Smectic A phase is restricted by the solidification fronts at 52.2°C and 29.0°C. The eutectic is found at 22.5°C.

Similar diagrams of state were observed in the binary liquid crystalline systems EBBA/CFPMBPB, EBBA/CFPPPB, EBBA/CFPDB and EBBA/CFPPHPB. All these systems showed uninterrupted miscibility of nematic* modification and a small area of induced smectic A phase. The highest induction temperatures at which smectic A modification appears on cooling from nematic are listed in Table 1. However, no induced smectic A phase was observed in the system EBBA/CFPDOB.

The difference in clearing points of the two components in these binary liquid crystalline systems

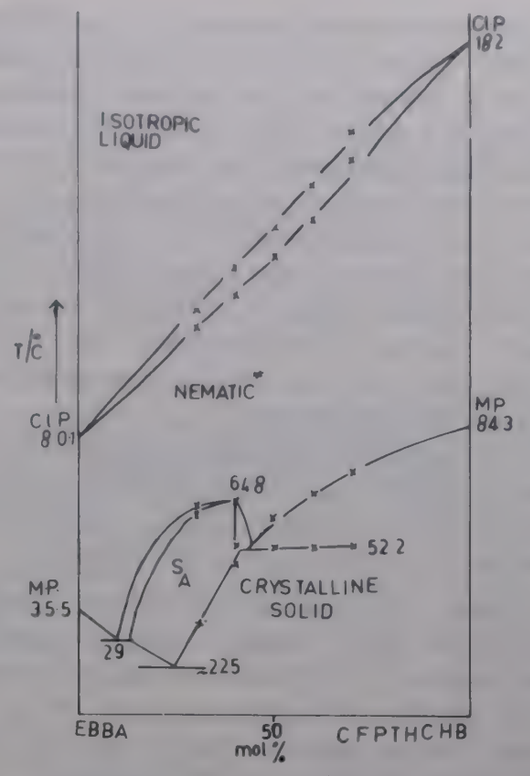

Fig. 1—Binary diagram of state between EBBA and CFPHCHB

Table 1—Highest induction temperature for nematic-smectic A (t_{N/S_A}) phases in different systems

Sl. No.	System	No. of induced phases	Induced modification	Highest induction temp. (t_{N/S_A})°C.
1	EBBA/CFPHCHB	1	Smectic A	64.8
2	EBBA/CFPMBPB	1	Smectic A	78.0
3	EBBA/CFPPPB	1	Smectic A	67.0
4	EBBA/CFPPDB	1	Smectic A	47.0
5	EBBA/CFPDOB	0	—	—
6	EBBA/CFPPHPB	1	Smectic A	163.0

is very large; hence, a smooth nematic*/isotropic heterogeneous region between the two clearing points is observed. On the contrary, a minimum is observed in nematic*/isotropic heterogeneous region in the system EBBA/CFPDB as the difference in the clearing points of the two components is small.

Interestingly, the induced smectic A of the system EBBA/CFPDB is not miscible with the smectic A of the pure component CFPDB. The compounds with cyano end group are said to possess a double layer structure[3] whereas induced smectic A phase is monolayer and the immiscibility may be due to two types of smectic A modifications.

EBBA is non-polar, whereas the compounds with 4-cyano-3-fluoro group should be highly polar. As the polar groups are at adjacent positions, the polarity of 4-cyano-3-fluoro group will be less than that of the compound with only $-CN$ or $-F$ substitution, which is evident from the investigations carried out by Schneider *et al.*[8] on the binary systems with EBBA as one of the components and alkyl or alkyloxy cyano biphenyls as the other component. Much higher enhancement in transition temperatures was observed in systems with cyano biphenyls than that in the systems with cyano fluoro phenyls. As against only induced smectic A in cyano fluoro systems, induced nematic, induced smectic A, induced smectic B and induced smectic E were observed in systems with cyano biphenyls.

Mixtures of non-polar-non-polar (N-N) or polar-polar (P-P) liquid crystals show no enhancement in the transition temperature but a binary system of polar-non polar (P-N) liquid crystals shows induced phases. All the systems investigated fall under the P-N category.

In compounds with cyano fluoro end group, electrons are withdrawn from the aromatic ring rendering it electron deficient. There is an increase in the electron affinity of the aromatic ring with the electron cloud protruding towards cyano fluoro substituents. The ethoxy and butyl substituents of EBBA are electron donating which release electrons to the aromatic ring rendering it electron rich. This results in the decrease in the ionisation potential of π-electrons on the side of ethoxy and σ-electrons on the side of butyl group. Two such moieties interact to form charge transfer complexes. This interaction tends to lead towards the formation and induction of smectic A phase in these systems. The effect of bridging group, $-CH=N-$, could not be ascertained, as also reported earlier[9,10].

References

1 Schneider F & Sharma N K, *Z Naturforsch*, 36a (1981) 1086.
2 Engelen B, Heppke G, Hopf R & Schneider F, *Ann Phys*, 3 (1978) 403.
3 Sharma N K, Pelzl G, Demus D & Weissflog W, *Z phys Chem*, 261 (1980) 579.
4 Griffin A C, Britt T R, Buckley N W, Fisher R W, Havens S J & Goodman D W, *Liquid crystals and ordered fluids*, Vol 3, edited by F Johnson & R S Porter (Plenum Press, New York) 1978.
5 de Jeu W H, Longa L & De mus D, *J chem Phys*, 84 (1986) 11.
6 Richter L, *Dissertation*, Martin Luther University, Halle, 1979.
7 Kelly S M & Schad H, *Helv chim Acta*, 67 (1984) 1580.
8 Schneider F & Sharma N K, *Z Naturforsch*, 36a (1981) 62.
9 Matsunaga Y, Kamiyama N & Nakayasu Y, *Mol Cryst Liq Cryst*, 147 (1987) 85.
10 Sharma N K, Sharma B L & Charak Anila, Indian J Chem 30A (1991) 831.

Indian Journal of Chemistry
Vol. 31A, September 1992, pp. 661-665

Chemical processing of hexagonal Sr-ferrite: Part II—Effect of mode of washing and filtration on the magnetic parameters†

A G Bagul, C E Deshpande, J J Shrotri, S D Kulkarni, Ila Nigam & S K Date*
Physical Chemistry Division, National Chemical Laboratory, Pune 411 008, India

Received 24 September 1991; revised 6 February 1992

Strontium hexaferrite has been prepared by coprecipitation technique. Controlled precipitation and subsequent low temperature processing results in the formation of ultrafine submicron particles. The coprecipitate has been washed using centrifugal filtration and decantation methods. It is then subjected to various calcination temperature ranging from 650 to 925°C and subsequent sintering in the range 1050-1150°C in air. The mode of washing affects the microstructure of strontium ferrite powder at the green stage, which is ultimately reflected in the magnetic properties of sintered ferrite. XRD, DTA/TG/DTG and magnetic hysteresis loop measurements have been carried out to characterize the powders and these results are discussed in the present paper.

To obtain highly uniform ultrafine powders, a variety of ultrastructure processing techniques are being perfected[1-3]. A number of solution techniques are available for the preparation of fine powders such as chemical coprecipitation, sol-precipitation, sol-gel, freeze drying, fast evaporation of solution, etc[4-7]. Amongst these techniques, the simplest is the simultaneous precipitation of various ions from a mixture of solutions. We have earlier reported[8,9] the controlled precipitation at high *p*H values and the subsequent low temperature synthesis of submicron sized strontium ferrite (Sr-ferrite, $SrFe_{12}O_{19}$) powders. During these extensive experiments, it was noticed that the various processing parameters like Fe/Sr ratio, alkali ratio, dilution, rate of precipitation, volume, temperature, *p*H of the wash, time and temperature of calcination govern the green microstructure of of the powders. These processing parameters are interrelated with each other in a complex way which, in turn, decides the performance parameters of the sintered materials/compacts.

The present paper describes (i) the preparative procedures followed under closely monitored conditions, (ii) the effect of a few important processing parameters on the properties of green and sintered compacts of chemically coprecipitated Sr-ferrite. In addition, XRD, DTA/TG/DTG and magnetic characterization results are presented. The experimental procedures are reproducible and can easily be scaled to higher production rates.

†NCL Communication No. 5273

Materials and Methods

Chemical co-precipitation

For chemical coprecipitation, processing parameters such as solution concentrations, temperature of precipitation, rate of addition, stirring speed, method of filtration and washing (centrifuge or decantation), etc., are very critical affecting the shape, size and nature of the coprecipitated particles. To study the effect of these processing parameters on the properties of Sr-ferrite powders, we prepared the sample S_1, S_2, S_3, S_4, S_1' and S_2' as described in Table 1. Coprecipitates S_1' and S_2' were prepared to see the effect of combined treatment of washing operations. Each sample was prepared on 50g scale. Appropriate quantities of LR grade chemicals namely ferric nitrate (1.3*M*), strontium nitrate (0.6 M), sodium hydroxide (2.5 *M*) and sodium carbonate (one-fourth the quantity of NaOH by weight) solutions were taken to give Fe:Sr:NaOH ratio = 10.8:1:68. The ratio was chosen after carrying out a series of ratio optimization experiments reported elsewhere[10] for a given set of experimental conditions which are used for the present work. The mixture of nitrate solutions was added to alkali solution at room temperature. The addition was done drop by drop at the rate of 3-4 ml/min with vigorous mechanical stirring to precipitate the mixed hydroxides of iron and strontium. The *p*H of the precipitated slurry was ≥ 13. The precipitate was washed with distilled water to remove Na^+ and NO_3^- ions either by centrifugal filtration or decantation method which brought down the *p*H of the

supernatant liquid to the values shown in Table 1. The coprecipitate was washed with 16 litres of distilled water divided into ten equal washings.

Calcination, pressing and sintering

The dried coprecipitates of the samples, S_1, S_2, S_3 and S_4 was calcined at different temperatures from 650°C to 925°C in air to see the extent of formation of hexagonal ferrite phase (Table 2). Calcined powder is referred to as "green" material in the text. Green powders were pressed at a pressure of about 2.2 tons/sq. cm after mixing with one per cent solution of polyvinyl alcohol (PVA). The green pellets were sintered at various temperatures ranging from 1050°C to 1150°C for two hours in air.

Physiochemical characterization

The analytical instruments used for characterization at various stages of processing were Netzsch STA 409, Philips PW 1730, Walker Scientific MH-1020, for thermal, XRD and magnetic measurements respectively.

Results and Discussion

Effect of alkali anions

As indicated earlier, samples S_1 and S_2 were precipitated using sodium hydroxide. A priori, one expects the coprecipitate to contain the hydroxides of iron and strontium. However, the XRD pattern of the coprecipitate S_1 shows the appearance of two

Table 1—Processing parameters used during precipitation of the samples S_1 to S_4

Sample number	Precipitating agent	Washing & filtration method	*p*H of the last filtrate	No. of hours for drying
S_1	NaOH	Centrifuge	8-9	16
S_1'	NaOH	Centrifuge followed by decantation (last wash)	—	64
S_2	NaOH	Decantation	10-11	64
S_2'	NaOH	Decantation followed by centrifuge (last wash)	—	16
S_3	NaOH + Na_2CO_3*	Centrifuge	8-9	16
S_4	NaOH + Na_2CO_3*	Decantation	10-11	64

*The amount of Na_2CO_3 used was one-fourth that of NaOH by weight.

Table 2—XRD and thermal analysis data of coprecipitates and calcined samples

Sample number	Coprecipitate		Calcined Sample	
	DTA	X-ray	Calcination temp. (°C)	Percentage ferrite formation Phases detected
S_1	Sharp exothermic peak at 690°C	Amorphous	650/5h	70% Ferrite + Fe_2O_3 + $SrCO_3$
			750/5h	85% Ferrite + Fe_2O_3
			850/5h	95% Ferrite + Fe_2O_3
			925/2h	almost complete ferrite
S_1'	Weak exothermic peak at 690°C	Crystalline (α-Fe_2O_3 + α-$Fe_2O_3.H_2O$ + $SrCO_3$) (Broad line widths	—	—
S_2	Weak exothermic peat at 690°C	Crystalline (α-Fe_2O_3 + α-$Fe_2O_3.H_2O$ + $SrCO_3$) (Broad line widths	650/5h	25% Ferrite + Fe_2O_3 + $SrCO_3$
			750/5h	45% Ferrite + Fe_2O_3 + $SrCO_3$
			925/2h	95% Ferrite + Fe_2O_3
S_2'	Sharp exothermic peak at 690°C	Amorphous	—	—
S_3	Sharp exothermic peak at 700°C	Amorphous	650/5h	65% Ferrite + Fe_2O_3 + $SrCO_3$
			750/5h	90% Ferrite + Fe_2O_3
			850/5h	Complete Ferrite
			925/2h	Complete Ferrite
S_4	No energy change around 700°C	Well crystalline (α-Fe_2O_3 + α-$Fe_2O_3.H_2O$ + $SrCO_3$	650/5h	5% Ferrite + Fe_2O_3 + SrCO3
			750/5h	20% Ferrite + Fe_2O_3 + $SrCO_3$
			850/5h	90% Ferrite + Fe_2O_3
			925/2h	95% Ferrite + Fe_2O_3

principal peaks of $SrCO_3$ at $2\theta = 25.2$ ($I/I_0 = 100$) and $2\theta = 25.9$ ($I/I_0 = 70$), the rest of the pattern showing amorphous nature of the coprecipitate. The coprecipitate S_2 shows crystalline phases, identified as α-Fe_2O_3, hydrated α-Fe_2O_3 and $SrCO_3$ (Table 2). The presence of $SrCO_3$ in these coprecipitates is obviously due to the chemisorption of atmospheric CO_2 on $Sr(OH)_2$ formed. Therefore, after drying the precipitate at 100°C in air, the $SrCO_3$ phase is seen clearly in XRD pattern.

Samples S_3 and S_4 were precipitated using $NaOH + Na_2CO_3$ mixture. The XRD pattern of the sample S_3 is more or less similar to that of S_1. The intensity of the characteristic peaks of $SrCO_3$ in sample S_3 is more than that in S_1. The obvious reason is that the sample S_3 was precipitated using $NaOH + Na_2CO_3$. Coprecipitate of sample S_4 is highly crystalline (narrow line widths) as observed from its XRD pattern. The various phases present are α-Fe_2O_3, hydrated α-Fe_2O_3 and $SrCO_3$ (Table 2). This is as expected, since the alkaline-earth elements preferably react with Na_2CO_3 to form carbonates[11].

Effect of washing and filtration procedure

(*A*) *XRD studies*

The samples washed by centrifugal filtration (S_1, S_3) are X-ray amorphous while those washed by decantation (S_2, S_4) are crystalline. This behaviour can be understood as follows. The decantation mode of washing allows the mother-liquor to remain in contact with the coprecipitate for a few hours; this is necessary for settling down of the coprecipitate. During this period and subsequent drying, crystallisation of F_2O_3 and $SrCO_3$ takes place. The extent of crystallinity depends upon the time required for the coprecipitate to settle since the drying conditions are identical. On the other hand, centrifugal washing removes the mother liquor quickly and completely, preventing the crystallization of hydroxides/carbonates under similar conditions of drying.

The precipitate was calcined at different temperatures ranging between 650°C and 925°C. The extent of the formation of ferrite phase was qualitatively determined from the analysis of the intense peak (114) in the powder XRD patterns of the calcined powders (Fig. 1). It is clearly seen that at a given temperature, the formation of the ferrite phase is relatively more in sample S_1 and S_3 than that in S_2 and S_4. The centrifuge method of washing leads to compaction of the precipitates S_1 and S_3 which enhances the solid-state diffusion at calcination temperature due to the close proximity of the reactants. It is generally accepted that amorphous materials are kinetically and thermodynamically unstable with respect to their crystalline forms[12]. These two factors result in higher percentage of formation of ferrite phase in S_1 and S_3 at 650°C, as compared to that in the case of S_2 and S_4.

(*B*) *Thermal studies*

DTA/DTG/TG plots of the two representative samples S_1 and S_4 are depicted in Fig. 2. DTA curves of all the samples show a broad exotherm between 150° and 500°C and a shallow and broad endotherm in the region 550°-900°C. The endotherm around 310°C and the exotherm around 700°C are superimposed on these broad peaks respectively. The broad exotherm may be the crystallisation of the coprecipitate and the broad endotherm may correspond to the solid-solid (molecular diffusion) reaction of $SrCO_3$ and Fe_2O_3.

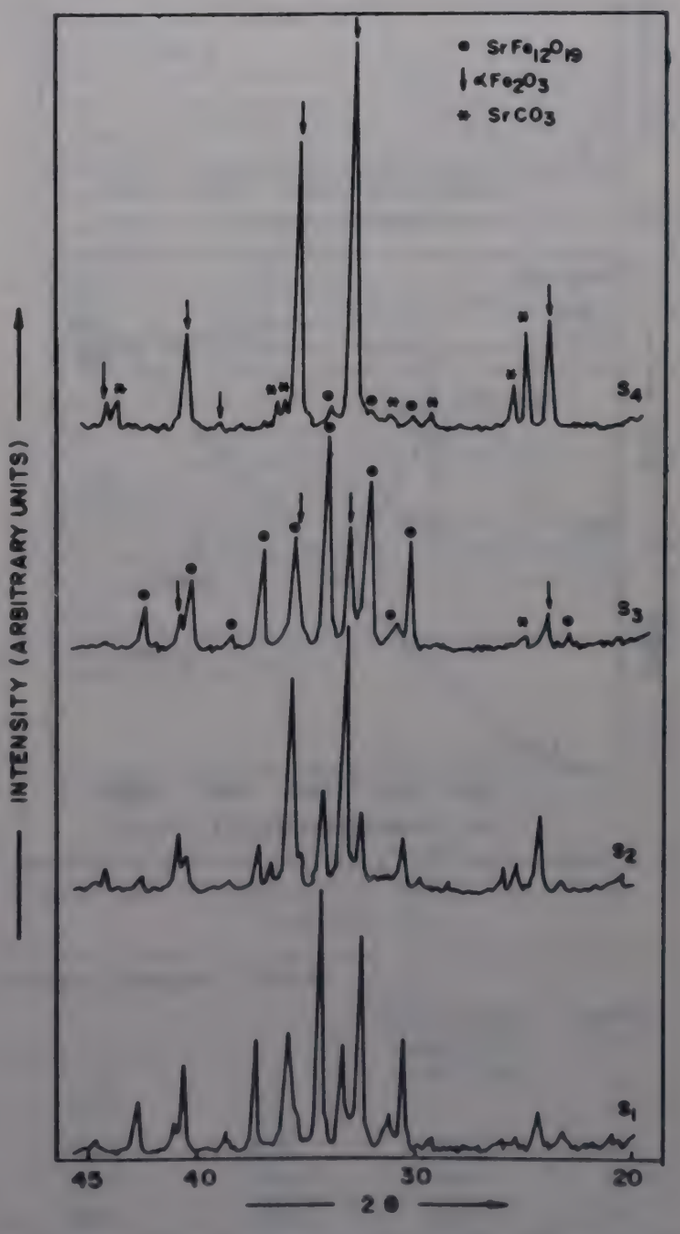

Fig. 1—XRD patterns of samples S_1, S_2, S_3 and S_4 calcined at 650°C/5 h

Adsorbed moisture goes off around 100°C from all the samples. The water of hydration of α-$Fe_2O_3.H_2O$ goes off at about 300°C in case of samples washed by decantation method. The corresponding weight changes are depicted in TG/DTG curves. Thus, above 500°C, the species are anhydrous α-Fe_2O_3 and $SrCO_3$, which are hereafter considered for ferrite formation reaction.

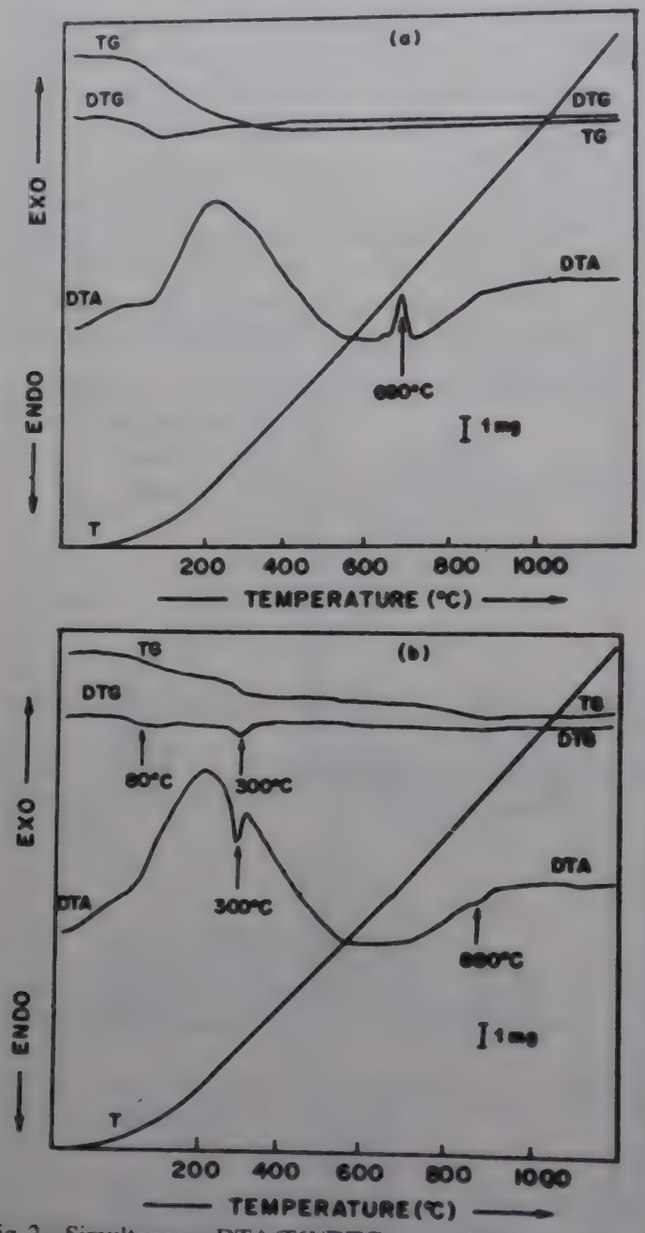

Fig. 2—Simultaneous DTA/TG/DTG scans of (a) sample S_1 and (b) Sample S_4 [weight of sample = 30 mg, heating rate = 10°C/min.]

Samples S_1, S_2 and S_3 show exothermic change around 690-700°C, indicating a chemical reaction of the precipitate forming ferrite phase, as has been discussed in our earlier communication[13] and reported by other researchers also[14,15]. The intensity of the peak is more for compacted samples S_1 and S_3 and less for sample S_2. The corresponding energy change was not detected in the case of sample S_4. These observations are explained on the basis of X-ray data. Samples S_1 and S_3 are X-ray amorphous, sample S_2 shows that crystallization has initiated, while sample S_4 is highly crystalline. Amorphous materials being unstable react faster in comparison to the corresponding crystalline ones. Therefore, the intensity of the peak around 700°C depends on the extent of crystallinity of the reactants.

(C) Magnetic studies

Intrinsic coercivity of ferrites is a function of magnetocrystalline anisotropy and contribution of single domain particles[16,17]. It is given by the equation:

$$ {}_iH_c = An_s \frac{2k}{M_s} $$

where n_s = contribution of single domain particles, A = constant, k = anisotropy constant and M_s = saturation magnetization.

The ${}_iH_c$ values for the green pellets of samples S_1 to S_4 (Table 3) are in concurrence. Though the percentage formation of S_1 and S_3 is comparable (65-70%), the intrinsic coercivity values differ by over 1000 Oe. Even in case of samples S_2 and S_4, the ${}_iH_c$ values are not proportional to their percentage formations.

Another observation is that the ${}_iH_c$ values of samples S_1 and S_3 are comparatively higher than those of S_2 and S_4. The difference is in their washing and filtration procedures resulting in the difference in their particle size and the coercivity values.

For sintered ferrite pellets, the most important property is the maximum energy product $(BH)_{max}$, which is a function of saturation induction, alignment factor and packing density[18]. Sintered pellets of samples S_1 and S_3 show higher B_r due to

Table 3—Magnetic properties of green and sintered samples

Sample No.	Green ${}_iH_c$ (Oe) (Cal. temp. 650°C/5hr.)	Sintered at 1100°C/2h					
		B_r (G)	H_c (Oe)	${}_iH_c$ (Oe)	$(BH)_{max}$ (MGOe)	D (g/cm³)	σ (emu/g)
S_1	4800	2350	1500	2650	1.10	4.21	51.03
S_2	4550	2050	1700	4250	0.9	4.13	50.15
S_3	5900	2450	1750	2750	1.24	4.51	46.75
S_4	4400	1950	1700	4650	0.85	4.06	42.07

better alignment of magnetic domains and higher density which result in higher $(BH)_{max}$ as compared to those for samples S_2 and S_4. Thus, starting from ultrafine coprecipitates, it is possible to control the grain growth during calcination and sintering. It has been possible for us to get $(BH)_{max}$ values in the range 1.35 to 1.42 MGOe, starting from submicron sized calcined powders of 0.2 μm[9].

Effect of the combined mode of washing and filtration

Samples S_1' and S_2' were prepared to see the effect of combined treatment of centrifugation and decantation mode of washing on the nature of coprecipitate. Table 2 describes the thermochemical behaviour and XRD data of samples S_1 and S_2 in comparison with the samples S_1' and S_2'. As the mode of the last washing is changed after the nine washings are over, the microcrystallinity of the coprecipitate changes (reflected in XRD patterns) and consequently the exothermic peak at T = 700°C becomes weak in intensity from samples S_1 to sample S_1'. The same peak becomes conspicuous in going from sample S_2 to S_2'. Thus compaction of the precipitate during washing is one of the factors governing the microcrystallinity of the precipitate which is turn affects the kinetics as well as thermodynamics of the reaction.

Conclusion

Between the two methods of washing and filtration of precipitate, centrifuge method was found to be advantageous resulting in superior performance parameters for Sr-ferrite.

Acknowledgment

We are thankful to Dr. S.D. Pradhan for many useful discussions on thermal studies. Thanks are also due to Mr. M.V. Kuber for XRD measurements and to Dr. V.G. Gunjikar for DTA/DTG/TG measurements. Financial assistance (Grant No. SP/S2/M41/87) from the Department of Science & Technology, Govt. of India is gratefully acknowledged.

References

1 Segal D, *Chemical synthesis of advanced ceramic materials* (Cambridge University Press, Cambridge), 1989.
2 Hench L L, *Ultrastructure processing of ceramics, glasses and composites*, edited by L L Hench & D R Ulrich (John Wiley and Sons, Inc, New York) 1984, pp 3.
3 Aksay I A, Shih W Y & Sarikaya M, *Ultrastructure processing of advanced ceramics*, edited by J D Machenzie & D R Ulrich (John Wiley and Sons, Inc, New York) 1988, pp 393.
4 Lange F F, *J Am ceram Soc*, 72(1) (1989) 3.
5 Roy R, *Science*, 238 (1987) 1664.
6 Haneda K, Miyakawa C & Kojima H, *J Am ceram Soc*, 59 (1974) 354.
7 Lucchini E, Meriani S, Delben F & Paoletti S, *J Mater Sci*, 19 (1984) 121.
8 Kulkarni S, Shrotri J, Deshpande C E & Date S K, *J Mater Sci*, 24 (1989) 3739.
9 Date S K, Deshpande C E, Kulkarni S D & Shrotri J J, in *Advance in ferrites*, edited by C M Shrivastava & M J Patni (Oxford & IBH Publishing Co Pvt Ltd, New Delhi) 1989, pp 55 (Hereafter this paper is referred to as Part-I).
10 Kulkarni S D, *PhD Thesis*, University of Poona, 1990.
11 Vogel I A, *Text book of quantitative inorganic analysis* (Longmans, London) 1961.
12 Angell C A, in *Preparation and characterization of materials*, edited by J M Honig & C N R Rao (Academic Prsss, New York), 1981, pp 449.
13 Kulkarni S D, Deshpande C E, Shrotri J J, Gunjikar V G & Date S K, *Thermochem Acta*, 153 (1989) 47.
14 Roos W, *J Am ceram Soc*, 63 (1980) 601.
15 Tang Z X, Nafis S, Sorensen C M & Hadjipanayis G C, *IEEE Trans MAG*, 25:5 (1989) 4236.
16 R K Tenzer, *J appl Phys*, 34 (1963) 1267.
17 Nomura T, Okutani K & Ochiai T, *Advanced Ceramics*, edited by S Saito (Oxford University Press and Ohmsha Ltd), 1988 pp 266.
18 *NMAB Report on magnetic materials*, 1985, National Research Council USA.

Indian Journal of Chemistry
Vol. 31A, September 1992, pp. 666-672

Synthesis and EPR of oligomeric manganese(II) complexes of a tripodal ligand tris(2-benzimidazolyl methyl)amine and its N-ethyl derivative

H N Pandey & Pavan Mathur*
Department of Chemistry, University of Delhi, Delhi 110 007

Received 22 July 1991; revised 14 October 1991; rerevised and accepted 27 February 1992

Three types of manganese(II) complexes of N,N',N''-tris(2-benzimidazolyl methyl)amine (NTB) and its N-ethyl (Et-NTB) derivatives have been synthesised and characterised. *Type I* complexes analyse for the formula [Mn(NTB) $(ClO_4)_2$]. A magnetic moment of 5.94 B.M./Mn indicates a monomeric manganese complex. EPR data find good correlation with $D = 0.15\ cm^{-1}$ and $\lambda = 0.067$. The Et-NTB analogue shows a broad $g_{eff.} = 2.0$ signal superimposed on which are fifteen hyperfine lines with a coupling constant of :A: = 83 ± 5 gauss. *Type II* complexes analyse for the formula $[Mn_3(L)X_5]$ where L = NTB and Et NTB, while X = Cl^-. These complexes show a strong single EPR line at $g_{eff.} = 2.0$. The complexes have slightly lowered magnetic moment of 5.56 B.M./Mn [$\mu_{eff.}$ trimer = 9.82, L = NTB] and 5.36 B.M./Mn [$\mu_{eff.}$ trimer = 9.26, L = Et NTB] at room temperature. *Type III* complexes analyse for the formula $[Mn(NTB)OAc]_2[OAc]_2$ with a room temperature magnetic moment of 5.99 B.M./Mn. EPR transitions at fields less than 3200 gauss, show a slightly enhanced temperature dependence.

The coordinating ability of the tripodal benzimidazole ligand tris(2-benzimidazolyl methyl)amine (NTB), has been earlier studied with metal ions like Cu(II), Ni(II), Co(II) and Zn(II)[1,2]. However, no Mn(II) complexes have been reported. Reports of manganese complexes with polyfunctional benzimidazole ligands are very few[3,4]; we were prompted to investigate the chemistry of the above ligand as it presents an opportunity for the preparation of discrete manganese aggregates in view of the incomplete coordination presented by the tripodal ligand; moreover, it contains aromatic nitrogen donors, mimetic of histidine imidazoles. Multinuclear manganese sites are of biological importance in the enzymes responsible for photosynthetic water oxidation[5] and the pseudocatalase of *L. plantanum*[6].

Here we report the synthesis, spectral and EPR properties of mononuclear and polynuclear manganese(II) complexes formed with tris(2-benzimidazolyl methyl)amine (NTB) and its N-ethyl derivatives (Et-NTB).

Materials and Methods

All the chemical were of AR grade and used without further purification except for acetonitrile which was dried by distillation over P_2O_5, and Mn(II) acetate that was recrystallised from hot acetic acid.

The free ligand, tris(2-benzimidazolyl methyl)amine was synthesized as described earlier[7]; its ethyl derivative was synthesised by the procedure of Reed *et al.*[8]. These were characterised by ^1H NMR.

NTB (DMSO-d_6) (rel. intensity in ppm): 12.1(s, 8.5), 7.60(m, 17), 7.19(m, 17), 4.12(s, 17).

Et-NTB (rel. intensity in ppm): 7.6-7.3 (asymmetric m, 12), 4.4(s, 6), 3.6(q, 6), 1.0(t, 9).

$[Mn(L)ClO_4]^+ [ClO_4]^-$ (*where L = NTB and Et-NTB*)

The Ligand (1 mmol) was suspended in 15 ml of acetonitrile. A solution of $M(ClO_4)_2$ (1 mmol) in CH_3CN was added to the above when a colourless clear solution was obtained. The solution was stirred for about 1 hr at room temperature and the volume was reduced to a few ml on a rotatory evaporator. To this, a small amount of ether was added to precipitate the crude product. The crude product was recrystallised from ether and acetonitrile mixture (1:10).

Anal.[Calc. for $C_{24}H_{21}N_7Cl_2O_8$ Mn.$2CH_3CN$: C, 45.2; H, 3.6; N, 16.9; Mn, 7.4. Found: C, 45.6; H, 4.0; N, 17.2; Mn, 8.0%].

Anal.[Calc. for $C_{30}H_{33}N_7Cl_2O_8$ Mn.$2CH_3CN$: C, 49.3; H, 4.7; N, 15.2; Mn, 6.6. Found: C, 49.9; H, 4.4; N, 14.7 Mn, 7.1%.

$[Mn(L)Cl]_2^{2+} [MnCl_4]^{2-}$ (*where L = NTB and Et-NTB*)

The ligand (1 mmol) was suspended in 20 ml of methanol and to this a slightly warm solution of $MnCl_2$ in methanol (5 ml) was added. Most of the ligand along with $MnCl_2$ went into solution forming a colourless solution. The solution was stirred for about 1 hr; it was then reduced to approximately 5 ml on a rotatory evaporator and a small amount of ether was added to precipitate the crude product. The col-

our of the product was off white. This crude product was recrystallized from (1:5) MeOH: ether mixture. A white compound crystallised on cooling.

Anal.[Calc. for $C_{48}H_{42}N_{14}Cl_6Mn_3.3H_2O$: C, 46.2; H, 3.8; N, 15.7; Mn 13.2. Found: C, 45.8; H, 4.5; N, 16.2; Mn, 12.8%].

Anal.[Calc. for $C_{60}H_{66}N_{14}Cl_6Mn_3.6H_2O$: C, 48.8; H, 5.3; N, 13.3; Mn, 11.2. Found: C, 48.2; H, 6.0; N, 13.2; Mn, 10.7%].

$[Mn(NTB)OAc]_2^{2+}$ $[OAc]_2^{2-}$

The ligand NTB (0.5 mmol) was suspended in 10 ml of ethanol and 1 ml of sodium acetate-acetic acid (2*M*) buffer solution (*p*H = 5.5). To this (0.5 mmol) of manganese acetate was added. A clear solution was obtained. The solution was stirred for 1 hr at room temperature and the solution was stripped off the solvent to dryness. The crude product so obtained was washed with water, dissolved in a small amount of ethanol and reprecipitated by diethyl ether. It was recrystallised from (1:3) mixture of ethanol: ether.

Anal.[Calcd. for $C_{56}H_{54}N_{14}O_8Mn_2.4H_2O$: C, 54.5; H, 5.0; N, 15.9; Mn, 8.9. Found: C, 55.1; H, 4.7; N, 15.1; Mn, 9.7%].

C, H, N were analysed micro-analytically at our University (USIC) facility. Manganese was estimated spectrophotometrically. It is not unusual for these complexes to crystallise as hydrates or solvates[9].

IR spectra were taken on a Shimadzu IR-435 spectrophotometer, electronic spectra were recorded on a Perkin Elmer-554 UV-visible spectrophotometer. X-band EPR were obtained with a JEOL JES-FE 3XG ESR spectrophotometer with a variable temperature liquid nitrogen cryostat. For EPR work, the Mn(II) complexes were diluted with (1) Analar ZnO[Mn-complexes: ZnO (1:20)] and (2) Zn-NTB complexes [Mn- complex: Zn NTB and Et NTB complex (1:20)]. The Zn-ligand complexes were prepared accordiing to published procedure[7]. ^1H NMR spectra were recorded on 90 MHz Perkin Elmer R-32 NMR spectrometer.

Results and Discussion

EPR spectroscopy

Figure 1 illustrates the X-band EPR spectrum of $[Mn(NTB)ClO_4]^+$ $[ClO_4]^-$. The complex has been examined as a solid diluted with a diamagnetic host [complex: ZnO (1:20)] at 143 K. The spectrum of $[Mn(NTB)ClO_4]^+$ $[ClO_4]^-$ reveals several transitions in the 5000 G scan. An intense transition is centred at $g = 2.0$ while medium to weak transitions are seen at $g \sim 3.6$, $g \sim 4.3$ and $g \sim 6.0$. The EPR and analytical data suggest an axially distorted Mn(II) complex in the above case (structure I). Dowsing and Gibson[10] have plotted the expected EPR transitions for a high spin d^5 ion experiencing various magnitudes of zero field splitting; utilising the various plots we found a good correlation at $\lambda = 0.067$ and $D \sim 0.15\,cm^{-1}$. The data are given in Table 1A. Fig.1(B) shows the EPR spectrum of the $[Mn(NTB)ClO_4]^+$ $[ClO_4]^-$ complex when diluted with analogous Zn-NTB complex. The number of lines observed is similar to that observed in Fig.1(A). Field positions are given in Table 1(A).

The data are given in Table 1A. Fig.1(B) shows the EPR spectrum of the $[Mn(NTB)ClO_4]^+$ $[ClO_4]^-$ complex when diluted with analogous Zn-NTB complex. The number of lines observed is similar to that observed in Fig.1(A). Field positions are given in Table 1(A).

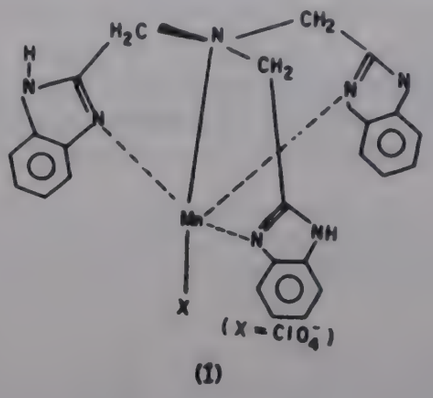

(I)

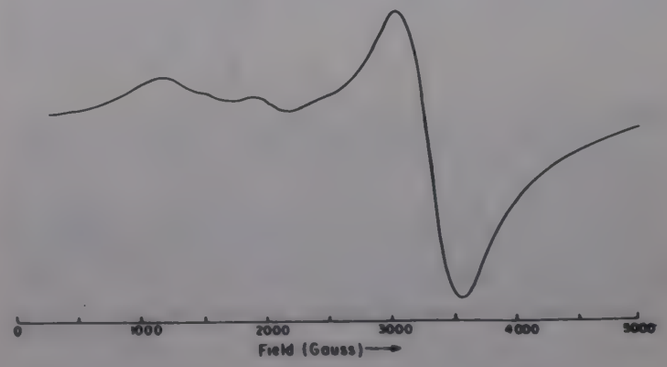

Fig. 1(A)—5000 G scan of $[Mn(NTB)ClO_4]$ $[ClO_4]$ complex, diluted in ZnO, at X-Band [microwave power 10.0 mW; microwave frequency, 9.20 GHz; modulation amplitude 5.0 G; receiver gain, 3.2×10^2. Temp = 143 K]

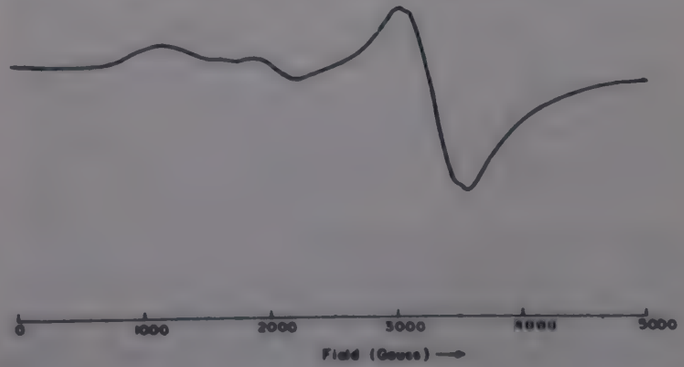

Fig. 1(B)—5000 G scan of $[Mn(NTB)ClO_4]ClO_4$ diluted with Zn-NTB complex [receiver gain, 1.0×10^2]

Figs.(2A) and (2B) illustrate the X-band EPR spectrum of $[Mn(NTB)Cl]_2^{2+}$ $[MnCl_4]^{2-}$ and $[Mn(Et\text{-}NTB)Cl]_2^{2+}$ $[MnCl_4]^{2-}$ examined as a solid, diluted in a diamagnetic host [complex: ZnO (1:20) at 142 K]. The spectra show a strong signal in the $g = 2.0$ region with a weak and broad shoulder arising in the region of $g \sim 4.0$. No other signal is observed in the 5,000 G scan spectra, as would have been expected for non-cubic Mn^{II}-complexes with an appreciable zero field splitting. Such a simple one-line spectrum devoid of any hyperfine structure has been interpreted as arising from a Mn(II) complex with a neighbouring atom magnetic interaction[10b]. For such complexes $\Delta m_s = 2$ (forbidden) transition is predicted to become weakly allowed. This transition occurs at about half field and in our case matches closely the weak transition observed around $g \sim 4$ (Table 1B). Moreover, the total width of the central isotropic resonance in the case of the $[Mn(Et\text{-}NTB)Cl]_2^{2+}$ complex is only 350 G at X-band (Fig.2B). Such a narrow isotropic resonance has been interpreted to arise from exchange narrowing phenomenon, where N divalent Mn(II) ions are coupled by an exchange interaction[11]. Fig.2(A)′, 2(B)′, show the EPR spectra of the $[Mn(NTB)Cl]_2^{2+}$ $[MnCl_4]^{2-}$ and $[Mn(Et\text{-}NTB)Cl]_2^{2+}$ $[MnCl_4]^{2-}$ complexes, when diluted with the analogous Zn-NTB and Zn-Et NTB complexes. In both the cases, spectra are similar to those shown in Fig.2(A) and 2(B), except that the line width in 2B′ is found to be 675 gauss.

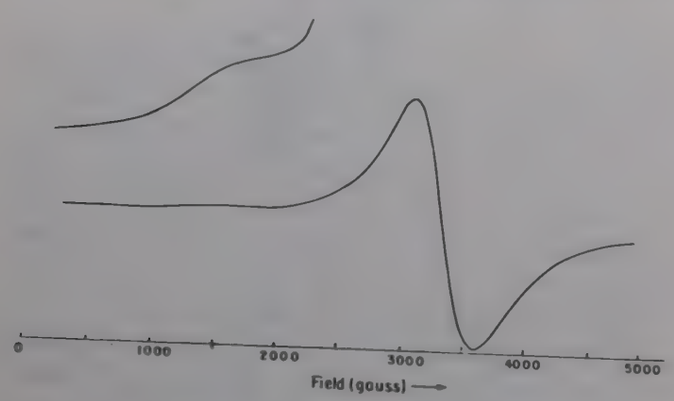

Fig. 2(A)—5000 G scan of $[Mn(NTB)Cl]_2^{2+}$ $[MnCl_4]^{2-}$ complex at X-band [microwave power, 10.0 mW; microwave frequency, 9.20 GHz; modulation amplitude, 5.0 G: receiver gain, 1.0×10^2; Temp = 143 K; inset: blow up of region between 1000 and 2000 G]

Table 1A—Observed and predicted transitions with assignments for $[Mn(NTB)ClO_4][ClO_4]$. $2CH_3CN$ doped in ZnO and in $[Zn(NTB)(ClO_4)_2]$ complex

Obs. position in ZnO	Obs. position in Zn-(NTB) complex	Calculated for $D \sim 0.15\ cm^{-1}$ & $\lambda = 0.067$		
		(x,y)H	Assignments	Z(H)
1150	1150	1050	$-3/2 \leftrightarrow -5/2$	1110 (low probability)
1500 (sh)	1625 sh	—		
1825	1875	1900 1950	$-1/2 \leftrightarrow -3/2$	2000 (low probability)
3000	3050	2800 3150	$+1/2 \leftrightarrow -1/2$	

Table 1B—X-band EPR data (peak position in Gauss) doped in ZnO

Complex	Peak positions
$[Mn(NTB)Cl]_2^{2+}$ $[MnCl_4]^{2-}$	3375($g_{eff.} \sim 1.98$) 1500 ($g_{eff.} \sim 4.0$)
$[Mn(Et\text{-}NTB)Cl]_2^{2+}$ $[MnCl_4]^{2-}$	3250($g_{eff.} \sim 2.0$) 1300($g_{eff.} \sim 5.0$)
$Mn(NTB)OAc]_2^{2+}$ $[OAc]_2^{2-}$	200, 1250, 1950, 3275, 5250
$[Mn(Et\text{-}NTB)ClO_4][ClO_4]$	3280
*$[Mn(tren)(NCO)_2](BPh_4)_2$	750, 1300, 2000, 2300 (sh) 3350, 5000

*Data taken from *Inorg Chem*, 17(2) (1978) 466; Fig. 4, T = 300°C

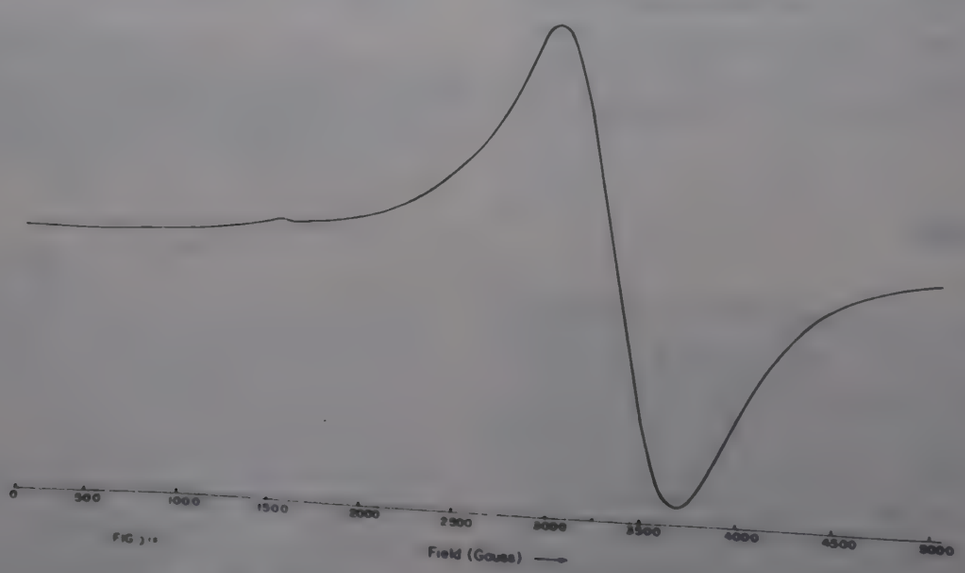

Fig. 2(A)′—Parameters same as in 2(A) except that the complex was diluted with Zn-NTB complex [receiver gain, 3.2×10^2]

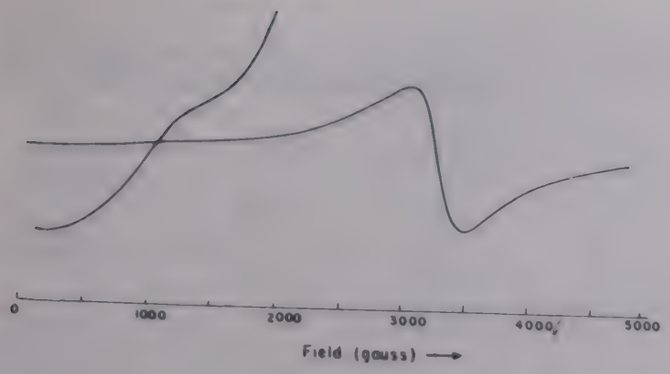

Fig. 2(B)—5000 G scan of $[Mn(Et\text{-}NTB)Cl]_2^{2+}$ $[MnCl_4]^{2-}$ complex at X-band [microwave power, 10.0 mW; microwave frequency, 9.20 GHz; modulation amplitude, 1.0 G; receiver gain, 1.25×10, Temp = 143 K; inset: blow up of region between 1000 and 2000 G: receiver gain, 2×10^2; all other conditions as above]

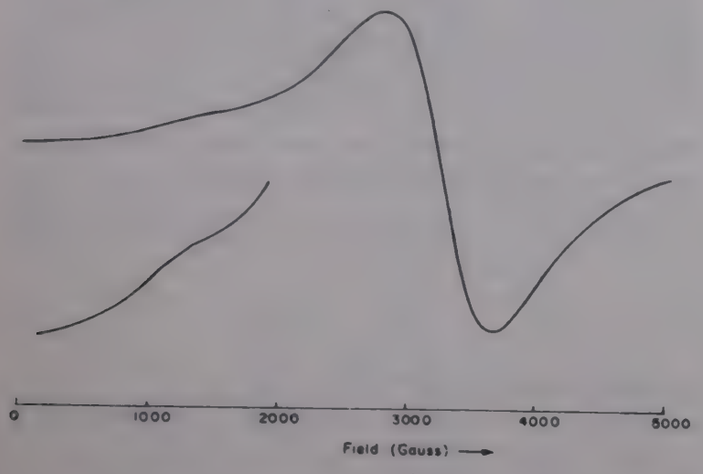

Fig. 2(B)'—Parameters same as in 2(B) except that the complex was diluted with Zn Et-NTB complex [receiver gain, 1.2×10^2]

Fig.3A represents the X-band EPR spectrum of $[Mn(NTB)OAc]_2^{2+}$ $[OAc]_2^{2-}$ studied as a solid, diluted with a diamagnetic host complex: ZnO (1:20); the 10,000 G spectrum shows the presence of five transitions spread over 6,000 G. At this stage, it is important to compare the spectrum of the above complex with that reported for a very similar tetradentate ligand 2, 2', 2''-triaminotriethylamine (tren) which has been reported to form simple monomeric trigonal-bipyramidal complexes with Mn(II) and also a series of outer sphere manganese dimers obtained from the parent trigonal-bipyramidal complex[12]. The EPR spectra of the monomeric trigonal-bipyramidal Mn(II) complexes are characterised by a very strong band at $g \sim 6$ (1100 G) with weak signals at $g \sim 2.0$ while the EPR spectra of the dimeric manganese complexes are characterised by an intense band at $g = 2$ alongwith relatively weak bands at both high and low fields. Moreover, the transitions at fields less than (3200 G) show a marked temperature dependence. The spectrum in Fig.3(A) has features which resemble closely those of

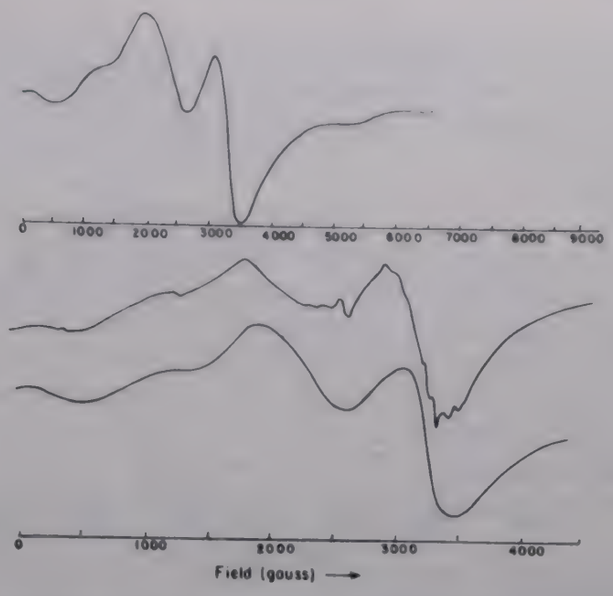

Fig. 3(A)—10,000 G scan of $[Mn(NTB)OAc]_2^{2+}$ complex at X-band [microwave power, 10.0 mW, microwave frequency, 9.2 GHz; modulation amplitude, 1.0 G: receiver gain, 5×10^2, Temp = 143 K]

Fig. 3(B)—5000 G scan of the above complex at X-band. [Upper trace: same conditions as in 3(A) except that Temp = 243 K & receiver gain 1×10^3. Lower trace: same conditions as in 3(B) except that Temp = 173 K & receiver gain = 5×10^2]

the dimeric Mn(II)—tren complexes rather than those of monomeric Mn(II)—tren complexes (data given in Table 1B).

A variable temperature study of the above complex is shown in the inset in Fig.3(B). The areas of the peaks at 1250 G, 1950 G have been evaluated using the formula given below:

$$\text{Area} = \frac{\text{Peak height} \times \text{half width}}{\text{Receiver gain}}$$

The data reported in Table (1C) show that the areas of the two peaks increase by 2 to 2.5 times as we go from 243 K to 143 K. The observation is again similar to that reported for Mn(II)—tren complex[12]. Fig.3(C) represents the EPR spectrum of $[Mn(NTB)OAc]_2^{2+}$ $[OAc]_2^{2-}$ complex diluted with the analogus Zn-NTB complex. The number of lines remains the same. However, there is a slight change in field positions (Table 1D).

Fig.4A shows the 5000 Gauss EPR spectrum of $[Mn(Et\text{-}NTB)ClO_4]$ $[ClO_4]$ also examined as a solid diluted in a diamagnetic host ZnO [complex: ZnO is 1:20]. The central part of the spectrum is blown up in Fig.4B; A 2000 G scan centered at 3000 G of the above complex shows a broad central transition at $g = 2$

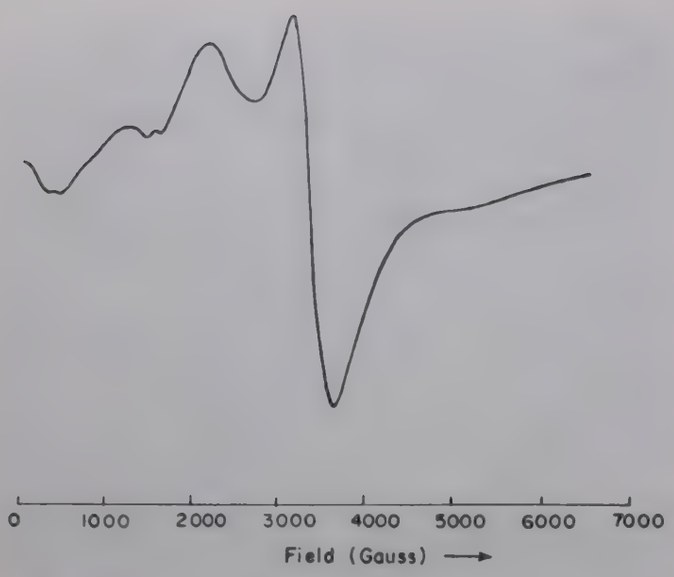

Fig. 3(C)—Parameters same as in 3(A), except that complex was diluted with Zn-NTB complex and receiver gain, 3.2 × 10^2

with a hyperfine structure of 15 lines superimposed on it (Fig.4B). The coupling constant is nominally 83 ± 5 G. A reasonable explanation of the above spectrum could be found in an exchange coupled tri-nuclear manganese complex; sixteen lines are theoretically expected if three Mn(II) are equivalently coupled to each other.

Ideally, it is possible to determine the nuclearity of super-exchanged coupled clusters of paramagnetic Mn(II) ions from the ^{55}Mn hyperfine pattern and its coupling constant[13]. For strongly coupled systems ($J > D$), the number of hyperfine lines increases while the coupling constant decreases. In contrast, when $J \sim D \sim h\nu$ the coupling constant does not decrease as the cluster size increases. This situation has been reported with a Mn(II) cluster with 2,6-diacetylpyridine dioxime[14]. The compound $[Mn(Et\text{-}NTB)ClO_4]^+ [ClO_4]^-$ may well fall in the above class as illustrated by its EPR. We are, therefore, prompted to propose the above complex as a minimum cluster of three Mn(II) ions coupled together via very weak exchange interaction, although in the absence of a crystal structure and variable temperature susceptibility data the above proposal is tentative. Fig.4C shows a 5000 gauss scan of $[Mn(Et\text{-}NTB)ClO_4]^+ [ClO_4]^-$ complex at X-band when diluted with the analogous Zn-Et NTB complex; the hyperfine structure on the $g \sim 2.0$ signal is similar to that in Fig.4B.

Magnetic susceptibility

The magnetic susceptibilities of manganese complexes were determined using a CAHN 2000 balance at 291 K in the solid state. The diamagnetic correction for each complex was estimated using Pascal's constants and was incorporated in experimental susceptibility. The magnetic moment data are given in Table 2.

Table 1C—Relative areas of peaks and their temperature dependence for $[Mn(NTB)OAc]_2^{2+} [OAc]_2^{2-}$ complex

Temp. (K)	R.A. (1250 G)	R.A. (1950 G)	R.A. (3250 G)
243	150	460	144
173	240	816	176
143	308	1120	224

R.A. = Relative area of the peak

Table 1D—X-band EPR data (peak positions in Gauss) doped in Zn(L) complexes, L = NTB & Et-NTB

Complex	Peak position
$[Mn(NTB)Cl_2^{2+}] [MnCl_4]^{2-}$	3362($g_{eff.} \sim 1.98$), 1500($g_{eff.} \sim 4.0$)
$[Mn(Et\text{-}NTB)Cl]_2^{2+} [MnCl_4]^{2-}$	3362($g_{eff.} \sim 1.97$), 1525($g_{eff.} \sim 4.0$)
$[Mn(NTB)OAc]_2^{2+} (OAc)_2^{2-}$	150, 1115, 2025, 3362, 5150
$[Mn(Et\text{-}NTB)ClO_4]^+ [ClO_4]^-$	3280, 1500

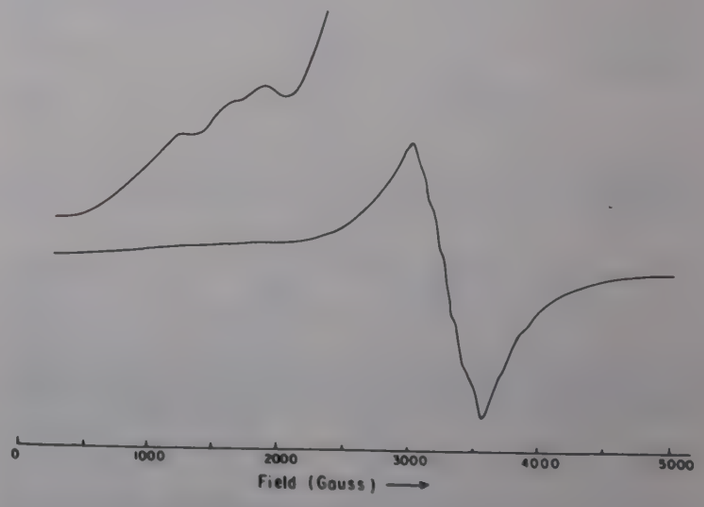

Figs.4(A)—5000 G scan of $[Mn(Et\text{-}NTB)ClO_4] [ClO_4)$ complex at X-band [microwave power, 10.0 mW; microwave frequency, 9.19 GHz; modulation amplitude, 2.5 G; receiver gain, 7.0 × 10, Temp = 223 K. Inset: blow up of region between 1000 and 2000 G; receiver gain, 7.9 × 10^2 all other conditions as above]

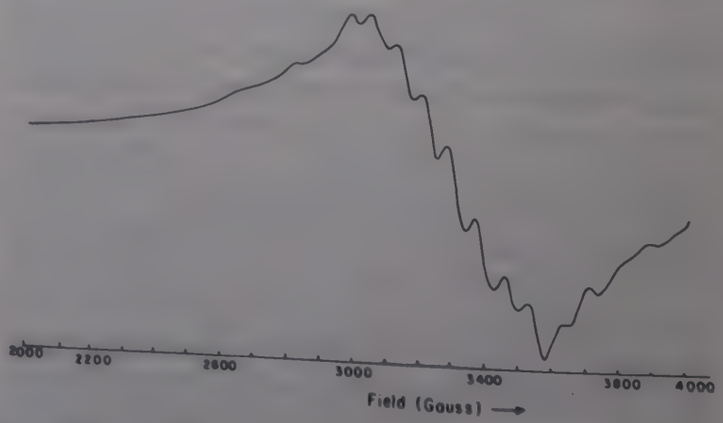

Fig. 4(B) - 2000 G scan of the above complex centred at 3000 G, at X-band [receiver gain, 4.0 × 10^2 Temp = 173 K]

The magnetic susceptibility data in all the cases support the formulation made on the basis of EPR.

The monomeric complex $[Mn(NTB)ClO_4]^+$ $[ClO_4]^-$ shows a magnetic moment of 5.94 B.M. The experimental $\mu_{eff.}$ lies in the range found for other Mn(II) complexes. The magnetic moment of $[Mn(NTB)OAc]_2^{2+}$ $[OAc]_2^{2-}$ is found to be 5.99 B.M./Mn which indicates practically no exchange coupling between the Mn(II) cations, and is quite expected for a outer sphere dimer[12].

The room temperature magnetic moments for the halide bridged $[Mn(L)X]_2^{2+}$ $[MnCl_4]^{2-}$ type complexes are slightly below those found for high spin monomeric Mn(II) complexes. The $\mu_{eff.}$ value is 5.56 B.M./Mn where L = NTB and 5.35 B.M./Mn where L = Et-NTB; this quenching in magnetic moment is expected for an exchange coupled Mn(II) dimeric complex[11]. The $\mu_{eff.}$ of 6.02 B.M./Mn for the $[Mn(Et\text{-}NTB)ClO_4)^+$ $(ClO_4)^-$ complex does not distinguish between a regular monomeric complex and an oligomeric one where exchange coupling is comparable to zero field splitting/microwave energy ($J \sim 0.2$-$0.3\ cm^{-1}$).

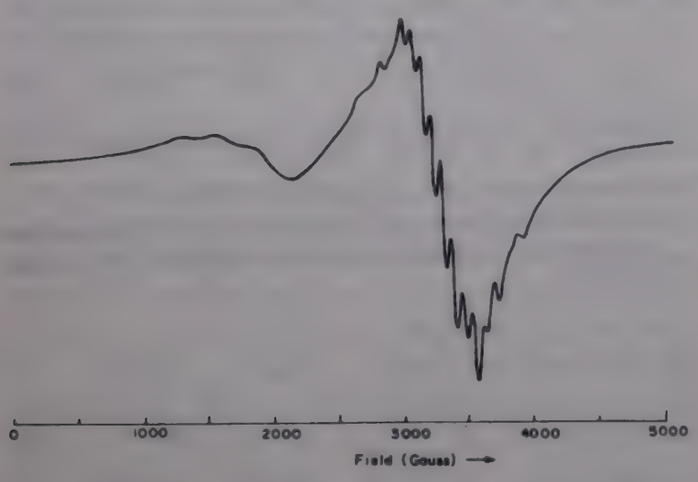

Fig. 4(C)—Parameters same as in 4(A) except that the complex was diluted with Zn-Et (NTB) complex and receiver gain, 2.9×10^2]

Ideally, one needs to compare the susceptibility of the complex at helium temperatures with that predicted by Fischers formula[14]. We expect to present this in a subsequent publication.

Electronic & IR spectroscopy

The ligands and their manganese complexes show characteristic UV spectra of the benzimidazolyl group; their absorption bands and extinction coefficients are reported in Table 3. The UV bands are all blue-shifted upon coordination and, in general, are enhanced in intensity. This includes the band at 245 nm in NTB and at 260 nm in ethyl NTB, which is associated with imidazole ring, showing clear evidence of C=N coordination to manganese centre.

IR spectra were taken in nujol mull. In free ligand, a strong band is found around $1460\ cm^{-1}$ alongwith a weaker band at $1440\ cm^{-1}$. In analogy with the assigned bands for imidazole, the $1440\ cm^{-1}$ band is attributed to ν-C=N-C=C-, while the other one is an overtone/or combination band[15]. The shift in the $1440\ cm^{-1}$ band is around $10\ cm^{-1}$ in the complexes. This implies direct coordination of all four imine nitrogen atoms to Mn(II). This is the preferred nitrogen atom for coordination as found for other metal complexes with benzimidazoles[16]. In the perchlorate complexes a strong peak present at 1115-1120 cm^{-1} suggests the presence of ionic perchlorate[17], $\nu_3(T_2)$, whilst a strong doublet occurs at 1150-1060 cm^{-1}, due to the $\nu_3(T_2)$ vibration which is split into $A_1 + E$ on lowering the symmetry of the perchlorate from T_d to C_{3v}. This splitting is indicative of a coordinated perchlorate group. The IR data clearly show that in both the perchlorato complexes, both ionic and coordinated perchlorate groups are present. This supports our formulation of the complexes on the basis of EPR study.

In the IR spectrum of $[Mn(NTB)OAc]_2^{2+}$ $[OAc]_2^{2-}$ bands present at 1560 and 1410 cm^{-1} are indicative of a free acetate group[18]; while the bands at 1620 and

Table 2—Solid state magnetic moment data at 300 K

Compound	$\mu_{eff.}$/Mn atom (B.M.)	$\mu_{eff.}$/Dimer (B.M.)	$\mu_{eff.}$/trimer (B.M.)
$[Mn(NTB)Cl]_2^{2+}$ $[MnCl_4]^{2-}$	5.56	7.85	9.82
$[Mn(Et\text{-}NTB)Cl]_2^{2+}$ $[MnCl_4]^{2-}$	5.35	7.54	9.26
$[Mn(NTB)OAc]_2^{2+}$ $[OAc]_2^{2-}$	5.99	8.42	
$[Mn(NTB)ClO_4]^+$ $[ClO_4]^-$	5.94		
$[Mn(Et\text{-}NTB)ClO_4]^+$ $[ClO_4]^-$	6.02		

$$\mu_{eff}/atom = \left[\frac{\mu^2_{dimer}}{2}\right]^{1/2}$$

$$\mu_{eff}/dimer = [\mu^2_{trimer} - \mu^2_{monomer}]^{1/2}$$

Table 3—Observed optical bands (nm) and their extinction coefficients

Compd.	Solvent	λ_{max} (logε) (nm)
NTB	Butanol	280(4.17), 270(4.12), 245.5(4.08)
$[Mn(NTB)OAc]_2^{2+}$ $[OAc]_2^{2-}$	EtOH	280(4.07), 272(4.00), 242(4.25), 220(4.25)
$[(Mn(NTB)Cl]_2^{2+}$ $[MnCl_4]^{2-}$	MeOH	280(4.53), 270(4.61), 238(4.09), 212(4.02)
$[Mn(NTB)ClO_4]^+$ $[ClO_4]^-$	MeOH	280(4.27), 272(4.30), 244(4.14)
Ethyl-NTB	MeOH	285(4.11), 275(4.27), 260(4.23), 250(4.23)
$[Mn(Et\text{-}NTB)ClO_4]^+$ $[ClO_4]^-$	Acetonitrile	280(4.00), 272(4.11), 256(4.00), 216(4.30)
$[Mn(Et\text{-}NTB)Cl]_2^{2+}$ $[MnCl_4]^{2-}$	MeOH	278(4.00), 270(4.00), 241(4.30), 210(4.30)

1380 cm^{-1} are assigned to a unidentate mode of binding of acetate group[18]. Thus, in this complex we have evidence of both the non-coordinated (free) and unidentate acetate groups. All the above noted IR bands are absent in the analogous $[Mn(NTB)Cl]_2^{2+}$ $[MnCl_4]^{2-}$ complexes.

Acknowledgement

Support of this research by the UGC, New Delhi (F.12-12/88 SR-III) is gratefully acknowledged. One of the authors (H N Pandey) acknowledges grant of a JRF from the UGC, New Delhi.

References

1 Thomson L K, Ramaswami B S & Dawe R D, *Can J Chem*, 56 (1978) 1311.
2 Hendriks H M J, Birker P J M W L, Verschoor G C & Jan Reedijk, *J Chem Soc Dalton*, (1982) 623.
3 Mathur P, Crowder M & Dismukes G C, *J Am Chem Soc*, 109 (1987) 5227.
4 Tripathi A K, Sharma K K & Mathur P, *Indian J Chem*, 30A (1991) 400.
5 Dismukes G C, *Photochem Photobiol*, 43 (1986) 99.
6 Beyer W F ,& Fridovitch (Jr) I, *Biochemistry*, 24 (1986) 6420.
7 Thompson L K, Ramaswami B S & Elizabeth Seymour A, *Can J Chem*, 55 (1977) 878.
8 McKee V, Zvagulis M, Dagdigian J V, Patch M G & Reed C A, *J chem Soc*, 106 (1984) 4765.
9 Addison A W, Hendriks H M J, Reedijk J & Thompson L K, *Inorg Chem*, 20 (1981) 103.
10 (a) Dowsing R D & Gibson J F, *Chem Phys*. 50(1) (1969) 294.
(b) Dowsing R D, Gibson J F, Goodgame D M L, Goodgame M & Hayward P J, *Nature*, 219 (1968) 1037.
11 Luneau D, Savarialt J M & Tuchagues J P, *Inorg Chem*, 27 (1988) 3912.
12 Edward E T & Hendrickson David N, *Inorg Chem*, 17 (1978) 2457.
13 Mathur P & Dismukes G C, *J Am chem Soc*, 105 (1983) 7093.
14 Unni Nair B C & Sheats J E, Pontociello R, Engen D V, Petrouleas V & Dismukes G C, *Inorg Chem*, 28 (1989) 1582.
15 Lane T J, Nakagawa I, Walter J L & Kandathil A J, *Inorg Chem*, 1 (1962) 267.
16 McKee V, Zvagulis M & Reed C A, *Inorg Chem*, 24 (1985) 2914.
17 Rosenthal M R, *J chem Educ*, 50 (1973) 331.
18 Nakamoto K, *Infrared and Raman spectra of inorganic and coordination compounds* (John Wiley & Sons, New York), 1978, 232.

Indian Journal of Chemistry
Vol. 31A, September 1992, pp. 673-677

Complexation of crosslinked polyacrylamide-supported aminoligands with Cu(II): Effect of crosslinking on complexation kinetics

Beena Mathew, P M Madhusudanan & V N Rajasekharan Pillai*
School of Chemical Sciences, Mahatma Gandhi University, Kottayam, Kerala 686 631

Received 1 October 1991; revised and accepted 20 January 1992

Kinetics of Cu(II) complexation of amino ligands supported on polyacrylamides with crosslinking agents which differ in their polarity and flexibility have been studied. The complexation is first order with respect to the metal ion. The rate of Cu(II) intake increases with the hydrophilic and flexible nature of the crosslinks. The Langmuir and Frumkin equations are used to evaluate the adsorption parameters of complexation which suggest that the phenomenon of adsorption depends on the nature of the crosslinking agent in the polymer matrix. The interaction between the complexed metal ions is more in the polymer support with rigid crosslinking.

Interaction of metal ions with ligand functions supported on crosslinked polymer matrices is of considerable significance in a number of areas like catalysis[1], metal ion separation[2] and in biology[3]. Generally, this interaction is a heterogeneous complex formation between an insoluble crosslinked macromolecular ligand and a metal ion in aqueous medium. The structural characteristics of the polymer matrix which affect the reactivity of the attached functional groups decide the nature and extent of the interaction of the metal ion with the ligand[4-6]. The dependence of the reactivity of the attached functional groups on the nature of the polymer matrix like the polarity of the support, molecular character and extent of crosslinking and the overall topographical nature has been reported earlier from this laboratory[7-9]. It was thought of interest to extend this approach to the interaction of metal ions with polymeric ligands. Thus we report here the results of the kinetic investigation on the complexation of Cu(II) ions with amino ligands incorporated in polyacrylamide matrices crosslinked with divinylbenzene (DVB), N,N'-methylene-bis-acrylamide (NNMBA) and tetraethyleneglycol diacrylate (TEGDA). For the adsorption studies, Langmuir and Frumkin equations were used. In Langmuir adsorption, assumptions are made that the adsorption sites are equivalent and the ability of the substrate to bind at these sites are independent of whether or not nearby sites are occupied, whereas in Frumkin equation, adsorption depends on the binding as well as the nearby active sites.

Materials and Methods

Polyacrylamides crosslinked with DVB, NNMBA and TEGDA (8 mole%) were prepared and functionalized with ethylenediamine following the procedure reported earlier[10]. The ligand capacities of these resins were determined by acid-titration. The resins with 0.5477 (DVB), 0.8417 (NNMBA) and 1.1075 (TEGDA) mmol NH_2/g were used in these studies. Copper sulphate used was the purest available sample (Merck).

General experimental procedure

For the kinetic studies of DVB-crosslinked amino resin, different sets of 8% DVB-crosslinked amino resin (100 mg each) with NH_2/g (0.5477 mmol) was mixed with Cu(II) salt solution (6.5×10^{-3} *N*, 100 ml) at two different temperatures in a thermostatically controlled system for different time intervals. The remaining [Cu(II) ions] in each system was estimated iodometrically. Similar studies were done for the 8% NNMBA- and TEGDA-crosslinked amino resins.

For the adsorption studies, different sets containing NH_2 functionalized resin (100 mg) in Cu(II) solution of varying concentrations were used at two different temperatures for the DVB-, NNMBA- and TEGDA-crosslinked systems. The Langmuir and Frumkin equations were used for following the adsorption.

Results and Discussion

Crosslinked polyacrylamides with DVB-, NNMBA- and TEGDA-crosslinks are represented in

Scheme 1. The respective crosslinking agents differ in their relative rigidity and polarity. Crosslinks given by DVB are rigid and hydrophobic while those given by TEGDA are hydrophilic and flexible due to the presence of the polar ethylene oxide units between the diacrylate functions. NNMBA-crosslinking has intermediate rigidity and polarity. The interaction of the polymer-supported ligand with the metal ions in aqueous medium is governed by the extent of availability of the ligands for the metal ions. This depends on the nature of the polymer backbone and molecular character and extent of crosslinking in the polymer matrix. (Scheme 1).

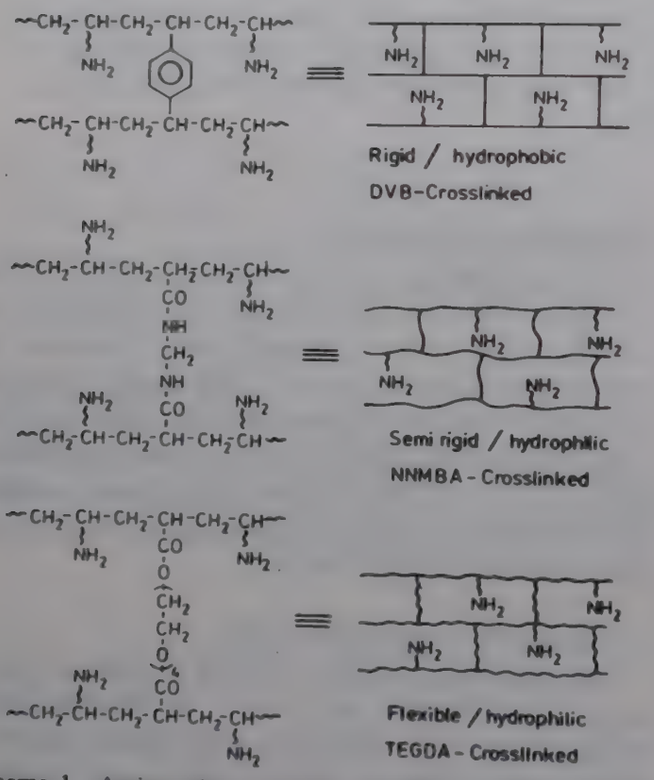

Scheme 1 – Aminopolyacrylamides with DVB-, NNMBA- and TEGDA-crosslinks

The results of the kinetic studies of the DVB-, NNMBA- and TEGDA-crosslinked systems are given in Fig. 1. In order to evaluate energy of activation (E) and entropy of activation ($\Delta S^{\neq}$) of complexation, a parallel run was carried out at higher temperature. The kinetic parameters for complexation was calculated from the Arrhenius equation.

For the DVB-crosslinked system the rate constant at 318 K is nearly double as that at 306 K. The activation energy for complexation is 82.410 kJ/mol, Arrhenius parameter is 1.145×10^9 s^{-1} and the entropy of activation is -71.628 J. These are comparable with those obtained for solution kinetics.

The nature of the complexation of NNMBA- and TEGDA-crosslinked amino resins was found to be different from that of the DVB-crosslinked system. The complexations of the NNMBA- and TEGDA-crosslinked systems occur faster than the DVB-crosslinked system. This appears to be due to the increased availability of the ligands by the diffusion of the solvent molecules with the metal ion into the polymer matrix. This increases with the increase in flexibility and hydrophilic nature of the crosslinking agent. Therefore the kinetics of the complexation of TEGDA-crosslinked resin could not be followed accurately at higher temperatures and they were carried out at 290 K and 303 K only. For the NNMBA-crosslinked system, the kinetic studies were carried out at temperatures 303 K and 316 K. The specific rate constant at higher temperature was found to be less in the case of NNMBA- and TEGDA-crosslinked resins. This can be ascribed to the exothermicity of the complexation process and the dissociation of the complex leading to an overall decrease in the rate. The diffusion of the solvent molecules into the polymer matrix increases with temperature[11]. In

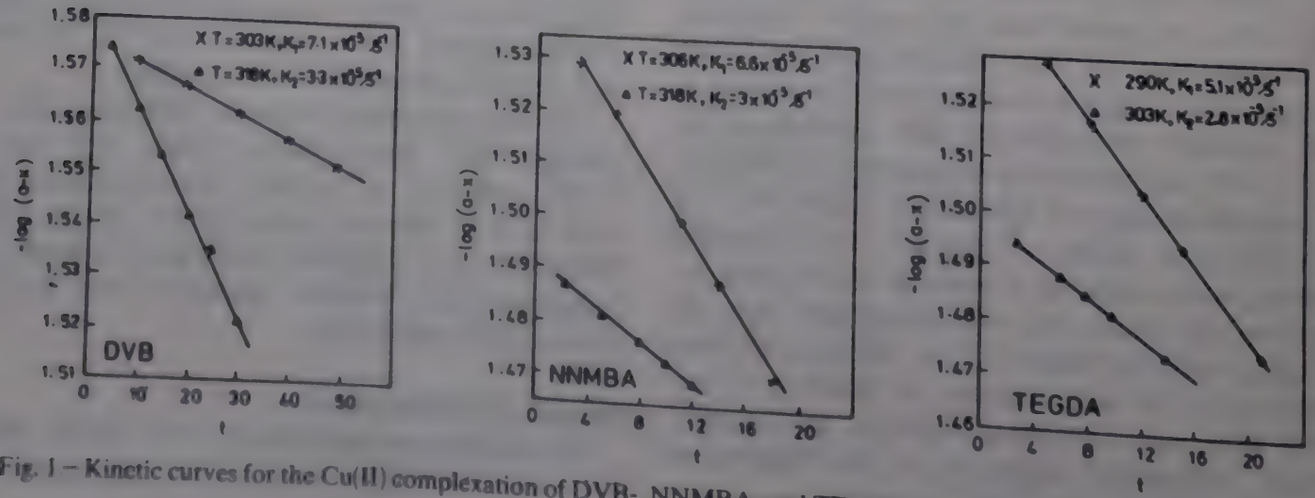

Fig. 1 – Kinetic curves for the Cu(II) complexation of DVB-, NNMBA- and TEGDA-crosslinked aminopolyacrylamides

TEGDA-crosslinked polyacrylamide-support, the hydrophilicity and flexibility of the crosslinking agent enhance the diffusion making the complexation process reversible with increase in temperature.

Diffusion, adsorption and interaction of metal ions with crosslinked polyacrylamide-supported amines

In the complexation of crosslinked polymer-supported ligands with metal ions which is a heterogeneous reaction, the following fundamental processes have to be considered: (i) diffusion of metal ions into the polymer matrix; (ii) adsorption on the surface and (iii) the reaction which may or may not be followed by desorption. In the case of adsorption, there are two possible approaches: (i) adsorption without any interaction with neighbours – Langmuir-type and (ii) adsorption invoking interaction between the neighbours – Frumkin-type[12,13].

(*i*) *Langmuir type*: The adsorption (complexation) of 8% DVB-, NNMBA- and TEGDA-crosslinked polyacrylamide-supported amines with Cu(II) ions was carried out at different temperatures with definite amount of the resin and varying concentrations of Cu(II) salt solution till equilibrium is reached. The Langmuir equation can be taken in the form

$$C_f/C_m = 1/KA_s + C_f/A_s \quad \ldots (1)$$

where C_f and C_m are the concentrations of uncomplexed and complexed Cu(II) ions, K is the stability constant and A_s is the surface area covered by the metal ions. The plot of C_f/C_m against C_f is linear (Fig. 2). The stability constant (K), surface area covered (A_s) and the free energy of activation ($\Delta G^{\neq}$) for the various systems at different temperatures are given in Table 1. For the DVB-crosslinked resin, the specific rate constant decreased with temperature whereas the surface area covered and the free energy of activation at the two different temperatures are almost same. This can arise from the rigid nature of the polymer-support. The activation energy for complexation, Arrhenius parameter and the entropy of activation are given in Table 1.

Parallel studies were carried out for the 8% NNMBA- and TEGDA-crosslinked poly(N-2-aminoethylacrylamide)s. The curves obtained by

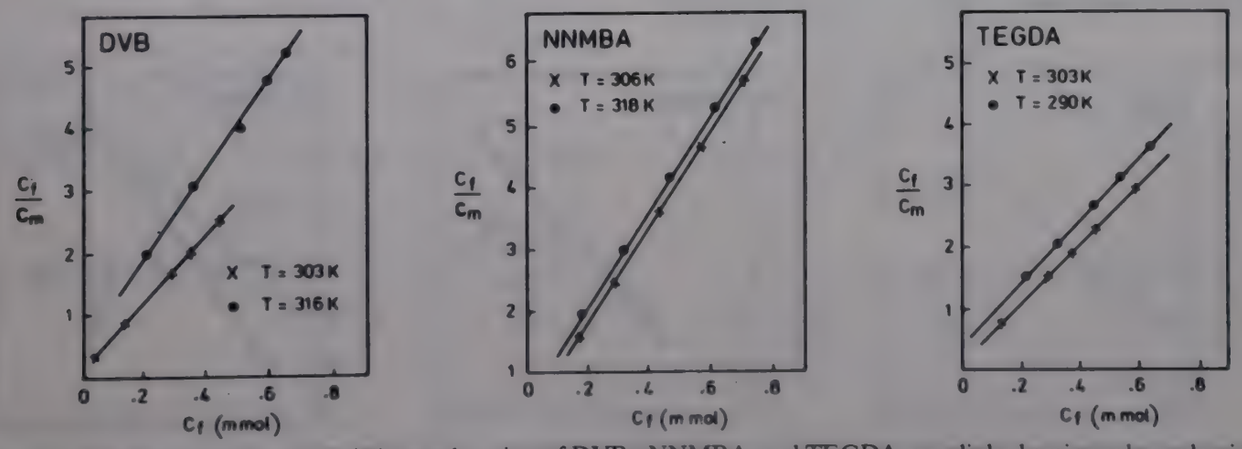

Fig. 2 – Langmuir plots for the Cu(II) complexation of DVB-, NNMBA- and TEGDA-crosslinked aminopolyacrylamides

Table 1 – Adsorption and kinetic parameters for the Cu(II) complexation of 8% DVB-, NNMBA- and TEGDA-crosslinked polyacrylamide-supported amines

Crosslinking (8%)	Kinetic Parameters			Temp. K	Adsorption Parameters		
	E kJ/mol	A (s^{-1})	$\Delta S^{\neq}$ J mol^{-1} k^{-1}		K kJ/mol	A_s	$\Delta G^{\neq}$ kJ/mol
DVB	31.9	8.9×10^9	+8.3	306	32.1	0.1301	−26.4
				318	20.1	0.1286	−26.2
NNMBA	18.6	1.1×10^5	+8.3	303	66.5	0.1871	−92.3
				316	1.6	0.3032	−61.1
TEGDA	88.8	2.2×10^{20}	−225.5	290	22.5	0.1740	−36.2
				303	109.3	0.1960	−96.5

plotting C_f/C_m versus C_m for the different temperatures are given in Fig. 2. The corresponding stability constants, surface area covered and the free energy of activation at different temperatures are given in Table 1. The specific rate constant decreases with increase in temperature but the free energy of activation becomes more positive. Larger the surface area covered, higher will be the repulsive force. This leads to an increase in the number of collisions for complexation to occur. A more positive value for the free energy of activation suggests a decrease in the spontaneity of the complexation. The kinetic parameters for the complexation are given in Table 1. The activation energy for complexation in the case of TEGDA-crosslinked system is less than that of the DVB-crosslinked system because of the former's low rigidity and hydrophobicity. The surface area covered by the metal ions at room temperature is 16% and at higher temperature it is 25%. This may be due to the increased availability of the reactive sites by the increased solvation at higher temperature.

In the case of the 8% TEGDA-crosslinked polyacrylamide-supported amino resin, the complexation was very fast at higher temperature. Hence, the adsorption studies were carried out at 290 and 303 K. The plots of the C_f/C_m against C_f at 290 and 303 K are given in Fig. 2. The specific rate constant, surface area covered and the free energy of activation at the two temperatures are given in Table 1. The high energy of activation, specific rate constant and the more negative value of free energy of activation support the view that increased complexation can occur at higher temperature. With increase in temperature, the latent reactive sites in the possibly coiled crosslinks become more exposed thereby enhancing the complexation. The entropy of activation at higher temperature delineates the disordering of the ordered structure of the polymer matrix by the increased diffusion of the solvents into the crosslinks, making them uncoiled and resulting in increased complexation. The surface area covered by Cu(II) ions at 290 K is 17.4% and at room temperature it is 19.6%.

(*ii*) *Frumkin type*: In order to investigate the interaction effect in complexation, Frumkin equation (Eq. 2) was chosen. Here C_f and C_m are the concentrations of uncomplexed and complexed Cu(II) ions and K_1 and K_2 are constants.

$$C_f = \frac{C_m}{(C_f - C_m)K_1} e^{-K_2 C_m/C_f} \quad \ldots (2)$$

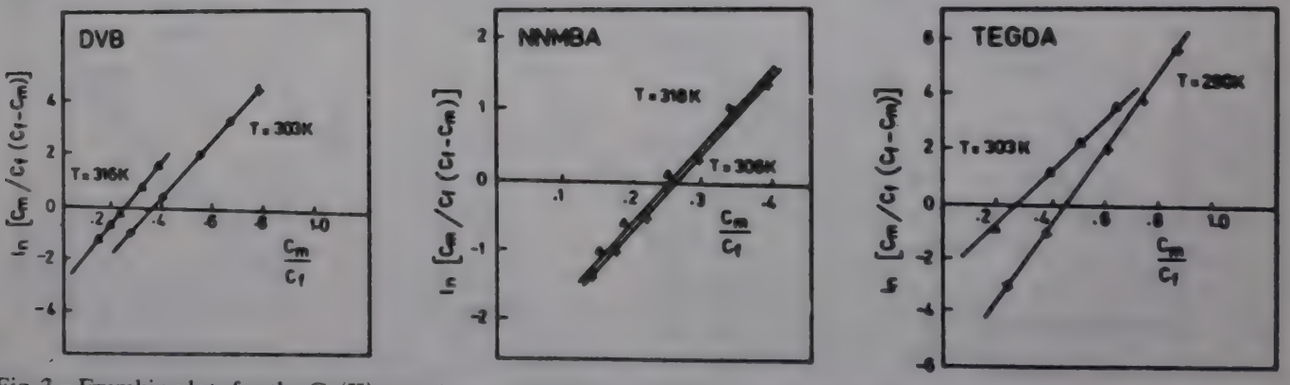

Fig. 3 – Frumkin plots for the Cu(II) complexation of DVB-, NNMBA- and TEGDA-crosslinked aminopolyacrylamides

Table 2 – Adsorption/interaction parameters and kinetic parameters of the Cu(II) complexation of 8% DVB-, NNMBA- and TEGDA-crosslinked polyacrylamide-supported amines

Crosslinking (8%)	Kinetic Parameters			Temp. K	Adsorption/Interaction Parameters		
	E kJ/mol	A (s^{-1})	$\Delta S^{\neq}$ $J\,mol^{-1}\,K^{-1}$		K_1 mol^{-1}	K_2 kJ/mol	$\Delta G^{\neq}$ kJ/mol
DVB	6.25	1.3×10^2	−204.7	306	19.05	11.08	−25.07/−23.69
				318	9.00	12.16	−24.90/−24.10
NNMBA	13.1	1.7×10^3	−183.1	303	2.94	9.62	−20.10/−23.10
				316	3.11	11.92	−21.10/−24.70
TEGDA	2.3	2.4×10^1	−218.63	290	2.30	9.70	−18.60/−22.10
				303	3.20	10.10	−20.30/−23.20

This can be transformed into Eq. (3)

$$\ln\left[\frac{C_m}{C_f(C_f - C_m)}\right] = \ln K_1 + K_2 \frac{C_m}{C_f} \quad \ldots (3)$$

For the complexations of DVB-, NNMBA- and TEGDA-crosslinked polyacrylamide-supported amines with Cu(II) ions, the experimental data obtained for the Langmuir type was used. The plots of $\ln[C_m/C_f(C_f - C_m)]$ versus C_m/C_f are given in Fig. 3. The interaction constant (K_2) and adsorption constant (K_1), free energy of activation at different temperatures, the energy of activation for interactions, Arrhenius parameter and the entropy of interaction are given in Table 2.

The free energy of activation for interaction is of the same order of magnitude for all systems. This is exemplified by the very low value of activation energy for interaction. Again it was found that the free energy of interaction is higher than the free energy of adsorption in the DVB-crosslinked system. This may be due to the possibility of increased interaction by the active sites in the DVB-crosslinked polymer matrix. The rigidity and hydrophobicity of the crosslinks make the active sites mainly on the surface resulting in increased interaction. For NNMBA- and TEGDA-crosslinked systems, the free energy of interaction is lower than the free energy of adsorption. This may arise from the flexibility of the crosslinking agents which results in extensive swelling in aqueous medium. But in the case of NNMBA-crosslinked system, the semi-rigidity of the polymer matrix needs higher activation energy for interaction. The entropies of interactions are negative and are of the same order of magnitude. Thus, the free energy of interaction depends on the nature of the polymer-support.

References

1 Ciardelli F, Carlini C, Pertici P & Valentini G, *J macromol Sci Chem*, A26(2&3) (1989) 327.
2 Warshawsky A, *Polymeric ligands in hydrometallurgy* in Sherrington D C & Hodge P (Eds.), *Syntheses and separations using functional polymers*, (J Wiley, Chichester) 1988, 325.
3 Palumbo M, Cosani A, Terbojerich M & Peggion E, *J chem Soc*, 99 (1977) 939.
4 Manecke G M & Heller H, *Makromol Chem*, 55 (1962) 51.
5 Drago R S & Gaul J H, *Inorg Chem*, 18 (1979) 2019.
6 Grote M, Wigge P & Kettrup A, *Fresenius Z Anal Chem*, 313 (1982) 297.
7 George B K & Pillai V N R, *J polym Sci polym Chem Ed*, 28 (1990) 2585.
8 Devaky K S, George B K & Pillai V N R, *Indian J Chem*, 29A (1990) 1045.
9 Jayakumari V G & Pillai V N R, *J appl polym Sci*, 42 (1991) 583.
10 Mathew B & Pillai V N R, *Polymer science: Contemporary themes*, Vol. 1, edited by S Sivaram, (Tata McGraw-Hill, New Delhi), 1991, 422.
11 Kahana N, Deshe A & Warshawsky A, *J polym Sci polym Chem Ed*, 23 (1985) 231.
12 Laidler K J, *Chemical kinetics*, (Harper & Row, New York) 1987, 231.

Indian Journal of Chemistry
Vol. 31A, September 1992, pp. 678-682

Kinetics and mechanism of complex formation between O-bonded(glycinato)pentaamminecobalt(III) and (glycinato)tetraethylenepentaminecobalt(III) ions with nickel(II) in aqueous medium

Nigamananda Das & Anadi C Dash*

Received 4 December 1991; revised and accepted 23 April 1992

The kinetics of the reversible complexation of $Ni(OH_2)_6^{2+}$ with oxygen bonded glycinatocobalt(III) substrates, $N_5Co(glyH)^{3+}$ ($N_5 = 5\ NH_3$ or tetraethylenepentamine; $glyH = H_2NCH_2COOH$) have been investigated by stopped flow technique at 25°C, $I = 0.3$ mol dm^{-3}. The values of formation and dissociation rate constants (k_f, k_r) for the binuclear species, $[N_5CoO_2CCH_2NH_2Ni]$ are 270 ± 37, 271 ± 41 $dm^3\ mol^{-1}\ s^{-1}$, and 0.140 ± 0.015, $0.100 \pm 0.007\ s^{-1}$ at 25°C ($I = 0.3$ mol dm^{-3}) for te tetraethylenepentaminecobalt(III) and pentaamminecobalt(III) substrates respectively. Lack of any dependence of k_f on the nature of the cobalt(III) moiety strongly suggests that the formation of the mono bonded species occurs by the entry of the pendant NH_2 group into the coordination sphere of Ni(II) via rate limiting $Ni-OH_2$ bond dissociation mechanism (I_d). The binuclear species exist in dynamic equilibrium between the monodentate and chelated forms with chelate form predominating. The small values of the dissociation rate constants despite the intrinsic electrostatic repulsion between the like charge centres also support the chelate nature of the binuclear species.

The kinetics of reversible formation of the binuclear species between $Ni(OH_2)_6^{2+}$ and ligands such as oxalate[1], pyridine-2- or 3-carboxylate[2], histidine[3], substituted salicylate[4], which are already bound to cobalt(III) have been studied in our laboratory. These studies point to a common mechanism where $Ni-OH_2$ bond dissociation controls the overall rate of formation of the binuclear complexes.

The stability constants of the binuclear species $(NH_3)_5CoglyM^{4+}$ ($M = Cu^{2+}$, Ni^{2+}, Co^{2+}) formed between O-bonded glycinate in $(NH_3)_5Co(gly)^{2+}$ and bivalent metal ions have been reported[5]. This work was undertaken as a part of our ongoing research investigation on metal-ligand complexation reactions where the denticity of the ligand can be altered by prior metal ion coordination. It was also of interest to investigate the kinetics of the formation and dissociation of Ni(II)-monoglycinatopentaamminecobalt(III) species so as to learn how the rate and mechanism of reversible complexation of glycine with $Ni(OH_2)_6^{2+}$ is affected by charges and steric properties of the cobalt(III) moieties to which it is bound.

Materials and Methods

$[Co(NH_3)_5glyH](ClO_4)_3.H_2O$ and $(\alpha\beta S)$-$[Co(tetren)glyH](ClO_4)_3$ were prepared by following the methods reported earlier[6,7]. The purity of the samples were checked by cobalt analysis and UV-visible spectral data which were in good agreement with the theoretical values and those reported in the literature[6,7].

Analar grade Ni(II) chloride was used for preparation of Ni(II) solution and the Ni(II) content in the stock solution was standardised by complexometric titration using Na_2EDTA[8]. Lutidine buffer was used for *p*H adjustment. Sodium perchlorate was used to maintain the ionic strength. All solutions were prepared in doubly distilled water. The *p*H measurement was made with a Elico digital *p*H-meter model LI 120 equipped with a combination electrode model CL 51. Standard NBS buffers (*p*H = 4.01, 6.86 and 9.2) were used for calibration of the *p*H meter. All UV-visible spectra were recorded using a JASCO model 7800 recording spectrophotometer using matched quartz cells of 10 mm path length.

Kinetics

The kinetics of complexation reaction was studied at 25°C, $I = 0.3$ mol dm^{-3} ($NaClO_4$) using a fully automated HI-TECH (UK) SF 51 stopped flow spectrophotometer with an Apple IIGS interface. The formation of binuclear species was followed under pseudo-first order conditions at 290 nm at which Ni(II) does not absorb significantly and only the cobalt(III) substrate and the resulting binuclear species are the dominant absorbing species (see Fig. 1). Absorbance of the reaction mix-

ture decreases with time for both the cobalt(III) substrates. All other kinetic details were similar to those described earlier[1]. The average value of the pseudo-first order rate constant and its standard deviation for any run was calculated from at least seven determinations.

Acid dissociation constant (K_{NH}) of $N_5CoO_2CCH_2NH_3^{3+}$

The *p*H-titration of an aqueous solution of both the complexes indicated only one inflexion point. The values of pK_{NH} of the N-protonated complexes were found to be 8.00 ± 0.2 and 7.79 ± 0.2 for $(NH_3)_5CoO_2CCH_2NH_3^{3+}$ and (tetren)$CoO_2CCH_2NH_3^{3+}$, respectively at 25°C and $I = 0.3$ mol dm^{-3}. These may be compared with the value of $pK_{NH} = 8.55 \pm 0.01$ at 27°C and $I = 0.3$ mol dm^{-3} for $(NH_3)_5CoO_2CCH_2NH_3^{3+}$ reported by Mohanty *et al.*[5].

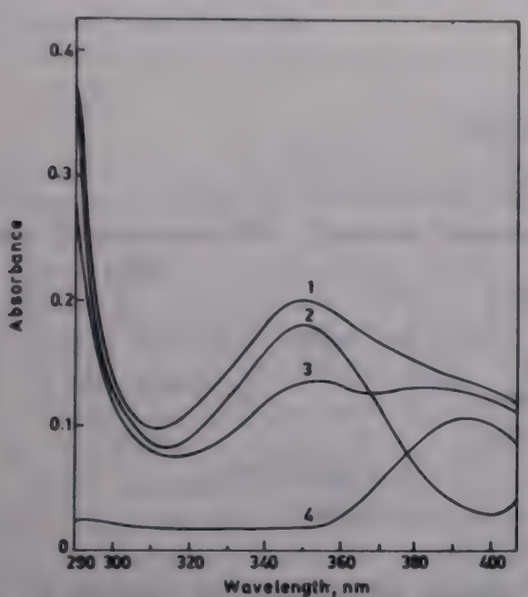

Fig. 1 – Spectral evidence of the interaction between glycinatopentaamminecobalt(III) with Ni(II). 1 Sum of absorbances of [Ni(II)] = 0.02 and [complex] = 2×10^{-3} mol dm^{-3}, at *p*H 6.8 taken separately; 2 Absorbance of cobalt(III) complex only at *p*H = 6.8 [complex] = 2×10^{-3} mol dm^{-3}; 3 Absorbance of reaction mixture, [Ni(II)] = 0.02 and [complex] = 2×10^{-3} mol dm^{-3} at *p*H = 6.8; 4 Absorbance of Ni(II) at *p*H = 6.8, [Ni(II)] = 0.02 mol dm^{-3}.

Results and Discussion

The interaction between Ni(II) and glycinatopentaamminecobalt(III) is evident from the spectral data presented in Fig. 1. Similar observation was also made for the corresponding tetren complex. The pseudo-first order rate constant (k_{obs}) for the reversible formation of binuclear species of $Ni(OH_2)_6^{2+}$ with $N_5Co(gly)^{2+}$ ($N_5 = 5NH_3$, tetren) at varying *p*H and $[Ni^{2+}]$ are collected in Tables 1 and 2. At a given *p*H, k_{obs} increases linearly with $[Ni^{2+}]$ in the range 5.0×10^{-3}-4.0×10^{-2} mol dm^{-3} (see Fig. 2). However, the plots of k_{obs} versus $[Ni^{2+}]$ at different *p*H's (6.0-6.9) converge to a common intercept indicating thereby that the dissociation rate constant of the binuclear species is *p*H-independent. The inverse acid dependence of gradient of the plots of k_{obs} versus $[Ni^{2+}]$ at different *p*H, however, is attributed to the involvement of the NH deprotonated glycinato species, $N_5CoO_2CCH_2NH_2^{2+}$. Also an earlier *p*H-titration study[5] of the thermodynamic stabilities of such binuclear species indicated that Ni(II) is most likely chelated by the pendant amine function and the carboxylato group bound to the cobalt(III) centre. Hence, considering these facts a possible reaction mechanism may be delineated as in Scheme 1.

In Scheme 1 k_{obs} takes the form (1)

$$k_{obs} = k_f(K_{NH}/([H^+] + K_{NH})[Ni^{2+}] + k_r \quad \ldots (1)$$

where, the overall formation rate constant (k_f) and the dissociation rate constant (k_r) for the binuc-

Table 1 – Rate data for the reversible formation of binuclear complex between $Ni(OH_2)_6^{2+}$ and $(NH_3)_5Co(gly)^{2+}$ at 25°C, $I = 0.3$ mol dm^{-3}, $\lambda = 290$ nm

pH_{av}	6.83 ± 0.02	6.64 ± 0.02	6.40 ± 0.02	6.23 ± 0.02	6.05 ± 0.02
10^2 [Ni^{2+}] (mol dm^{-3})			$10^2 k_{obs}^{(a)}$ (s^{-1})		
0.5	16.9 ± 0.8 (16.1)	13.4 ± 0.2 (14.0)	12.0 ± 0.5 (12.3)	11.7 ± 0.2 (11.6)	10.9 ± 0.5 (11.0)
1.0	21.6 ± 0.2 (22.2)	16.6 ± 0.9 (18.0)	15.1 ± 0.2 (14.7)	13.6 ± 0.4 (13.2)	11.9 ± 0.2 (12.1)
1.5	27.5 ± 0.8 (28.3)	19.9 ± 0.8 (22.0)	— —	16.3 ± 0.7 (14.8)	12.7 ± 0.4 (13.1)
2.0	33.9 ± 0.5 (34.4)	25.0 ± 0.4 (26.0)	20.5 ± 0.9 (19.4)	18.1 ± 1.1 (16.4)	12.4 ± 0.4 (14.2)
3.0	41.9 ± 0.6 (46.7)	30.0 ± 1.0 (34.1)	25.8 ± 0.8 (24.1)	20.7 ± 0.9 (19.6)	16.8 ± 0.5 (16.3)
4.0	— —	38.5 ± 1.2 (42.0)	31.1 ± 0.3 (28.7)	26.0 ± 0.9 (22.7)	19.7 ± 0.6 (18.5)

k_f(av) (dm^3 mol^{-1} s^{-1}) = 271 ± 41; k_r(av) (s^{-1}) = 0.100 ± 0.007

[a] Values in parentheses are $10^2 k_{calc}$ (s^{-1}) (see Eq. 1)

Table 2 – Rate data for the reversible formation of binuclear complex between $Ni(OH_2)_6^{2+}$ and $(tetren)Co(gly)^{2+}$ at 25°C, $I = 0.3$ mol dm^{-3}, $\lambda = 290$ nm

pH_{av}	6.83 ± 0.02	6.61 ± 0.02	6.39 ± 0.02	6.21 ± 0.01	6.05 ± 0.02
10^2 [Ni^{2+}] (mol dm^{-3})			$10^2 k_{obs}^{(a)}$ (s^{-1})		
0.5	22.7 ± 1.5 (23.6)	18.4 ± 1.8 (19.9)	17.6 ± 1.2 (17.6)	16.4 ± 0.5 (16.4)	15.4 ± 0.5 (15.7)
1.0	33.3 ± 0.8 (33.2)	24.1 ± 2.7 (25.9)	21.5 ± 1.1 (21.3)	19.6 ± 1.1 (18.9)	17.5 ± 0.8 (17.4)
1.5	40.7 ± 0.2 (42.8)	29.7 ± 0.6 (31.9)	— —	22.0 ± 0.9 (21.3)	18.2 ± 1.3 (19.0)
2.0	51.3 ± 1.1 (52.5)	35.5 ± 3.5 (37.9)	30.5 ± 0.9 (28.6)	25.2 ± 0.5 (23.8)	21.4 ± 0.9 (20.8)
3.0	63.1 ± 1.1 (71.7)	46.0 ± 3.3 (49.8)	39.8 ± 1.0 (33.9)	31.8 ± 0.9 (28.6)	25.6 ± 0.7 (24.1)
4.0	— —	56.3 ± 0.2 (61.7)	45.7 ± 1.7 (43.2)	39.2 ± 2.3 (33.5)	29.2 ± 1.4 (27.6)

k_f(av) (dm^3 mol^{-1} s^{-1}) = 270 ± 37; k_r(av) (s^{-1}) = 0.140 ± 0.015

(a) Values in parentheses are $10^2 k_{calc}$ (s^{-1}) (see Eq. 1)

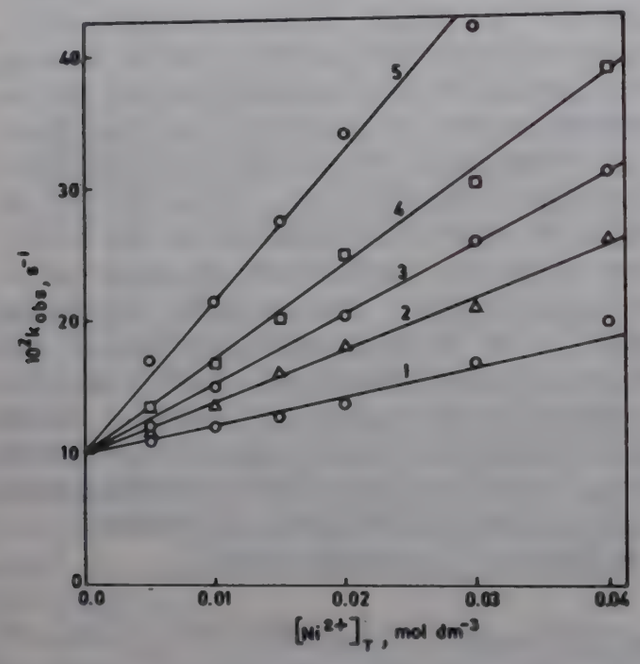

Fig. 2 – Plots of k_{obs} versus $[Ni^{2+}]$ at 25°C for $(NH_3)_5Co(gly)^{2+}$. 1 $pH = 6.05$, 2 $pH = 6.23$, 3 $pH = 6.40$, 4 $pH = 6.64$ and 5 $pH = 6.83$.

lear species, $N_5CoO_2CCH_2NH_2Ni^{4+}$, are given by Eqs (2) and (3), respectively.

$$k_f = K_{OS} k_{11} k_{22} / (k_{22} + k_{-11}) \quad \ldots (2)$$

$$k_r = k_{11} k_{-22} / (k_{-11} + k_{22}) \quad \ldots (3)$$

In Eqs (2) and (3), k_{11} and k_{-11} denote the first order constants for the formation and dissociation of the monobonded species derived from the encounter complex, $[N_5CoO_2CCH_2NH_2, Ni(OH_2)_6]^{4+}$ respectively; k_{22} and k_{-22} are the intramolecular chelation and dechelation rate constants for the mono ⇌ chel equilibrium respectively and K_{OS} is the equilibrium constant for the

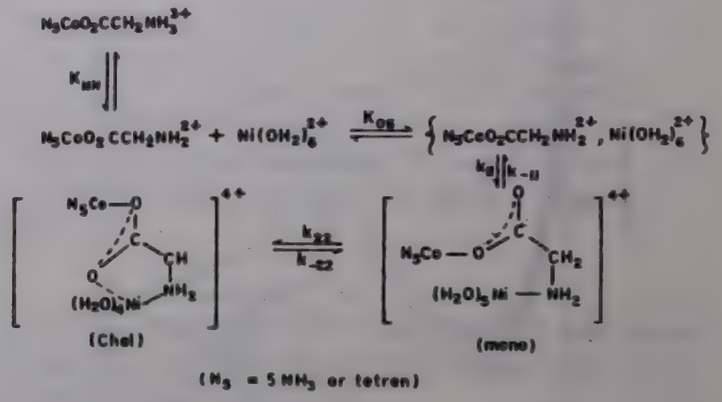

SCHEME 1

outer sphere association of $Ni(OH_2)_6^{2+}$ with $N_5CoO_2CCH_2NH_2^{2+}$. Initially the values of k_f and k_r were calculated from the gradients and intercepts of the least squares best line plots of k_{obs} versus $[Ni^{2+}]$. Since k_r turned out independent of pH, k_f was then calculated from all rate data using the mean value of k_r and the value of K_{NH} obtained from potentiometric measurement. The values of k_f, k_r along with K_{NH} reproduce the rate constants (see for k_{cal}, Tables 1 and 2) satisfactorily supporting the validity of the proposed rate law (see Eq. 1).

It is worth noting that the values of k_r for $N_5CoO_2CCH_2NH_2Ni^{4+}$ ($N_5 = 5NH_3$ or tetren) are $\sim 5 \times 10^4$ and ~ 70 times smaller than those for monoacetato Ni(II)[9] and monomethylamineNi(II)[10] and only 1.7 times larger than the value of the dissociation rate constant of monoglycinatoNi(II) species[11] despite the fact that the interionic repulsion between the two positively charged centres {Co(III) and Ni(II)} of the binuclear complex under consideration acts in favour of its dissociation (see Table 3). The location of rate determining step in the dissociation of the binuclear species

Table 3 – Comparison of rate parameters for the reversible formation of binuclear species between Ni(II) and $N_5Co(gly)^{2+}$ with related systems at 25°C

Reacting species	I (mol dm^{-3})	k_f (dm^3 mol^{-1} s^{-1})	k_r (s^{-1})	Ref.
Glycinate ion	0.10	$(1.5\text{-}4.1)\times10^4$	5.7×10^{-2}	11,14
Ethylamine	0.10	8.65×10^2	—	10
Acetate	0.0	—	5.0×10^3	9
Methylamine	0.10	—	9.6-13.6	11
$(NH_3)_5Co(gly)^{2+}$	0.30	$(2.71\pm0.41)\times10^2$	0.10 ± 0.007	This work
$(tetren)Co(gly)^{+2}$	0.30	$(2.70\pm0.37)\times10^2$	0.14 ± 0.015	This work

can now be considered referring to Eq. (4), a rearranged form of Eq. (3),

$$k_r = k_{-11}Q/f \quad \ldots (4)$$

where $f = 1 + k_{-11}/k_{22}$ and $Q = k_{-22}/k_{22}$ i.e. the equilibrium constant for monodentate and chelate forms of the binuclear complex. Assuming that the value of k_{22} is comparable to the water exchange rate constant of the $Ni(OH_2)_6^{2+}$ $\{k_{ex} = (2.7\text{-}3.6)\times10^4$ s^{-1} at 25°C$\}$[12] and that of k_{-11} equal to that of $CH_3CH_2NH_2Ni(OH_2)_5^{2+}$ ($k_{-11} \simeq 10$ s^{-1} at 25°C)[10] the value of the ratio k_{-11}/k_{22} turns out to be $\simeq 3.3\times10^{-4}$. Hence $f = 1.0$ appears to be reasonable estimate for which $k_r = k_{-11}Q$. Thus it appears that the dissociation rate of the monobonded form (k_{-11}) limits the overall dissociation of the binuclear species to the reactants[1,13]. The small value of the dissociation rate constant must be due to a relatively lower value of Q. Assuming $k_{-11} \simeq 10$ s^{-1}, $f \simeq 1.0$ and $k_r = 0.1$ s^{-1}, a tentative value of Q is found to be 0.01, which means that the mono $\rightleftharpoons$ chel equilibrium is strongly driven to the chelate form.

The overall rate constant for the forward reaction (k_f) (see Eq. 2) takes the form of Eq. (5)

$$k_f = K_{OS}k_{11}/f \quad \ldots (5)$$

The values of k_f for both the cobalt(III) substrates indicate that the rates of formation of $N_5CoO_2CCH_2NH_2Ni^{4+}$ species are vitually independent of N_5 ligand. However, the k_f values ($\sim 2.7\times10^2$ dm^3 mol^{-1} s^{-1}, 25°C (see Tables 1 and 2) are smaller than the same for glycinate ($NH_2CH_2COO^-$)[11,14] and for ethylamine[10] (see Table 3). This rate difference may be attributed at least partly to lower values of K_{OS} for the substrate under consideration. The values of the outer sphere association constant can only be summarised. For (2+)(+1) charge type association, using Fuoss equation based on a = 5 Å at 25°C and $I = 0.1$ mol dm^{-3}, the value of K_{OS} may be calculated to be 0.05 dm^3 mol^{-1} (ref. 13). A value of $K_{OS} = 0.01$ dm^3 mol^{-1} (for (2+/2+) ion pair) and $f = 1.0$ for the present investigation, yielded $k_{11} \simeq 2.7\times10^4$ s^{-1}, which is comparable to the water exchange rate constant of $Ni(OH_2)_6^{2+}$ $\{k_{ex} = (2.7\text{-}3.6)\times10^4$ s^{-1} at 25°C$\}$[12]. It is thus interesting to note that alteration in the mode of coordination of glycinate {i.e. O- for glycinate and N- for glycinatopentaminecobalt(III)} has virtually no effect on the intimate mechanism; the I_d mechanism involving $Ni(II)-OH_2$ bond dissociation largely controls the rate determining process for the formation of binuclear complex.

It is worthwhile to compare the overall formation equilibrium constant, K_M ($= k_f/k_r$) obtained from kinetic study with those obtained from potentiometric titration. Values of $K_M = 2.7\times10^3$ and 1.93×10^3 dm^3 mol^{-1} at 25°C for $(NH_3)_5$ and (tetren) complexes respectively obtained from the kinetic data compare satisfactorily with those reported from potentiometric titration $k_M = 8.13\times10^3$ and 5.13×10^3 dm^3 mol^{-1} at 25°C, $I = 0.3$ mol dm^{-3} for $(NH_3)_5Co(glyH)^{3+}$ (ref. 5) and $(tetren)Co(glyH)^{3+}$ respectively. This further convincingly supports the proposed scheme of reaction.

Acknowledgement

ND thanks the CSIR, New Delhi for the award of a senior research fellowship. We are grateful to DST, New Delhi for providing funds to purchase the stopped flow spectrophotometer.

References

1 Dash A C, Nanda R K & Acharya A, *Indian J Chem*, 30A (1991) 769.
2 Dash A C, Nanda R K & Das N N, (Mss submitted to IJC).
3 Dash A C, Nanda R K & Das R, *Indian J Chem*, 31A (1992) 1001.
4 Dash A C & Acharya A, (unpublished results).

5 Mohanty P, Tripathy P C, Dash A C & Nanda R K, *Indian J Chem*, 26A (1987) 392.
6 Fujita J, Yasui T & Shimura Y, *Bull chem Soc Japan*, 38 (1965) 654.
7 Dash A C, Das S & Nanda R K, *Indian J Chem*, 29A (1990) 227.
8 Vogel A I, *A text book of quantitative inorganic analysis* (*Longmans*) (1962) pp. 435.
9 Margerum D W, Cayley G R, Weatherburn D C & Pagenkopf G K in *Coordination chemistry, ACS Monograph* 174, edited by A E Martell (American Chemical Society, Washington D C) Vol. 2, Ch. 1, pp. 435 (1978).
10 Rorabacher D B & Melendez-Cepeda C A, *J. Am chem Soc*, 93 (1971) 6071.
11 Davies G, Kustin K & Pasternack R F, *Inorg Chem*, 8 (1969) 1535.
12 Ref. 9, pp. 5.
13 Dash A C & Pradhan J, *Int J chem Kinet*, 24 (1992) 155.
14 Ref. 9, pp. 74.

Indian Journal of Chemistry
Vol. 31A, September 1992, pp. 683-687

Surface-mediated autoxidation of aqueous SO_2 in ceramic powder suspensions

Rachna Bhargava, Ashu Rani & K S Gupta*

Atmospheric Chemistry Laboratory, Department of Chemistry, University of Rajasthan, Jaipur 302 004, India

Received 18 November 1991; revised and accepted 10 March 1992

In acetate buffered ceramic suspensions, if the ceramic concentration is not too high, the kinetics of autoxidation conforms to the rate law

$$R_{obs} = R_{un} + k_5[H^+]^{-1}[\text{Ceramic}][S(IV)]^2$$

where R_{un} is the rate of uncatalyzed reaction and k_5 is the rate constant for the surface catalyzed path. The rate of autoxidation is unaffected by oxygen partial pressure. Interestingly, the rate versus [ceramic] profile passes through a maximum indicating that the autoxidation mechanism involves the adsorption of both sulphur(IV) and dioxygen on particle surface.

So far most of the work on the studies of autoxidation of sulphur(IV) is limited to homogeneous metal ion catalysis[1], aerosol studies[2], catalysis by metal oxides[3-4], e.g., CoO[3], Ni_2O_3[4], CdO[5], CuO[6] and some other solid materials like fly ash[7,8] dust[9], glass[10], carbonaceous particles[11] and minerals and rocks[12]. These studies intend to delineate relative importance of these materials in atmospheric acid generation. These studies are also useful in searching new desulphurization catalysts.

Recently, the kinetics of S(IV)-autoxidation in silica[6] suspensions have been investigated in our laboratory. Our desire to carry out a comparative rate analysis made us to look into the chemistry of the aqueous suspension of ceramic powder. The other motivating factor was to assess the efficacy of this material in promoting conversion of S(IV) into S(VI) and its relevance to atmospheric processes because ceramic, which is largely a man-made material, is being released to the atmosphere as fine dust by its industrial users.

Materials and Methods

Ceramic powder was prepared by grinding thoroughly the small pieces of broken tea cups (Bharat make), washed with acid dichromate, water, EDTA-NaOH mixture and doubly distilled water, and using sieves the powder was separated into four fractions having different particle sizes, r, viz. $r \leq 53$; $53 \leq r \leq 75$; $75 \leq r \leq 120$; $120 \leq r \leq 180$ μm. pH was maintained with acetate buffer. Kinetics were followed by estimating S(IV) iodometrically[3,4,9,10]. Reaction mixtures were continuously stirred at 1500 ± 100 rpm, as at this stirring speed the reaction was shown, by varying stirring speed between 200-1800 rpm, not to be oxygen mass transfer-controlled. The treatment of kinetic results was based on the initial rates. The reproducibility of duplicate rate measurements was better than $\pm 10\%$. All calculations were done on APPLE IIe computer using curve fitter and scientific plotter programmes of Interactive Microwave Inc. In the presentation of rate data later the statistical parameters have been abbrreviated as follows: CC = correlation coefficient, CD = coefficient of determination and SEE = standard error of estimate.

Product analysis

Sulphate was estimated gravimetrically by precipitating it as $BaSO_4$ using standard procedure. Stoichiometry was found as in Eq. (1).

$$S(IV) + \tfrac{1}{2}O_2 \xrightarrow{\text{Ceramic}} S(VI) \qquad \ldots (1)$$

There was no evidence for the formation of dithionate.

Results

Chemical analysis of ceramic powder (done in CGCRI, Calcutta) revealed the following percentage of substances: SiO_2-69.42; Al_2O_3-20.64; Fe_2O_3-0.81; TiO_2-0.69; CaO-2.75; MgO-0.40; K_2O-3.69, CoO-0.02, MnO-0.01, ZnO-0.15 and with Cr_2O_3, CuO and NiO in traces.

In line with practically insoluble nature of ceramic powder, its recovery from final product so-

lution, under varying *p*H was more than 99%, the rest being lost. Uncatalysed and leachate reactions, which are trace metal ion catalysed[13], are completely seized by an EDTA concentration of 5×10^{-6} mol dm^{-3}, whereas the reaction in suspension, in the presence of the same amount of EDTA, is only slowed down slightly but not seized.

The kinetics were studied in suspension and in corresponding leachate solution in otherwise identical conditions. In a suspension ([ceramic] = 1.0 g dm^{-3}, [S(IV)] = 2×10^{-3} mol sm^{-3}, *p*H = 5.06 and t = 30°) initial rate of autoxidation, R_{obs}, was determined to be 8.0×10^{-7} mol dm^{-3} s^{-1}. Now the leachate of the same amount of ceramic was prepared and keeping all other conditions same as in previous experiment, the kinetic measurements yielded a R_{obs} value of 2.0×10^{-7} mol dm^{-3} s^{-1} which is the same as the uncatalysed rate (2.5×10^{-7} mol dm^{-3} s^{-1}) determined separately. Had the catalysis in the suspension been wholly due to trace metal ion catalysis, the rates in suspension and in leachate would have been of the same magnitude. However this is not so. This leads us to conclude that in suspension the catalysis is not due to trace metal ions and is most likely surface-mediated.

In a few kinetic runs, the reaction was studied in nitrogen atmosphere excluding O_2 completely. No perceptible reaction occurred over a period of one hour.

At a fixed *p*H, on increasing buffer concentration the rate of autoxidation decreased. A plot of $[R_{obs}]^{-1}$ versus $[CH_3COONa]$ is linear passing through the origin. In all further experiments overall $[CH_3COONa]$ was maintained at 0.14 mol dm^{-3} and wherever needed $[CH_3COOH]$ was changed for obtaining desired *p*H. Since the particle size, affects the rate of reaction in all experiments, unless otherwise stated, ceramic powder fraction, $r \leq 53$ μm, was used.

Kinetic results

The effect of [ceramic] on R_{obs} is shown in Fig. 1. On increasing [ceramic] upto 4 g dm^{-3} the rate increases and thereafter a further increase in [ceramic] leads to a continuous decrease in the rate of reaction. However, the results of [ceramic] variation between 0.5 to 4.0 g dm^{-3} displayed a linear relationship between R_{obs} and [ceramic]. The plots of R_{obs} versus [ceramic] were found to be linear with a non-zero intercept (Fig. 2). The intercept is ascribed to the uncatalysed reaction and thus the results are in agreement with the rate law (2).

$$R_{obs} = R_{un} + k_2[\text{ceramic}] \quad \ldots (2)$$

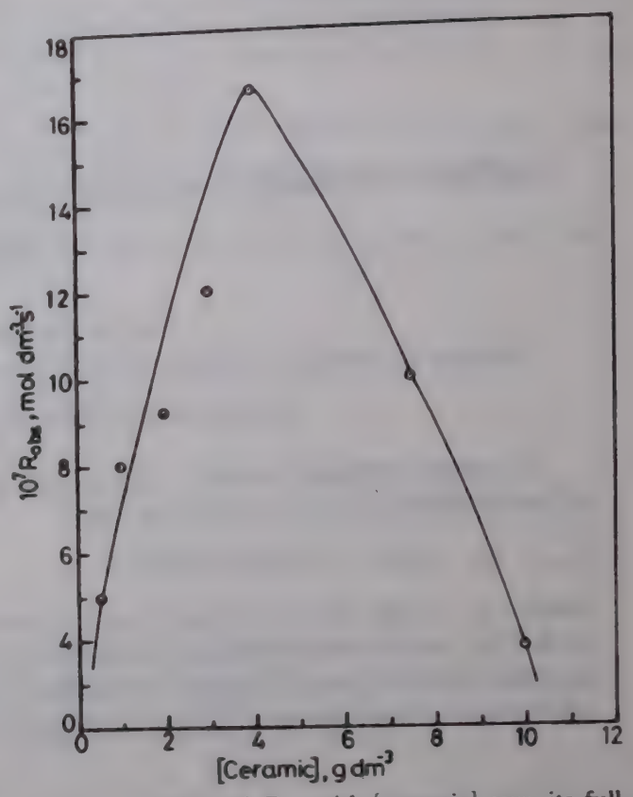

Fig. 1 – The variation of R_{obs} with [ceramic] over its full concentration range at *p*H = 5.06, [S(IV)] = 2×10^{-3} mol dm^{-3} and 30°C

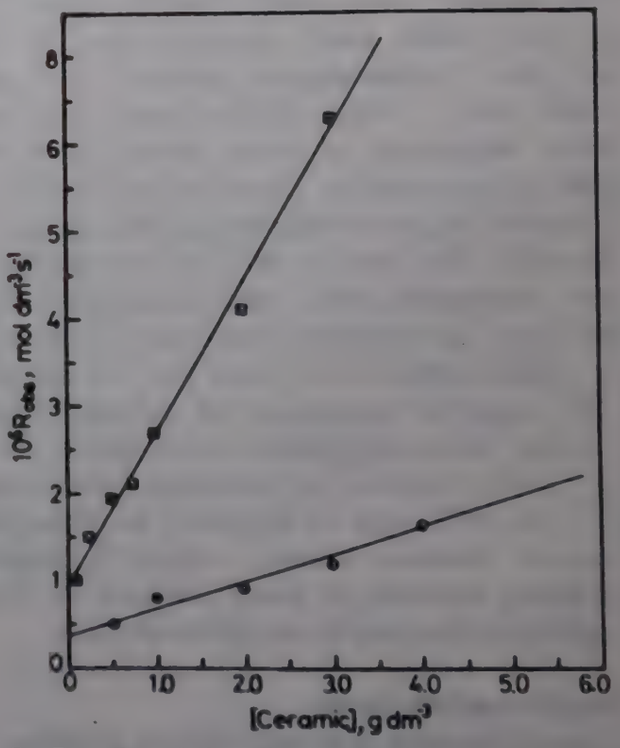

Fig. 2 – The plot of R_{obs} with [ceramic] in the autoxidation of sulphur(IV) at 5.06 *p*H and 30°C. ⊙, [S(IV)] = 2×10^{-3} mol dm^{-3}; ⊡, [S(IV)] = 4×10^{-3} mol dm^{-3}.

where R_{un} represents the rate of uncatalysed path and k_2 is the rate constant of the catalysed path.

The results of S(IV) variation at fixed [ceramic] and *p*H showed an order of 1.6 ± 0.05 in S(IV). The kinetic data pertaining to both [S(IV)] and

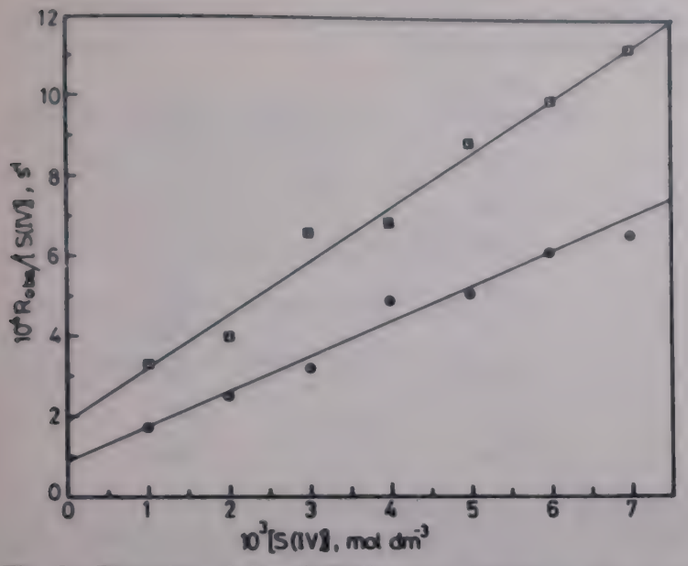

Fig. 3 – The plot of $R_{obs}/[S(IV)]$ versus [S(IV)] at pH = 5.06 and at 30°. ⊙, [ceramic] = 0.5 g dm^{-3}, ⊡, [ceramic] = 1.0 g dm^{-3}

[ceramic] variations fitted rate law (3) as shown in Fig. 3.

$$R_{obs} = k_1[S(IV)] + k_4[ceramic][S(IV)]^2 \quad \ldots (3)$$

The values of k_1 and k_4 are given in Table 1. A comparison of k_4 values shows these to vary in the range 0.08-0.16 dm^6 mol^{-1} g^{-1} s^{-1}. This variation in k_4 is probably due to the inhomogenity of the powder sample itself. Sulphur(IV) autoxidation, even in homogeneous studies, shows invariably a large scatter leading to relatively higher uncertainty[14].

Like k_4, the values of k_1 (Table 1) also display variation in their magnitude. This is probably due to the fact that the contribution of uncatalyzed rate, except at low [ceramic], is not sizeable and one does not expect to extract k_1 values with a high degree of precision. However, it is gratifying to note that the average value of k_1 (Table 1) is in good agreement with the value of 2.0×10^{-4} s^{-1} determined independently using same reagent samples and reaction conditions. The dependence of k_1 on pH is of interest to us. In general the rate of uncatalyzed S(IV) autoxidation based on the reactive SO_3^{2-} species is described by rate law (4)[15].

$$R_{un} = k_{SO_3}[SO_3^{2-}] \quad \ldots (4)$$

In the pH range (4.65-5.91), S(IV) would be present largely as HSO_3^- with some SO_3^{2-}. In terms of S(IV), which represents the analytical concentration of all sulphur(IV) species, Eq. (4) takes the form (5).

$$R_{un} = \frac{k_0[S(IV)]}{[H^+]} \quad \ldots (5)$$

Rate law (5)[15,16] has generally been found to be valid for uncatalysed reaction. On comparing Eqs (3) and (5)

$$k_1 = \frac{k_0}{[H^+]} \quad \ldots (6)$$

Using the k_1 value of 1.8×10^{-4} at pH = 5.06 and 30°, we obtained $k_0 = 1.57 \times 10^{-9}$ s^{-1} at 30°. This value of k_0 has been used in estimating R_{un} values at different pH and [S(IV)] in terms of rate law (5).

The $[H^+]$ dependence of the reaction was investigated by varying pH in the range 4.65 to 5.91. The rate increases with increase in pH. However, for an analysis of $[H^+]$ dependence of the ceramic catalysed reaction, the values of R_{un} (Rate law 3) at different pH are required. These values were obtained at $[S(IV)] = 4 \times 10^{-3}$ mol dm^{-3} using Eqs (5) and (6).

Rate law (3) can be written as (7).

$$R_{obs} - R_{un} = R_{cat} = k_4[ceramic][S(IV)]^2 \quad \ldots (7)$$

The values of R_{cat} are given in Table 2 and these values were used for obtaining k_4 at different pH. The plot of k_4 versus $[H^+]^{-1}$ was found to be linear with negligible intercept showing that

$$k_4 = \frac{k_5}{[H^+]} \quad \ldots (8)$$

Rate law (8), therefore, can be written as

$$R_{obs} = R_{un} + \frac{k_5}{[H^+]}[ceramic][S(IV)]^2 \quad \ldots (9)$$

At 30°, k_5 was determined to be 9.28×10^{-7} dm^6 mol^{-1} g^{-1} s^{-1}.

Table 1 – Values of k_1 and k_4 obtained from [S(IV)] and [Ceramic] variation at pH = 5.06, temp. = 30°

$10^4 k_1$ (s^{-1})	k_4 ($dm^6\ mol^{-1}\ g^{-1}\ s^{-1}$)	Method
1.92	0.08	[Ceramic] variation
2.46	0.10	[Ceramic] variation
0.94	0.16	[S(IV)] variation
1.88	0.13	[S(IV)] variation
Av = 1.8 ± 0.43	Av = 0.117 ± 0.027	

Table 2 – The values of k_4 at various *p*H values and at 30°

*p*H	$10^6 R_{obs}$* (mol dm^{-3} s^{-1})	$10^6 R_{un}$** (mol dm^{-3} s^{-1})	$10^6 R_{cat}$ (mol dm^{-3} s^{-1})	k_4 (dm^6 mol^{-1} g^{-1} s^{-1})
5.91	17.12	5.12	12.0	0.75
5.60	7.78	2.50	5.28	0.33
5.38	4.55	1.51	3.04	0.19
5.28	3.27	1.19	2.08	0.13
5.18	2.71	0.95	1.76	0.11
5.06	2.16	0.72	1.44	0.09
4.86	1.57	0.45	1.12	0.07
4.65	0.92	0.28	0.64	0.04

*Average of two independent measurements at [Ceramic] = 1.0 g dm^{-3}, [S(IV)] = 4×10^{-3} mol dm^{-3}.
**Calculated from the rate law (5) using $k_0 = 1.5 \times 10^{-9}$ s^{-1} at 30°.

The catalytic activity of the ceramic powder decreases with increase in particle size, *r*. The log-log plots of R_{obs} and *r* were linear with a slope of −1 indicating an inverse first order in particle size.

The rate of reaction was unaffected on varying O_2 partial pressure by passing O_2:N_2 mixtures in varying proportions showing a zero order in O_2.

A value of 110 kJ mol^{-1} for overall energy of activation was determined by studying the reaction in the temperature range 30-40°C.

Reaction profiles in unbuffered suspensions

The reaction profiles for unbuffered suspensions, in which the initial *p*H was adjusted by addition of dilute $HClO_4$, showed the occurrence of the reaction in two stages; the first of which is rapid and the second a slower one. Similar rate profiles have been obtained in carbon[11], CoO[3], and $CaSO_3$[17] suspensions.

Discussion

There are several lines of arguments which suggest the mechanism of autoxidation to involve the adsorption of dioxygen and S(IV) on the particle surface as has been assumed by several previous workers[3,4,10,18,19]. Surface area decreases with increase in particle size. The fact that the rate decreases with increase in particle size points to the surface nature of the autoxidation. Autoxidation occurs only in the presence of oxygen. The adsorption of both oxygen and S(IV) on particle surface is also indicated by the rate profile which passes through a maximum; the observance of which can be explained if the operation of a Langmuir-Hinshelwood type of mechanism[20] is assumed. This, in effect, requires that both S(IV) and O_2 must be adsorbed on the adjacent sites on the ceramic surface to facilitate the oxidation. When [catalyst] is very high, a large number of active sites are available for adsorption of S(IV) and O_2 on remote sites. The inhibitory effect of buffer also points to the catalysis being surface mediated. The adsorption of one or more of the buffer constituents on the particle surface results in the reduced availability of the active sites for the adsorption of O_2 and S(IV).

Although, on increasing *p*H the rate increases, the observed effect may not be real and may have its origin in variation of [acetic acid] (cf. buffer effect) which accompanies a variation in *p*H. Hence, it is considered advisable not to take $[H^+]$-dependence into consideration in proposing the mechanism. In the *p*H range of this study, S(IV) will be largely present as HSO_3^- (dissociation constant values of 1.26×10^{-2} for $K_{d(1)}$ and 6.24×10^{-8} for $K_{d(2)}$[22]. The nature of the kinetics, which is first order in ceramics, second order in S(IV) and zero order in O_2 may be explained by following mechanism in Scheme 1.

$$>Cer + HSO_3^- \rightleftharpoons Cer.HSO_3^- \text{ (fast)}$$

$$>Cer.HSO_3^- + HSO_3^- \rightleftharpoons Cer.(HSO_3^-)_2 \text{ (slow)}$$

$$>Cer.(HSO_3^-)_2 + O_2 \rightleftharpoons Cer.(HSO_3^-)_2.O_2 \text{ (fast)}$$

$$>Cer.(HSO_3^-)_2.O_2 \rightarrow Cer. + S_2O_7^{2-} + 2H^+ \text{ (fast)}$$

$$S_2O_7^{2-} + H_2O \rightarrow 2SO_4^{2-} + 2H^+ \text{ (fast)}$$

Scheme 1

The results can also be explained by involving metabisulphite ion in an alternative mechanism (Scheme 2).

$$2HSO_3^- \overset{K_D}{\rightleftharpoons} S_2O_5^{2-} + H_2O,\ K_D = 1.75 \times 10^{-3}$$

$$Cer. + S_2O_5^{2-} \rightleftharpoons Cer.S_2O_5^{2-} \text{ (slow)}$$

$$Cer.S_2O_5^{2-} + O_2 \rightleftharpoons Cer.S_2O_5^{2-}.O_2 \text{ (fast)}$$

$$Cer.S_2O_5^{2-}.O_2 \rightarrow Cer + S_2O_7^{2-} \text{ (fast)}$$

$$S_2O_7^{2-} + H_2O \rightarrow 2SO_4^{2-} + 2H^+, \text{ (fast)}$$

Scheme 2

The formation of disulphate ion in Schemes 1 and 2 has been proposed in the light of the work of Batterton and Hoffmann[23]. Both the proposed mechanisms will lead to the same experimental rate law (9).

It is of interest to compare the results of this study with those of silica[12], glass[10], CdO[5] and carbon suspensions[11]. In CdO[5], silica[6] and glass[10] a clear-cut second order dependence in S(IV), as in the present study, was noted. In case of carbon[11], the order varied from two to zero. However, a distinctive feature of this study, same as in the case of glass, is the observance of rate maximum in rate profile on varying [ceramic]. This phenomenon was absent in other studies and probably supports the operation of a Hinshelwood-Langmuir mechanism[20]. An initial rapid drop in [S(IV)] in unbuffered suspensions has been found in all these studies except CdO[5]. The phenomenon of induction period, which was observed in glass catalyzed reaction[10] below *p*H 5, was absent in all other cases.

The results obtained in this study have relevance to the environmental chemistry of SO_2. Ceramic is mainly composed of such material which is an important constituent of suspended particulate matter. These materials are, therefore, likely to catalyze the atmospheric transformation of S(IV) into S(VI) in various forms of atmospheric water. Moreover, in real atmosphere the size of suspended particles is much smaller ($1 \times 10^{-2} - 10^{-1}$ μm)[24] and so the rate of autoxidation is expected to be much higher due to large surface area, in agreement with the inverse relationship between rate and particle size.

Acknowledgement

The work was supported by an Indo-US Subcommission Research project CE-2.

References

1 Hoffmann M R & Boyce S D in *Trace atmospheric constituents: properties, transformations and fates*, edited by S E Schwartz (John Wiley, New York) (1983) pp. 147-189.
2 Berresheim H & Jaeschke W, *J atmos Chem*, 4 (1986) 311-334.
3 Prasad D S N, Ashu Rani, Madnawat P V S, Bhargava R & Gupta K S, *J mol Catal*, 69 (1991) 393-405.
4 Bhargava R, Prasad D S N, Rani A, Bhargava P, Jain U & Gupta K S, *Transition met Chem*, accepted (1991).
5 Ashu Rani, Prasad D S N, Bhargava R & Gupta K S, *Bull chem Soc Japan*, 64 (1991) 1956.
6 Prasad D S N, Rani A & Gupta K S, *Environ Sci Technol* Accepted (1991).
7 Cohen S, Chang S G, Markowitz S S & Novakov T, *Environ Sci Technol*, 15 (1981) 1498-1502.
8 Madnawat P V S, Prasad D S N, Rani A, Sharma M & Gupta K S, Unpublished work.
9 Rani Ashu, Prasad D S N, Madnawat P V S & Gupta K S, *Atmos Environ*, 26A (1992) 667-673.
10 Rani A, Prasad D S N, Jain U & Gupta K S, *Indian J Chem Sect A*, 30 (1991) 756-764.
11 Brodzinsky R, Chang S G, Markowitz S S & Novakov T, *J phys Chem*, 84 (1980) 3354-3358.
12 Gupta K S, Madnawat P V S, Bhargava R, Prasad D S N, Sharma M & Rani A in *Proc V int. conf on precipitation scavenging and atmosphere surface exchange processes*, edited by S E Schwartz (Hemisphere, New York) accepted (1991).
13 Huss Jr A, Lim P K & Eckert C A, *J Am chem Soc*, 100 (1978) 6252-6253.
14 Martin L R in *SO_2, NO and NO_2 oxidation mechanisms: Atmospheric considerations* edited by J G Calvert (Butterworth, Boston) (1984), pp. 70-71.
15 Beilke S, Lamb D & Miller J, *Atmos Environ*, 9 (1975) 1083-1090.
16 Hoather R C & Goodeve C F, *J phys Chem*, 30 (1934) 1149.
17 Weisnicht W L, Overman J, Wang C C, Wang H J, Erwin J & Hudson J L, *Chem engng Sci*, 35 (1980) 463-468.
18 Faust B C, Hoffmann M R & Bahnemann D W, *J phys Chem*, 93 (1989) 6371-6381.
19 Hong A P, Boyce S D & Hoffmann M R, *Environ Sci Technol*, 23 (1989) 533-540.
20 Laidler K J, *Chemical kinetics*, (Harper & Row, New York) (1987) pp. 229-275.
21 van Eldik R & Harris G M, *Inorg Chem*, 19 (1980) 880.
22 Tartar H V & Garretson H H, *J Am chem Soc*, 63 (1941) 808.
23 Betterton E A & Hoffmann M R, *J phys Chem*, 92 (1988) 3962-3965.
24 Spedding D J, *Air pollution* (Oxford University Press, London) (1974) p. 8.

Indian Journal of Chemistry
Vol. 31A, September 1992, pp. 688-692

Kinetic and mechanistic studies on substitution reaction of aqua-ligands from *cis*-diaqua-bis[2-(*m*-tolylazo)-pyridine]ruthenium(II) ion with 2,2′-bipyridine in aqueous medium

Bibekananda Mahanti & G S De*
Department of Chemistry, University of Burdwan, Burdwan 713 104

Received 17 January 1992; revised and accepted 23 March 1992

The kinetics of substitution of aqua-ligands from *cis*-diaqua-bis[2-(*m*-tolylazo)pyridine]ruthenium(II) ion by 2,2′-bipyridine in aqueous medium has been studied spectrophotometrically at different temperatures (40-55°C). A rate law has been established. The reaction rates are found to be *p*H dependent in the *p*H range of 4.5 to 6.0. Ionic strength has a very little effect on the rate constants. Activation parameters ($\Delta H^{\neq}$ and $\Delta S^{\neq}$) have been evaluated and compared with the reactions by 8-hydroxyquinoline and 1,10-phenanthroline. All the experimental results are consistent with a dissociative mechanism. The effect of variation of dielectric constant of the medium has been used to verify the mechanistic conclusion.

In recent years much attention has been devoted to the aqua-ligands substitution reactions of ruthenium (II) complexes as they do not follow a single mechanism. Thorough literature survey[1-7] reveals a general pattern of the mechanism in which replacement of water molecules occurred through either purely dissociative or dissociative interchange pathway. Deviations from the above mechanism are also noticed in which associative mechanism has been suggested[8]. In view of the conflicting mechanisms proposed so far, we have studied the kinetics of substitution of aqua-ligands from *cis*-diaqua-bis[2-(*m*-tolylazo(pyridine]ruthenium(II) ion by 8-hydroxyquinoline[9], 1,10-phenanthroline[10] and 2,2′-bipyridine to see whether any mechanistic generalisation can be made.

The present paper is related to the findings of the reaction:

$$cis\text{-}[Ru(tap)_2(H_2O)_2]^{2+} + bipy \rightarrow [Ru(tap)_2(bipy)]^{2+} + 2H_2O$$

where tap and bipy represent 2-(*m*-tolylazo)pyridine and 2,2′-bipyridine respectively.

Materials and Methods

Reactant complex *cis*-$[Ru(tap)_2(H_2O)](ClO_4)_2.H_2O$ (complex-I) was prepared by following literature method and characterised by elemental analysis, and spectral data obtained were compared with the data reported in the literature[11,12]. Absorption spectra of 1×10^{-4} mol dm^{-3} solutions at *p*H 5.6, recorded on a Hilger UVISPEK spectrophotometer, exhibited λ_{max} at 536 nm. The ionic strength of the reaction medium was adjusted by adding recrytallised $NaClO_4$. The *p*H of the medium was adjusted by adding NaOH or $HClO_4$. The product (complex-II) resulting from the reaction between complex-I and 2,2′-bipyridine (L) was prepared by mixing the reactants in different molar ratios of 1:1, 1:2 and 1:3 ([complex-I], [L], [complex-I] being 1×10^{-4} mol dm^{-3}) and thermostating at 50°C for 48 hr at *p*H 5.6. The absorption spectra of the resultant solutions wee taken and found that all the three compositions exhibited identical natures having λ_{max} at 518 nm. The 1:1 metal-ligand composition of complex-II in solution was verified by Jobs method of continuous variation.

In all the experiments AR grade chemicals were used and doubly distilled water was used for preparing solution. The course of the reaction was followed by measuring the absorbances at 560 nm (using a Hilger UVISPEK spectrophotometer) where a substantial difference existed in the spectra of complex-I and complex-II. The reaction rate was monitored from the decrease of intensity at 560 nm. Equal volumes of complex-I and L of desired concentrations were mixed in such a way that the pseudo-first order rate law becomes applicable. The pseudo-first order rate constant values (k_{obs}) were obtained by plotting $\ln [(D_0 - D_\alpha)/(D_t - D_\alpha)]$ versus time where D_0, D_α and D_t are the optical density values at the beginning of the reaction, at infinite time and at the end of time t respectively. The pseudo-first order plots were linear passing through the

origin. This linearity is observed from the beginning to the end of the reaction which ruled out the possibility of any kind of consecutive reactions. The rate constants were reproducible within ± 3%.

Results and Discussion

(i) *Effect of varying [complex-I] on rate constant*

The [complex-I] was varied in the range of 0.5×10^{-4} to 1.5×10^{-4} mol dm^{-3} under the conditions of *p*H = 5.6, [L] = 2×10^{-3} mol dm^{-3} and ionic strength = 0.01 mol dm^{-3}. The $k_{obs} \times 10^5$ (s^{-1}) values were found to be 20.14, 20.06, 20.30 and 20.11 at [complex-I] of 0.5×10^{-4}, 0.75×10^{-4}, 1.0×10^{-4} and 1.5×10^{-4} mol dm^{-3} respectively at 50°C in aqueous medium. The rate of reaction is first order with respect to the [complex-I]. The rate law is represented by Eq. (1).

$$\frac{d[\text{complex-II}]}{dt} = k_{obs}[\text{complex-I}] \qquad \ldots(1)$$

(ii) *Effect of ionic strength on rate constant*

Under the conditions of *p*H = 5.6, [complex-I] = 1×10^{-4} mol dm^{-3} and [L] = 2×10^{-3}mol dm^{-3} the ionic strength was varied by $NaClO_4$. A very little change in the k_{obs} values at 50°C in aqueous medium was observed with increase in ionic strength. The $k_{obs} \times 10^5$ (s^{-1}) values are 20.30, 20.14, 20.65, 20.05 and 20.29 at different ionic strengths 0.01, 0.05, 0.1, 0.2 and 0.3 respectively. The incoming ligand is not protonated at *p*H = 5.6. The rate of reaction between an ion and a neutral molecule in solution should have been independent of ionic strength of the medium[13], hence the variation of ionic strength produces no appreciable change in rate constant values.

(iii) *Effect of pH on rate constant*

Under the conditions of [complex-I] = 1×10^{-4} mol dm^{-3}, [L] = 2×10^{-3} mol dm^{-3}, ionic strength = 0.01 mol dm^{-3} and temperature = 50°C the *p*H of the aqueous medium was varied in the range of 4.5 to 6.0. The $k_{obs} \times 10^5$ (s^{-1}) values were 1.49, 5.65, 13.37, 20.30 and 26.34 at *p*H values 4.5, 5.0, 5.3, 5.6 and 6.0 respectively. The increasing rate of reaction with the increase in *p*H must be attributed to two acid dissociation equilibria of the ligand L and the complex-I. The acid dissociation equilibrium of 2,2′-bipyridine (i.e. L) is represented by Eq. (2)

$$LH^+ \overset{K_a}{\rightleftharpoons} L + H^+ \qquad \ldots(2)$$

where the value of pK_1 is observed[14] to be 4.44 at 25°C. Since the donor ability of the nonprotonated species is much higher than that of the protonated species, the reaction rate increases with the increase in *p*H. The acid dissociation equilibrium of complex-I is represented by Eq. (3)

$$[Ru(tap)_2(H_2O)_2]^{2+} \overset{K_1'}{\rightleftharpoons} [Ru(tap)_2(OH)(H_2O)]^+ + H^+ \qquad \ldots(3)$$

where the pK_1' value is observed to be 6.55 at 25°C. The reactivity of hydroxoaqua complex is usually higher than that of diaqua complex by the well known labilising effect of the coordinated hydroxide ion[15]. Hence the reaction rate increases again with the increase in *p*H. Notwithstanding in the present kinetic runs, the substitution reactions were followed at a constant *p*H of 5.6 to avoid complications caused by adding an additional parameter of [H$^+$] to the rate equation. At *p*H 5.6 complex-I exists mainly in the diaqua form.

(iv) *Effect of varying [ligand] on rate constant*

The concentration of 2,2′-bipyridine was varied in the range of 1×10^{-3} to 3×10^{-3} mol dm^{-3} under the conditions of [complex-I] = 1×10^{-4} mol dm^{-3}, *p*H = 5.6 and ionic strength = 0.01 mol dm^{-3}. The results presented in Table 1 show that the rate increases with increase in [L], and tend to approach a limiting value at higher [ligand] at each temperature. Though the rate of reaction is dependent on [L], outersphere association is not considered since the incoming ligand species are either neutral or positively charged under the reaction conditions. The unimolecular reaction mechanism showsn in Scheme 1 can be proposed to explain the variation of rate with [L].

$$[Ru(tap)_2(H_2O)_2]^{2+} \underset{k_{-1}\,(fast)}{\overset{k_1\,(slow)}{\rightleftharpoons}} [Ru(tap)_2(H_2O)]^{2+} + H_2O$$

Table 1—Variation of rate constants with [L] at different temperatures

[complex-I] = 1×10^{-4} mol dm^{-3}, ionic strength = 0.01 mol dm^{-3}, *p*H = 5.6

[L] × 10^3 (mol dm^{-3})	$k_{obs} \times 10^5$ (s^{-1})			
	40°	45°	50°	55°C
1.0	2.9	5.6	10.6	21.9
1.5	4.2	8.2	15.4	31.4
2.0	5.6	10.7	20.3	42.9
2.5	6.7	13.0	24.6	50.0
3.0	7.7	15.0	27.6	55.8

$$[Ru(tap)_2(H_2O)]^{2+} + L \underset{fast}{\overset{k_2}{\rightarrow}} [Ru(tap)_2L]^{2+} + H_2O$$

Scheme 1

The rate of formation of the final product can be obtained by applying steady state principle (Eq. 4).

$$\frac{d[Ru(tap)_2L^{2+}]}{dt} = \frac{k_1 k_2 [Ru(tap)_2(H_2O)_2^{2+}][L]}{k_{-1} + k_2[L]} \quad \ldots(4)$$

Two limiting cases of this rate expression can be achieved: (a) If [L] is low and $k_{-1} \gg k_2[L]$, then Eq. (4) reduces to Eq. (5)

$$\frac{d[Ru(tap)_2L^{2+}]}{dt} = \frac{k_1 k_2 [Ru(tap)_2(H_2O)_2^{2+}][L]}{k_{-1}} \quad \ldots(5)$$

i.e. a second order rate dependent on [ligand] would be obtained. (b) If [L] is high and $k_2[L] \gg k_{-1}$, then Eq. (4) is reduced to Eq. (6)

$$\frac{d[Ru(tap)_2L^{2+}]}{dt} = k_1 [Ru(tap)_2(H_2O)_2^{2+}] \quad \ldots(6)$$

i.e. a first order reaction rate independent of [ligand] would be observed. Thus the reaction rate may or may not depend on the concentration of the entering ligand under different reaction conditions. Generally a gradual change from second order to first order kinetics is expected with the increase in [ligand]. A limiting rate is reached at high concentration of ligand. From the effect of variation in [complex-I] on the rate it has already been concluded that Eq. (1) holds. Eq. (7) has been obtained from Eq. (1).

$$\text{Rate} = k_{obs}[Ru(tap)_2(H_2O)_2^{2+}] \quad \ldots(7)$$

Equation (8) is obtained from Eqs (4) and (7)

$$k_{obs} = k_1 k_2 [L]/(k_{-1} + k_2[L]) \quad \ldots(8)$$

$$\text{or, } 1/k_{obs} = 1/k_1 + k_{-1}/(k_1 k_2).1/[L] \quad \ldots(9)$$

It is evident from Eq. (9) that a plot of $1/k_{obs}$ versus $1/[L]$ should be linear with an intercept of $1/k_1$. Actually such linear plots were obtained (Fig. 1). From such linear plots at different temperatures k_1 values and k_{-1}/k_2 values were obtained from the intercepts $(1/k_1)$ and the ratios of the slope to the intercept respectively. The k_1 and k_{-1}/k_2 values, reproducible within ±4%, are given in Table 2. The k_1 value increases and k_{-1}/k_2 value decreases with increase in temperature. These rate data were compared with that of aqua ligand substitution of *cis*-$[Ru(tap)_2(H_2O)_2]^{2+}$ by 1,10-phenanthroline[10] (Table 2). The k_{-1}/k_2 values reveal that 1,10-phenanthroline (i.e. phen) is a better nucleophile for $[Ru(tap)_2(H_2O)_2]^{2+}$ than 2,2′-bipyridine. The k_1 values at a given tem-

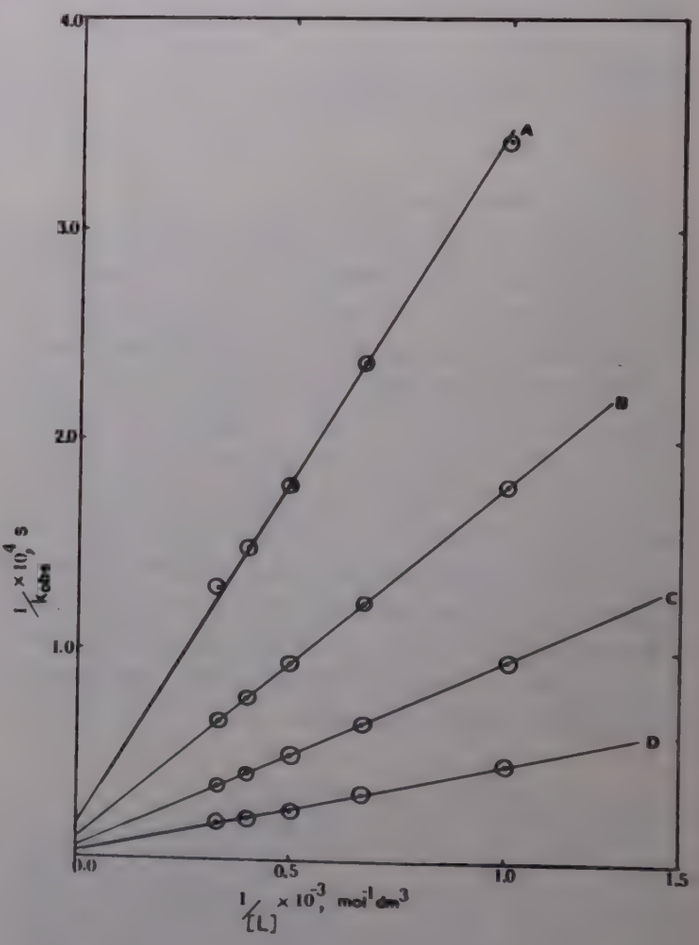

Fig. 1—Plot of $1/k_{obs}$ versus $1/[L]$ at different temperatures (A) 40°, (B) 45°, (C) 50°, and (D) 55°C.

Table 2—Values of k_1 and (k_{-1}/k_2) at different temperatures [complex-I] = 1×10^{-4} mol dm^{-3}, ionic strength = 0.01 mol dm^{-3}, pH = 5.6

System	$k_1 \times 10^4$ (s^{-1})				k_{-1}/k_2			
	40°	45°	50°	55°C	40°	45°	50°	55°C
Complex-I + 2,2′-bipyridine	6.5	11.4	19.2	33.3	0.022	0.019	0.017	0.014
Complex-II + 1,10-phenanthroline	6.2	10.7	17.8	32.0	0.013	0.011	0.010	0.009

perature are almost identical for both the ligands indicating that both the reactions proceed with a common dissociative pathway as proposed in the reaction Scheme 1.

(v) *Effect of varying dielectric constant of the medium on the rate constant*

The solvent effect of the aqua substitution reaction between complex-I and 2,2′-bipyridine has been studied in three ethanol-water mixtures (10, 20 and 30% v/v) at 50°C. In this experiment [ligand] was varied from 1×10^{-3} to 3×10^{-3} mol dm^{-3} under the conditions of [complex-I] = 1×10^{-4} mol dm^{-3}, pH = 5.6, and ionic strength = 0.01 mol dm^{-3}. It has been observed that the pseudo-first order rate constants (k_{obs}) decrease with decrease in dielectric constant of the medium. The k_{obs} values are given in Table 3. From the plots of $1/k_{obs}$ versus 1/[L], k_1 and k_{-1}/k_2 values were calculated. The $k_1 \times 10^4$(s^{-1}) values are 16.67, 14.29 and 11.63 at 10%, 20% and 30% (v/v) ethanol-water mixtures respectively. It is observed that the k_1 values decrease with the increase in organic component of the medium. This result is also consistent with the dissociative mechanism proposed. Laidler-Eyring equation can be used to explain the above facts (Eq. 10).

$$d(\ln k_1)/d(1/D) = e^2Z^2(1/r - 1/r^*)/(2\,kT) \quad \ldots(10)$$

where r and r* are the effective radii of the reactant and activated species respectively, Z is the net charge on the complex ion, k = Boltzman constant, T = temperature in absolute degree and D represent the varying dielectric constant of the medium. Since one water molecule is lost in the activated state of the dissociative process, the size of the activated complex gets reduced i.e. r* becomes smaller than r. Hence, the plot of ln k_1 versus 1/D should be linear with a negative slope according to Eq. (10). That a good linear plot with a negative slope is obtained indicates the dissociative pathway for the reaction process.

(vi) *Effect of temperature on rate constant*

The substitution reaction of aqua ligands from complex-I by 2,2′-bipyridine has been studied at four different temperatures for different [ligand] in aqueous medium. Activation parameters ($\Delta H^{\neq}$ and $\Delta S^{\neq}$) of this system were evaluated from the Eyring plot of ln (k_1h/kT) versus 1/T. The activation parameters thus obtained have been compared with that for the substitution of aqua-ligands of the complex-I by 8-hydroxyquinoline[9] (i.e. oxine) and 1,10-phenanthroline[10]. The almost identical $\Delta H^{\neq}$ value for these systems (Table 4) suggests a dissociative mechanism for the reaction process.

Considering all the above results we suggest a dissociative mechanism for the reaction process. On the slow step complex-I first dissociates into a pentacoordinated intermediate, $[Ru(tap)_2(H_2O)]^{2+}$ with the loss of one water molecule. Then this intermediate reacts rapidly with 2,2′-bipyridine to form [Ru(tap)$_2$(bipy)]. Attachment of one donor nitrogen atoms of 2,2′-bipyridine to the intermediate increases the electron density on ruthenium(II) and as a result the second water molecule is labilised, leading to rapid chelation.

Table 3—Values of rate constants (10^5 k_{obs}, s^{-1}) in various ethanol-water mixtures

[complex-I] = 1×10^{-4} mol dm^{-3}, pH = 5.6 and ionic strength = 0.01 mol dm^{-3}

[L] × 10^3 (mol dm^{-3})	10%	20%	30% (v/v)
1.0	8.7	7.1	5.5
1.5	12.9	10.5	8.1
2.0	16.7	13.6	10.6
2.5	20.1	16.5	12.8
3.0	23.3	19.2	15.0

Acknowledgement

We are thankful to the UGC, New Delhi for providing the financial assistance and a junior research fellowship to BM.

Table 4—Activation parameters

System	$\Delta H^{\neq}$ (kJ mol^{-1})	$\Delta S^{\neq}$ (JK^{-1}mol^{-1})	Ref.
cis-$[Ru(tap)_2(H_2O)_2]^{2+}$ + bipy	89.9 ± 0.5	− 19.1 ± 0.3	This work
cis-$[Ru(tap)_2(H_2O)_2]^{2+}$ + oxine	82.4	− 37.1	9
cis-$[Ru(tap)_2(H_2O)_2]^{2+}$ + phen	88.7	− 23.2	10

References

1 Allen R J & Ford P C, *Inorg Chem*, 11 (1972) 696.
2 Ojo J F, Olubuyide O & Oyetunji O, *J chem Soc Dalton Trans*, 4 (1987) 957.
3 Mallick D & De G S, *Trans met Chem*, 16 (1991) 289.
4 Mallick D & De G S, *Indian J Chem*, 30A (1991) 509.
5 Hoddenbagh J M A & Macartney D H, *Inorg Chem*, 25(3) (1986) 380.
6 Filho J C N & Franco D W, *Inorg chim Acta*, 113(1) (1986) 55.
7 Kallan T W & Earley J E, *J chem Soc Chem Commun*, (1970) 851.
8 Davies N R & Mullins T L, *Aust J Chem*, 21 (1968) 915.
9 Mahanti B & De G S, *Trans met Chem* (in press).
10 Mahanti B & De G S, *Bull chem Soc Jpn* (in press).
11 Goswami S, Chakravarty A R & Chakravarty A, *Inorg Chem*, 20 (1981) 2246.
12 Goswami S, Chakravarty A R & Chakravarty A, *Inorg Chem*, 22 (1983) 603.
13 Glasstone S, *Text book of physical chemistry* (Macmillan, London) 1977, p. 1116.
14 Martell A E & Calvin M, *Chemistry of the metal chelate compounds* (Prentice-Hall, New Jersey) 1962, p. 524.
15 Kruse W & Taube H, *J Am chem Soc*, 83 (1961) 1280.

Indian Journal of Chemistry
Vol. 31A, September 1992, pp. 693-698

Electrochemical oxidation of 5, 6-dihydroxytryptamine at solid electrodes

R N Goyal
Department of Chemistry, University of Roorkee, Roorkee 247 667

Received 18 November 1991; revised and accepted 24 February 1992

The electrochemical oxidation of indolic neurotoxin 5, 6-dihydroxytryptamine has been studied at solid electrodes in *p*H 7.2 phosphate buffer. The oxidation of 5, 6-DHT occurs in one 2e, $2H^+$ step associated with adsorption complications at glassy carbon and pyrolytic graphite electrodes, whereas, purely diffusion controlled electrode process has been observed at platinum electrode. The analysis of cyclic voltammograms indicated the process to be an EC mechanism. The major product of oxidation has been isolated by using HPLC and has been identified as 2, 7′-bi(5, 6-dihydroxytryptamine). The intracranial injection of 2, 7′-bi(5, 6-DHT) in albino mice has been found to produce a substantial neurotoxic effect.

Over the last few years, it has been established that 5, 6-dihydroxytryptamine (5, 6-DHT) induces a substantial degree of chemical degeneration of indoleamine containing neurons in the rat brain[1,2]. A single 50 μg dose of 5, 6-DHT has been found to produce relatively specific depletion of serotonin after intraventricular injection to 40-60% of control values[3,4]. As the neurotoxicity of 5, 6-dihydroxy-tryptamine is believed from its ease of oxidation. a large number of autooxidation studies on 5, 6-DHT have been carried out and various theories have been suggested to account for the autooxidation of 5, 6-DHT to its neurodegenerative activity[5,8]. Literature survey revealed that inspite of chemical lesioning property of serotonergic neurons of 5, 6-DHT, no attempt has been made so far to study its electrochemical behaviour. This paper describes the electrochemical behaviour of 5, 6-DHT at three solid eletctrodes at physiological *p*H using variety of techniques. It is observed that oxidation of 5, 6-DHT at glassy carbon (GCE) and pyrolytic graphite electrodes (PGE) is associated with adsorption complications, whereas a purely diffusion controlled oxidation occurred at platinum electrode. The major product of oxidation has been identified by use of High performance Liquid Chromatography—mass spectrometry and has been found to be neurotoxic in mice. Information on the electrode mechanism is also presented.

Materials and Methods

5, 6-dihydroxytryptamine (creatinine sulfate salt) (Sigma, USA) was used as such. Preliminary experiments on linear and cyclic sweep voltammo-grams were carried out by using the equipments as reported earlier[9]. More elaborate experiments were carried out using a BAS 100A system after correcting for IR drop. All potentials are referred to the SCE at ambient temperature (22 ± 2°C). The area of electrodes were measured using a potentiostatic method with 4.0 m*M* potassium ferrocyanide in 0.5 *M* KCl as reported by Adams[10] and were 0.025, 0.021 and 0.020 cm^2 for platinum, PGE and GCE respectively. Phosphate buffers of ionic strength 0.1*M* were prepared by the reported method[11], All test solutions were thoroughly bubbled with purified nitrogen for 8-10 min before voltammograms were recorded.

Controlled potential electrolysis was carried out in a conventional electrolysis cell using platinum counter electrode and SCE as a reference electrode. The working electrode was either a pyrolytic graphite plate (6×1.5 cm^2), platinum foil (4×1 cm^2) or two glassy carbon rods (6×0.2 cm^2). Purified nitrogen was bubbled continuously throughout the course of electrolysis. The electrolysis was fast for first 15-20 min and then became slow and only background oxidation was observed after 40-50 min. At this stage the electrodes were found heavily coated with a thin film of black shining material. The proper cleaning of electrodes caused electrolysis to continue again. Several such cleanings were required to achieve about 90-95% oxidation of 5, 6-DHT. High performance chromatography employed a BioRad gradient instrument equipped with dual pumps, an apple IIe controller and an ISCO model UV detector. A Rheodyne model 7125 loop injector was used to inject 2.0 ml solution in a reversed phase column (Brownlee RP-18) to which a short guard column was attached. The mobile phase solvents were prepared as follows: Solvent 1 was prepared by adding 10 ml of NH_4OH and 20 ml of methanol to 970 ml of water. The *p*H of

this solution was adjusted to 3.25 by adding formic acid. Solvent 2 was prepared by adding 10 ml of NH_4OH and 400 ml of methanol to 590 ml of water and *p*H was adjusted to 3.25 with formic acid. The gradient employed in HPLC was as follows: 0-16 min 100% solvent 1 at flow rate of 1.5 ml/min; 16 to 35 min linear gradient to 5% solvent 2 with increase in flow rate to 2.5 ml/min; 35 to 50 min linear gradient to 60% solvent 2, which was maintained for 5 min and then returned to 100% 1 over 5 min. The column was equilibrated for 10 to 15 min with 100% of 1 before making another injection.

The mass spectrum of the product was recorded using Hewlett Packard 5985 B instrument and ^{1}HNMR spectrum was recorded with a Varian 300 XL spectrometer.

The neurotoxic studies were carried out in male albino mice (15-20 g), which were housed ten per cage with access to water and food *ad libitum*. They were maintained on a 12 hr light/12 h dark schedule and the temperature of the room was maintained at 21 ± 1°C. The product of electrooxidation was dissolved in an appropriate volume of isotonic saline. The animals were anesthetized with diethyl ether and 5 µl of the solution was injected in the vicinity of the lateral ventricle with a 25 µl Hamilton syringe employing a disposable needle. A teflon stop was placed on the needle so that the penetration depth in the brain, as measured from the outside of the skin covering skull, was fixed at 3 mm. The behavioural changes were then monitored.

Results and Discussion

Linear and cyclic sweep voltammetry

Linear sweep voltammetry of 5, 6-dihydroxy-tryptamine in the *p*H range 3.2-8.8 exhibited a single well defined oxidation peak at PGE, GCE and platinum electrodes at a sweep rate of 5 mVs^{-1}. The peak at platinum electrode was more broad in comparison to PGE and GCE. The peak potential of the oxidation peak I_a was dependent on *p*H and shifted to less positive potential with increase in *p*H, nevertheless, the potential of oxidation peak I_a was practically similar at all the three electrodes at a particular *p*H. The broad shape of peak at lower *p*H values did not permit determination of accurate E_p at a sweep rate of 5 or 10 mVs^{-1} and hence the relation of E_p versus *p*H are plotted at a sweep rate of 200 mVs^{-1}, where the oxidation peak was well observed at all the three electrodes used. The dependence of E_p versus *p*H can be represented by the equation

$$E_p(pH\ 3.2\text{-}8.8) = [0.057\ pH - 0.51] \text{ versus SCE}$$

at all the three electrodes. The peak current (i_p) of the oxidation peak I_a was found practically independent of *p*H in the range 3.0-8.8 at all the three electrodes used. The i_p values at platinum electrode were quite reproducible, whereas at GCE and PGE, average of atleast three replicate determinations was taken to calculate the peak current. The values thus obtained gave a deviation of ±5% and hence indicated *p*H independent nature of the peak current.

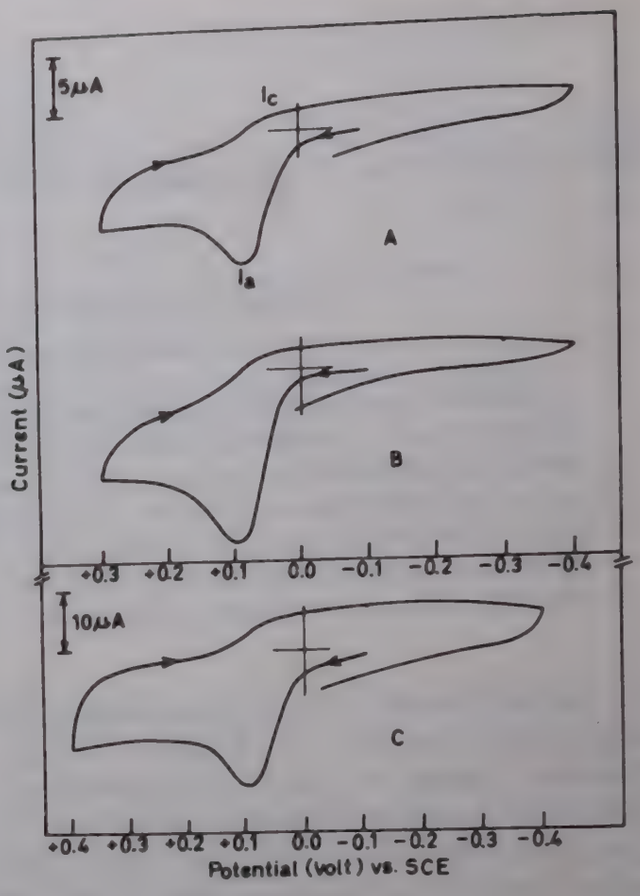

Fig. 1—Typical cyclic voltammograms of 0.5 m*M* 5, 6-DHT at different solid electrodes; (A) Pt; (B) GCE and (C) PGE electrode; *p*H 7.2 and sweep rate 200 mVs^{-1}

Cyclic sweep voltammetry of 0.5 m*M* solution of 5, 6-DHT at 200 mVs^{-1} exhibited a well defined oxidation peak (Ia) when sweep was initiated in the positive direction. In the reverse sweep, a cathodic peak I_c was observed which formed a quasi-reversible couple with peak I_a. Peak I_c was not clearly observed in the *p*H range 3.2-7.2 at a sweep rate > 100 mVs^{-1} at all the electrodes rather it had a bump shape, whereas with increase in sweep rate the peak I_c became more clear and took a well-defined shape at sweep rate > 500 mVs^{-1}. A comparison of cyclic voltammograms of 5, 6-DHT at *p*H 7.2 at the three electrodes is presented in Fig. 1. The increase in sweep rate from 100 mVs^{-1} to 20.4 Vs^{-1} caused a sharp increase in the peak currents for peak I_a and peak I_c and the ratio of peaks I_c/I_a increased from 0.34 to 0.75 at PGE, whereas, this ratio varied from 0.1 to 0.46 at GCE and platinum electrodes. The increase in

Table 1—Dependence of peak I_c on the sweep rate at PGE for 0.5 m*M* 5, 6-dihydroxytryptamine in phosphate buffer of *p*H 7.2

V, mVs^{-1}	i_a, μA	i_c, μA	i_c/i_a
200	35.7	12.1	0.34
500	73.2	29.8	0.41
1000	131.0	64.5	0.49
2003	233.0	139.5	0.59
5007	342.1	203.1	0.59
10240	402.0	288.0	0.71
20480	510.0	382.5	0.75

peaks I_a and I_c with increase in sweep rate is presented in Table 1. Hence, it was concluded that the species generated in peak I_a reaction is highly unstable and rapidly undergoes chemical reactions to give the ultimate products. The cyclic voltammograms observed at different electrodes were also analysed for various criterions suggested by Nicholson and Shain[12] to detect if the electrode process is coupled with chemical reactions. It was observed that the plots of i_a/i_c versus log V and $\Delta E_{p/2}/\Delta \log V$ versus log V were S-shaped at all the electrodes and hence confirmed the redox mechanism of 5,6-DHT as EC mechanism in which charge transfer is followed by an irreversible chemical reaction. Some of the typical i_a/i_c versus log V and $\Delta E_{p/2}/\Delta$ log V versus log V relations obtained are depicted in Fig. 2. The effect of concentration on peak I_a was studied in the concentration range of 20 μ*M* to 1.5 m*M* at all the three electrodes. It was observed that the peak current for peak I_a increased with increasing concentration of 5, 6-DHT. However, the plots of i_p versus concentration provided an interesting information that the plot was linear upto ~ 0.25 m*M* at PGE and had a tendency to limit at higher concentrations. Almost similar behaviour was observed at GCE, whereas, a linear relation is observed in the entire concentration range at platinum electrode. Thus, it was concluded that the electrode reaction for peak I_a is associated with adsorption complications at PGE and GCE[15,16] whereas, purely diffusion controlled reaction is occurring at platinum electrode. The adsorption complications at GCE and PGE are further confirmed by determining the peak current function with variation in sweep rate in the range 5 mVs^{-1} to 20 Vs^{-1}. The plots of peak current ratio ($i_p/\sqrt{V}$) versus log V for 5, 6-DHT at PGE and GCE are presented in Fig. 3A and 3B and clearly indicate that the peak current function increases with increase in sweep rate even at 2 m*M* concentration of 5, 6-DHT and hence provided further evidence that the electrode reaction at PGE and GCE are associated with adsorption complications. On the other hand, the plot of i_p versus log V at 0.5 m*M* concentration of 5,

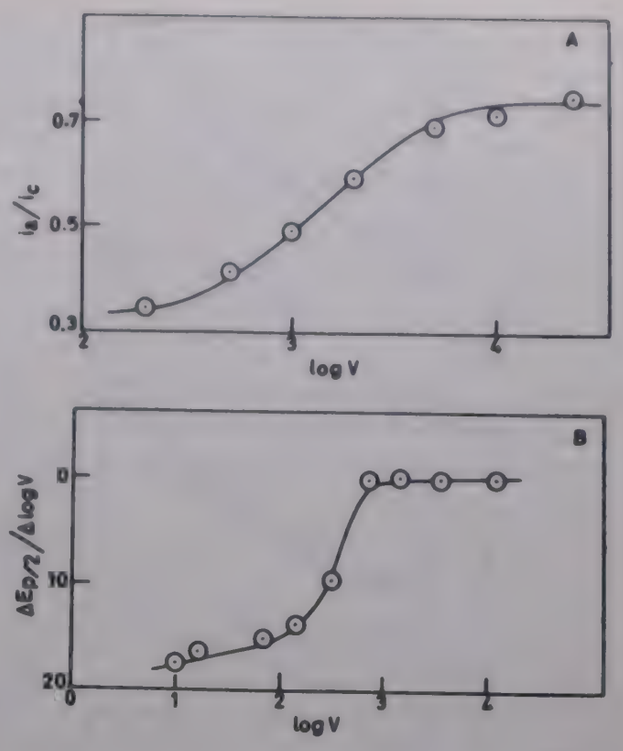

Fig. 2—Observed dependence of (A) i_a/i_c and (B) $E_{p/2}$/log V on log V for 0.5 m*M* DHT at *p*H 7.2

6-DHT at platinum electrode is presented in Fig. 3C and is practically constant, suggesting thereby purely diffusion controlled nature of the electrode reaction. To eliminate adsorption complications observed at PGE and GCE, attempts were made to record voltammograms in presence of anionic surfactants, viz., sodium octylsulfate (SOS) and sodium dodecylsulfate (SDS). It was observed that at *p*H 7.2, the concentrations of SOS or SDS upto ~ 18 m*M* (4 mg/ml) were not sufficient to completely eliminate the adsorption complications as evidenced by the increase in peak current function with increase in sweep rate.

The peak potential for peak I_a was also found to shift to more positive potentials with increase in sweep rate at all the three electrodes. used. The plots of E_p versus log V for different concentrations of 5, 6-DHT at all the three electrodes were linear in nature with correlation coeff. 0.98. The value of dE_p/dlog V obtained at platinum electrode was found as 18 mV and 30 mV for 0.1 and 2.0 m*M* concentration of 5, 6-DHT.

The value of n, number of electrons involved in oxidation, were determined by controlled potential electrolysis at *p*H 7.2 at all the three electrodes used and it was found that ~ 0.5 m*M* solution of 5, 6-DHT generally took ~ 4 hr for complete oxidation at GCE and platinum, whereas much longer time was required at PGE probably due to excessive adsorption complications. The values of n

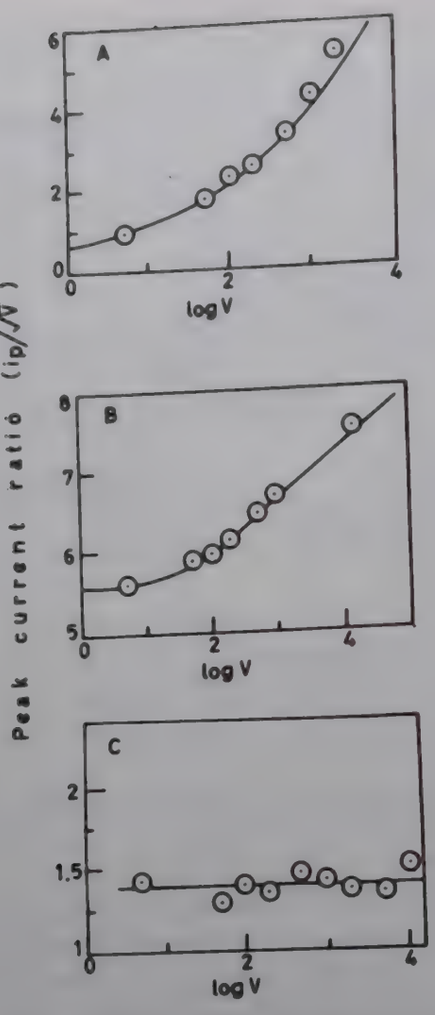

Fig. 3—Dependence of peak current (I_a) on log V at (A) PGE; (B) GCE and (C) platinum. Concentration of 5, 6-DHT for A and C is 0.5 mM and for B is 2.0 mM

determined at various concentrations of 5, 6-DHT were 1.87 ± 0.07 (0.1 mM); 2.04 ± 0.06 (0.2 mM) and 2.04 ± 18(0.5 mM) respectively. In general, it was observed that n-values at PGE exhibited a large deviation from the average value. This behaviour is probably due to the adsorption and rapid polymerization of the products generated in the electrode reaction.

High performance liquid chromatography

The progress of electrolysis of oxidation of 5, 6-DHT was also monitored by using HPLC. Fig. 4A presents chromatogram observed for 1 mM 5, 6-DHT at pH 7.2 just before electrooxidation at PGE, and exhibited a peak at ~19.4 min. The peak at 12 min is due to creatinine and hence no attempt was made to identify it. With progress of electrolysis, peak 3 systematically decreased (Fig. 4) and two new peaks 2 and 4 immerged in the chromatogram. Peak 4 increased up to ~ 90 min and then became almost constant. Peak 2, on the other hand, did not increase and remained constant throughout the course of electrolysis at all the electrodes and hence is considered as a minor product of oxidation. The material collected under peak 2 was never sufficient to get information on its structure. However, the UV spectrum of the volume collected in mobile phase (pH 3.25) exhibited λ_{max} at 302 nm. The UV spectrum of HPLC peak 4 in mobile phase gave a well defined band at 236 nm. Several injections of 2.0 ml each were made in HPLC and volume under peak 4 was collected and lyopholized. The freeze dried material thus obtained was desalted to remove the mobile phase and buffer constituents (see Experimental) and the light orange coloured material obtained had a m.p. 230°C (decomposed). The mass spectrum of this product gave a clear molecular ion peak at m/e = 382. The other high mass peaks observed in the spectrum were at 369(5.5%); 368(7.8%); 256(2.6%); 242(1.0%); 236(1.1%); 227(1.2%); 209(1.5%); 208(2.1%) and 193(1.6%). However, no attempt was made to explain the fragmentation pattern. The molar mass of 382 indicated that the product formed from 5, 6-DHT should be a dimer. Several dimers and oligomers have been reported during autooxidation as well as electrochemical oxidation of 5-hydroxytryptamine[15,16]. The ^{1}HNMR spectrum of the material gave signals at $\delta = 10.38$ (s, 1H, N – H);

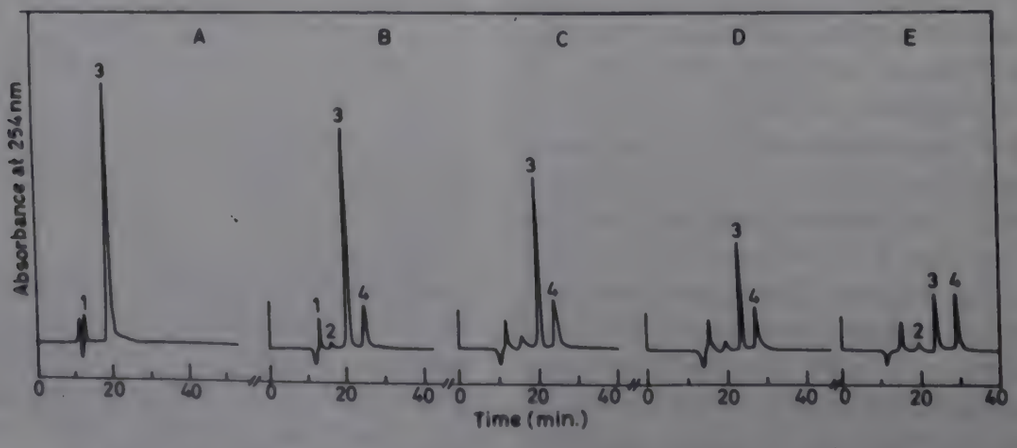

Fig. 4—HPLC chromatograms observed during oxidation of 0.5 mM 5, 6-DHT at pH 7.2 PGE pot. 800 mV versus SCE. (A) 0 min; (B) 45 min; (C) 75 min; (D) 135 min and (E) 240 min of electrolysis

9.90(s, 1H, N−H); 8.90(s, 1H, N−H); 8.68(s, 1H, OH); 8.16(s, 1H, OH); 8.12(s, 3H, $-NH_3^+$); 8.0 (s, 1H, OH); 7.74 (s, 3H, NH_3^+); 6.89(s, H); 6.84(s, H) and 6.84(s, H). The aliphatic protons were observed as a multiplet at 2.85 (m, 4H, $-CH_2CH_2$) and 2.75(m, 4H, $-CH_2CH_2$). The protons attached to carbon were identified by adding D_2O, which caused the disappearance of peaks except at 6.87, 6.84 and 6.80. The NMR and UV spectra obtained were also compared with the autooxidation product of 5,6 -DHT and it was interesting to observe that the NMR and UV spectra were basically similar to 2, 7′-bi(5, 6-DHT) as reported by Singh *et al.*[17]. Thus, it was concluded that the major product of electrochemical oxidation of 5, 6-DHT at the solid electrodes is similar to the autooxidation product and found to be 2, 7′-bi(5, 6-DHT).

The cyclic voltammogram of a dilute solution of 2, 7′-dimer of 5, 6-DHT was also recorded in phosphate buffer of *p*H 7.2 and it was interesting to observe that it is electroactive in nature. A well defined oxidation peak at slightly more positive potential than 5, 6-DHT was observed when sweep was initiated in the positive direction. Hence, it was concluded that a part of 2, 7′-bi(5, 6-DHT) undergoes further oxidation at peak I_a potential to give black polymeric products, which deposited at the electrode surface and hence the frequent cleaning of electrodes was required during controlled potential electrolysis. Nevertheless, analysis of cyclic voltammograms always indicated the electrode process to be an EC process. Thus it was concluded that under cyclic voltammetric conditions, electrode reaction is basically EC process, whereas, under controlled potential conditions, the reaction has a tendency to change from EC to ECE process.

Redox mechanism

The electrochemical oxidation of 5, 6-dihydroxytryptamine appears to be a complex process and under CV and controlled potential conditions the mechanisms are basically EC and ECE process respectively. Under controlled potential conditions and cyclic voltammetric conditions at platinum electrode, 5, 6-DHT oxidised in 2e, $2H^+$ reaction to give 2, 7′-bi(5, 6-dihydroxytryptamine) as the major product of oxidation. The 2e, $2H^+$ oxidation of 5, 6-DHT may occur in a single 2e step or two 1e steps. As no radical species has ever been detected in the autooxidation or electrochemical oxidation of 5, 6-DHT, it seems reasonable to conclude that 5, 6-DHT oxidizes in a single 2e, $2H^+$ step to quinonoid intermediate (II) as shown in Scheme 1. At high voltage sweep, the cathodic peak I_c involves reduction of species II_a to I, whereas, at low sweep rate, kinetic step of attack of nucleophile becomes more important and generation of III becomes fast. Species II is electron deficient and hence can be attached at position 4 or 7 by a nucleophile OH^- or the substrate 5, 6-DHT itself. These positions have been considered more susceptible for nucleophilic attack during synthesis of a series of methyl substituted 5, 6-dihydroxytryptamines[18]. Thus, the attack of OH^- on II can lead to a mixture of 4, 5, 6- and/or 4, 5, 7-trihydroxytryptamines, which are expected to rapidly undergo polymerization as reported in literature[17,19,20]. Position 2 of 5, 6-DHT is expected to be most nucleophilic as reported for indoles[15] and hence the attack of substrate through position 2 at species II_b can lead to the formation of 2, 4′- or 2, 7′-bi(5, 6-DHT). Analysis of the product formed and comparison of NMR spectrum with 2, 7′-dimer of 5, 6-DHT clearly indicated that the product formed during oxidation of 5, 6-DHT at all the three electrodes is 2 7′-bi(5, 6-dihydroxytryptamine). It is very likely that HPLC peak 2 is due to the formation of trihydroxy compounds and their rapid polymerization did not permit the increase in HPLC peak 2.

Preliminary neurotoxic studies

5, 6-Dihydroxytryptamine has been reported to be a selective neurotoxin for 5-hydroxytryptamine depletion in mice brain. So it was considered worthwhile to evaluate the behavioural changes after intracranial injection of its electrochemical oxidation product. The behavioural changes in mice were observed after intracranial injections of different amounts of 2,

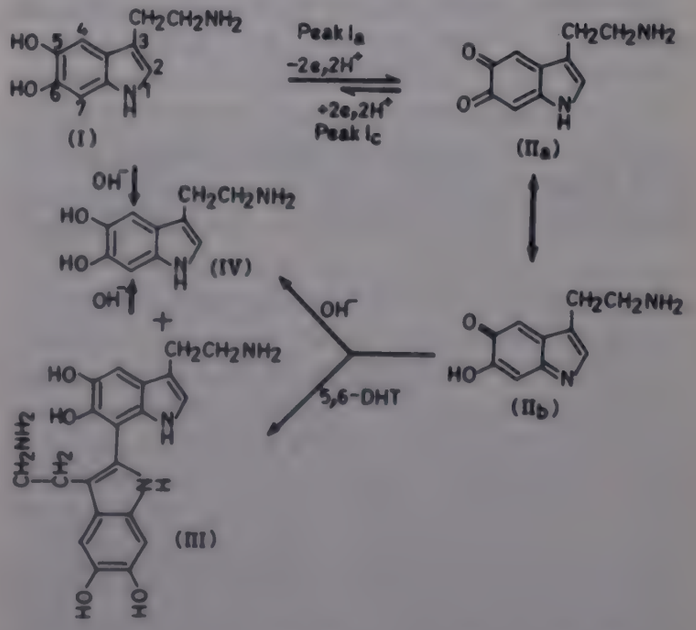

Scheme 1—Tentative mechanism proposed for the EC oxidation of 5, 6-DHT at physiological *p*H.

7′-bi(5, 6-dihydroxytryptamine). An injection of 50 μg of the oxidation product caused a contralateral motion after ~ 30 min of injection followed by trembling. After ~ 90 min, the animal started rolling in the cage and trembling increased. This behaviour continued for about 20-30 min and then the animal became almost normal. At higher doses (125 and 150 μg), the contralateral motion was followed by rapid rolling over and jumping. The animal had difficulty in walking and died after 3 hr of injection. Thus, the preliminary studies clearly indicated that the oxidation product of 5, 6-dihydroxytryptamine produces substantial degree of neurtotoxicity in mice, which caused behavioural changes. It is possible that the formation of 2, 7′-bi(5, 6-dihydroxytryptamine) by the oxidation of 5, 6-DHT in the brain is responsible for the neurotoxicity of this compound.

The results presented above clearly indicate that electrooxidation of serotonergic neurotoxin, 5, 6-dihydroxytryptamine occurs in a 2e, $2H^+$ reaction at all the three electrodes used to give quinonoid species(II). The nucleophilic attack by 5, 6-dihydroxytryptamine on II ultimately gives 2, 7′-bi(5, 6-DHT) as the main product of oxidation. It is of some interest to note that the electrode reaction at both PGE and GCE is associated with adsorption complications, which could not be eliminated even by adding 2.0 m*M* concentration of sodium octylsulfate or sodium dodecyl sulfate. However, the electrode reaction at platinum electrode was free from adsorption complications and hence this electrode is suitable for determination of 5, 6-DHT in a large concentration range of 20 μ*M* to 1.5 m*M*.

The electroactive nature of the main oxidation product, 2, 7′-bi(5, 6-DHT) at slightly positive potential than 5, 6-DHT implies that a part of 2, 7′-bi(5, 6-dihydroxytryptamine) further undergoes oxidation. Nevertheless, an almost constant HPLC peak height of peak 4, even after several hours of electrolysis, clearly indicated that 2, 7′-dimer remains in solution for quite a long time and hence its further oxidation is only a side reaction, which was confirmed by an EC mechanism. The electro-oxidation of 5, 6-dihydroxytryptamine in acidic *p*H appears to give more than one product and is presently under investigation.

Acknowledgement

I am thankful to M/s Pfizer, USA for providing a gift sample of pyrolytic graphite.

References

1 Baumgarten H G, Klemn H P, Lachenmeyer L, Lovenberg W & Schlossberger H G, *Ann N Y Acad Sci*, 305 (1978) 3.
2 Wolf W A & Bobik A, *J Neurochem*, 50 (1988) 534.
3 Massoti M, Scotti A & Longo V G, *Pharmacol Biochem and Behaviour*, 2 (1974) 769.
4 Baumgarten H G, Lachenmeyer L & Schlossberger H G, *Zellforsch Z*, 125 (1972) 553.
5 Creveling C R & Rotman A, *Ann N Y Acad Sci*, 305 (1978) 57.
6 Johnson G, *Ann Rev Neurosçience*, 3 (1980) 169.
7 Baumgarten H G, Klemn H P, Sievers J & Schlossberger H G, *Brain Res Bull*, 9 (1982) 131.
8 Baumgarten H G, Jenner S, Bjorklund, Klemn H P & Schlossberger H G, *Biology of serotonergic neurotransmission*, edited by N N Osborne, (Wiley, N Y) 1983.
9 Goyal R N, *Indian J Chem*, 26A (1987) 656.
10 Adams R N, *Electrochemistry at solid electrodes* (Marcel Dekker, N Y) 1969, 202.
11 Christian G D & Purdy W C, *J electroanal Chem*, 3 (1962) 363.
12 Nicholson R S & Shain I, *Analyt Chem*, 36 (1964) 706.
13 Wopschall R H & Shain I, *Analyt Chem*, 39 (1967) 1514.
14 Brown E C & Large R F, *Techniques of chemistry*, edited by A Weissberger & R W Rossiter (Wiley Interscience, N Y) 1974, 423.
15 Anne A & Moiroux J, *J org Chem*, 53 (1988) 2816.
16 Wrona M Z & Dryhurst G, *Bioorg Chem*, 18 (1990) 291.
17 Singh S, Jen J F & Dryhurst G, *J org Chem*, 55 (1990) 1484.
18 Sihnababu A G, Ghosh A K & Borchardt R T, *J Med Chem*, 28 (1985) 1273.
19 Klemn H P, Baumgarten H G & Schlossberger H G, *J Neurochem*, 35 (1980) 1400.
20 Wrona M Z, Westmark P, Goyal R N & Dryhurst G, *Electroorganic synthesis*, edited by R D Little & N L Weinbereg (Marcel Dekker, Inc., New York) 1991, 289.

Indian Journal of Chemistry
Vol. 31A, September 1992, pp. 699-701

Notes

σ-Bonded organometallics of iron and their facile conversion into π complexes

I Ahmed, J U Ahmad, M M Karim, S I Sarder & S S Ullah*
Department of Chemistry, Jahangirnagar University, Savar, Dhaka, Bangladesh

Received 17 July 1991; revised and accepted 15 January 1992

The metal carbonylate anion, $Na[Fe(\eta^5\text{-}C_5H_5)(CO)]$ reacts at room temperature with halogeno organic ligands 1,3,5-tris(bromomethyl)benzene and 1,2,4,5-tetrakis-(bromomethyl)benzene to give the complexes 1,3,5-tris-(σ-methylene) benzene{tris(η^5-cyclopentadienyl)hexacarbonyliron} (**1**) and 1,2,4,5-tetrakis(σ-methylene)benzene{tetrakis(η^5-cyclopentadienyl) octacarbonyliron} (**3**). The complex (**1**) undergoes thermal transformation to the corresponding π complex whereas, complex (**3**) does not due to the 18-electron rule formalism.

Metal-carbon σ-bonded organometallic compounds are prepared usually by the reaction of metal carbonylate anions and their derivatives with halogeno organic ligands[1-7]. Various halogeno organic ligand complexes with transition metals and their derivatives have been reported from our laboratory, such as 1,2-bis(σ-methylene)-benzenetetracarbonyliron, 4,5-dimethyl-1,2-bis-(σ-methylene)benzenetetracarbonyliron, 2,3,5,6-tetramethylenebicyclo[2,2,0]hexanehexacarbonyldiiron and 1, 2, 3, 4,5,6-hexamethylenecyclohexanenonacarbonyltriiron, etc. In continuation of these studies, we report herein, the results of our investigations on the reactions of $Na[CpFe(CO)_2]$ with 1,3,5-tris(bromomethyl)benzene, and 1,2,4,5-tetrakis(bromomethyl)benzene.

Experimental

All reactions and workups were carried out under nitrogen atmosphere. Infrared spectra were recorded on a PE-983 spectrophotometer and PMR spectra on a Varian XL-200 spectrometer.

The starting materials and $Na[CpFe(CO)_2]$ were prepared according to the known procedure[8]. Tetrahydrofuran (THF) was distilled over sodium and benzophenone prior to use.

1,3,5-Tris(bromomethyl)benzene and 1,2,4,5-tetrakis(bromomethyl)benzene were prepared by the known procedure[9].

Preparation of 1,3,5-*tris*(σ-methylene)benzene{-tris(η^5-*cyclopentadienyl*)*hexacarbonyliron*} (**1**)

To a suspension of sodium cyclopentadienyldicarbonyliron (6.0g, 30.0 mmol) in THF (30 cm^3) was added dropwise a solution of 1,3,5-tris(bromomethyl)benzene (3.6g, 10.0 mmol). The reaction mixture was stirred at room temperature for 24 hr, the solvent removed *in vacuo* and the residue extracted twice with petroleum ether (40-60°C), filtered and the filtrate conentrated *in vacuo* to obtain a deep yellow crystalline solid, m.p. 88-90°C (1.40g, 32%) [Found: C, 56.07 H, 3.35. $C_{30}H_{24}O_6Fe_3$ requires: C, 56.00; H, 3.30%[5].

Thermal reaction of 1,3,5-*tris*(*bromomethyl*)*benzene with sodium* (η^5-*cyclopentadienyl*)*dicarbonylferrate*

A THF solution (30 cm^3) of 1,3,5-tris(bromomethyl)benzene (3.6g, 10 mmol) was added dropwise to a suspension of sodium (η^5-cyclopentadienyl)dicarbonylferrate (6.0g, 30 mmol) and refluxed for 5 hr. The colour of the reaction mixture changed from reddish-black to red.

The solvent was removed *in vacuo* and the residue extracted twice with petroleum ether (40-60°C), filtered through the Kieselguhr. The filtrate was concentrated *in vacuo* to get a deep red solid. Chromatographic separation of the red solid on a column of silica gel (60-120 mesh) eluted with petroleum ether (40-60°C) afforded 1,3,5-tris(η^3-allylene)cyclohexane {tris-(η^5-cyclopentadienyl)tricarbonyltriiron (**2**) (1.60g, 45%), m.p. 103-105°C [Found: C, 56.85; H, 4.50. $C_{27}H_{24}Fe_3O_3$ requires: C, 57.47; H, 4.26%].

Preparation of 1,2,4,5-*tetrakis*(σ-*methylene*)*benzene*{*tetrakis*(η^5- *cyclopentadienyl*)*octacarbonyltetrairon*} (**3**)

To a suspension of sodium (η^5-cyclopentadienyl)dicarbonylferrate (0.8g, 4 mmol) in freshly distilled THF (30 cm^3) was added dropwise 1,2,4,5-tetrakis-(bromomethyl)benzene , (0.46g, 1 mmol) at room temperature with stirring for 24 hr. The solvent was removed *in vacuo* and the residue extracted twice with petroleum ether (40-60°C) (40 cm^3) and filtered through the kieselguhr.

The filtrate was dried *in vacuo* to get a deep red solid mass which when chromatographed on silica eluting with petroleum ether (40-60°C) gave a deep red solid (0.16g, 34%), m.p. 99-101°C [Found: C, 55.50; H, 3.15. $C_{38}H_{30}O_8Fe_4$ requires: C, 54.30; H,3.50%].

Thermal reaction of 1,2,4,5-*tetrakis*(*bromomethyl*)-*benzene with sodium* (η^5-*cyclopentadienyl*)*dicarbonylferrate*

1,2,4,5-Tetrakis(bromomethyl)benzene (0.46g, 1.0 mmol) in freshly distilled THF (40 cm^3) was added to a suspension of sodium (η^5-cyclopentadienyl)-dicarbonylferrate (0.8g, 4 mmol) and heated under reflux for 4 hr. The solvent was removed *in vacuo* and the residue extracted twice with petroleum ether (40-60°C) (40 cm^3) and filtered through the kieselguhr. Removal of solvent from the filtrate gave a red solid. Chromotographic separation of the red solid on silica eluting with petroleum ether (40-60°C) afforded a deep red solid, m.p. 95-97°C (0.15g, 29%) [Found: C, 55.65; H, 4.05. $C_{34}H_{30}O_4Fe_4$ requires: C, 56.18; H, 4.13%].

Results and discussion

The reaction of 1,3,5-tris-(bromomethyl)benzene with $Na[CpFe(CO)_2]$ in THF at room temperature under nitrogen resulted in the isolation of 1,3,5-tris-(σ-methylene) benzene(tris(η^5-cyclopentadienyl)hexacarbonyltriiron) (**1**) (32%) as a deep yellow crystalline solid. The compound (**1**) undergoes thermal transformation of the π-complex to 1,3,5-tris(η^3-allylene)cyclohexane{tris-(η^5-cyclopentadienyl)tricarbonyltriiron} (**2**). Although we did not heat directly the complex 1,3,5-tris(σ-methylene) benzene {tris(η^5-cyclopentadienyl)hexacarbonyltriiron}, by analogy with the reaction of other σ-complexes, we could come to a conclusion that 1,3,5-tris(σ-methylene)-benzene{tris(η^5-cyclopentadienyl)hexacarbonyltriiron} first formed from 1,3,5-tris(bromomethyl)benzene and sodium (η^5-cyclopentadienyl)-dicarbonylferrate converts to 1,3,5-tris(η^3-allylene)-cyclohexane {tris(η^5-cyclopentadienyl)tricarbonyltriiron}.

The IR spectrum of the complex (**1**) in nujol mull exhibited two sharp ν CO bands at 2003 and 1957 cm^{-1} in agreement with a *cis*-dicarbonyl arrangement. The PMR spectrum of complex (**1**) displayed a singlet at δ 2.30, which accounts for the methylene protons. This type of high field shift for methylene protons is also observed for analogous complexes[1,2,4]. The signal at δ7.16 clearly indicates that the aromaticity of the benzene ring is retained. The signal at δ4.66 is assigned to the cyclopentadienyl protons.

The mass spectrum of the complex showed molecular ion peak, m/z at 648, and the successive loss of three cyclopentadienyl groups and 6 CO groups was also observed.

The π complex (**2**) was prepared by the elimination of CO from the corresponding σ complex by pyrolysis. Spectral data show that the complex (**2**) contains three Fe(CO) (Cp) moieties where the aromaticity of the benzene ring is totally lost. This type of examples are known where benzene ring behaves as a diene or triene ligand[6], with all the π electrons of the benzene ring grouped into three butadiene fragments for coordination. The IR spectrum of the complex in cyclohexane exhibited only one ν(CO) band at 1945 cm^{-1}. The PMR spectrum of (**2**) in $CDCl_3$ at 25°C displayed resonances at δ0.34 (d, 3H, J = 3Hz, Hc), 0.87 (t, 3H, J = 4Hz, Hb), 1.15 (d, 3H, J = 3Hz, Ha) and 4.65 (s, 15H, Cp protons) with the intensity ratio 1:1:1:5.

The protons Hc being nearer to the metal are expected to be more shielded as has been observed in most cases. The mass spectrum of the complex (**2**) showed the molecular ion peak, m/z at 564 and stepwise loss of CO and cyclopentadienyl units. With

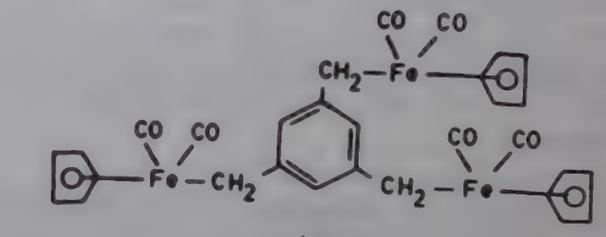

(1)

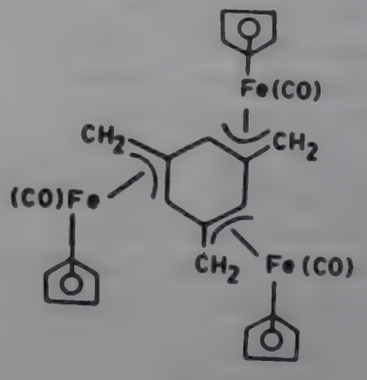

(2)

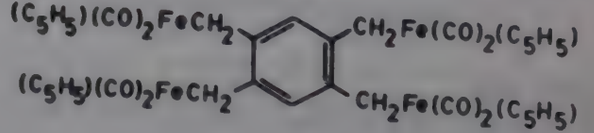

(3)

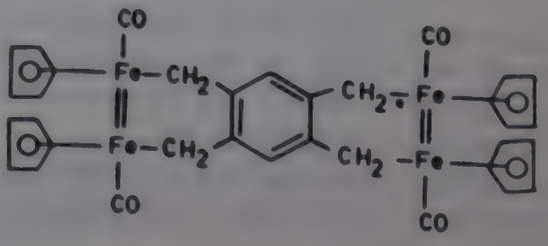

(4)

Fig. 1—Structures of iron complexes

a view to studying the conversion of analogous 1,2,4,5-tetrakis(bromoethyl)benzene complexes, we have synthesized 1,2,4,5-tetrakis(σ-methylene)-benzene {tetrakis(η^5-cyclopentadienyl)tetra-ironoctacarbonyl} (**3**) and shown that the thermal conversion of the complex to the corresponding π-complex is not possible due to the eighteen electron rule formalism.

The complexes (**3**) and (**4**) have been characterised by spectral data. Complex (**3**) shows two ν(CO) bands at 2005 and 1957cm^{-1} which is typical for a *cis*-dicarbonyl complex; this also indicates that the carbonyls are terminal. The PMR spectrum exhibited three types of protons resonances at δ 2.17 (s, 8H, methylene), δ 4.67 (s, 20H, cyclopentadienyl) and δ 7.11 (s, 2H, aromatic protons).

The mass spectrum of (**3**) gave molecular ion peak, *m/z* at 830 and some other important peaks due to the stepwise loss of eight CO and four cyclopentadienyl units.

Complex (**4**) showed ν(CO) band at 1940 cm^{-1} indicating the presence of only one terminal CO group. PMR spectrum showed three types of protons. A resonance at δ 2.11 (s, 8H, methylene) clearly shows the bonding of Fe atoms with methylene groups and the consequent upfield shift compared to that observed for the halogenated ligand. The resonance at δ 7.02 (4H) is due to the aromatic protons while that at δ 4.56 is due to the cyclopentadienyl protons. Elemental analysis also corresponds to the proposed molecular formula for (**4**). The structure of the complex is thus tentatively proposed as shown in (Fig. 1). It may be mentioned that an Fe = Fe bonding had to be invoked in order to account for the eighteen electron role; we have, however, no further evidence for such bonding.

The conversion of σ-complex to the π-complex significantly lowers the delocalization energy of the benzene ring so that the energetically favourable electron distribution can be achieved for the complex.

Acknowledgement

The authors are thankful to Dr. A. K. F. Rahman, Research School of Chemistry, The Australian National University, Australia for the PMR, mass spectra and analytical data.

References

1 Ullah S S, Kabir S E, Rahman A K F & Karim M M, *Indian J Chem*, 23B (1984) 103.
2 Ullah S S, Molla M E & Karim M M, *J Bangladesh Acad Sci*, 8 (1984) 75.
3 Ullah S S, Hashem M A, Karim M M & Khan S M A, *Indian J Chem*, 24A (1985) 607.
4 Ullah S S, Azam K A, Hashem M A, Ahmed I, Karim M M & Khan S M A, *Indian J Chem*, 26A (1987) 831.
5 Azam K A, Das P C, Hasan M K & Kabir S E, *Indian J Chem*, 28A (1989) 906.
6 Ullah S S, Azam K A, Kabir S E, Rahman A K F & Begum R, *Indian J Chem*, 29A (1990) 22,
7 Ullah S S, Molla M E, Karim M M & Begum R, *Indian J Chem*, 24A (1985) 412.
8 Burlitch J M, Leonowiez M E, Peterson R B & Hughes R E, *Inorg Chem*, 18(4) (1979) 1097.
9 Ried W & Bodem H, *Chem Ber*, 87 (1956) 2328.

Indian Journal of Chemistry
Vol. 31A, September 1992, pp. 702-703

Monopyridineiodine(I) chloride in ethanol as a new iodinating reagent for metal β-diketones and ketoneimines

S K Ramalingam*, K Jeyasubramanian & S Abdulsamath
Department of Inorganic Chemistry, School of Chemistry, M.K. University, Madurai 625 021, Tamilnadu, India

Received 7 October 1991; revised and accepted 2 April 1992

A direct iodination procedure is described for the introduction of iodine in the 3-position of the metal β-diketonates of Cr(III), Co(III), Al(III), Be(II), oxovanadium(IV), Ni(II) and Cu(II) employing monopyridineiodine(I) chloride in ethanol or methanol medium as a new iodinating reagent for β-diketonates. Unlike the reagents known already, monopyridineiodine(I) chloride gamma-iodinates at room temperature (in 10 min) giving 75-90% yield. On iodination, $Ni(bzac)_2$ changes from the high spin to a low spin state due to steric factors. 3-Iodovandylacetylacetonate has been prepared for the first time using the present reagent.

Electrophilic γ-halogenation studies of many metal β-diketonates are well documented[1,2]. However, among the reported halogenation reactions, iodination is quite scarce. Hitherto, only the metal β-diketonates of Co(III), Cr(III), Fe(III), Al(III), Rh(III), Be(II), Cu(II), Ni(II) and Pd(II) have beeen sucessfully γ-iodinated using reagents like N-iodosuccinimide[1,3,4], or iodine monochloride[2], in chloroform or buffered acetic acid medium. Even for the reported cases of Be(II), Cu(II) and Al(III) chelates, the iodo products could be obtained only indirectly[5] first by iodinating the ligand and then complexing it with the metal ion. The direct reaction between N-iodosuccinimide and copper(II) acetylacetonate in chloroform[6] is reported to end in decomposition. In this communication we report the first use of monopyridine(I) chloride[7] (a stable solid) in EtOH/MeOH for the iodination of some metalβ-diketones as well as diketoneimines.

Experimental

The reagent monopyridineiodine(I) chloride, an yellow crystalline solid (m.p. 136°C) and metal β-diketonates were prepared by the literature methods[1,7].

Typical iodination procedures adopted are as follows.

(1) *Iodination of Cu(II), Co(III), Cr(III), Fe(III), Al(III) and Be(II) diketonates (ethanol medium)*

An ethanolic solution of the metal acetylacetonate (20 ml, 2 mmol) was mixed with an ethanolic solution of the reagent monopyridineiodine(I) chloride (10 ml, 4 and 6 mmol for bis and tris chelates respectively). The solution was stirred for about 10 min, cooled in an ice-bath and the solution mixture poured into ice-cold water (200 ml). The solid product obtained was allowed to settle down, filtered and washed with water and dried in an oven at 80°C. The iodo compounds were recrystallised from chloroform-pet. ether mixture.

(2) *Iodination of $VO(acac)_2$ and $Ni(acac)_2$ (methanol medium)*

The reaction is more facile in methanol medium compared to ethanol. The vanadyl product was recrystallised from a mixture of chloroform and pet. ether. Unlike in the previous case the solid product, if wahsed with water, was found to decompose. For iodinating $Ni(bzac)_2$, the *p*H was raised to 7 by adding liquor ammonia.

Results and discussion

The compositions of the new iodo products as arrived at on the basis of their microanalytical data, their physical characteristics, the UV-vis and important IR spectral data are presented in Table 1. That the iodo substitution has taken place at the γ-carbon is revealed by a comparison of the IR spectra of the iodinated product with that of the substrate chelate. As expected, the medium intensity band at 790 cm^{-1} (out of plane bend of C-H) and the weak band at 1195 cm^{-1} (in plane bend of C-H) of the IR spectrum of the substrate disappear in the spectrum of the product. The other bands that are affected by substitution are the two strong ones, one at 1585 cm^{-1} and the other at 1520 cm^{-1}. The former band is attributable to a mixed vibration of νC=O(75%) and νC=C(25%) and the latter to νC=C(75%) and νC=O(25%) in the unsubstituted substrate[8]. Normally, halogenation, e.g., chlorination, does not affect these two bands. However, in the IR spectrum of iodinated compound, these two bands merge to form one strong band spanning the region 1530-1550 cm^{-1}. This fact may be attributed to the mass effect of the iodine atom.

An approximately linear correlation between the masses of chlorine, bromine and iodine atoms and the corresponding νC=O and νC=C vibrations has

Table 1—Characterization data for the new iodo compounds

Complex (colour)	M.P. (°C)	Yield (%)	Found (calc.), %				IR frequencies $\nu C=O$ & $\nu C=C$ (cm^{-1})	UV-vis data λ_{max}(nm)
			C	H	N	M		
$VO(I\text{-}acac)_2$ green	168	75	23.21 (23.15)	2.32 (2.38)	– –	9.96 (9.85)	1535	316
$Cu(I\text{-}bzac)_2$ (green)	180	95	37.63 (37.85)	2.54 (2.09)	– –	10.08 (9.05)	1548	322.5
$Ni(I\text{-}bzac)_2$ (red)	76	60	37.93 (38.28)	2.55 (2.60)	– –	9.35 (9.14)	1550	372,750
$Be(I\text{-}bzac)_2$ (brown)	164	80	41.25 (40.92)	2.74 (2.38)	– –	1.62 (1.54)	1560	321
$Al(I\text{-}bzac)_3$ (pink)	135	75	40.52 (40.14)	2.74 (2.84)	– –	3.14 (3.09)	1554	316
$Cu(I_2\text{-}baen)$ (brown)	100	90	26.83 (26.62)	3.09 (2.84)	5.22 (5.04)	11.83 (11.92)	1538	321.2
$Ni(I_2\text{-}baen)$ (red)	260 dec	70	27.03 (26.82)	3.01 (3.15)	5.36 (5.42)	11.02 (10.74)	1550	342,684

bzac = Benzoylacetone
baen = Bisacetylacetoneethylenediimine

been arrived at by comparing the present data for iodine with those reported in literature[1,9] for chlorination and bromination reactions. This is evidenced by the IR spectra of $VO(Iacac)_2$ which shows only a broad band at 1535 cm^{-1}.

Attempts to iodinate vanadyl acetylacetonate by Singh and Sahai[1] were unsuccessful. In the present investigation iodination of this complex has been readily accomplished. The IR spectrum of the iodo product, nevertheless, is analogous to that of other iodo β-diketonates. However, a noteworthy feature is that $\nu V=O$ vibration observed at 997 cm^{-1} for the substrate gets shifted to as low a value as 900 cm^{-1} $VO(Iacac)_2$.A comparison of the $\nu V=O$ shift for $VO(Clacac)_2$ (907 cm^{-1}) and $VO(acacBr)_2$[10] (906 cm^{-1}) with the present data demonstrates the mass effect.

Electronic spectra

A salient feature of the electronic spectrum of the iodinated complex is the observed progressive bathochromic shift from the chloro to iodo through bromo compounds. This may be attributed to an increase in delocalisation of electron density in the same order.

The UV-visible spectrum of $Ni(acac)_2.2H_2O$ is typical of a weakly tetragonal Ni(II) species and is dominated[2] by two absorption band at ~310 and ~1000 nm. Generally, no significant shifts in the frequencies of these ligand field bands have been observed for the solvated species. Introduction of iodine in the 3-position of the $Ni(bzac)_2$ chelate ring, however, has been reported to shift these bands to 327 nm and 750 nm respectively. But no such feature has been observed in the iodination of $Ni(acac)_2.2H_2O$. This indicates a transformation of the tetragonal geometry of the substrate to a square planar geometry for the 3-iodobenzoylacetonato Ni(II) product. This may probably be due to steric and conjugation effects. The iodo product is found to be diamagnetic as expected of a planar molecule. The observed electronic spectra of the iodinated products of the other metal β-diketonates are found to be similar to those reported earlier[1].

NMR spectra

A comparison of the ^1H NMR spectra of the diamagnetic $Ni(Ibzac)_2$, $Be(Iacac)_2$ and $Al(Iacac)_3$ with the corresponding unsubstituted complexes shows the absence of characteristic signal at 4.9-5.0 δ (ppm) for the γC-H proton demonstrating thereby that substitution has taken place only at the γ-positions of the diketone ring.

References

1 Singh P R & Sahai R, *Aust J Chem*, 20 (1967) 639.
2 Mehrotra R C, Bohra R & Gaur D P, *Metal β-diketonates and allied derivatives* (Academic Press, New York), 1978.
3 Yamakawa K & Kaneoya H, *Chem Pharm Bull*, 24 (1976) 1931.
4 Kasahara A, UJI-IE & Tanaka K, *Bull chem Soc Japan*, 39 (1966) 3318.
5 Kavathekar B J, Khanvilkar J N, Sahakari M P & Mukhedkar A J, *Radio Chim Acta*, 23 (1976) 88.
6 Holtzclaw H F & Collman J P, *J Am chem Soc*, 79 (1963) 3318.
7 Kauffman G B, Stevens K L & Royer D J, *Inorg Synth*, 7 (1963) 176.
8 Nakamoto K, McCarthy P J, Ruby A & Martell A E, *J Am chem Soc*, 83 (1961) 1066.
9 Holm R H & Cotton F A, *J Am chem Soc*, 80 (1958) 5658.
10 Mannix C E & Zipp A P, *J inorg nucl Chem*, 41 (1979) 59.

Indian Journal of Chemistry
Vol. 31A, September 1992, pp. 704-705

1,3-Bis(salicylidineamino)thiourea dihydrate as an analytical reagent for the direct spectrophotometric determination of Co(II) in natural samples

L D Prabhakar*, C Umarani, V Thanikachalam & C B Palanivelu

Department of Chemistry, Annamalai University, Annamalainagar 608 002, India

Received 3 September 1991;
revised and accepted 13 January 1992

A simple, rapid, selective and sensitive spectrophotometric method for the determination of microamounts of Co(II), alone or in presence of associated metals has been developed. Co(II) forms a 1:2 complex with 1,3-bis(salicylidineamino)thiourea dihydrate which obeys Beer's law in the concentration range of 0.1 to 100 ppm of Co(II). The molar absorptivity and Sandell's sensitivity of the method are 1.8924×10^4 dm^3 mol^{-1} cm^{-1} and 0.049 μg cm^{-1} respectively.

A number of complexing reagents have been used for the spectrophotometric determination of Co(II) in the form of its thiocarbohydrazide[1-6], diamine[7,8], oxime[9], carbothioamide[10], aldoxime[11], isonitroso-thio[12], and thiocarbamide[13] complexes. But no attempt has been made to determine the Co(II) content present in natural samples like human hair. In the present note we report the use of 1,3-bis(salicylidineamino)thiourea dihydrate (SAT.2H_2O) for Co(II) determination.

Experimental

All the chemicals used were of analytical reagent grade (BDH/E. Merck Chemicals).

Synthesis of SAT.2H_2O

A solution containing 0.05 mol (5.3 g) of thiocarbohydrazide and 0.1 mol of salicylaldehyde and 3 ml of glacial acetic acid in 100 ml of ethanol-water (1:1) was slightly warmed with constant stirring. A yellow coloured product which quickly separated, was filtered off, recrystallized from 50% ethanol-acetone mixture (MF C_{15} N_4 H_{18} O_4 S, m.p. 191-192°C, yield 85-90%).

Stock solution of the reagent was prepared by dissolving SAT.2H_2O (0.625 g) in 250 ml of DMF and solutions of lower concentrations (1×10^{-2} *M*) were obtained by dilution with DMF.

A stock solution of cobalt(II) was prepared by dissolving 2.38146 g of AR cobalt(II) chloride hexahydrate in 250 ml and was standardised gravimetrically by the pyridine thiocyanate method[14].

The *p*H measurements were done with an ITL digital *p*H/MV meter having a glass electrode, model DPH-14, C, H and N analyses were carried out with a CHNO Rapid Analyser. IR spectra were recorded on a Perkin Elmer 781 spectrophotometer. A spectrophotometer model UV-DEC 340 was used for absorbance measurements.

Analytical procedure

To an aliquot of the sample solution containing 0.1 to 100 ppm of cobalt(II) in a 25 ml of standard flask, 3 ml of buffer (*p*H 3.5) and 5 ml of 5×10^{-3} *M* reagent solution were added and the absorbance of cobalt complex was measured at 416 nm, against a blank prepared identically, keeping DMF-water ratio 50%. The amount of cobalt(II) was determined from a calibration curve.

Preparation of solid Co-SAT complex, $[Co(H_2-L)_2Cl_2]2H_2O$

A solution of $CoCl_2.6H_2O$ (0.08 mol) in 50 ml of doubly distilled water was added to 0.16 mol of reagent in 30 ml of DMF with an appropriate amount of *p*H 3.5 buffer solution. The contents were stirred at room temperature for 15 min. The yellowish green solid which separated out, was filtered, washed thoroughly with aqueous acetone and dried in vacuo over $CaCl_2$ at room temperature.

Results and discussion

SAT.2H_2O was characterised on the basis of its elemental analysis and the IR data.

Its ionisation constant in 50% DMF-water medium[18] (4 ml of 1×10^{-3} *M* SAT.2H_2O) was found to be 6.5.

The absorption spectrum of Co-SAT.2H_2O showed λ_{max} at 416 nm, where the reagent shows comparatively low absorbance. Hence, in all further studies the absorption was measured at 416 nm against the corresponding reagent blank. The optimum *p*H range was found to be 3.0-4.0.

The composition of the Co-SAT.2H_2O complex was established by Job's method of continuous variation and Yoe's mole ratio method. In both methods, cobalt to reagent ratio was found to be 1:2.

The system obeys Beer's law over the concentration range 0.1-100 ppm of Co(II) ions. The

Table 1—Results of analysis of Co(II) in human hair

Sample No.	Amount of Co(II) estimated in hair samples by	
	Pyridinethiocyanate method (ppm)†	Present method (ppm)
1.	50.03	50.44
2.	50.05	50.43
3.	50.15	50.43

† Ref. 14.

molar absorptivity and Sandell's sensitivity of the method was 1.8928×10^4 dm^3 mol^{-1} cm^{-1} and 0.049 μg cm^{-2} respectively.

Effect of foreign ions

Among the ions examined only oxalate, Fe^{2+} and Cu^{2+} interferred. The interferences from Fe^{2+} and Cu^{2+} could be eleminated by masking with citrate (40 fold) and tartrate (10 fold), respectively.

Application of the reagent for estimation of Co(II) in natural samples

A sample of human hair (5 g) was taken in a 250 ml beaker and 50 ml of conc. perchloric acid was added. The contents were digested for one hour carefully when the sample dried. Then 50 ml of conc. H_2SO_4 was added and evaporated to dryness. Then 50 ml of con. HCl was added and evaporated to dryness. The acid treatment of the sample was repeated three times. Finally the dried mass was taken in 50 ml of doubly distilled water, and ultracentrifuged. The centrifugation was repeated with fresh water. Filtrates were combined and heated to reduce the volume to 50 ml. The filtrate was transferred to a 100 ml standard flask, two drops of hydrochloric acid were added and volume was made upto the mark. An aliquot of solution (10 ml) was taken for the determination of Co(II) content by the spectrophotometric method as described above. The results are given in Table 1.

References

1 Daniel Rosales, Jose Gomez Ariza L & Juan Munoz Leyva A, *Mikro chim Acta (Wien)* 1 (1985) 77.

2 Daniel Rosales & Jose Gomes Ariza L, *Anal Chem*, 57 (1985) 1411.

3 Daniel Rosales, Isabel Milan & Jose Gomez Ariza L, *Talanta*, 33(7) (1986) 607.

4 Salagado M, Urene E, Garcia A, De Tortes & Ganopvaon J M, *J mole Struct*, 143 (1986) 477.

5 Daniel Rosales & Jose Gomez Ariza L, *Anal chem Acta*, 169 (1985) 367.

6 Daniel Rosales, Jose Gomez Ariza L & Aguestion Asuero G, *Analyst*, 111(4) (1986) 449.

7 Furukawa, Masamichi, Nakashima, Ryozo, Kanata, Eijiro, Shibata, Shouzo, Nagayo, Kugya, *Gijuetsu Shikensho Kagaku*, 30(II) (1981) 187.

8 Lorenzo Ferriro Rosa A & Bermiji Martinez F, *Rev Soc Quim Mex*, 25(5) (1981) 550.

9 Mathur C P, Thakur R S, Baterja S & Bhandary C S, Bangaladesh, *J Scient ind Res*, 16(1-4) (1981) 41.

10 Gowda, Sanke H, Thimmaias N & Ahmed Magbools, *Indian J Chem*, 22A(6) (1983) 551.

11 Yamageuchi Shigeroleu & Vesugi Katsvya, *Bunseki Kagaku*, 33(2) (1984) 112.

12 Pria P K & Majumdar S K, *Indian J Chem*, 24A(11) (1985) 1989.

13 Ambhane D P & Joshi A P, *Indian J Chem*, 25A(!7) (1986) 699.

14 Vogel A I, *A text book of quantitative inorganic chemistry*, (Longmans, London) 1978.

15 Harris C M, Palit H R H & Singh E, *Inorg Chem*, 6 (1967) 1102.

16 Satapathy S & Sahoo B, *J inog nucl Chem*, 31 (1970) 2223.

17 Rajeshwar Singh & Srivastava J P, *Indian J Chem*, 15A (1977) 805.

18 Chakrabarthi J & Sahoo B, *Indian J Chem*, 20A (1981) 431.

19 Prakash K M M S, Prabhakar L D & Venkata Reddy, *Analyst*, 111 (1986) 1301.

20 Borissova R, *Talanta*, 22 (1975) 797.

Indian Journal of Chemistry
Vol. 31A, September 1992, pp. 706-709

Correlation analysis of reactivity in the oxidation of substituted mandelic acids by pyridinium fluorochromate

Rachna Asopa, Pallavi Bhatt & Kalyan K Banerji*
Department of Chemistry, J.N.V. University, Jodhpur 342 005

Jodhpur 342 005
Received 13 December 1991; revised and accepted
17 March 1992

Kinetics of oxidation of nine substituted mandelic acids by pyridinium fluorochromate (PFC) have been studied. The main product is the corresponding arylglyoxylic acid. The reaction is first order in [PFC] and Michaelis-Menten type kinetics has been observed with respect to the reductant. The formation constants of the complexes and the rates of their decomposition have been calculated. The formation constants are not sensitive to substitution in the benzene ring. The rates of decomposition of the complexes showed an excellent correlation with Brown's σ^+ values with negative reaction constants. The effect of solvent has been analysed using multiparametric equations and mechanistic aspects are discussed.

Hydroxy acids may either be oxidised as alcohols, yielding corresponding oxoacids[1] or undergo oxidative decarboxylation to yield a ketone[2]. Pyridinium fluorochromate (PFC) is a highly versatile oxidant[3]. Several reports concerning the kinetics and mechanism of oxidation of organic compounds including that of mandelic acid have emanated from our laboratory[4-8]. Herein we report the effect of substituents and solvents on the oxidation of mandelic acid by PFC.

Experimental

The preparation and specification of the substituted mandelic acids have been described earlier[9]. PFC was prepared by the reported method[3] and its purity checked by iodometric determination. Solvents were purified by the usual methods[10].

Kinetic measurements were carried out in DMSO as a solvent spectrophotometrically at 356 nm as described earlier[8]. Reactions too fast to be studied by the conventional method were studied by a stopped-flow technique using a Hi-Tech SFL-44 stopped-flow spectrophotometer coupled to an MCS-1 data processing system. All other experimental procedures have been described earlier[8].

Results and discussion

The main product of oxidation is the corresponding arylglyoxylic acid. The overall reaction can be represented as Eq. (1).

$$ArCH(OH)COOH + CrO_2FOPyH \rightarrow ArCOCOOH + H_2O + CrOFOPyH \quad \ldots(1)$$

PFC undergoes a 2-electron change. This accords with the earlier observations[11,12].

The reaction is first order in [PFC] and Michaelis-Menten type kinetics are observed with respect to the reductant (Table 1). This points to the following overall mechanism (Eqs 2 and 3) and rate law (4).

$$\text{Mandelic acid} + \text{PFC} \overset{K}{\rightleftarrows} \text{Complex} \quad \ldots(2)$$

$$\text{Complex} \xrightarrow{k_2} \text{Products} \quad \ldots(3)$$

$$-d[\text{PFC}]/dt = Kk_2[\text{PFC}][\text{mandelic acid}]/(1 + K[\text{mandelic acid}]) \quad \ldots(4)$$

The dependence on [reductant] was studied at different temperatures and values of K and k_2 were calculated from the linear plots of $1/k_{obs}$ versus 1/[mandelic acid]. The thermodynamic parameters of the complex formation and the activation parameters of its decomposition were evaluated from

Table 1—Rate constants for the oxidation of *p*-methylmandelic acid by PFC at 288 K

[Hydroxy acid] (mol dm^{-3})	10^3 [PFC] (mol dm^{-3})	$10^4 k_{obs}$ (s^{-1})
0.010	1.0	4.17
0.015	1.0	5.63
0.020	1.0	7.90
0.030	1.0	8.83
0.040	1.0	10.0
0.060	1.0	12.1
0.080	1.0	13.5
0.110	1.0	15.0
0.170	1.0	16.0
0.080	2.0	13.2
0.080	4.0	13.7
0.080	8.0	13.5
0.080	10.0	13.4
0.080†	2.0	13.6

†contained 10^{-3} mol dm^{-3} acrylonitrile

the values of K and k_2 at different temperatures respectively (Tables 2 and 3).

The oxidation of *p*-methylmandelic acid was studied in 19 different organic solvents. The choice of solvents was limited by the solubility of PFC and its reaction with primary and secondary alcohols. There was no noticeable reaction with the solvent chosen. The kinetics were similar in all the solvents. The values of K and k_2 were determined (Table 4).

The entropy and enthalpy of activation of the oxidation of the ten compounds are linearly related ($r = 0.9818$) and the value of isokinetic temperature, evaluated from the slope of this plot, is 416 ± 28 K. The validity of the isokinetic relationship was checked and found genuine by using Exner's criterion[13]. A linear isokinetic relationship is a necessary condition for the validity of linear free energy relationships[14].

A perusal of values in Tables 2 and 3 showed that the formation constants of the substituted mandelic acids-PFC complexes are not much sensitive to substitution in the aromatic ring. Similar observations have earlier been made in the oxidation of substituted benzyl alcohols by PFC[5] and by ceric ammonium nitrate[15], and in the oxidation of mandelic acids by ceric ammonium nitrate[16]. But the rates of decomposition of the complexes showed considerable variation with the substitution.

The rate of decomposition is increased by the introduction of electron-releasing groups; electron-withdrawing groups have an opposite effect. The rates did not yield a significant correlation with

Table 2—Formation constants and thermodynamic parameters of the substituted mandelic acid-PFC complexes

Subst.	K (dm^{3}mol^{-1})				ΔH^0 (kJ mol^{-1})	ΔS^0 (J mol^{-1}K^{-1})	ΔG^0 (kJ mol^{-1})
	288	298	308	318 K			
H[a]	26.0	20.7	17.3	10.5	−25.0	−51	−9.9
p-F	30.3	25.0	19.5	14.1	−21.8	−39	−10.4
p-Cl	28.5	23.0	17.7	12.3	−23.6	−46	−10.2
p-Br	24.5	18.0	14.3	9.0	−27.0	−59	−9.6
p-Me	26.7	21.0	15.8	10.3	−26.3	−55	−9.9
p-Pr^i	28.0	23.0	16.3	11.0	−26.3	−55	−9.9
p-OMe	30.7	26.0	19.7	14.2	−22.0	−40	−10.4
m-Cl	27.5	21.3	16.5	10.7	−25.9	−54	−10.0
m-NO_2	24.7	17.5	13.8	9.0	−27.3	−60	−9.6
p-NO_2	25.6	20.1	15.8	10·2	−25.2	−52	−9.9

Average errors: K, ±1.3 dm^{-3}mol^{-1}; ΔH^0, ±1.8 kJ mol^{-1}; ΔS^0, ±6 J mol^{-1}K^{-1}; ΔG^0, ±1.4 kJ mol^{-1}

[a]Data from ref. 8

Table 3—Rates of decomposition of the complexes and the activation parameters

Subst.	$10^6 k_2$ (s^{-1})				$\Delta H^{\neq}$ (kJ mol^{-1})	$\Delta S^{\neq}$ (J mol^{-1}K^{-1})	$\Delta G^{\neq}$ (kJ mol^{-1})
	288	298	308	318 K			
H[a]	41.0	80.2	161	337	50.8	−134	90.6
p-F	60.4	110	208	462	48.7	−138	89.7
p-Cl	22.8	46.0	108	225	56.2	−120	91.9
p-Br	20.1	40.4	88.1	185	50.1	−129	92.2
p-Me	198	318	636	1140	42.7	−149	87.0
p-Pr^i	165	282	473	960	41.5	−155	87.5
p-OMe	2150	3020	3960	6360	24.2	−193	81.6
m-Cl	6.24	14.0	35.7	90.6	65.6	−98	94.8
m-NO_2	1.21	3.07	10.0	28.3	78.3	−68	98.5
p-NO_2	0.79	2.10	6.64	19.0	78.7	−70	99.5

Average errors: $\Delta H^{\neq}$ 1.7 kJ mol^{-1}; $\Delta S^{\neq}$ 7 J mol^{-1}K^{-1}; $\Delta G^{\neq}$ 1.4 kJ mol^{-1}

[a]Data from ref. 8

Table 4—Effect of solvents on the oxidation of *p*-methylmandelic acid by PFC at 298 K

Solvent	K (dm^3mol^{-1})	$10^6 k_2$ (s^{-1})
Chloroform	24.1	93.7
Carbon disulphide	22.5	15.8
1,2-Dichloroethane	18.5	113
Dichloromethane	20.7	108
Dimethylsulphoxide	21.0	318
Acetone	24.3	110
Dimethylformamide	23.9	170
Butanone	22.5	78.3
Nitrobenzene	21.4	134
Benzene	25.3	37.7
Cyclohexane	19.7	4.25
Toluene	18.8	31.0
Acetophenone	23.0	140
Tetrahydrofuran	22.7	52.0
t-Butyl alcohol	19.6	38.7
Dioxane	20.7	54.5
1,2-Dimethoxyethane	23.5	28.0
Acetic acid	24.6	17.3
Ethyl acetate	22.2	42.0

Hammett's σ substituent constants ($r=0.9419$). However, an excellent correlation ($r>0.9980$) is obtained when the rates are correlated with Brown's σ^+ values[17]; the reaction constants being negative (-2.18, -2.00, -1.76 and -1.59 at 288, 298, 308 and 318 K respectively).

The formation constant, K, of *p*-methylmandelic acid-PFC complex is not much sensitive to the nature of medium but the rate of decomposition showed considerable variation.

The rate constants for the decomposition, k_2, in 17 solvents (CS_2 and acetic acid were not considered as the complete range of the solvent parameters were not available) were correlated in terms of linear solvation energy relationship of Kamlet *et al.*[18].

$$\log k_2 = A_0 + p\pi^* + a\alpha + b\beta \quad \ldots(5)$$

In Eq. (5) π^* represents the solvent polarity for the solvent-solute interaction of non-specific type, β is a scale of solvent hydrogen-bond acceptor basicity while α represents the solvent hydrogen-bond donor acidity of the solvent. A_0 is the intercept term. It may be mentioned here that out of the 17 solvents, α for 12 solvents has a value of zero. The analyses in terms of the triparametric LSER (Eq. 5), a biparametric equation involving π^* and β, and separately with π^* and β gave the following results (Eqs 6-9).

$$\log k_2 = (1.70 \pm 0.13)\pi^* + (0.05 \pm 0.11)\beta + (0.45 \pm 0.18)\alpha - 0.65 \quad \ldots(6)$$

$R^2 = 0.9344$; sd $= 0.12$; n $= 17$; $\psi = 0.26$

$$\log k_2 = (1.58 \pm 0.25)\pi^* + (0.16 \pm 0.12)\beta - 0.72 \quad \ldots(7)$$

$R^2 = 0.9025$; sd $= 0.14$; n $= 17$; $\psi = 0.31$

$$\log k_2 = (1.62 \pm 0.15)\pi^* - 0.75 \quad \ldots(8)$$

$r^2 = 0.8904$; sd $= 0.15$; n $= 17$; $\psi = 0.36$

$$\log k_2 = (0.45 \pm 0.34)\beta - 1.64 \quad \ldots(9)$$

$r^2 = 0.1030$; sd $= 0.41$; n $= 17$; $\psi = 0.84$

Here n is the number of data points and ψ is Exner's statistical parameter[19]. The results show that about 93% of the data on the solvent effect are explained by Kamlet and Taft's triparametric equation (*cf.* Eq. 6). By Exner's criterion[19] however, the correlation is poor. The major contribution is by the solvent polarity term, π^* (*cf.* Eq. 8), both α and β play relatively insignificant roles.

The data on the solvent effect were also analysed in terms of Swain's equation[20] of cation-solvating and anion-solvating concept (Eq. 10).

$$\log k_2 = aA + bB + C \quad \ldots(10)$$

In this equation, A represents the anion-solvating power of the solvent and B the cation-solvating power, C is the intercept term and (A+B) is postulated to represent the solvent polarity. The results of correlation analysis in terms of Eq. (10), individually with A and B, and with (A+B) are given in Eqs (11)-(14).

$$\log k_2 = (0.55 \pm 0.02)A + (1.68 \pm 0.01)B - 0.51 \quad \ldots(11)$$

$R^2 = 0.9993$; sd $= 0.01$; n $= 19$; $\psi = 0.02$

$$\log k_2 = 1.31 \pm 0.15\,(A+B) - 0.54 \quad \ldots(12)$$

$r^2 = 0.8260$; sd $= 0.19$; n $= 19$; $\psi = 0.24$

$$\log k_2 = (0.31 \pm 0.55)A - 1.67 \quad \ldots(13)$$

$r^2 = 0.0178$; sd $= 0.46$; n $= 19$; $\psi = 1.02$

$$\log k_2 = (1.64 \pm 0.10)B - 0.69 \quad \ldots(14)$$

$r^2 = 0.9437$; sd $= 0.11$; n $= 19$; $\psi = 0.14$

The rates of decomposition of the complex show an excellent correlation in Swain's equation (*cf.* Eq. 11) with both cation- and anion-solvating powers contributing towards the observed effect of the solvents, though the contribution of the cation-solvating power is more. In fact the cation-solvating power

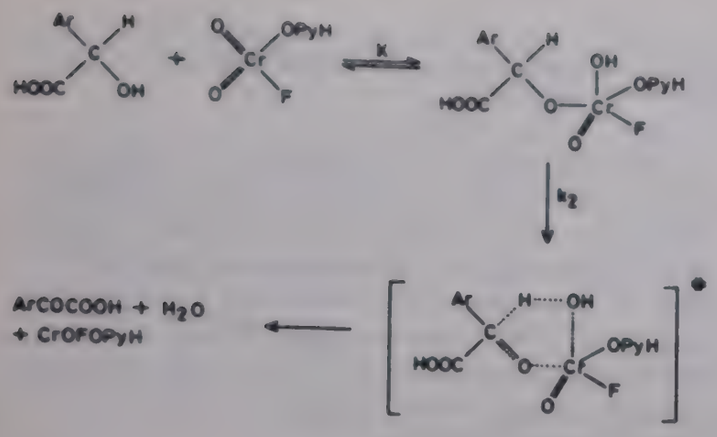

Scheme 1

alone accounts for about 94% of the data (Eq. 14). The value of Exner's statistical parameter points to an excellent correlation in Eq. (11) and a satisfactory correlation in Eq. (14).

Mechanisms

Absence of any effect of acrylonitrile on the reaction discounts the possibility of a one-electron oxidation, leading to the formation of free radicals. The presence of a substantial kinetic isotope effect in the oxidation of mandelic acid[8] confirms the cleavage of the α-C − H bond in the rate-determining step. The large negative reaction constants together with the excellent correlation with Brown's σ^+ values point to a highly electron-deficient carbon centre in the transition state. The transition state thus approaches a carbocation in character. This is supported by the solvent effect also. Greater role played by the cation-solvating power of the solvents supports the postulation of a carbocationic transition state. Therefore, the correlation analysis of substituent and solvent effects on the oxidation of mandelic acid supports a mechanism involving a hydride-ion transfer via a chromate ester (Scheme 1).

Acknowledgement

Thanks are due to the UGC, New Delhi, for financial assistance.

References

1 Banerji K K, *J chem Res (S)*, (1978) 193.
2 Levesley P & Waters W A, *J chem Soc*, (1955) 215.
3 Bhattacharjee M N, Chaudhuri M K, Dasgupta H S, Roy N & Kathing D, *Synthesis*, (1982) 588.
4 Banerji K K, *J chem Soc Perkin Trans*, 2, (1988) 547.
5 Banerji K K, *J org Chem*, 53 (1988) 2154.
6 Banerji K K, *J chem Soc Perkin Trans*, 2 (1988) 2065.
7 Agarwal A, Chowdhury K & Banerji K K, *J chem Res (S)*, (1990) 86.
8 Asopa R, Agarwal A & Banerji K K, *Proc Indian Acad Sci, Chem Sci*, 103 (1991) 563.
9 Jain A L & Banerji K K, *J Indian chem Soc*, 59 (1982) 645.
10 Perrin D D. Armarego W L & Periin D R, *Purification of organic compounds*, (Pergamon Press, Oxford) 1966.
11 Bhattacharjee M N, Chaudhuri M K & Purakayastha S, *Tetrahedron*, 43 (1987) 5389.
12 Brown H C, Rao C G & Kulkarni S U, *J org Chem*, 44 (1979) 2809.
13 Exner O, *Collect Czech Chem Commun*, 29 (1964) 1094.
14 Leffler J E, *J org Chem*, 31 (1966) 1535.
15 Young L B & Trahanovsky W S, *J Am chem Soc*, 91 (1969) 5060.
16 Banerji K K, *J Indian chem Soc*, 53 (1975) 575.
17 Brown H C & Okamoto Y, *J Am chem Soc*, 80 (1958) 4979.
18 Kamlet M J, Abboud J L H, Abraham M H & Taft R W, *J org Chem*, 48 (1983) 2877 and refs. cited therein
19 Exner O, *Collect Czech Chem Commun*, 31 (1966) 3222.
20 Swain C G, Swain M S, Powell A & Alunni S, *J Am chem Soc*, 105 (1983) 502.

Indian Journal of Chemistry
Vol. 31A, September 1992, pp. 710-713

Influence of sodium lauryl sulfate micelles on the oxidation of malonic acid by chromic acid

G P Panigrahi* & S K Mishra
Department of Chemistry, Berhampur University
Berhampur 760 007

Received 31 October 1991; revised 7 February 1992;
accepted 10 March 1992

Malonic acid oxidation by Cr(VI) in the presence of sodium lauryl sulfate micelle is first order each in [Cr(VI)] and [H^+] but second order in malonic acid. The oxidation is inhibited by NaLS. The observed reactions can be explained with the model proposed by Menger and Portnoy but does not fit to Berezin's model. The treatment leads to the conclusion that the reaction occurs in the aqueous phase and the active Cr(VI) species is H_2CrO_4.

Recently it has been reported[1] from this laboratory that malonic acid oxidation by Cr(VI) in aqueous $HClO_4$ medium conformed to a pathway in which a complex of enol form of malonic acid with $HCrO_4^-$ changes over to a complex of Cr(IV) in the rate limiting step and the Cr(IV) complex is taken up in a fast step by a second molecule of $HCrO_4^-$ to yield glyoxylic acid. Our interest to understand catalytic behaviour of surfactants[2] on redox-reactions prompted us to carry out the oxidation of malonic acid by Cr(VI) in the presence of sodium lauryl sulfate in order to throw light on the nature of the species of the reactants capable of affecting the reaction.

Experimental

All the chemicals are of AR grade. Malonic acid (Riedel) and chromic acid (S. Merck) were used as such. All solutions were prepared in deionised water. The surfactant, sodium lauryl sulfate (NaLS), was used after recrystallisation. Stock solutions of the surfactant (0.5 mol dm^{-3}) and chromium (VI) oxide (0.1 mol dm^{-3}) were prepared and diluted appropriately. Surfactant was always added to the oxidant flask. Chromic acid was found to be unstable in the presence of the surfactant (NaLS). The decomposition of CrO_3 with different [surfactant] under a particular set of experimental conditions was constructed by plotting k_{decomp} versus [NaLS]. The reaction was initiated by mixing equal volumes of thermally equilibrated reactant solutions and the progress of the reaction was followed by withdrawing aliquots (5 ml) of the reaction mixture at regular time intervals and discharging it into a carbon dioxide atmosphere. The liberated iodine was then titrated with standard thiosulfate solution using starch as indicator. The pseudo-first order rate constant with respect to Cr(VI) in the presence of NaLS was computed after deducting the k_{decomp} from the gross rate constant. Results were reproducible within the limits of experimental error.

Determination of critical micelle concentration

The critical micelle concentration (cmc) for sodium lauryl sulfate has been determined by conductometry in aqueous media in the presence of substrate malonic acid by using literature procedure[3]. The value was found to be 5×10^{-3} mol dm^{-3} which is considerably smaller than the reported value of 8×10^{-3} mol dm^{-3} The cmc value suggests that the substrate molecule, namely malonic acid, is able to induce micellisation.

Results and discussion

The kinetics of malonic acid oxidation by Cr(VI) in the presence of NaLS was carried out under the conditions [malonic acid] > > [Cr(VI)] (100 fold) in the [H^+] range from 0.2 to 0.5 mol dm^{-3}. The kinetic data conformed to unit dependence each in Cr(VI) and [H^+]. The order in malonic acid was obtained by varying the initial [malonic acid] in the range 0.3 to 0.7 mol dm^{-3}, keeping all other concentrations fixed. The pseudo-first order constant (k_ψ, s^{-1}) increased with increase in [malonic acid but k_ψ/[malonic acid]^2 values were found to be constant (1.90 ± 0.06 s^{-1} mol^{-2} dm^6). This observation is at variance with that obtained in the absence of lauryl sulfate. Also the reaction is catalysed by added Mn^{2+} ions when carried out in the presence of added manganese sulfate ($0.5\text{-}3 \times 10^{-3}$ mol dm^{-3}).

Activation parameters in the absence and presence of the surfactant have been computed from rate constants at 35°, 40° and 45°C using the Arrhenius plot. The activation energy and entropy of activation values have been given in Table 1. It is observed from Table 1 that the activation energy values continuously increase with [NaLS].

The observation is consistent with the accepted view that slow reaction would require higher energy of activation. But the observed increase in the entropy of activation with [NaLS] is in contrast with the trend in the energy of activation, so much so the

Table 1—Rate constants, activation parameters and $[H^+]$ in micellar phase for the oxidation of malonic acid by Cr(VI) in the presence of sodium lauryl sulfate at different temperatures.

{$[Cr(VI)] = 0.0005$ mol dm^{-3}, [Malonic acid] = 0.5 mol dm^{-3} and aqueous medium}

$[H^+]$ (mol dm^{-3})	10^2[NaLS] (mol dm^{-3})	$10^5[H_m^+]$ (mol dm^{-3})	$10^5 k_\psi$ s^{-1}			E_a (kJ mol^{-1})	$\Delta S^\neq$ (JK^{-1} mol^{-1})
			35°	40°	45°C		
0.25	0.00	—	1.675	2.400	2.931	49.28	180.49
	0.70	1.716	0.997	1.488	1.722	61.60	144.82
	0.80	2.564	0.776	1.110	1.499	64.06	139.51
	0.90	3.406	0.548	0.903	1.332	72.07	115.80
	1.04	4.577	0.397	0.710	1.150	86.24	72.50
	1.10	5.069	0.329	0.654	1.088	96.10	41.91
	1.22	6.055	0.272	0.557	0.978	105.10	14.39
0.38	0.00	—	3.290	4.300	6.700	57.20	149.49
	0.70	1.732	1.582	2.293	3.444	64.06	133.20
	0.80	2.592	1.046	1.850	2.998	85.87	65.64
	0.90	3.447	0.756	1.350	2.702	103.78	10.47
	1.04	4.636	0.525	0.986	2.297	121.01	−42.22
	1.10	5.144	0.477	0.831	2.170	125.22	−54.76
	1.22	6.153	0.357	0.735	1.927	138.81	−96.71
0.50	0.00	—	5.038	6.200	10.468	60.06	136.91
	0.70	1.740	2.285	3.427	5.123	66.07	123.56
	0.80	2.605	1.374	2.575	4.547	97.78	24.75
	0.90	3.467	0.858	1.725	4.006	128.13	−69.44
	1.04	4.668	0.602	1.203	3.503	144.15	−118.26
	1.10	5.180	0.539	1.066	3.515	155.74	−154.68
	1.22	6.202	0.400	0.865	3.030	168.82	−194.64

negative entropy of activation values change over to positive entropy of activation values showing that there is a greater degree of freedom for the reactants in the micellar phase. This may probably be attributed to the loss of water molecule from the hydration cell of the Cr(VI) species.

Effect of [surfactant] on the oxidation rate

To understand the nature of influence of the NaLS micelle on the oxidation of malonic acid by Cr(VI), oxidation rates in the presence of 0.0035 to 0.012 mol dm^{-3} NaLS have been measured in various acidities. The data are given in Table 1. Inspection of data in Table 1 indicates inhibition of oxidation rates in the presence of sodium lauryl sulfate as the rates rapidly fall with increase in [sodium lauryl sulfate]. For an observation of this type it is likely that one of the reactants may be partly incorporated in the micellar phase with the other reactant completely in the aqueous phase. This is borne out from the following consideration. Assuming that the reaction is occurring in both the phase, Scheme 1 can be written to describe the reaction.

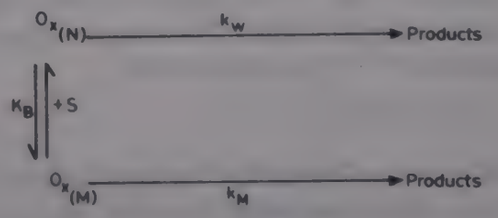

Scheme 1

Scheme 1 would relate the k_ψ (i.e., observed pseudo-first order rate constant) to the micellar concentration through the relationship (1).

$$k_\psi = \frac{k_W + k_M K_B ([D]\text{-cmc})}{1 + K_B ([D]\text{-cmc})} \quad \ldots (1)$$

Equation 1 can be rearranged to Eq. (2).

$$\frac{1}{k_W - k_\psi} = \frac{1}{k_W - k_M} + \frac{1}{(k_W - k_M) K_B ([D]\text{-cmc})} \quad \ldots (2)$$

Applicability of the relationship can be verified from the plots of $(k_W - k_\psi)^{-1}$ against $([D]\text{-cmc})^{-1}$ These plots are linear (Fig. 1) and from the ratios of intercepts to slopes K_B values (i.e., binding constant

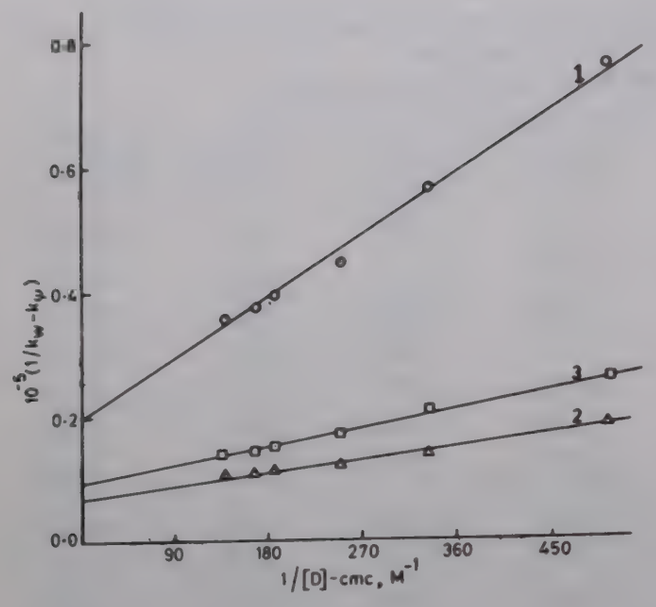

Fig.1—Plots of $\frac{1}{k_w - k_\psi}$ versus $\frac{1}{[D]\text{-cmc}}$ for malonic acid at different [acid] at 35°C: 1, $[H^+]=0.248$ mol dm^{-3}; 2, $[H^+]=0.5$ mol dm^{-3} and 3, $[H^+]=0.376$ mol dm^{-3} (40°C).

of Cr(VI) with the micelle) at different acidities and temperatures are obtained. These values are given in Table 2. Further, from the intercepts, attempt was made to compute k_M values which were found to be negative at once suggesting that no reaction occurs in the micellar phase.

The fact that a part of the Cr(VI) is bound to the surface is seen from the small magnitude of transfer free energy of the Cr(VI) species from aqueous phase to the micellar phase. The transfer free energy was calculated[6,7] by the relationship,

$$\Delta\mu_T^0 = -RT \ln (55.5\ K_B) \quad \ldots (3)$$

and are given in Table 2. The conclusions drawn above are quite compatible with the observations of Carbone *et al.*[8a] who have observed small magnitude of transfer free energy in the reaction of Fe(III) with substituted ferrocenes. The surface interaction of the solute in cationic and anionic micelles for substituted phenols[6,8b,c] and benzoic acid and anilines[8b] has been also concluded from an observed smaller magnitude of transfer free energy. A similar situation occurs for substituted phenothiazines as well as with anionic micelle[11].

As the binding constant of Cr(VI) species, (K_B), is now available, the partition constant, P_B, for Cr(VI) species between the micellar phase and aqueous phase was calculated by the relationship[9,10].

$$K_B = (P_B - 1)\,V \quad \ldots (4)$$

where V is the molar volume of the micelle. The molar volume of NaLS micelle is ~ 0.25 mol^{-1} dm^{-3}

Table 2—Binding constant (K_B), transfer free energy ($-\Delta\mu^0$) and partition coefficient values at different temperatures {[Cr(VI)] = 0.0005 mol dm^{-3}; [Malonic acid] = 0.5 mol dm^{-3}}

$[H^+]$, mol dm^{-3}	35°C	40°C	45°C
		K_B, (dm^3 mol^{-1})	
0.25	191.26	253.87	385.00
0.38	277.20	316.59	561.02
0.50	316.91	329.78	610.50
		$-\Delta\mu^0$, (kcal mol^{-1})	
0.25	2.46	2.58	2.74
0.38	2.56	2.63	2.84
0.50	2.60	2.65	2.86
		P_B	
0.25	761.99	1011.43	1533.87
0.38	1104.38	1261.31	2235.14
0.50	1262.59	1313.86	2430.28

(ref. 11). The P_B values at different acidities and temperatures are given in the Table 2.

The P_B values range between 700-2400. Relatively large P_B vaues for Cr(VI) indicate that a greater fraction of the oxidant is solubilized in NaLS micelle leaving a smaller fraction in the aqueous phase. There is a decisive decrease in [oxidant] in the aqeous phase. As no reaction takes place in the micellar phase ($k_M = -$ve mostly), the overall reaction in the aqueous phase slows down. The phenomenon of inhibition of rate in the presence of NaLS again points to H_2CrO_4 species as the oxidant rather than $HCrO_4^-$, because $HCrO_4^-$ being negatively charged will not bind to the negatively charged NaLS micelle. Also, there is increase in $[H^+]$ as shown by the following considerations.

In order to have an understanding of the magnitude of $[H^+]$ in the presence of micelles, the following exchange equilibrium between H^+ and Na^+ counterions in the micellar surface has been considered[11].

$$H_m^+ + Na_w^+ \overset{K_{Na}^H}{\rightleftharpoons} H_w^+ + Na_m^+ \quad \ldots (5)$$

The equilibrium constant for the ion exchange process is given as

$$K_{Na}^H = \frac{[H_w^+][Na_m^+]}{[H_m^+][Na_w^+]} \quad \ldots (6)$$

The magnitude of K_{Na}^H is broadly close to unity and in the circumstances $[H_m^+]$ is defined by the relationship

$$[H_m^+] = \frac{[H_T^+][D_n]\beta}{[H_T^+] + [Na_T^+]} \quad \ldots (7)$$

where D_n is defined as ([NaLS]-cmc)/N and β is defined as the fraction of micellar head group neutralised. Since β can be obtained by conductivity measurements, as ratios of the slope above and below the cmc, the value of β thus obtained is equal to 0.6. Making use of Eq. (7), $[H_m^+]$ has been computed and given in Table 1. As is very clear from the data in Table 1, $[H_m^+]$ values increase with increase in [micelle], or in other words, $[H^+]$ decreases in the aqueous phase, which is reasonable for a lowering of the reaction rate in the aqueous phase.

The foregoing discussion amply demonstrates that one of the reactants, namely, Cr(VI), is partitioned between the aqueous and micellar phases resulting in the decrease in [Cr(VI)] in the aqueous phase. However malonic acid being present only in the aqueous phase, the reaction mainly occurs in the aqueous phase.

Acknowledgement

Financial assistance by the UGC (New Delhi) is gratefully acknowledged.

References

1 Senapati M, Panigrahi G P & Mohapatro S N, *J org Chem*, 50 (1985) 365.

2 Panigrahi G P & Mishra S K, *J chem Res* (*M*), (1990) 1259.

3 Shinoda K, Nakagawa T, Tamamushi B & Isemuna T, *Colloidal surfactants* (Academic Press, New York) (1963) 98.

4 Menger F M & Portnoy C E, *J Am chem Soc*, 89 (1967) 4698.

5 Bunton C A & Sepulveda L, *J phys chem*, 83 (1979) 680.

6 Hirose C & Sepulveda L, *J phys chem*, 85 (1981) 3689.

7 (a) Carbone A I, Cavasino F P & Sbriziolo C, *Ber Bunsenges phys Chem*, 87 (1985) 31; (b) Hirose C & Sepulveda L, *J phys Chem*, 85 (1981) 3689; (c) Pramauro E & Pelizzetti E, *Anal Chim Acta*, 126 (1981), 253; *Ann Chim* (Rome), 72 (1982) 117.

8 Berezin I V, Martinek K & Yatsimirskii Y K, *Russ chem Rev* (*Eng Trans*), 42 (1973) 787.

9 Bhalekar A A & Engberts J B F N, *J Am chem Soc*, 100 (1978) 5914 and references therein.

10 Hodges H L & de Araujo M A, *Inorg Chem*, 21 (1982) 3236.

11 Perez E Benito & Rodenas E, *Langmuir*, 7 (1991) 232.

Indian Journal of Chemistry
Vol. 31A, September 1992, pp. 714-715

Kinetics and mechanism of the substitution reaction of ethylenediaminetetraacetatoruthenate(III) with cyanide in aqueous solution

M M Taqui Khan*, Debabrata Chatterjee, H C Bajaj, K N Bhatt & S Sanal Kumar

Discipline of Coordination Chemistry and Homogeneous Catalysis, Central Salt & Marine Chemicals Research Institute, Bhavnagar 364 002, India

Received 3 December 1991; revised and accepted 5 March 1992

The kinetics of the ligand substitution of $Ru^{III}(EDTA)(H_2O)^-$ (EDTA-ethylenediaminetetraacetate anion) with CN^- has been studied spectrophotometrically as a function of ligand concentration, *p*H (5.0-11.0) and temperature (20-50°C). The kinetic and activation parameters are consistent with an associative interchange (Ia) mechanism.

The kinetics of ligand substitution reactions of $Ru^{III}(EDTA)/H_2O)^-$ with monodentate and bidentate ligands is of current interest[1-3] Although a series of thio-ligands and different N-aromatic heterocycles[4] were used for these studies, cyanide a potentially strong π-acidic ligand was not used for the substitution of H_2O in $Ru^{III}(EDTA)(H_2O)^-$ complex. We report for the first time in this paper the kinetics of the substitution of $Ru^{III}(EDTA)(H_2O)^-$ with CN^- in aqueous solution.

Experimental

The complex $K[Ru^{III}(EDTA\text{-}H)Cl]$ **1** was prepared by following the published procedure[5]. Complex **1** rapidly gets aquated when dissolved in water, to give $[Ru^{III}(EDTA)(H_2O)]^-$ **1a** species[4] at *p*H 4.0. All other chemicals used were of AR grade. Doubly distilled water was used to prepare the experimental solutions.

The substitution reactions were followed spectrophotometrically at 380 nm where substantial difference in absorbance exists. A Shimadzu UV vis 160 spectrophotometer coupled with TCC-240A temperature controller was used for this purpose. All the experimental solutions were preequilibrated at the desired temperature (±0.1°C) before mixing in the spectrophotometric cell. Acetate, citrate, phosphate and borate buffers were used to control the *p*H of the experimental soltuion. A Digisun *p*H meter was used to carry out the *p*H measurements. Ionic strength of the solutions for kinetic studies was adjusted with KCl. Under pseudo-first order conditions of excess CN^- the pseudo-first order rate constants were calculated in the usual way from the absorbance versus time traces which were linear up to 2-3 half-lives. The rate constant data (average of duplicate runs) were reproducible with ±4%.

Results and discussion

In some preliminary kinetic experiments it was observed that in the presence of CN^- ligand the buffer components used to control the *p*H of the reaction mixture did not interfere with the substitution reaction under the experimental conditions. The 1:1 stoichiometry of the reaction was confirmed by mole-ratio method at three different *p*H (!5, 7.5 and 10). However, in the presence of excess CN^-, formation of 1:2 and 1:3 complexes were observed to take place over a longer period.

The rate of substitution reaction was found to be first order each with respect to complex **1a** and ligand concentrations. The rate of reaction was found to be independent of *p*H in the *p*H range 5-6. The rate decreased slowly with *p*H in the *p*H range 6.0 to 9.0. Further increase in *p*H (9.0-10.5) enhanced the reaction rate slightly (Fig. 1) which attained a limiting rate above *p*H 10.5. On the basis of the above kinetic observation a mechanism of substitution of $Ru^{III}(EDTA)(H_2O)^-$ with CN^- has been proposed (Scheme 1).

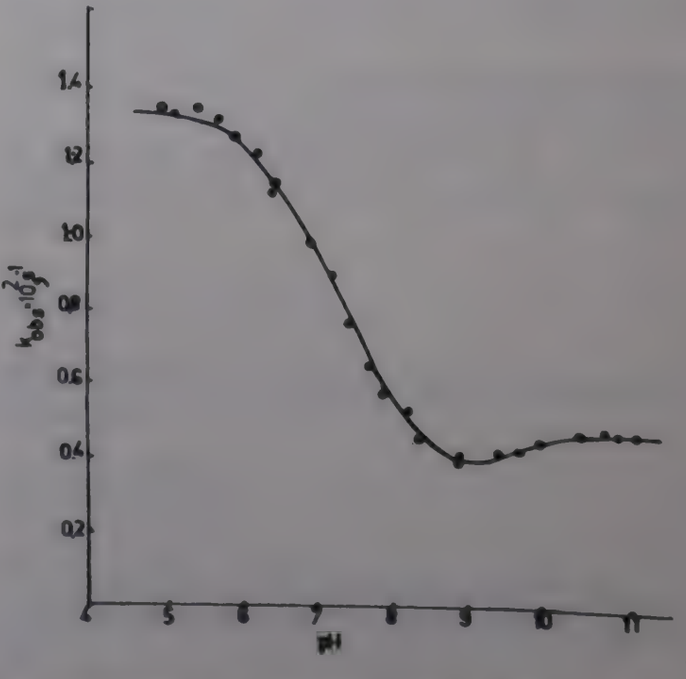

Fig. 1—Variation of k_{obs} with *p*H at 30°C {$[Ru^{III}] = 5 \times 10^{-4}$ *M*, $[CN]_T = 5 \times 10^{-3}$ *M*, $\mu = 0.2$ *M* (KCl). ○—observed rate constant, ●—Calculated by using resolved rate constants}

$$Ru^{III}(EDTA)(H_2O)^- \overset{K_1}{\rightleftharpoons} Ru^{III}(EDTA)(OH)^{2-} + H^+$$

$$pK_1 = 7.6 \quad \ldots (1)$$

$$HCN \overset{K_2}{\rightleftharpoons} CN^- + H^+ \qquad pK_2 = 9.0 \quad \ldots (2)$$

$$Ru^{III}(EDTA)(H_2O)^- + HCN \xrightarrow{k_1}$$

$$Ru^{III}(EDTA)(CN)^{2-} + H_3O^+ \quad \ldots (3)$$

$$Ru^{III}(EDTA)(OH)^{2-} + HCN \xrightarrow{k_2}$$

$$Ru^{III}(EDTA)(CN)^{2-} + H_2O \quad \ldots (4)$$

$$RU^{III}(EDTA)(OH)^{2-} + CN^- \xrightarrow{k_3}$$

$$Ru^{III}(EDTA)(CN)^{2-} + OH^- \quad \ldots (5)$$

Scheme 1

On the basis of Scheme 1, rate expression (6) can be derived for the substitution process.

$$k_{obs} = \frac{k_1[H^+]^2 + k_2K_1[H^+] + k_3K_1K_2}{[H^+]^2 + [K_1 + K_2)[H^+] + K_1K_2}[CN]_T \quad \ldots (6)$$

At low *p*H (6), $[H^+] > > K_1k_2$. Eq. (6) reduces to $k_{obs} = k_1[CN]_T$ from which k_1 was calculated as 2.7 $M^{-1}s^1$ The values of k_2 and k_3 were calculated by assuming reactions (4) and (5) are taking place only at the *p*H range 9.0 to 11.0. In this *p*H range (9-11), the reaction of Ru^{III}-OH_2 species with CN^- may be neglected and Eq. (6) can be reduced to Eq. (7).

$$k_{obs} = \frac{k_2[H^+] + k_3K_2}{K_2 + [H^+]} \; (9 < pH < 11) \quad \ldots (7)$$

The values of k_2(0.68 $M^{-1}s^{-1}$) and k_3(1.01 M^{-1} s^{-1}) were calculated from the plot of k_{obs} $(K_2 + [H^+])$ versus $[H^+]$ which gives the slope k_2 and intercept k_3K_2. The calculated rate—*p*H profile superimposes with that of experimentally obtained (Fig. 1) thereby substantiates the various assumptions made in the rate equations (1-5) in Scheme 1.

In the *p*H region 5-7 the ligand exists predominantly as HCN which is less nucleophile than CN^-. The observed decrease in rate from 6.5 to 9.0 due to the decrease in the concentration of reactive Ru^{III} $(EDTA)(H_2O)^-$ species in solution. Further, increase in *p*H increase the reaction rate slowly because of increase in CN^- concentration. The species $Ru^{III}(EDTA)(OH)^{-2}$ formed above *p*H 9 is less reactive towards substitution than Ru^{III} $(EDTA)(H_2O)^-$ species. However, appreciable build up of concentration of CN^- which is a stronger nucleophile than HCN, occurs in the *p*H range 9-11. This altogether makes the reaction less sensitive to the *p*H in the higher *p*H range (9-11.0) than that observed in the region 6.0 to 9.0. Further, the concentration of CN^- does not change appreciably in the *p*H range 10.5-11.0, which is reflected by attaining the limiting rate in the *p*H range 10.5-11.0 (Fig. 1).

The substitution reaction was studied at four different temperatures. The activation parameters $\Delta H^{\neq}$ (33.5 kJ/mol) and $\Delta S^{\neq}$ (-126.2 J/deg. mol) are quite comparable to those reported for other substitution reactions[1-3]. The low positive $\Delta H^{\neq}$ and large negative $\Delta S^{\neq}$ values clearly support the operation of an associatively mode of activation in the substitution process.

References

1 Bajaj H C & Eldik R V, *Inorg Chem*, 27 (1988) 4052.

2 Toma H E, Santos P S, Mattioli M P D & Oliveira L A A, *Polyhedron*, 6 (1987) 603.

3 Taqui Khan M M, Chatterjee D, Hussain A & Moiz M A, *Polyhedron*, 9 (1990) 2681.

4 Matsubara T & Creutz C, *Inorg Chem*, 18 (1979) 1956.

5 Diamentis A A & Dubrawakl J V, *Inorg Chem*, 20 (1980) 1142.

Indian Journal of Chemistry
Vol. 31A, September 1992, pp. 716-720

A study on ion-solvent interactions of some tetra-alkyl and multicharged electrolytes in water at different temperatures

M L Parmar*, Ch V Nageshwara Rao & S K Bhardwaj

Department of Chemistry, Himachal Pradesh University, Shimla 171 005

Received 20 December 1991; revised and accepted 26 March 1992

The partial molar volumes and viscosities of some common electrolytes, tetra-alkyl salts and multicharged electrolytes, viz., ammonium nitrate and ammonium sulphate, tetramethyl ammonium chloride and tetraethyl ammonium iodide, ammonium ceric nitrate and ammonium cerium (iv) sulphate, respectively, have been determined in water at different temperatures. The density data have been analysed by means of Masson's equation. The experimental results of viscosity have been analysed using the Jones-Dole equation. All the different types of electrolytes behave similarly and act as structure breakers. The activation parameters of viscous flow have also been obtained to throw light on the mechanism of viscous flow.

In our previous studies on multicharged electrolytes, it was reported[1-2] that these types of electrolytes behave like symmetrical tetra-alkyl salts but not like common electrolytes in binary aqueous organic liquid mixtures on the criterion of partial molar expansibilities. In order to verify this fact, on actual measurement basis, present study was undertaken with some common electrolytes viz; ammonium nitrate and ammonium sulphate; as well as with some tetra-alkyl salts viz; tetramethyl ammonium chloride and tetraethyl ammonium iodide in water at different temperatures. A survey of literature showed that such studies on multicharged ions are limited[3], reflecting the difficult experimental problems associated with the study of these ions. Also, nowhere, the comparison of the various studies on the multi-charged ions with those of common and tetra-alkyl salts is available and hence the title investigation.

Experimental

Ammonium nitrate, ammonium sulphate, tetramethyl ammonium chloride, tetraethyl ammonium iodide, ammonium ceric nitrate and ammonium cerium (iv) sulphate were of AR grade and used as such, without further purification, after drying over P_2O_5 in a desiccator. Doubly distilled water (sp. cond. $\sim 10^{-6}$ Ω^{-1} cm^{-1}) was always prepared afresh.

The solutions of the electrolytes were made by weight, and conversion of molality into molarity was done by using the standard expression described elsewhere[4].

For density measurement, an apparatus similar to the one reported by Ward and Millero[5] and described elsewhere[6] (accuracy in density measurements, $\pm 0.1 \times 10^{-4}$ g cm^{-3}) was used. The relative viscosities were measured at the desired temperature (accuracy ± 0.01°C) using a Ostwald's suspended level type viscometer, with a flow time 450s for water at 303.15 K. Runs were repeated until three successive determinations were obtained within ± 0.1s. Because all the flow times were greater than 100s, the kinetic energy correction was not necessary.

The apparent molar volumes, ϕ_v, and relative viscosities of the solutions (η_{rel}) were calculated by the usual procedure[7,8].

The density and viscosity measurements were made in a water bath whose temperature was controlled to ± 0.01°C.

Results and discussion

The densities of ammonium nitrate, ammonium sulphate, tetramethyl ammonium chloride, tetraethyl ammonium iodide, ammonium ceric nitrate and ammonium cerium (iv) sulphate in water, measured at 303.15, 308.15, 313.15 and 318.15 K have been used to calculate the apparent molar volume (ϕ_v) of the solute. The plots of ϕ_v against square root of concentration were found to be linear with negative slopes in case of common, tetra-alkyl as well as multicharged electrolytes, at all temperatures, reported here. A representative plot for ammonium cerium (iv) sulphate in water at different temperatures is shown in Fig. 1. The limiting apparent molar volumes, (ϕ_v^0), were calculated using least squares fit to the plots of the experimental values of ϕ_v against the square root of molar concentration, C, using Masson's equation[9] (Eq. 1).

$$\phi_v = \phi_v^0 + S_v^* \cdot C^{1/2} \qquad \ldots (1)$$

where $\phi_v^0 = \bar{V}_2^0$, is the partial molar volume at infinite dilution and S_v^* the experimental slope. The values of ϕ_v^0, S_v^* and standard errors, obtained in

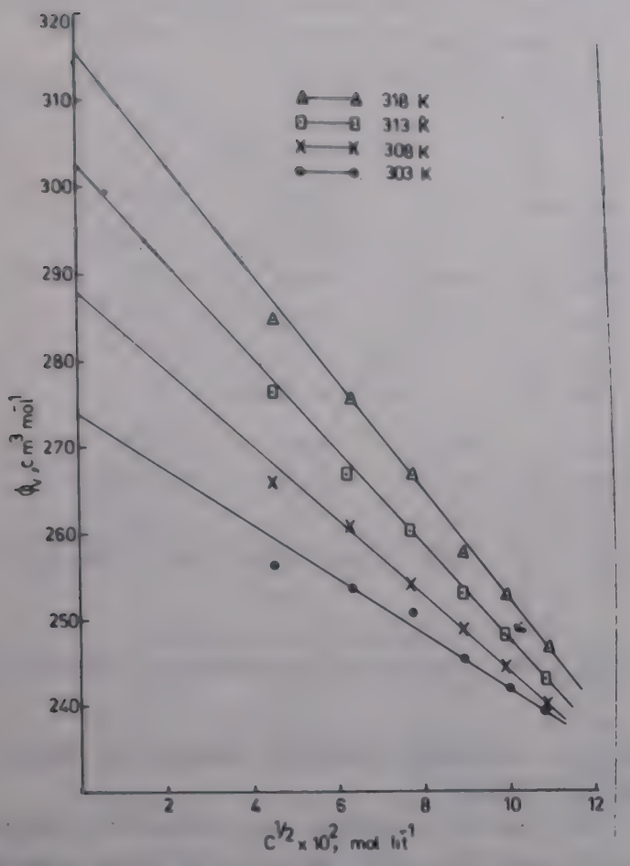

Fig. 1—Plots of ϕ_v versus $\sqrt{C}$ for ammonium cerium(IV) sulphate in water at different temperatures

water at 303.15, 308.15, 313.15 and 318.15 K are listed in Table 1.

The negative vlaues of S_v^* (Table 1, Fig. 1) indicate the presence of weak ion-ion interactions for all the electrolytes, which are further weakened with the rise in temperature. At a particular temperature, the ion-ion interactions, for the three different types of electrolytes, follow the following order: NH_4NO_3 > $(NH_4)_2SO_4$ > Me_4NCl > Et_4NI > $(NH_4)_2Ce(NO_3)_6$ > $(NH_4)_4Ce(SO_4)_4$.

Further in water these salts may be completely ionized at fairly high concentrations. Therefore, appreciable interionic penetration occurs and this gives rise to a negative slope in the ϕ_v versus $C^{1/2}$ curves.

Since ϕ_v^0 is a measure of ion-solvent interactions (as ion-ion interactions vanish at infinite dilution), therefore, it is evident from Table 1 that the values of ϕ_v^0 are positive and large for all the electrolytes in water at different temperatures, indicating the presence of strong ion-solvent interactions. These interactions are further strengthened with the rise in temperature. At a particular temperature the ion-solvent interactions follow the order: NH_4NO_3 < $(NH_4)SO_4$ < Me_4NCl < Et_4NI < $(NH_4)_2Ce(NO_3)_6$ < $(NH_4)_4Ce(SO_4)$.

The increase in ϕ_v^0 with increase in temperature, for individual electrolyte, may be attributed to increase in solvation. The temperature dependence of ϕ_v^0 for the various electrolytes, studied here, in water can be expressed by the general equation (Eq. 2)

$$\phi_v^0 = a + bT + cT^2 \quad \ldots (2)$$

Table 1—Partial molar volume (ϕ_v^0), experimental slope (S_v^*) for ammonium nitrate, ammonium sulphate, tetramethyl ammonium chloride, tetraethyl ammonium iodide, ammonium ceric nitrate and ammonium cerium (IV) sulphate in water at different temperatures[1]

Temp. T (K)	ϕ_v^0 (cm^3 mol^{-1})	S_v^* (cm^3 l$^{1/2}$ mol$^{-3/2}$)
	Ammonium nitrate	
303.15	49.73 (±0.02)[1]	−3.57 (±0.08)[1]
308.15	50.41 (±0.04)	−4.26 (±0.14)
313.15	51.01 (±0.02)	−4.46 (±0.54)
318.15	51.90 (±0.03)	−4.95 (±0.12)
	Ammonium sulphate	
303.15	55.41 (±0.52)[1]	−3.99 (±0.15)[1]
308.15	55.71 (±0.04)	−4.27 (±0.16)
313.15	55.98 (±0.24)	−4.50 (±0.18)
318.15	56.71 (±0.05)	−6.19 (±0.21)
	Tetramethyl ammonium chloride	
303.15	101.61 (±0.42)[1]	−7.07 (±0.15)[1]
308.15	103.74 (±0.08)	−11.68 (±0.41)
313.15	104.39 (±0.02)	−13.03 (±0.07)
318.15	105.78 (±0.03)	−16.41 (±0.13)
	Tetraethyl ammonium iodide	
303.15	185.80 (±0.02)[1]	−3.32 (±0.11)[1]
308.15	188.67 (±0.14)	−14.73 (±0.94)
313.15	189.60 (±0.07)	−17.01 (±0.85)
318.15	189.82 (±0.12)	−20.09 (±0.78)
	Ammonium ceric nitrate	
303.15	233.45 (±0.60)[1]	−133.54 (±7.75)[1]
308.15	245.34 (±1.31)	−195.40 (±0.80)
313.15	252.30 (±0.16)	−245.36 (±2.16)
318.15	259.57 (±0.37)	−284.93 (±4.19)
	Ammonium cerium (IV) sulphate	
303.15	273.44 (±0.12)[1]	−308.50 (±1.36)[1]
308.15	288.34 (±0.71)	−441.21 (±8.48)
313.15	302.83 (±0.30)	−546.34 (±3.55)
318.15	315.53 (±0.50)	−629.89 (±0.58)

[1]Standard errors are given in parentheses.

Table 2—Various coefficients of Eq. 2 for different salts†

Salt	a	b	c
Ammonium sulphate	−19	0.43	−0.001
	(±0.98)†	(±0.00)†	(±0.000)†
Ammonium nitrate	−141	1.11	−0.022
	(±0.60)	(±0.00)	(±0.000)
Tetramethyl ammonium chloride	−2790	18.15	−0.030
	(±0.82)	(±0.00)	(±0.000)
Tetraethyl ammonium iodide	−3609	24.28	−0.039
	(±0.97)	(±0.01)	(±0.000)
Ammonium cerium(IV) sulphate	−1395	8.00	−0.008
	(±15.16)	(±0.44)	(±0.000)
Ammonium ceric nitrate	−9689	62.62	−0.009
	(±5.71)	(±0.02)	(±0.000)

†Standard errors are given in parentheses.

Table 3—Partial molar expansibilities (ϕ_E^0) for ammonium nitrate, ammonium sulphate, tetra methyl ammonium chloride, tetra ethyl ammonium iodide, ammonium ceric nitrate, and ammonium cerium (iv) sulphate in water at different temperatures

Electrolyte	Partial molar expansibility ϕ_E^0 [ml/(mole)(deg)]			
Temp. T (K)	303.15	308.15	313.15	318.15
NH_4NO_3	0.144	0.128	0.112	0.096
$(NH_4)_2SO_4$	0.063	0.062	0.051	0.045
Me_4NCl	0.574	0.278	−0.018	−0.314
Et_4NI	0.768	0.380	0.008	−0.396
$(NH_4)_2Ce(NO_3)_6$	2.870	1.885	0.899	−0.087
$(NH_4)_4Ce(SO_4)_4$	3.020	2.930	2.850	2.770

The various coefficients for different salts, along with standard errors are given in Table 2.

The partial molar expansibilities, $\phi_E^0 = (\partial \phi_v^0 / \partial T)$ calculated from general Eq. (2) are given in Table 3. It is evident from Table 3 that ϕ_E^0 decreases with increase in temperature, for all the electrolytes in water, indicating thereby that the behaviour of all the electrolytes is just like common salts, because in the case of common salts the molar expansibility should decrease with the increase in temperature[10,11].

The variation of ϕ_E^0 with temperature for all the electrolytes in water, is linear (a sample plot is shown in Fig. 2 for ammonium ceric nitrate). The decrease in ϕ_E^0 with the increase in temperature, for the different types of electrolytes in water, shows the absence of caging or packing effect[12].

It is also observed from Eq. 2 that $(\partial^2 \phi_v^0 / \partial T^2)_p$ for all the electrolytes in water, reported here, behave as structure breakers keeping in view the work of Hepler[13].

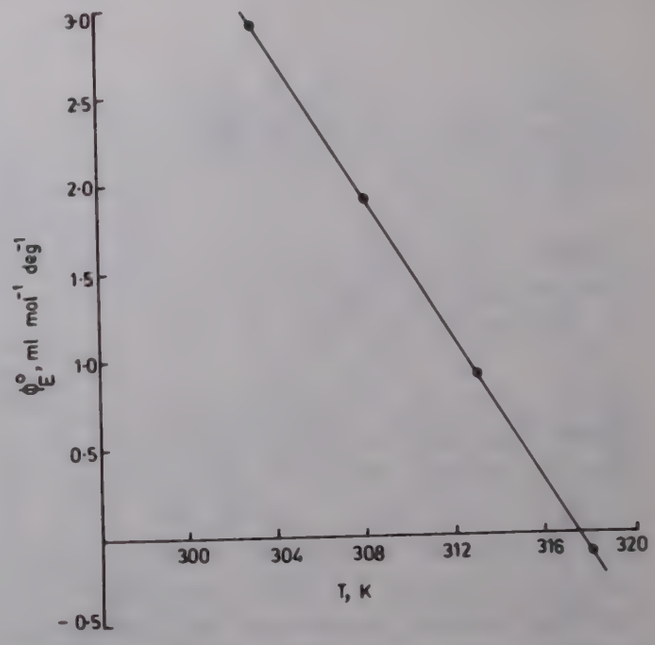

Fig. 2—Plot of ϕ_E^0 versus T for ammonium ceric nitrate.

The relative viscosities and densities of salts in water were also determined at different temperatures. The viscosity data were analysed by Jones-Dole[14] Eq. (3).

$$\eta_{rel} = \eta / \eta_0 = 1 + AC^{1/2} + BC \quad \ldots (3)$$

where η_{rel} is the relative viscosity of electrolytic solutions. A is the Falkenhagen[15] coefficient and B, the Jones-Dole coefficient[14]. A and B values were calculated by the method of least-squares by fitting the experimental results in the Jones-Dole equation and these values are given in Table 4.

A perusal of the data in Table 4 shows that the values of the coefficient A are very small in water for all the electrolytes at different temperatures indicating the presence of weak ionic interactions. Further, the value of A decreases with the increase in temperature meaning thereby that ionic interactions are weakened with the rise in temperature, which may be attributed to the increase in solvation of ions.

The B coefficients for all the electrolytes are positive and large in the entire temperature range indicating thereby the existence of strong ion-solvent interactions. The magnitude of B increases with the increase in temperature for all the electrolytes meaning thereby that ion-solvent interactions increase with the increase in temperature.

The dB/dT is a better criterion[16,17] for determining the structure making/breaking nature of any electrolyte rather than simply the B-coefficient. Viscosity study of a number of salt solutions showed that structure makers have negative

Table 4—Values of A ($cm^{3/2}$ $mol^{-(1/2)}$) and B (cm^3 mol^{-1}) parameters[†] for some common, tetra-alkyl and multicharged electrolytes in water at different temperatures

Temp. (K)	303.15	308.15	313.15	318.15
	Ammonium nitrate			
A	0.011	0.008	0.002	−2.006
	(±0.001)[†]	(±0.000)	(±0.001)	(±0.001)
B	0.089	0.090	0.098	0.115
	(±0.003)	(±0.002)	(±0.006)	(±0.002)
	Ammonium sulphate			
A	0.008	0.003	−0.005	−0.018
	(±0.000)	(±0.001)	(±0.001)	(±0.002)
B	0.264	0.273	0.288	0.305
	(±0.003)	(±0.003)	(±0.003)	(±0.008)
	Tetramethyl ammonium chloride			
A	0.043	0.039	0.031	0.027
	(±0.001)	(±0.001)	(±0.001)	(±0.000)
B	0.035	0.039	0.051	0.054
	(±0.000)	(±0.003)	(±0.007)	(±0.002)
	Tetraethyl ammonium iodide			
A	0.084	0.075	0.068	0.058
	(±0.003)	(±0.004)	(±0.001)	(±0.005)
B	0.116	0.132	0.139	0.162
	(±0.002)	(±0.003)	(±0.001)	(±0.004)
	Ammonium ceric nitrate			
A	0.062	0.058	0.048	0.041
	(±0.002)	(±0.004)	(±0.005)	(±0.005)
B	0.183	0.206	0.249	0.276
	(±0.003)	(±0.006)	(±0.006)	(±0.006)
	Ammonium cerium (IV) sulphate			
A	0.107	0.09	0.087	0.078
	(±0.005)	(±0.003)	(±0.002)	(±0.001)
B	0.419	0.430	0.506	0.624
	(±0.007)	(±0.005)	(±0.003)	(±0.003)

[†]Standard errors are given in parentheses.

values of dB/dT whereas structure breakers, positive values. It is evident from Table 4 that the value of dB/dT is positive, thereby suggesting the structure breaking nature of all the electrolytes in water. This conclusion from dB/dT is in excellent agreement with that drawn from $(\partial^2 \phi_v^0/\partial T^2)_p$.

Table 5—Values of $\bar{V}_2^0$ and $\Delta\mu_2^{0*}$ ($\Delta\mu_1^{0*} = 9.04$ kJ mol^{-1}) for ammonium nitrate, ammonium sulphate, tetramethyl ammonium chloride, tetraethyl ammonium iodide, ammonium ceric nitrate and ammonium cerium (iv) sulphate in water at 303.15 K

Electrolyte	$\bar{V}_2^0$ (cm^3 mol^{-1})	$\Delta\mu_2^{0*}$ (kJ mol^{-1})
Ammonium nitrate	49.73	25.72
Ammonium sulphate	55.41	50.91
Tetramethyl ammonium chloride	101.61	25.42
Tetraethyl ammonium iodide	185.80	48.45
Ammonium ceric nitrate	233.45	64.43
Ammonium cerium (IV) sulphate	273.44	103.05

The viscosity data were also analysed on the basis of the transition state treatment of relative viscosity of the electrolytic solutions as suggested by Feakins *et al*[18]. The B-parameter in terms of this theory is given by Eq. (4),

$$B = \frac{\bar{V}_1^0 - \bar{V}_2^0}{1000} + \frac{\bar{V}_1^0}{1000}\left[\frac{\Delta\mu_2^{0*} - \Delta\mu_1^{0*}}{RT}\right] \quad \ldots (4)$$

where $\bar{V}_1^0$ is the partial molar volume of the solvent and $\bar{V}_2^0$ is the partial molar volume of the solute. The free energy of activation per mole of the pure solvent ($\Delta\mu_1^{0*}$) and the free energy of activation per mole of solute ($\Delta\mu_2^{0*}$) were calculated with the help[19] of Eqs (5) and (6) respectively.

$$\Delta\mu_1^{0*} = RT \ln(\eta_0 \bar{V}_1^0/hN) \quad \ldots (5)$$

and

$$\Delta\mu_2^{0*} = \Delta\mu_1^{0*} + \frac{RT}{\bar{V}_1^0}[1000B - (\bar{V}_1^0 - \bar{V}_2^0)] \quad \ldots (6)$$

where h is the Planck constant, N the Avogadro number, η_0 is the viscosity of the solvent (water). The value of $\Delta\mu_1^{0*}$ in water at 303.15 K was found to be 9.04 (kJ mol^{-1}) by taking the standard partial molar volume of water at 303.15 K as 18.08 cm^3 mol^{-1}. The values of $\Delta\mu_2^{0*}$ for the different electrolytes, at 303.15 K are recorded in Table 5. It is evident from Table 5 that the values of $\Delta\mu_2^{0*}$ are positive and larger than $\Delta\mu_1^{0*}$. This suggests that the formation of the transition state is less favoured in presence of the salts, meaning thereby that formation of the transition state is accompanied by the breaking and distortion of the intermolecular bonds.

The different types of electrolytes viz; common, tetra-alkyl and multicharged electrolytes in water

have similar behaviour i.e. all of them behave similar to common electrolytes in water but dissimilar to n-Bu_4N^+ and n-Pr_4N^+ ions, which are strong hydrophobic structure makers. If we focus our attention to the present results only for Me_4NCl and Et_4NI, the conclusions drawn from partial molar volume and viscosity are in agreement with literature, as reported by Kay and coworkers, from the measurement of conductance[20] and viscosity[21], which indicate that the Me_4N^+ ion is a structure breaker, but Et_4N^+ ion is in the transition region between a structure maker and a structure breaker. This is because of the reason that Me_4N^+ ion is just small enough so that the water structure around the ions is still under the influence of its charge and the Et_4N^+ ion is just large enough that the effect of charge on the water structure is slightly overshadowed by the hydrophobic or clathrate effect.

Acknowledgement

The authors are highly grateful to the University Grants Commission, New Delhi (India) for financial assistance.

References

1 Parmar M L & Khanna A, *Proc Indian natn Sci Acad*, **55** (1989) 35.
2 Parmar M L & Rao Ch V N, *Indian J Chem*, 29A (1990) 958.
3 Hedwing G R, Owensky D A & Parker A J, *J Am chem Soc*, 97 (1974) 3888.
4 Shoemaker D P & Garland C W, *Experiments in physical chemitry* (Mc Graw Hill, New York) 1967, 131.
5 Ward G K & Millero F J, *J soln Chem*, 3 (1974) 417.
6 Parmar M L & Kundra A, *Electrochim Acta*, 28 (1983) 1655.
7 Parmar M L & Khanna A, *J phys Soc Japan*, 55 (1986) 4122.
8 Parmar M L & Khanna A, *Indian J Chem*, 25A (1986) 1044.
9 Masson D O, *Phil Mag*, 8 (1929) 218.
10 Millero F J & Drost Hansen W, *J phys Chem*, 72 (1968) 1758.
11 Millero F J, *Chem Rev*, 71 (1971) 147.
12 Millero F J, in *Structure and transport processes in water and aqueous solutions*, edited by R A Horne (Wiley-Interscience, New York) 1971, Chapter 15, p. 622.
13 Hepler L G, *Can J Chem*, 47 (1969) 4613.
14 Jones G & Dole M, *J Am chem Soc*, 51 (1929) 2950.
15 Falkenhagan H & Vernan E L, *Z Phys*, 33 (1932) 140.
16 Gurney R W, *Ionic processes in solutions* (McGraw Hill, New York) 1954.
17 Sarma T S & Ahluwalia J C, *Rev chem Soc*, 2 (1973) 217.
18 Feakins D, Freemantle J D & Lawence K G, *J chem Soc Faraday Trans I*, 70 (1974) 795.
19 Glasston S, Laidler K & Eyring H, *The theory of rate processes* (McGraw Hill, New York) 1941, 477.
20 Kay R L & Evans D F, *J phys Chem*, 69 (1965) 4216; **70** (1966) 2325.
21 Kay R L, Vituccio T, Zawosky C & Evans D F, *J phys Chem*, 70 (1966) 2376.

Indian Journal of Chemistry
Vol. 31A, September 1992, pp. 721-722

Excess molar volumes of binary mixtures containing nitrotoluene at 308.15 K

V K Sharma* & Sanjeev Maken
Department of Chemistry, Maharshi Dayanand University, Rohtak 124 001

Received 17 January 1992; revised and accepted 22 April 1992

Excess molar volumes, V^E, for *m*-nitrotoluene (i) + cyclohexane (j), + *n*-hexane (j), + *n*-heptane (j) and + *n*-hexadecane (j) have been determined as a function of composition at 308.15 K. The data for an equimolar composition vary as *n*-hexane < *n*-heptane < *n*-hexadecane and suggest that while *m*-nitroluene (i) + *n*-hexane mixture is characterized by dipole-induced dipole interactions, the remaining mixtures are influenced by additional steric repulsion between the terminal CH_3 substituents of alkane and the CH_3 substituent of *m*-nitrotoluene.

Recent studies[1-3] have shown that V^E data for aromatic hydrocarbons + *n*-alkane binary mixtures depend on the positive inductive effect of CH_3 substituent in benzene and is independent of a number of carbon atoms of aliphatic chain on the aromatic ring. It would then be interesting to see as to how the excess volumes of aromatic hydrocarbons + *n*-alkane binary systems would be affected if both electron-withdrawing and electron releasing substituents are present in the benzene ring of such systems. This prompted us to undertake the present study.

Experimental

Cyclohexane, *n*-hexane, *n*-heptane (Sisco, Bombay) were purified by standard methods[4-6] *n*-Hexadecane (Fluka, Purris-quality) with stated purity of ≥99.5 mol % was used without further purification. Prior to actual measurements, *n*-alkanes were dried with molecular seive (union carbide type 4A, beads from Fluka). *m*-Nitrotoluene (99%, Sisco, Bombay) was distilled under vacuum and fractionated at 100 mm of Hg (b.p. 156°C)[7]. The purities of the purified compounds were checked by measuring their densities at 298.15 ± 0.01 K (recorded in Table 1) and these values agreed to within $\pm 5 \times 10^{-5}$ gm cm^{-3} with their corresponding literature[8-12] values. (The density of *m*-nitrotoluene at 298.15 K was calculated from the density versus temperature data[8]).

The molar excess volumes were determined in a dilatometer by the procedure described elsewhere[13]. The temperature of the water bath was controlled within ± 0.01 K by means of a toluene regulator. Two degassed liquids in the dilatometer were separated by means of a mercury column and the change in the level of liquid in the dilatometer was measured by a cathetometer with a precision of ± 0.001 cm. To ensure complete mixing in the capillary, the dilatometer was removed from the water bath after mixing, placed in a cold bath (so that there was minimum liquid in the capillary) and then again placed in the experimental bath. The process was repeated two to three times. The uncertainty in V^E results is about 0.5%.

Table 1—Comparison between the pure component densities measured at 298.15 ± 0.01 K and the corresponding literature values

Compound	Density (gm cm^{-3})	
	Experimental	Literature
m-Nitrotoluene	1.15237	1.15239[8]
Cyclohexane	0.77388	0.77392[9]
n-Hexane	0.65483	0.65479[10]
n-Heptane	0.67951	0.67955[11]
n-Hexadecane	0.76989	0.76991[12]

Results and discussion

The excess molar volumes, V^E, of binary mixtures as a function of composition at 308.15 K are recorded in Table 2 and plotted in Fig. 1. The V^E data were expressed as

$$\frac{V^E}{x_i x_j} = [a + b(x_i - x_j) + c(x_i - x_j)^2] \quad \ldots (1)$$

Table 2—Values of the parameters a, b and c of equation 1 along with standard deviation $\sigma(V^E)$ values of the molar excess volumes for the various (i + j) mixtures at 308.15 K

System	a	b	c	$\sigma(V^E)$ cm^3 mol^{-1}
m-Nitrotoluene (i) + *n*-heptane (j)	−3.6099	0.5046	−0.4212	0.002
m-Nitrotoluene (i) + *n*-heptane (j)	−2.2279	0.1153	−0.2653	0.002
m-Nitrotoluene (i) + *n*-Hexadecane(j)	1.3096	−0.4201	0.0289	0.003
m-Nitrotoluene (i) + Cyclohexane (j)	1.7799	−0.2701	0.0257	0.002

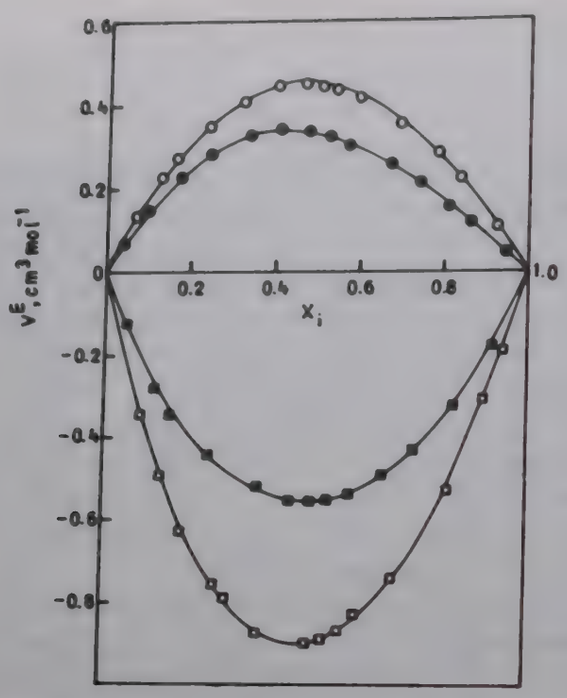

Fig. 1—Variation of V^E with mole fraction, x_i for nitrotoluene with ○ cyclohexane, ■ *n*-hexane, □ *n*-heptane, ● *n*-hexadecane at 308.15 K.

where x_i is the mole fraction of component i and a, b and c are parameters (Table 2) which were evaluated by the least squares method to give the standard errors defined by

$$\sigma(V^E) = [\Sigma[V^E_{expt} - V^E_{cal}]^2/(m-p)]^{1/2} \quad \ldots (2)$$

We have not compared our data with any of the existing data on such systems. The V^E data for the present mixtures (for an equimolar composition) vary as *n*-hexane < *n*-heptane < *n*-hexadecane. V^E data of *m*-nitrotoluene + *n*-alkane mixtures can be explained if it is assumed that these mixtures are characterized by dipole-induced dipole interactions. Since *m*-nitrotoluene is polar, strong dipole-induced dipole interactions would render *m*-nitrotoluene + *n*-hexane mixtures to have negative V^E values. Further an increase in C – C chain length of *n*-hexane would envisage that *m*-nitrotoluene + *n*-heptane or + *n*-hexadecane mixtures would be characterized not only by dipole-induced dipole interactions but also by steric repulsion between the terminal CH_3 substituents of *n*-heptane or *n*-hexadecane with the CH_3 substituents of *m*-nitrotoluene; the steric repulsion would be maximum in *m*-nitrotoluene + *n*-hexadecane mixture than that in *m*-nitrotoluene + *n*-heptane mixtures. The V^E data of *m*-nitrotoluene + *n*-hexane, + *n*-heptane and + *n*-hexadecane mixtures should thus vary as *n*-hexane < *n*-heptane < *n*-hexadecane which is indeed true.

Acknowledgement

We are thankful to the Head of the Chemistry Department and the authorities of MD University, Rohtak for providing the necessary research facilities.

References

1 Caceres Alonso M & Nunez Delgado J, *J chem Engng Data*, 28 (1983) 61.
2 Caceres Alonso M & Nunez Delgado J, *J chem Thermodyn*, 13 (1981) 1133.
3 Caceres Alonso M & Nunez Delgado J, *J chem Engng Data*, 27 (1982) 331.
4 Morgan S O & Lowry H H, *J phys Chem*, 34 (1930) 2385.
5 Crow R W & Smyth C P, *J Am chem Soc*, 73 (1951) 5406.
6 Herold W & Wolf K L, *Z phys Chem*, Abt B, 12 (1982) 194.
7 *CRC hand book of chemistry and physics* (edited by C R Weast), 59th edn.
8 Timmermans J, *The physico-chemical constants of pure organic compounds* (Elsevier, New York), 1950.
9 Aicart E, Tardojos G & Diaz Pena M, *J chem Engng Data*, 25 (1980) 140.
10 Diaz Pena M & Nunez Delado J, *J chem Thermodyn*, 7 (1975) 201.
11 Treszczanowicz A J, Halpin C J & Benson G C, *J chem Engng Data*, 27 (1982) 321.
12 Deanesly R M & Carleton L T, *J phys Chem*, 45 (1941) 1104.
13 Singh P P & Sharma S P, *J chem Engng Data*, 30 (1985) 477.

Indian Journal of Chemistry
Vol. 31A, September 1992, pp. 723-725

Kinetics of oxidation of nitrite by peroxomonosulphate

Madhu Sharma, D S N Prasad & K S Gupta*
Atmospheric Chemistry Laboratory, Department of Chemistry
University of Rajasthan, Jaipur 302 004, India

Received 24 October 1991; accepted 12 March 1992

Rate studies on peroxomonosulphate-nitrite reaction show that the reaction obeys the rate equation,

$$-\frac{d[HSO_5^-]}{dt} = \frac{\{k_0K_a + k_1[H^+] + k_2K_2[H^+]^2\}[PMS][NO_2^-]_t}{(K_a + [H^+])}$$

where K_a is the dissociation constant of HNO_2. Values of k_0, k_1 and k_2K_2 are 0.14, 0.31 and 6.4×10^2 dm^3 mol^{-1} s^{-1}, respectively at 25°C. A comparison with oxidation of HSO_3^- by peroxomonosulphate shows that, in atmosphere, NO_2^- will not be able to compete with HSO_3^-.

Concentration of peroxomonosulphate (PMS) has been predicted to be only one order of magnitude less than that of H_2O_2 in remote marine and continental clouds[1]. PMS radical is formed[2] in the first propagation step of the metal ion catalysed atmospheric oxidation of SO_2. Moreover, PMS ion is reported to be formed as an intermediate in surface catalysed autoxidation of aqueous SO_2 in suspensions of several metal and non-metal oxides[3-8]. Besides sulphur dioxide, oxides of nitrogen are other important acid rain precursors. A recent modelling exercise by Luria and Sievering[9] has shown that HNO_2, in atmosphere, may be present to the extent of 0.1-0.4 parts per trillion by volume. Reaction of NO_2^- with S(IV) (refs 10-12) is considered to be one of the paths contributing to atmospheric acid precipitation. In remote marine and continental clouds, both nitrite and sulphur(IV) may compete for PMS. The kinetics of oxidation of S(IV) by PMS have been studied recently[13]. It was, therefore, of interest to study the oxidation of nitrite by PMS in order to compare the relative reactivities of NO_2^- and PMS in the *p*H region of interest to atmospheric situations. Previously, a preliminary investigation on kinetics of nitrite-PMS reaction has been made[14].

Experimental

Oxone (Aldrich), which is a triple salt ($2KHSO_5.KHSO_4.K_2SO_4$), was the source of peroxomonosulphate. Sodium nitrite (BDH, AnalaR) and all other chemicals of reagent grade were used. Iodometric assay revealed the PMS content in the triple salt to be around 85%. Sodium nitrite solutions were standardised cerimetrically and only fresh solutions were used. Acetate buffer was used for maintaining the *p*H of reaction mixtures. The reactions were initiated by mixing temperature equilibrated solution of sodium nitrite with the solution of PMS containing buffer and maintained at the same temperature (±0.1°C). For following the kinetics, the nitrite was decomposed by addition of sulphamic acid to the aliquots. Now potassium iodide was added and the liberated iodine was titrated against standard sodium thiosulphate solution using starch as an indicator. The duplicate rate measurements were reproducible within ±5%.

Stoichiometry

The stoichiometry was determined by keeping [PMS] in some, and [nitrite] in other experiments, in excess and the unreacted PMS was determined iodometrically and unreacted nitrite was determined cerimetrically. Both the methods of stoichiometric measurements led to Eq. (1). The product nitrate was detected

$$HSO_5^- + NO_2^- \rightarrow SO_4^{2-} + NO_3^- + H^+ \quad \ldots (1)$$

by usual qualitative tests as well as by appearance of a peak in the visible spectrur of final product solution at 302 nm.

Results

The kinetic results of [PMS] and [nitrite] variations are consistent with the experimental rate law (2),

$$-\frac{d[PMS]}{dt} = k[PMS][NO_2^-]_t \quad \ldots (2)$$

where [PMS] and $[NO_2^-]_t$ represent the analytical concentrations of PMS and nitrite respectively. From the kinetic runs in which $[NO_2^-]_t$ was in excess over [PMS], the pseudo-first order rate constants, k_{obs} (Table 1), were obtained by using Eq. (3),

$$-\frac{d[PMS]}{dt} = k_{obs}[PMS] \quad \ldots (3)$$

where $k_{obs} = k[NO_2^-]_t$

In some kinetic runs, [PMS] and $[NO_2^-]_t$ were either equal or comparable and, the values of second or-

der rate constants are in good agreement with those derived from k_{obs}. On increasing *p*H the rate of reaction decreases and tends to attain a limiting value at *p*H > 5 (Table 1). The variation of ionic strength (0.1-1.0 mol dm^{-3}) with sodium perchlorate did not affect the rate of the reaction.

Discussion

The first dissociation constant of peroxomonosulphate is reported to be high ($pK_1 < 0$) and the second dissociation constant to be low ($pK_2 = 9.8$) (ref. 16). Thus, in the *p*H range of 2.08-7.01 used in this study, PMS will be present largely as HSO_5^-.

Table 1—The values of pseudo-first order constant, k_{obs}, and second order rate constant, k, at 25°C

10^4 [PMS] (mol dm^{-3})	10^3 [NO_2^-]$_i$ (mol dm^{-3})	*p*H	10^4 k_{obs} (s^{-1})	k (dm^3 mol^{-1} s^{-1})
5.00	5.0	3.69	10	0.20
9.35	5.0	3.69	—	0.22
11.90	5.0	3.69	—	0.19
15.30	5.0	3.69	—	0.21
18.70	5.0	3.69	—	0.25
23.80	5.0	3.69	—	0.24
2.55	10.0	3.69	—	0.19
5.10	10.0	3.69	—	0.26
8.50	10.0	3.69	—	0.26
12.75	10.0	3.69	—	0.23
25.50	10.0	3.69	—	0.24
2.55	0.5	3.69	—	0.23
2.55	1.0	3.69	—	0.19
2.55	2.0	3.69	4.6	0.23
2.55	3.0	3.69	6.1	0.20
2.55	4.5	3.69	9.0	0.20
2.55	6.0	3.69	13	0.21
2.55	7.5	3.69	17	0.23
2.55	9.0	3.69	21	0.23
2.55	10.0	3.69	24	0.24
10.0	1.0	7.01	—	0.14
10.0	1.0	6.22	—	0.14
10.0	1.0	5.01	—	0.14
10.0	1.0	4.65	—	0.14
10.0	1.0	3.71	—	0.16
10.0	1.0	3.69	—	0.21
10.0	1.0	3.30	—	0.32
10.0	1.0	3.14	—	0.40
10.0	1.0	2.80	—	0.60
10.0	1.0	2.69	—	1.3
10.0	1.0	2.39	—	2.4
10.0	1.0	2.08	—	5.1

The observed [H^+] dependence is thus most likely related to involvement of nitrite ion and its various protonated forms, as shown in the following Scheme 1.

$$HNO_2 \overset{K_a}{\rightleftharpoons} NO_2^- + H^+$$

$$HNO_2 + H^+ \xrightarrow{K_2} NO^+ + H_2O$$

$$NO_2^- + HSO_5^- \xrightarrow{k_0} NO_3^- + SO_4^{2-} + H^+$$

$$HNO_2 + HSO_5^- \xrightarrow{k_1} NO_3^- + SO_4^{2-} + 2H^+$$

$$NO^+ + HSO_5^- + H_2O \xrightarrow{k_2} NO_3^- + SO_4^{2-} + 3H^+$$

Scheme 1

Scheme 1 leads to the rate law (4).

$$k = \frac{k_0K_a + k_1[H^+] + k_2K_2[H^+]^2}{(K_a + [H^+])} \quad \ldots (4)$$

Dissociation constant, K_a, of HNO_2 is reported to be 5.1×10^{-4} and so in the *p*H range 5-7, nitrite will be almost wholly present as NO_2^-. Hence the rate of reaction in this region can be ascribed to mainly NO_2^--HSO_5^- reaction and contributions from k_1 and k_2 paths may be ignored. On this basis second order rate constants determined in *p*H region 5-7 may be taken equal to k_0.

On rearranging Eq. (4) becomes Eq. (5).

$$\frac{k(K_a + [H^+]) - k_0K_a)}{[H^+]} = k_1 + k_2K_2[H^+] \quad \ldots (5)$$

The plot of left hand side of Eq. (5) against [H^+] was linear (Fig. 1) and from the intercept and slope the

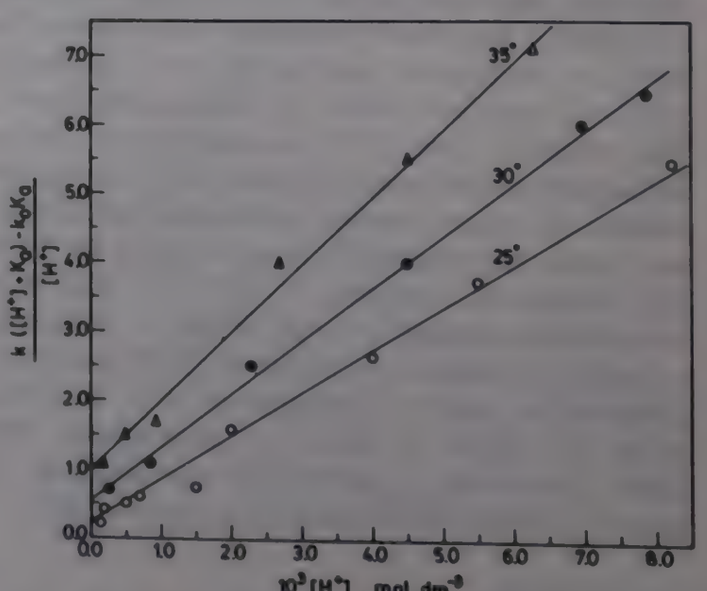

Fig. 1—The effect of [H^+] on the rate of nitrite-peroxomonosulphate reaction at I = 1.0 mol dm^{-3}

Table 2—The values of k_0, k_1 and k_2K_2 at different temperatures

Rate constants ($dm^3\ mol^{-1}\ s^{-1}$)	Temperature, °C			E_a kJ mol^{-1}	$\Delta S^{\neq}$ ($J\ mol^{-1}\ K^{-1}$)
	25	30	35		
k_0	0.14	0.19	0.26	47	−104
k_1	0.31	0.50	0.95	85	27
k_2K_2	640	780	870	31	−150

values of k_1 and k_2K_2 were determined. These values together with k_0 are given in Table 2 which also includes energies and entropies of activation for k_0, k_1 and k_2K_2.

The value of equilibrium constant, K_2, is reported[17] to be 3×10^{-7}. From the k_2K_2 value, k_2 is estimated to be 2.1×10^9 $dm^3\ mol^{-1}\ s^{-1}$ at 25°C. This value of k_2 suggests the reaction of NO^+ with HSO_5^- to be diffusion controlled. The reaction of NO_2^- and H_2O_2 has also been studied in the $[H^+]$ range of 0.1-1.0 mol dm^{-3}. Using the same K_2 value, from the data of Benton and Moore[18], the value of k_2 for NO^+ and H_2O_2 reaction is estimated to be 5×10^9 $dm^3\ mol^{-1}\ s^{-1}$. Thus, both NO^+-H_2O_2 and NO^+-HSO_5^- reactions are diffusion controlled and take place at nearly the same rates. Incidentally, Betterton and Hoffmann[13] found a similar behaviour of HSO_5^- and H_2O_2 towards HSO_3^-.

It is of interest to compare the results of this study with those of Edwards and Mueller[14]. k (25°C) and E_a values of 0.14 $dm^3\ mol^{-1}\ s^{-1}$ and 11.0 kcal/mol compare favourably with those (0.31 $dm^3\ mol^{-1}\ s^{-1}$ and 13.2 kcal/mol) of earlier workers[14]. In the previous study the main contributing path to the overall rate was NO_2^--HSO_5^- reaction as their study was done in the high *p*H range. In the present case, two additional paths manifest themselves in the low *p*H region. In atmosphere, both H_2O_2 and HSO_5^- may compete for oxidising nitrite. A comparative rate analysis carried out by Edwards and Mueller[14] has shown HSO_5^- to be several orders of magnitude more reactive than H_2O_2 in the *p*H range of interest to atmospheric chemists. Thus if both HSO_5^- and H_2O_2 are present, NO_2^- will be preferentially oxidised by HSO_5^-.

A comparison of the rates of oxidation of S(IV) and nitrite ion by PMS is in order. At *p*H 2.08, Betterton and Hoffmann[13] determined the overall second order rate constant to be 4.11×10^4 $dm^3\ mol^{-1}\ s^{-1}$ at 5°C. In the present reaction at the same *p*H value but at 25°C the overall second order rate constant has a value of 4.38 $dm^3\ mol^{-1}\ s^{-1}$. It is therefore concluded that, in atmosphere, HSO_5^- will oxidise HSO_3^- at a rate much faster than NO_2^-.

Acknowledgement

The work was supported by Indo-US Subcommission and UGC research projects.

References

1 Jacob D J, *J geophys Res*, 91 (1986) 9807.
2 Backstrom H, *Z phy Chem*, 25B (1934) 122.
3 Prasad D S N, Rani A & Gupta K S, *Environ Sci Technol*, (1992) (in press).
4 Rani A, Prasad D S N, Madnawat P V S & Gupta K S, *Atmos Environ*, 26A (1992) 667.
5 Rani A, Prasad D S N, Bhargava R & Gupta K S, *Bull chem Soc Japan*, (1991) 1955.
6 Rani A, Prasad D S N, Jain U & Gupta K S, *Indian J Chem*, 30A (1991) 756.
7 Prasad D S N, Madnawat P V S, Rani A, Bhargava R & Gupta K S, *J mol Catal*, 69 (1991) 393.
8 Gupta K S, Madnawat P V S, Rani A, Sharma M, Prasad D S N, Jain U, Bhargava P & Saxena D in *Chemical kinetics and reaction mechanism* edited by K S Gupta (RBSA Publishers, Jaipur) 1991, pp 117-164.
9 Luria M & Sievering H, *Atmos Environ*, 25A (1991) 1489.
10 Prasad D S N & Gupta K S, *Bull Soc Kinet Ind*, 12(1) (1990) 1.
11 Oblath S B, Markowitz S S, Novakov T & Chang S G, *J phys Chem*, 85 (1981) 1017.
12 Seel F & Dagner E, *Z anorg allg Chem*, 284 (1956) 101; Yamamoto S & Kaneda T, *Nippon Kagaku Zasshi*, 80 (1959) 1908; Seel F & Knorre H, *Z anorg allg Chem*, 313 (1961) 70.
13 Betterton E A & Hoffmann M R, *J phys Chem*, 92 (1988) 5962.
14 Edwards J O & Mueller J J, *Inorg Chem*, 1 (1962) 696.
15 Alock N W, Benton D J & Moore P, *Trans Faraday Soc*, 66 (1970) 2210.
16 Spiro M, *Electrochem Acta*, 24 (1979) 313.
17 Wischart J F, Taube H, Breslauer K J & Isied S S, *Inorg Chem*, 25 (1986) 1497.
18 Benton D J & Moore P, *J chem Soc A* (1970) 3179.

Indian Journal of Chemistry
Vol. 31A, September 1992, pp. 726-727

Kinetics of release of dithizone from mercury(II) dithizonate by triphenylphosphine

Tarlok S Lobana*, M S Sidhu, Sanjeev Kumar & Randhir Singh
Department of Chemistry,
Guru Nanak Dev University, Amritsar 143 005

Received 16 August 1991; revised and accepted 14 February 1992

Reaction of mercury(II) dithizonate with triphenylphosphine releases free dithizone in the presence of acetic acid and follows a pseudo-first order kinetics with rate constant, $k = 7.38 \times 10^{-5}\ s^{-1}$.

Dithizone (H_2Dz) has been extensively used for the extractive photometric determination of heavy metals (e.g. Pb, Hg, Ag, Cd etc.)[1]. Free H_2Dz exists in tautomeric equilibrium in organic solvents:

In chloroform, the thione and thiol forms absorb light at 605 nm ($\varepsilon = 41490\ dm^3\ mol^{-1}\ cm^{-1}$) and 422 nm ($\varepsilon = 16000\ dm^3\ mol^{-1}\ cm^{-1}$) respectively[2].

Mercury(II) dithizonate $Hg(HDz)_2$ ($\lambda_{max} = 490$ nm) exhibits photochromism in solvents like $CHCl_3$, CCl_4 etc. (colour of the solution changes from orange to dark blue or violet when its solutions are placed either in the sunlight or irradiated with light, $\lambda > 450$ nm)[3]. In the present investigation, it was intended to explore the effect of organo-phosphorus reagents like triphenylphosphine to stabilize the colour of $Hg(HDz)_2$ when exposed to light. However, we observed the release of free dithizone on addition of triphenylphosphine – a rare phenomenon in phosphine chemistry[4-6].

Experimental

Analytical grade reagents, mercury(II) acetate and chloroform were procured from Ranbaxy (Chandigarh). $Hg(OOCCH_3)_2$ was standardized before use[7]. Dithizone (E. Merck, Bombay) and triphenylphosphine (AG Fluka, Switzerland) were used as such. Acetic acid (Sisco, Bombay) was purified by the reported method[8].

A stock solution of mercury(II) acetate (3.482×10^{-4} mol dm^{-3}) was prepared in deionized distilled water and that of H_2Dz (8.44×10^{-4} mol dm^{-3}) was prepared in chloroform. Experimental solutions were prepared as follows: Added one ml each of the above two stock solutions into the stoppered round bottomed flask, followed by 4 ml each of water and chloroform, stirred the contents on a magnetic stirrer for 10 min. to establish the equilibrium, solution was transferred to a separating funnel, the organic layer was taken out in a measuring flask (25 ml) followed by the addition of 10 mg of PPh_3 and 6-7 drops of acetic acid and the volume made upto the mark using chloroform. The release of dithizone from $Hg(HDz)_2$ complex was monitored at 25 ± 2°C using Shimadzu UV-visible recording spectrophotometer UV-240.

Results and discussion

The reagent H_2Dz extracted Hg(II) quantitatively from the aqueous phase to the non-aqueous phase (Eq. 1)

$$Hg^{2+}(II) + 2H_2Dz \rightleftharpoons Hg(HDz)_2 + 2H^+ \quad \ldots (1)$$

The addition of excess PPh_3 to the solution of $Hg(HDz)_2$ in chloroform liberated H_2Dz ... (2)

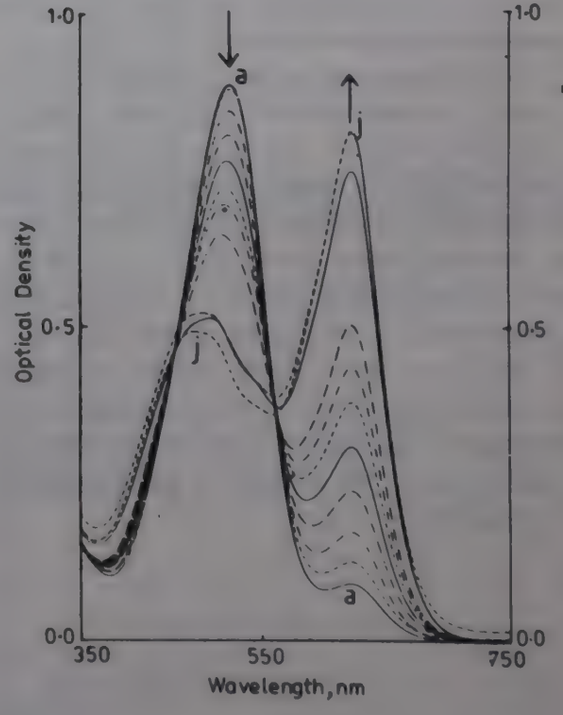

Fig. 1 – Electronic absorption spectra of the release of dithizone from mercury(II) dithionate (1.39×10^{-5} mol dm^{-3}) with triphenyl phosphine (1.52×10^{-3} mol dm^{-3}) after (a) 0.0; (b) 14.0; (c) 39.0; (d) 80.0; (e) 110.0; (f) 141.0; (g) 168.0; (h) 191.0; (i) 280.0; (j) 300.0 minutes.

$$Hg(HDz)_2 + 2CH_3COOH + 2PPh_3 \rightleftharpoons Hg(OOCCH_3)_2(PPh_3)_2 + 2H_2Dz \quad \ldots (3)$$

It may be noted that mercury(II) salts form 1:2 complexes with tertiary phosphines, e.g., $HgX_2(PPh_3)_2$ (where X = Cl, CN, NCS and $OOCCF_3$)[9-12]. The liberation of H_2Dz (Fig. 1) followed pseudo-first order kinetics with respect to $Hg(HDz)_2$ and the first order rate constant ($k = 7.38 \times 10^{-5}$ s^{-1}) was calculated from linear first order plot. The reaction seems to be autocatalyzed as the rate of reaction increases with the passage of time. In contrast, triphenylphosphine sulphide (Ph_3PS) fails to liberate H_2Dz from $Hg(HDz)_2$. PPh_3 is a much stronger lewis base as compared to Ph_3PS.

It is significant that H_2Dz is liberated even in the absence of added acetic acid, but the rate of the reaction is immeasurably slow. It was observed that when $Hg(OOCCH_3)_2$ reacts with H_2Dz, the liberated CH_3COOH also gets transferred to the organic layer (*p*H of the aqueous solution after Hg(II) extraction was nearly 7).

Acknowledgement

Two of us (SK and RS) are thankful to the Guru Nanak Dev University, Amritsar for laboratory facilities.

References

1 Sandell E B & Onishi H, '*Photometric determination of traces of metals*, Part 1 (John Wiley, New York) (1978).
2 Ramakrishna R S & Irving HMNH, *Anal chim Acta*, 48 (1969) 252.
3 Meriwether L S, Breitner E C & Sloan C L, *J Am chem Soc*, 87 (1965) 4441, 4448.
4 McAulife C A, *Transition metal complexes of phosphorus, arsenic and antimony ligands* (McMillan, London) (1973).
5 McAulife C A & Levason W, *Phosphine arsine and stibine complexes of transition elements: Studies in inorganic Chemistry*, Vol. 1, (Elsevier, Amsterdam) (1979).
6 Lobana T S, '*The chemistry of organophosphorus compounds*' edited by F R Hartley, (John Wiley, Chichester) Vol. 2 (1992) p. 409.
7 Vogel A I, *A text book of quantitative inorganic analysis*, (ELBS, London) (1961).
8 John A Riddick & William B Bunger, *Organic solvents*, (Wiley-Interscience, New York) (1970).
9 Colton R & Dakternieks D, *Aust J Chem*, 34 (1981) 323.
10 Buergi H B, Fischer E, Kunz R W, Parvez M & Pregosin P S, *Inorg Chem*, 21 (1982) 1246.
11 Lobana T S, Sandhu M K, Snow M R & Tiekink E R T, *Acta Crystallogr*, C44 (1988) 1979.
12 Lobana T S, Sandhu M K, Povey D C, Smith G W & Ramdas V, *J chem Soc Dalton Trans*, (1989) 2339.

Indian Journal of Chemistry
Vol. 31A, September 1992, pp. 728-731

Kinetics of oxidation of thioacetic acid by methylene blue in methanol-water medium

K Chansoria & K K Mishra*

Department of Postgraduate Studies and Research in Chemistry, R D University, Jabalpur 482 001

Received 4 December 1991; revised 28 February 1992; accepted 2 April 1992

Thioacetic acid (TA) and methylene blue (MB) interact to form corresponding disulphide and the leuco base. The order in MB is two in the initial part (40-50%) of the kinetic runs and in the latter part it changes to 1/2. The order in [TA] is unity. The second order rate constant increases linearly with increase in $[H^+]$ while the half order rate constant shows a fractional dependence on $[H^+]$ at low concentrations. At higher $[H^+]$ (ca. $\geq 4.0 \times 10^{-2}$ mol dm^{-3}) however, again a linear relationship between $k_{1/2}$ and $[H^+]$ has been noticed. The rate decreases with increase in [MB]. The variation in ionic strength does not affect the rate. The psuedo-second order rate constant decreases and attains a limiting value while the half order rate constant continuously decreases on decreasing the dielectric constant of the medium. Addition of the products does not affect the rate but second order behaviour in [MB] observed in the initial part disappears in the presence of leuco base. The order in TA remains unity while the pseudo-half order rate constant is not influenced by varying [MB] under these conditions. The addition of methyl methacrylate does not affect the rate initially but appreciably retards the rate of the latter part of the reaction. Activation parameters have been evaluated and the participation of semireduced methylene blue is shown to cause the kinetic deviations.

A wide and varied involvement of sulphydryl compounds in human metabolism has received enormous attention in the recent past and thus, kinetics of oxidation of thioacetic acid by methylene blue in the presence of HCl is reported herewith. Methylene blue is known to participate in the electron transfer reactions used as model systems for mechanistic investigations on the oxidation of flavin-bound enzymes[1] and recently, the kinetics of V(V)-catalysed oxidation of bromate ion by this oxidant have been reported[2]. The reaction systems investigated presently are highly dependent on steric factors as revealed by the diversity in kinetic features recorded for thioacetic acid and for mercaptosuccinic and *o*-mercaptobenzoic acids[3,4] reported earlier.

Experimental

The solution of thioacetic acid (TA or RSH) was prepared by diluting the sample (E. Merck) in methanol (E. Merck, GR) and was standardised iodimetrically[5]. It was stored under nitrogen atmosphere. The solution of methylene blue (Farbwerke Hoechst, Germany) was prepared in doubly distilled water. Dithiodiacetic acid (the disulphide) was prepared by oxidising TA with iodine[6]. The leuco base was prepared by passing purified SO_2 gas in a solution of methylene blue as described earlier[3].

The reaction was followed colorimetrically by employing a Klett-Summerson photoelectric colorimeter in terms of the decrease in absorbance of methylene blue ($\varepsilon_{max} = 4.5 \times 10^4$ dm^3 mol^{-1} cm^{-1} at 660 nm). The spectral interference in this region due to the thiol acid, the disulphide and the leuco base was ruled out. The runs were made in Pyrex vessels (coated black) under nitrogen atmosphere although its absence did not make any significant change in the rate of reaction. Other details are the same as described previously.

Results

The stoichiometric investigations showed that two moles of thiol are oxidised by one mole of MB to form the disulphide and the leuco dye (H_2MB). The IR spectra of the product also confirmed the formation of the disulphide.

$$2\,RSH + MB \rightarrow RSSR + H_2MB$$

The order in MB was determined by making a number of runs having 150-420 fold excess [TA] over the oxidant and it was found to be two in [MB] up to the initial 50% completion of the

Table 1—Effect of variation in [TA] on rate constant {$[MB] = 3.0 \times 10^{-5}$ mol dm^{-3}; $[HCl] = 4.0 \times 10^{-2}$ mol dm^{-3}; methanol = 80% (v/v); $I = 9.0 \times 10^{-2}$ mol dm^{-3}; temp = 30°C}

$[TA] \times 10^3$ (mol dm^{-3})	k_2 (dm^3 mol^{-1} s^{-1})	$k_{1/2} \times 10^6$ ($mol^{1/2} dm^{-3/2} s^{-1}$)
1.8	9.0	1.0
3.6	12.2	1.6
4.5	18.1	2.1
5.4	27.2	2.7
7.2	37.2	3.9
9.0	49.6	5.0
10.8	83.0	7.5

reaction which gradually changed to half in a given kinetic run as given in Table 1. The actual behaviour of a representative kinetic run has been shown in Fig. 1.

The order in the oxidant was further confirmed by the graphical as well as van't Hoff's differential methods. The reaction followed a first order kinetics in the substrate which was unchanged in spite of a transition in order in [MB].

The pseudo-second order rate constant increases linearly on increasing $[H^+]$. A plot of log $k_{1/2}$ against log $[H^+]$ is linear with a slope of 0.4 at low $[H^+]$ (ca. $\leqslant 4.0 \times 10^{-2}$ mol dm^{-3}) but at higher $[H^+]$ the order in $[H^+]$ increases to unity (slope 0.8; Fig. 2). The ionic strength of the system was maintained constant (0.15 mol dm^{-3}) by adding the requisite amount of potassium chloride

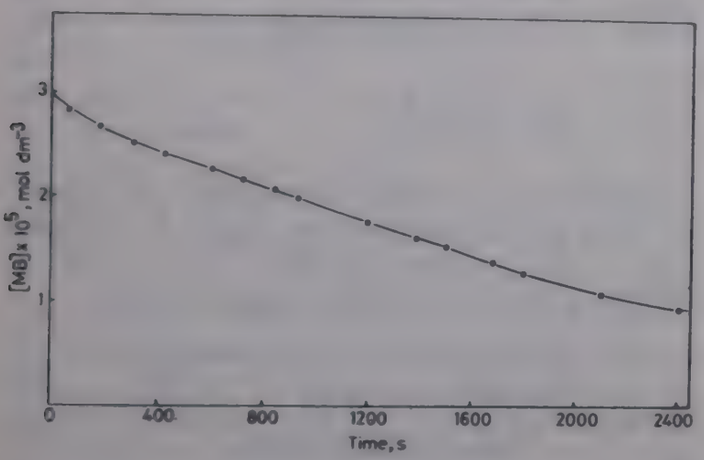

Fig. 1—Concentration-time curve {$[TA] = 4.5 \times 10^{-3}$ mol dm^{-3}; $[MB] = 3.0 \times 10^{-5}$ mol dm^{-3}; $[HCl] = 4.0 \times 10^{-2}$ mol dm^{-3}; $[KCl] = 5.0 \times 10^{-2}$ mol dm^{-3}; $CH_3OH = 80\%$ (v/v); $I = 9.0 \times 10^{-2}$ mol dm^{-3}, temp = 30°C.}

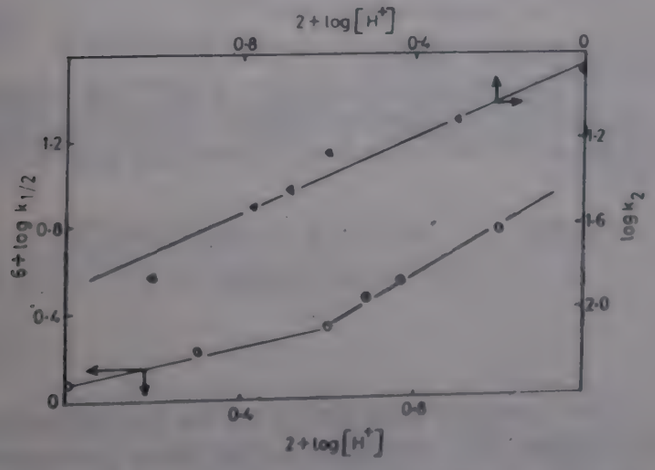

Fig. 2—Plots of $K_{1/2}$ versus log $[H^+]$ and K_2 versus log $[H^+]$ {$[TA] = 4.5 \times 10^{-3}$ mol dm^{-3}; $[MB] = 3.0 \times 10^{-5}$ mol dm^{-3}; $CH_3OH = 80\%$ (v/v); $I = 15.0 \times 10^{-2}$ mol dm^{-3}; temp = 30°C; $[HCl] \times 10^{-2}$ mol dm^{-3} = 1.0, 2.0, 4.0, 5.0, 6.0, 10.0 ○, $k_{1/2}$; Δ, k_2}

in the reaction mixture. The rate decreases with increase in initial [oxidant] but the rate constants tend to attain a limiting value at higher [MB] (Table 2).

The rate is not influenced by the addition of electrolytes such as KCl, NaCl, $NaNO_3$ and Li_2SO_4. The dielectric constant of the medium was altered by varying the methanol content of the reaction mixture. The pseudo-second order rate constant decreases and attains a limiting value while the half order rate constant continuously decreases with decrease in the dielectric constant of the medium.

The addition of dithiodiacetic acid did not influence the rate of reaction. However, on adding leuco methylene blue the second order dependence of rate on [MB] in the initial part of reaction almost disappeared and a half order dependence was noticed even from the initial stages. The order in [substrate] remained unity but unlike the runs given in Table 2, the rate constant was not affected on varying [MB] under these conditions. For example, under the same conditions as in Table 2, in the presence of $[H_2MB] = 6.66 \times 10^{-6}$ mol dm^{-3}, $k'_{1/2} \times 10^6$ values were 2.8, 2.9 and 3.0 mol$^{1/2}$ dm$^{-3/2}$ s^{-1} respectively for $[MB] \times 10^5$ of 3.0, 2.6 and 2.1 mol dm^{-3}.

The activation parameters evaluated by studying the effect of temperature on the second order as well as on half order rate constants show that the latter part of the reaction requires a highly specific conformational orientation of the reacting species. When the order in [MB] is two, $\Delta H^\dagger = 61.3$ kJ mol^{-1}, $\Delta S^\dagger = -21.9$ JK^{-1} mol^{-1} and $\Delta G^\dagger = 68.0$ kJ mol^{-1}; when the order in [MB] is half, the corresponding values are 31.6, −246.0 and 106.2 respectively.

Discussion

It is reported that methylene blue is protonated (MBH^+) in acidic medium[7-10] and is predominantly present in the monomeric form in alcohol while

Table 2—Effect of variation in [MB] on rate constant
{$[TA] = 4.5 \times 10^{-3}$ mol dm^{-3}; $[HCl] = 4.0 \times 10^{-2}$ mol dm^{-3}; methanol = 80% (v/v); $I = 9.0 \times 10^{-2}$ mol dm^{-3}; temp = 30°C}

$[MB] \times 10^5$ (mol dm^{-3})	k_2 (dm^3 mol^{-1} s^{-1})	$k_{1/2} \times 10^6$ (mol$^{1/2}$ dm$^{-3/2}$ s^{-1})
3.50	20.0	2.7
3.00	18.1	2.1
2.50	23.2	2.3
2.00	47.0	2.5
1.50	89.0	2.8
1.25	133.1	3.7

the dimeric species is prevalent in aqueous medium[11]. Further, methylene blue cation excited to a triplet state is known to form a dimer (D) on interaction with MB in ground state. The present kinetic findings for the initial part of the reaction are best explained by presuming the interaction of dimer with RSH as the rate determining step. Thus,

$$MB + H^+ \overset{K_1}{\rightleftharpoons} MBH^+ \quad \ldots(1)$$

$$MBH^+ + MB \overset{K_2}{\rightleftharpoons} D \quad \ldots(2)$$

$$D + RSH \overset{k_1}{\rightarrow} RS^{\cdot} + HM^{\cdot} + MBH^+ \quad \ldots(3)$$

$$HM^{\cdot} + RSH \overset{k_2}{\rightarrow} RS^{\cdot} + H_2M \quad \ldots(4)$$

$$2\,RS^{\cdot} \overset{k_3}{\rightarrow} RSSR \quad \ldots(5)$$

The participation of the radical $HM^{\cdot}$ (semi reduced MB) is reported in a variety of electron transfer reactions[12] while the formation of $RS^{\cdot}$ radical is quite prevalent in literature[13]. The rate of reaction would be given by Eq. (6)

$$-\frac{d[MB]}{dt} = k_1[D][RSH] \quad \ldots(6)$$

On substituting $[D] = K_1K_2[MB]^2[H^+]$

$$-\frac{d[MB]}{dt} = k_1K_1K_2[MB]^2[H^+][RSH] \quad \ldots(7)$$

Thus, Eq. (7) explains the second order kinetics in methylene blue observed in the initial part of the reaction. Moreover, it also explains a linear dependence of rate on $[H^+]$. It has been shown that the rate constant decreases with increase in [MB] which indicates the possibility of the participation of inhibiting species during the course of reaction and it seems that in the latter part, recombination of radicals $RS^{\cdot}$ and $HM^{\cdot}$ becomes predominant to make step (3) reversible. Thus,

$$D + RSH \underset{k'_{-1}}{\overset{k'_1}{\rightleftharpoons}} RS^{\cdot} + HM^{\cdot} + MBH^+ \quad \ldots(8)$$

$$HM^{\cdot} + RSH \overset{k'_2}{\rightarrow} RS^{\cdot} + H_2M \quad \ldots(9)$$

$$RS^{\cdot} \overset{k'_3}{\rightarrow} 1/2\,RSSR \quad \ldots(10)$$

Under these conditions, the rate of reaction would be given by Eq. (11)

$$-\frac{d[MB]}{dt} = k'_1[D][RSH] - k'_{-1}[RS^{\cdot}][HM^{\cdot}][MBH^+] \quad \ldots(11)$$

On assuming steady state for $RS^{\cdot}$ and $HM^{\cdot}$,

$$[RS^{\cdot}] = \frac{2k'_1[D][RSH]}{2k'_{-1}[HM^{\cdot}][MBH^+] + k'_3} \quad \ldots(12)$$

$$\text{and } [HM^{\cdot}] = \frac{\left\{\begin{matrix} -k'_2k'_3[RSH] \pm k'^2_2k'^2_3[RSH]^2 \\ +8k'_{-1}k'_2k'_3[RSH]^2[MBH^+][D]\end{matrix}\right\}^{1/2}}{4k'_{-1}k'_2[RSH][MBH^+]} \quad \ldots(13)$$

or,

$$[HM^{\cdot}] = \frac{\left\{\begin{matrix} \pm(k'^2_2k'^2_3[RSH]^2 + 8k'_{-1}k'_1k'_2k'_3 \\ [RSH]^2[MBH^+][D]\end{matrix}\right\}^{1/2}}{4k'_{-1}k'_2[RSH][MBH^+]} - \frac{k'_3}{4k'_{-1}[MBH^+]} \quad \ldots(14)$$

Activation parameters (specifically ΔS^*) indicate that k'_{-1} is comparatively larger in the latter part of the reaction; therefore, Eq. (12) can be written as (after neglecting the negative root)

$$[HM^{\cdot}] = \frac{\left\{\begin{matrix} (k'_2k'^2_3[RSH]^2 + 8k'_{-1}k'_1k'_2k'_3 \\ [RSH]^2[MBH^+][D]\end{matrix}\right\}^{1/2}}{4k'_{-1}k'_2[RSH][MBH^+]} \quad \ldots(15)$$

Thus, the rate expression is given by

$$-\frac{d[MB]}{dt} = \frac{2k'_1k'_2k'_3[D][RSH]}{(k'^2_2k'^2_3 + a[MBH^+][D])^{1/2} + 2k'_2k'_3} \quad \ldots(16)$$

where $a = 8k'_{-1}k'_1k'_2k'_3$

On substituting the value of [D] and putting $[MBH^+] = K_1[MB][H^+]$; Eq. (14) becomes Eq. (17).

$$-\frac{d[MB]}{dt} = \frac{2k'_1k'_2k'_3K_1K_2[RSH][MB]^2[H^+]}{(k'^2_2k'^2_3 + aK_1^2K_2[MB]^3[H^+]^2)^{1/2} + 2k'_2k'_3} \quad \ldots(17)$$

The increased probability of the recombination of radicals $RS^{\cdot}$ and $HM^{\cdot}$ in the latter part would result in a decrease in the magnitude of k'_2 and k'_3 and under these conditions, Eq. (17) will be valid resulting in half order kinetics in [MB] and a fractional order in $[H^+]$ as has been observed (Fig. 2). However, at higher $[H^+]$ the monomeric species

predominates[9] which would tend to decrease [D] in denominator of Eq. (16) and in turn, tend to increase the order in $[H^+]$ as has been noticed.

The deviations in kinetic features in methylene blue have been attributed to the prominence of radical participation in the latter part of the reaction and this postulate was experimentally verified by adding methyl methacrylate to the reaction system. It was observed that the rate of the initial part (about 30%) remained unaffected on such additions but the rate of the latter part considerably decreased on adding the monomer which indicates that the rate determining step involves the participation of free radical(s) at a latter stage[14].

Further, the reaction scheme also qualitatively explains the effect of solvent on the rate. As already mentioned the pseudo-second order rate constant tends to attain a limiting value at higher methanol content while $k_{1/2}$ gradually decreases. The influence on the second order rate constant may be attributed to the limiting rate of dimerisation of MB at higher methanol content whereas a solvent cage around the reacting species is likely to hinder the sterically controlled interactions in the latter part and will retard the rate of reaction. The reaction scheme, however, does not explain the disappearance of second order behaviour in MB on adding the leuco base to the system. It may be mentioned here that semiquinone radicals are known to undergo disproportionation to produce the leuco dye along with the parent molecule[15].

$$HD + HD \rightarrow H_2D + D$$

It is, therefore, likely that the addition of leuco base on interaction with MB favours the formation of $HM^{\cdot}$ and decreases the magnitude of velocity constants k'_2 and k'_3 to give an overall half order kinetics in methylene blue as explained earlier. It may also result in an increase in the magnitude of k'_{-1} due to the recombination of radicals with MBH^+ as shown in step (8). This reversibility may lead to a limiting concentration of MB and thus, the rate is not affected by variation in [MB]. Incidentally, a similar behaviour in hexacyanoferrate (III) ion has been observed in the oxidation of 1-butanethiol and 2-butanethiol when the runs are made in the presence of externally added hexacyanoferrate(II) ions[16].

Acknowledgement

The authors are thankful to M P Council of Science and Technology, Bhopal, for providing financial assistance for this project.

References

1 Lehninger A L, *Biochemistry*, (Kalyani Publishers, India) (1978) 447.
2 Muthakia G K & Jonnalogadda S B, *J phy Chem*, 93 (1989) 4751.
3 Mishra K K & Chansoria K, *Oxid Commun*, 11 (1988) 285.
4 Mishra K K & Bhargava R, *Phos Sulf Silicon*, 54 (1990) 39.
5 Kramer H, *J Assoc agri Chem*, 35 (1952) 285.
6 Kolthoff I M, Anastasi A & Tan B H, *J Am chem Soc*, 80 (1958) 3235.
7 Mukerjee P & Ghosh A K, *J Am chem Soc*, 92 (22) (1970) 6408.
8 Mukerjee P & Ghosh A K, *J Am chem Soc*, 92 (22) (1970) 6413.
9 Ghosh A K, *J Am chem Soc*, 92 (22) (1970) 6415.
10 Mukerjee P & Ghosh A K, *J Am chem Soc*, 92 (22) (1970) 6419.
11 Mukerjee P & Ghosh A K, *J Am chem Soc*, 92 (22) (1970) 6403.
12 *Annual review of physical chemistry*, edited by H Eyring, C J Christensen & H S Johnston, Vol. 18, (Annual Review Inc) (1947) 415, 425.
13 Patai S, *The chemistry of the thiol group* (Wiley Interscience, London) Part I (1974) 313.
14 Kolthoff I M & Meehan E J, *J polymer Sci*, 11 (1953) 71.
15 Rohtagi Mukherjee K K, *Fundamentals of photochemistry* (Wiley Eastern, New Delhi) (1986) 254.
16 Kalla K G & Mishra K K, *Phos Sulf*, 35 (1988) 183.

Indian Journal of Chemistry
Vol. 31A, September 1992, pp. 732-734

Voltammetry of 1-(*m*-chlorophenyl)-3-phenyl-1,2-epoxypropan-3-one

G Srinivasulu Reddy & S Jayarama Reddy*
Department of Chemistry, Sri Venkateswara University, Tirupati 517502

Received 15 April 1991; revised 8 October 1991; accepted 6 February 1992

Electrochemical reduction of 1-(*m*-chlorophenyl)-3-phenyl-1,2-epoxypropan-3-one has been carried out in the *p*H range 2.0 to 12.0 in 25% aqueous DMF by differential pulse polarography, AC polarography, DC polarography and cyclic voltammetry. The electrochemical reduction mechanism given is consistent with the data obtained. The kinetic parameters, such as transfer coefficient, diffusion coefficient and heterogeneous forward rate constant value have been evaluated and reported.

In an earlier investigation on the electroreduction of simple epoxychalcone it was shown that the epoxy group is reduced at d.m.e. In the present investigation, DC polarography, cyclic voltammetry, AC polarography, differential pulse polarography and millicoulometry are employed to study the reduction of the title compound in 25% aqueous DMF as solvent.

Experimental

1-(*m*-chlorophenyl)-3-phenyl-1,2-epoxy propan-3-one (Aldrich Chemicals, U.S.A.) was used as solvent and its solution was prepared by dissolving it in DMF and the required concentration of the solvent made up with the supporting electrolyte in triply distilled water. The universal buffers used were prepared from 0.2 *M* boric acid, 0.05 *M* citric acid and 0.1 *M* trisodium orthophosphate. The test solution was made oxygen-free before taking the voltammograms. All experiments were carried out at 27 ± 1°C.

'Metrohm unit' model E 506 polarecord coupled with E 612 VA Scanner, E 608 VA Controller and model X-Y/t Digigraphic recorder were used for cyclic voltammetry, differential pulse polarography and AC polarography techniques. DC polarograms were recorded on a PARC unit, model-364 coupled with Kipp and Zonen recorder. Techno potantiostat coupled with digital multimeter were used for controlled potential electrolysis measurements. Mercury pool was used as working electrode, platinum as the auxiliary electrode, and saturated calomel electrode (SCE) as the reference electrode. The solution was stirred by means of a magnetic stirrer. The d.m.e. at a flow rate 2.4805 mgs^{-1} was used as working electrode and SCE/Ag/AgCl(s), Cl^- as the reference electrodes in DC polarography. However in the case of cyclic voltammetry, hanging mercury drop electrode (hmde) was used as the working electrode. Platinum served as the auxiliary electrode for all techniques.

Results and discussion

1-(*m*-chlorophenyl)-3-phenyl-1,2-epoxy-propan-3-one exhibits a single well-defined cathodic wave/peak in the *p*H range of 2.0 to 6.0. Whereas in the *p*H range of 8.0 to 12.0, besides this cathodic peak/wave an additional second wave/peak is observed. The cathodic peak observed in the entire *p*H range of 2.0 to 12.0 may arise as a result of reduction of epoxy group, whereas peak observed in the *p*H range of 8.0 to 12.0 may be the reduction of keto group to the hydroxy group. Typical cyclic voltammogram is shown in Fig. 1.

The number of electrons involved in the reduction process has been calculated from the results obtained with millicoulometry[6]. At all *p*Hs, the number of electrons with reduction process are found to be two. Controlled potential electrolysis has been carried out in 25% DMF (*p*H 10.0) solution at − 1.52 V (vs. SCE) and the isolated product has been identified as the corresponding hydroxy compound by IR spectral data (KBr, 3280, 2975 cm^{-1}). In this method 55% yield of 1-(*m*-chlorophenyl)-3-phenyl-1,3-di-hydroxy-propane is obtained.

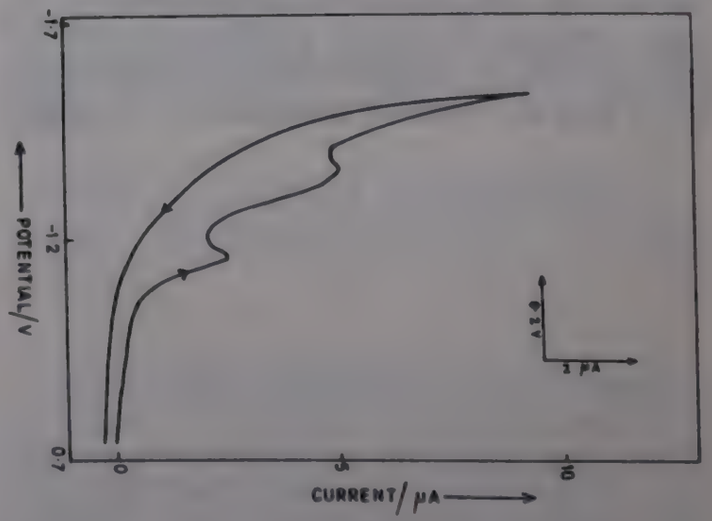

Fig. 1—Typical cyclic coltammogram of 1-(*m*-chlorophenyl)-3-phenyl-1,2-epoxypropan-3-one in *p*H 8.0 (Concentration: 0.5 m*M*; scan rate: 40 mVs^{-1}; solvent: 25% DMF).

The plots of i_d versus $h^{1/2}$, i_p versus $v^{1/2}$ and i_m versus $t^{2/3}$ are all linear passing through the origin in each of the supporting electrolytes employed indicating adsorption-free and diffusion-controlled nature of the electrode process. The decrease in the base current is not observed before or after the AC peaks, indicating that the electrode process is free from adsorption complications. Variation of current function $i_p/Cv^{1/2}$ with scan rate (v) in cyclic voltammetry is found to be almost negligible indicating the electrode process to be free from any kinetic complications.

The reduction process for the two waves/peaks is irreversible in all the techniques employed as evidenced from the disobedience of Tome's criterion, log-plot analysis and dependence of half-wave potential on the concentration of the electroactive species, in DC polarography and the absence of anodic peak in the reverse scan and the variation of peak potential with scan rate in cyclic voltammetry. The marginal variation of peak potential (E_m) with concentration and non-linearity in the plot of i_m versus $1-\sigma/1+\sigma$ in differential pulse polarography also confirm the irreversible nature of the electrode process.

The values obtained for the transfer coefficient, diffusion coefficient and heterogeneous forward rate constants in various supporting electrolytes in different techniques are given in Table 1. The diffusion coefficient values evaluated from all the techniques are in good agreement. The decrease in diffusion coefficient with increase in *p*H may be attributed to the decrease in the availability of protons with increase in *p*H of the supporting electrolyte. The DC polarographic diffusion coefficient values are considered as more reliable, since it is a slow technique and the renewal of the surface of mercury drops at d.m.e. also adds to the credibility of the values. The number of protons involved in the rate determining step as evaluated from $E_{1/2}$ versus *p*H plot is found to be two in both the cases. The heterogeneous forward rate constants are found to decrease with increase in *p*H and percentage at DMF in aq. DMF as solvent indicates that the electrode reaction tends to become more and more irreversible. The rate constants obtained in AC polarography are found to be high as compared to other techniques since the rate constants are evaluated at standard potentials in AC polarography.

Electrode mechanism

In the entire *p*H range of 2.0 to 12.0, the reduction process may be represented by Eq. (1)

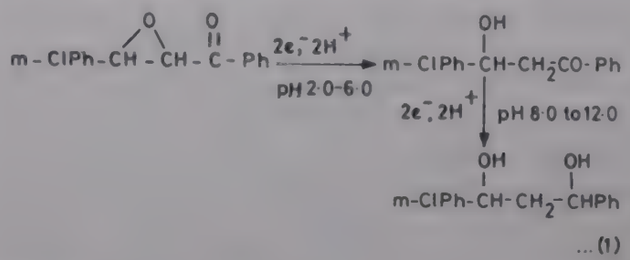

...(1)

Analysis

In the present investigation, the peak obtained at *p*H 4.0 (potential = −0.79 V) in differential pulse polarography is well resolved and may be utilized for the estimation of title compound. Using the calibration method, the peak height is found to be linear in the concentration range of 2.5×10^{-4} *M* to 4.5×10^{-6} *M*. The lower detection limit is found to be 4.3×10^{-6} *M*.

Table 1—Typical electrode kinetic data for reduction of 1-(*m*-chlorophenyl)-3-phenyl-1,2-epoxypropan-3-one (Concentration: 0.5 m*M*; Solvent: 25% DMF)

*p*H	DC Polarography (Drop time = 3 sec)			Cyclic voltammetry (Scan rate = 40 mV s^{-1})			AC Polarography (Drop time = 3 sec)			Diff. pulse polarography (Drop time = 2 sec)		
	$-E_{1/2}$ V	$D\times10^6$ $cm^2\,s^{-1}$	$K^0_{f,h}$ cm s^{-1}	$-E_p$ V	$D\times10^6$ cm^2s^{-6}	$K^0_{f,h}$ cm s^{-1}	$-E_s$ V	$D\times10^6$ $cm^2\,s^{-1}$	$K^0_{f,h}$ cm s^{-1}	$-E_m$ V	$D\times10^6$ $cm^2\,s^{-1}$	$K^0_{f,h}$ cm s^{-1}
2.0	0.70	3.42	2.97×10^{-9}	0.71	3.45	4.09×10^{-9}	0.70	3.38	4.17×10^{-8}	0.70	3.37	1.29×10^{-9}
4.0	0.78	3.27	7.49×10^{-10}	0.78	3.37	8.17×10^{-10}	0.79	3.29	4.92×10^{-9}	0.79	3.19	8.42×10^{-10}
6.0	0.87	3.16	1.92×10^{-10}	0.89	3.26	2.09×10^{-10}	0.88	3.26	8.97×10^{-10}	0.88	3.04	7.43×10^{-11}
8.0	a) 1.00	3.08	6.49×10^{-11}	1.01	3.15	7.49×10^{-11}	0.99	3.11	1.89×10^{-10}	1.02	2.97	9.21×10^{-12}
	b) 1.36	3.01	8.43×10^{-13}	1.35	3.52	3.73×10^{-12}	1.34	3.31	4.92×10^{-11}	1.33	3.23	4.32×10^{-13}
10.0	a) 1.13	2.87	4.72×10^{-12}	1.13	3.04	4.72×10^{-12}	1.14	2.83	9.67×10^{-11}	1.14	2.86	2.72×10^{-13}
	b) 1.44	2.65	1.92×10^{-15}	1.45	3.41	6.49×10^{-14}	1.44	3.24	4.82×10^{-12}	1.44	3.11	6.42×10^{-15}
12.0	a) 1.26	2.42	8.43×10^{-14}	1.27	2.99	7.23×10^{-13}	1.28	2.49	8.21×10^{-12}	1.28	2.58	2.79×10^{-14}
	b) 1.58	2.52	4.73×10^{-17}	1.59	3.42	8.42×10^{-17}	1.59	3.11	3.49×10^{-14}	2.73	2.73	8.03×10^{-18}

a) First wave/peak; (b) Second wave/peak.

Acknowledgement

The authors are thankful to the DNES, New Delhi, for providing financial assistance.

References

1 Hine C & Rowe V K, *Epoxy compounds* (John Wiley, UK) Ch. 32 (1981) 2141.

2 Clayton G D & Clayton F E, *Industrial toxicology* Vol. 2A, *Toxicology* (Interscience), (1961) 2878.

3 Kaiser E M, Charbs G, Grubb S D, Smith J W & Tramb D, *J org Chem*, 36 (1971) 330.

4 Kamernitskii V & Listsina N K, *Izv Akad Nack SSSR Ser Khim S*, (1984) 1901.

5 Reddy G S, Raju N V, Reddy T N & Jayarama Reddy S, *Indian J Envi Pro*, (1989) 595.

6 Devries T & Kroon T L, *J Am chem Soc*, 75 (1953) 2484.

Indian Journal of Chemistry
Vol. 31A, September 1992, pp. 735-736

Separation of platinum and palladium using a chelating resin containing quinaldinic acid amide group

B Konar, S Basu* & (Late) J Das
Analytical Chemistry Laboratory, Department of Chemistry, University of Burdwan, Burdwan 713 104

Received 22 November 1991; revised 3 February 1992; accepted 17 March 1992

A new chelating polystyrene divinyl-benzene based resin containing quinaldinic acid amide group has been used for the quantitative separation of Pt(IV) and Pd(II). Maximum sorption values of 0.19 and 0.36 mmol g^{-1} respectively, were observed around *p*H 1 for both. The method has been successfully applied for the separation of Pt(IV) and Pd(II) from each other and from noble-base mixtures, as well as from native silver solutions, the average recovery being above 99.9% with 4(*M*) HCl.

Quinaldinic acid is a well established analytical reagent, predominantly used for the gravimetric determination of several cations[1]. A new chelating resin containing quinaldinic acid amide as the functional group incorporated into the macro-reticular styrene divinyl benzene copolymer beads was synthesised[2] and used for the determination of a number of cations[3] in our laboratory. The present work describes the use of this exchanger in the quantitative separation of Pt(IV) and Pd(II) from their mixtures.

Experimental

Palladium(II) chloride, chloroplatinic acid, and rhodium(III) chloride (Johnson-Mathey) were dissolved in dilute HCl, and gold(III) chloride (Johnson-Mathey) in deionised water and the solutions were standardized by literature methods[4,5]. The metal ions were determined with a Shimadzu UV-vis double beam spectrophotometer (Model UV-160). A Sambros digital *p*H meter (Model 335) was used for adjustment of *p*H. IR spectra were recorded on a Shimadzu instrument (IR-408).

The metal ion uptake at different *p*H (0.1-5.0) were determined both by batch equilibration and column technique, followed by its spectrophotometric estimation[6,7] after eluting the metals by suitable eluting agents. For the separation of Pt(IV) and Pd(II) in different binary mixtures containing the two cations in different proportions, a glass column (30 × 1 cm) was packed with 20 g of resin and preconditioned with a buffer solution of *p*H 1. The mixture, at *p*H 1, was percolated through the column maintaining a constant flow rate of 0.5 ml min^{-1}. After complete sorption, Pd(II) was eluted by 1% DMG-$CHCl_3$ mixture. After its quantitative recovery, Pt(IV) was eluted by 4 *M* HCl. The results are given in Table 1.

Results and discussion

Recovery of Pt(IV) and Pd(II) with various eluting agents (2*N* and 4*N* H_2SO_4, HNO_3 and HCl) was studied in detail. The results showed that the recovery of Pt(IV) and Pd(II) was above 99% with 4 *M* HCl.

Several synthetic solutions containing Pd(II), Pt(IV) and associated noble or base metals or a mixture of both were used to test the applicability of the proposed method for the quantitative recovery of both the cations using the present method. We also analysed a few synthetic solutions having the same compositions after separation of silver from native Kongsberg silver sample[8]. Microgram quantities of noble metals in different quantities were incorporated into these synthetic solutions and silver was separated as AgCl by double precipitation. The solutions so obtained were subjected to resin treatment by the proposed method. Pd(II) and Pt(IV) were recovered using 1% DMG-$CHCl_3$ mixture and 4*M* HCl as eluting agents respectively (Table 2).

Quinaldinic acid has been reported to form insoluble complexes with Pd and Pt[1]. The resin with

Table 1—Separation of Pt(IV) and Pd(II) in several binary mixtures

Metal ion	Amount taken (ppm)	Amount found (ppm)†	Recovery (%)
1.(a) Pd(II)	100	99.0	99.0
(b) Pt(IV)	80	80.3	100.3
2.(a) Pd(II)	60	59.4	99.0
(b) Pt(IV)	80	79.6	99.5
3.(a) Pd(II)	100	100.1	100.1
(b) Pt(IV)	120	120.0	100.0
4.(a) Pd(II)	60	60.08	100.1
(b) Pt(IV)	120	118.0	98.3
5.(a) Pd(II)	100	100.1	100.1
(b) Pt(IV)	5	4.5	90.0
6.(a) Pd(II)	5	4.7	94.0
(b) Pt(IV)	100	100.4	100.4
7.(a) Pd(II)	20	19.7	98.5
(b) Pt(IV)	120	120.0	100.0
8.(a) Pd(II)	120	119.0	99.1
(b) Pt(IV)	20	19.4	97.0

† Average of three determination.

Table 2—Analysis of native Kongsberg silver samples

[Approx. comp. Ag=98.45%, Au=0.004%, Cu=0.011%, Fe=0.024%, Sb=0.581%, Hg=1.13%]

Sample No.	Pd(μg)		Pt(μg)		Recovery (%)	
	Taken	Found	Taken	Found	Pd(II)	Pt(IV)
Native silver 1	2.0	1.99	16.0	17.0	100.0	106.0
Native silver 2	1.0	1.00	12.0	11.5	100.0	95.8
Native silver 3	2.0	2.00	10.0	10.0	100.0	100.0

the acid amide functional group falls into the border line to soft base region and is expected to complex with soft cations like Pt(IV) and Pd(II). The maximum sorption capacity of Pt(IV) and Pd(II) (0.19 and 0.36 mmol g^{-1} respectively) was observed at *p*H 0.8 and 1.0 respectively. The separation of Pt(IV) and Pd(II) from associated noble-base mixtures as well as from native silver solution is achieved on the basis of the differential sorption capacities; the sorption capacities of Au(III), Rh(III), Ir(III), Cu(II), Ni(II), recorded at *p*H 1 are 3.98, 0.049, 0.05, 0.01, 1.6×10^{-3} mmol g^{-1} respectively. The capacities of the remaining cations of the synthetic solutions are zero at *p*H 1. Hence most of the cations remain unabsorbed and come out by simple washing of the column with a buffer solution of *p*H 1. Since Pd(II) forms a very strong DMG complex[7], extractable into $CHCl_3$, it was eluted by this reagent which did not however effect elution of Pt(IV), Rh(III) and Ir(III) were then eluted by 1:1 sodium oxalate:potassium oxalate (5%) solution. Pt(IV) is not eluted by this oxalate mixture due to its higher sorption capacity as well as weak complexation with oxalate[9]. Finally, Pt(IV) was eluted by 4 *M* HCl which does not effect the elution of Au(III), which in turn, is eluted by 10% thiourea in 4 *M* $HClO_4$. The time required for 50% uptake ($t_{1/2}$) of the metal ions by the resin was found to be 72 and 85 min for Pd(II) and Pt(IV) respectively. The present method is very simple and yields quantitative separation of these important noble metal pair.

Acknowledgement

The authors thank Thermax (P) Ltd., Poona, India, for the gift samples of Styrene-DVB beads. Thanks are also due to Miss M Pobi for valuable suggestions.

References

1 Vogel A I, *A text book of quantitative inorganic analysis including elementary instrumental methods*, 4th Edn (Longman, New York) (1978) 428.
2 Das J & Das N, *Analyt Lett*, 21 (1988) 1735.
3 Das N, *Separation and preconcentration of metal ions using chelating ion exchange resin containing quinaldinic acid amide group* (Ph D Thesis), Burdwan University (1989).
4 Pal T & Das J, *Talanta*, 30(7) (1983) 519.
5 Kodama K, *Quantitative inorganic analysis* (Intersciences, New York) (1963) 228.
6 Shome S C, Majumdar M & Chakrabarty M R, *J Indian chem Soc*, LIV (1977) 225.
7 Davis W F, *Talanta*, 16 (1979) 1330.
8 Dana J D & Dana E S, *The system of minerology*, 7th Edn (John Wiley, New York) (1946) 97.
9 Sidgwich N V, *The chemical elements and their compounds*, Vol. 2 (Oxford University Press, England) (1962) 1525, 1545-1600.

ANNOUNCEMENT

INTERNATIONAL CONFERENCE ON ENERGY ENVIRONMENT AND ELECTROCHEMISTRY

The International Conference on Energy, Environment and Electrochemistry, scheduled to be held at CECRI, Karaikudi during 9-11 September 1992, has been postponed to 10-12 February 1993. The new deadline for submission of papers/registration is 30 November 1992. Further information regarding the conference may be obtained from Dr K C Narasimhan, Conference Convenor, Central Electrochemical Research Institute, Karaikudi 623 006, Tamilnadu, India.

GOLDEN OFFER

You can now book your copies of the attractive, lavishly illustrated popular science titles under CSIR GOLDEN JUBILEE SERIES in advance and also get a

FREE GIFT

Titles in print

BODY'S BATTLES

By **Bal Phondke**

Unfolds the story of the inner defence organisation of the body, the diversity and specificity of its armament and its round the clock vigil that meets every threat to it.

84 pages; Price: Rs.15 (Paperback), Rs. 18 (Hardcover)

MINING THE OCEAN

By **T K S Murthy**

Reveals, the timeless secrets of the seas and the secret bounty that they hold in reserve.

106 pages; Price: Rs. 12 (Paperback), Rs. 20 (Hardcover)

HIS MASTER'S SLAVE

By **Tapan Bhattacharya**

Tells the non-specialist the riveting story of the modern day genie of the bottle, the PC.

88 pages; Price: Rs. 10 (Paperback), Rs. 18 (Hardcover)

INSIDE STARS

By **Biman Basu**

Provides a privileged glimpse into star nurseries, tracking the luminescent trail to fiery senescence and death of stars to reveal the mysteries and marvels of cosmic drama.

90 pages; Price: Rs. 10 (Paperback), Rs. 18 (Hardcover)

PLASTIC FEAST

By **Subodh Jawadekar**

Celebrates the dawn of the plastics era and elaborates the myriad ways in which plastics touch our lives. A veritable feast of plastics, very palatable to the readers.

96 pages; Price: Rs. 12 (Paperback) Rs. 20 (Hardcover)

CERAMICS ARE FOREVER

By **B C Sharma**

Highlights the fascinating versatility of ceramics and provides an excellent close-up of the symbiotic relationship between man and materials.

84 pages; Price: Rs. 11 (Paperback), Rs. 20 (Hardcover)

ARTIFICIAL INTELLIGENCE

By **K.D. Pavate**

Unveils the many facts of Artificial Intelligence

98 pages; Price: Rs.13 (Paperback), Rs.21 (Hardcover)

Forthcoming Titles

HARDY COMPOSITES

MAN IN SPACE

MIND MASTER

You may place an order for all 10 titles by sending Rs.120.00 (for paperback) or Rs.200.00 (for Hardcover) including postage by Demand Draft/M.O. payable to "Publications and Information Directorate". The titles already published will be sent to you as soon as the payment is received and the forthcoming titles will be sent by post as soon as they are published, one every month. With every order you will receive a free gift.

For further information write to:
Sales and Distribution Officer
Publications and Information Directorate (CSIR)
Dr. K S Krishnan Marg, New Delhi 110 012

OUR AGENTS: – BANGALORE, Navakarnataka Publications Pvt. Ltd., Embassy Centre, 11, Crescent Road, Kumara Park East, Bangalore - 560 001; BHOPAL, Ajay Publishers & Distributors, 74, Motia Park, Behind Moti Masjid, Bhopal-460 001; BOMBAY, Strand Book Stall, Sir Ferozeshah Mehta Road, Fort, Bombay - 400 001, Universal Book Corporation, 546, Kalabadevi Road, Dhobi Talao, P.B. No.2540, Bombay - 400 00; CALCUTTA, Manisha Granthalaya (P) Ltd., 4/3 B, Bankim Chatterjee Street, Calcutta-700 073; MYSORE, People's Book House, J.M. Place Road, Mysore - 570 024; NEW DELHI, Sangam Book Depot, 4378/4B, Ansari Road, Darya Ganj, New Delhi - 110 002, UBS Publishers Distributors Ltd., 5, Ansari Road, Darya Ganj, New Delhi - 110 002; PATNA, Sunil News Agency, Yogiatoli, Patna - 800 001; PUNE, Satish Book Distributors, 27/B, Siddharth Chambers, Opp. Balwant Chowk, Budhwar Peth, Pune 411 002.

Printed & Published by Dr. G.P. Phondke, Director, Publications & Information Directorate (PID)
Dr. K.S. Krishnan Marg, New Delhi 110 012, at PID.

DL-18023/92
RN 7090/63